QA: NA

July 2004

Technical Basis Document No. 7: In-Package Environment and Waste Form Degradation and Solubility

Revision 1

Prepared for:
U.S. Department of Energy
Office of Civilian Radioactive Waste Management
Office of Repository Development
1551 Hillshire Drive
Las Vegas, Nevada 89134-6321

Prepared by:
Bechtel SAIC Company, LLC
1180 Town Center Drive
Las Vegas, Nevada 89144-6363

Under Contract Number
DE-AC28-01RW12101

CONTENTS

Page

CONTENTS (Continued)

Page

CONTENTS (Continued)

Page

CONTENTS (Continued)

Page

CONTENTS (Continued)

Page

INTENTIONALLY LEFT BLANK

FIGURES

Page

FIGURES (Continued)

Page

TABLES

Page

TABLES (Continued)

Page

ACRONYMS AND ABBREVIATIONS

AIN	additional information needed
BWR	boiling water reactor
DOE	U.S. Department of Energy
EBS	engineered barrier system
FEP	feature, event, or process
GEN	general items
HLW	high-level radioactive waste
KTI	Key Technical Issue
LA	license application
NRC	U.S. Nuclear Regulatory Commission
PWR	pressurized water reactor
RMEI	reasonably maximally exposed individual
SNF	spent nuclear fuel
TSPA	total system performance assessment
TSPA-LA	total system performance assessment for the license application
TSPA-SR	total system performance assessment for the site recommendation

INTENTIONALLY LEFT BLANK

1. INTRODUCTION

This technical basis document summarizes the technical basis and conceptual understanding of the chemical environment within breached waste packages after water has come into contact with the waste form, the subsequent degradation of the waste forms, and the mobilization of radionuclides from degraded waste forms.

This document is one in a series of technical basis documents that are being prepared for the different components relevant to predicting the likely postclosure performance of the Yucca Mountain repository system. The relationship of in-package chemistry, waste form degradation, and radionuclide solubility to the other repository system components is illustrated in Figure 1-1.

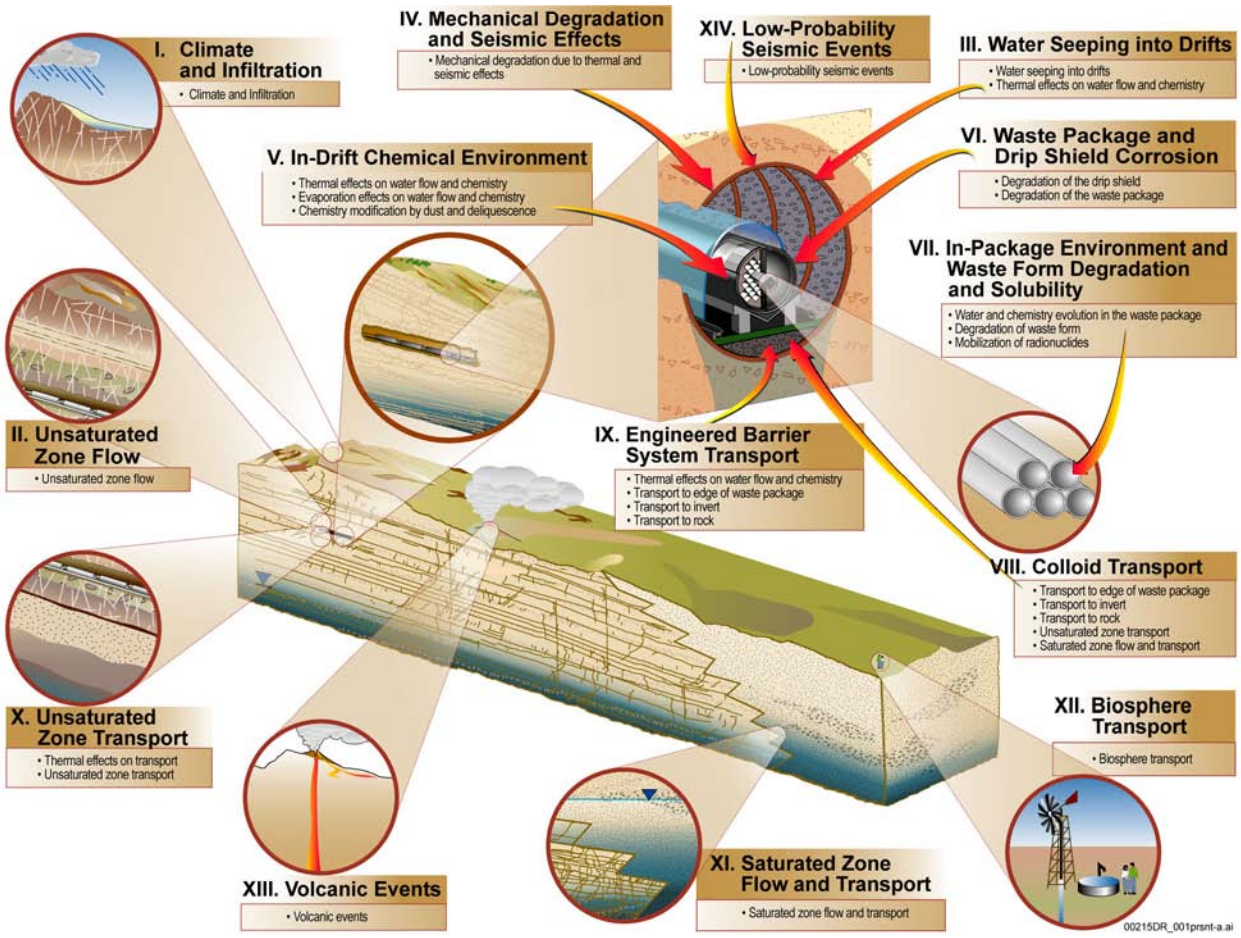

Figure 1-1. Components of the Postclosure Technical Basis for the License Application

To predict the chemical environment within a breached waste package, the degradation of the waste form, and the mobilization of radionuclides, the models discussed in this technical basis document rely on input from other models shown in Figure 1-1. Specifically, models for water seepage into the drifts and for waste package and drip shield corrosion are used to predict the evolution of the chemical environment within breached waste packages, the degradation of the waste forms, and the mobilization of radionuclides from degraded waste forms. Output from the models discussed in this document provides the source term for modeling radionuclide transport

as dissolved species and as associated with colloids through the different components of the engineered barrier system (EBS) (waste package, corrosion products, and invert) and subsequent migration through the unsaturated zone, the saturated zone, and discharge to the biosphere. The technical understanding of the waste package environment, waste form degradation, and radionuclide mobilization is based on 13 reports written to support the license application (LA):

- *Radionuclide Screening* (BSC 2002a)
- *Clad Degradation — FEPs Screening Arguments* (BSC 2004a)
- *Pitting Model for Zirconium-Alloyed Cladding at YMP* (BSC 2003a)
- *Clad Degradation — Summary and Abstraction for LA* (BSC 2003b)
- *Seismic Consequence Abstraction* (BSC 2003c)
- *Initial Radionuclide Inventories* (BSC 2003d)
- *CSNF Waste Form Degradation: Summary Abstraction* (BSC 2003e)
- *In-Package Chemistry Abstraction* (BSC 2004b)
- *DSNF and Other Waste Form Degradation Abstraction* (BSC 2003f)
- *Defense HLW Glass Degradation Model* (BSC 2003g)
- *Dissolved Concentration Limits of Radioactive Elements* (BSC 2004c)
- *Waste Form and In-Drift Colloids-Associated Radionuclide Concentrations: Abstraction and Summary* (BSC 2003h).
- *Igneous Intrusion Impacts on Waste Package and Waste Form* (BSC 2004d).

This technical basis document uses the information provided in these 13 reports to present a coherent perspective of the impact that water ingress into waste packages has on the chemical environment within the waste packages, the degradation of the waste forms, and the mobilization of radionuclides. In addition, this technical basis document provides the context for responses to Key Technical Issue (KTI) agreements (and associated general (GEN) items) and Additional Information Needed (AIN) requests made between the U.S. Nuclear Regulatory Commission (NRC) and the U.S. Department of Energy (DOE) related to in-package chemistry and commercial spent nuclear fuel (SNF) cladding. Technical responses to the following KTI agreements and AIN requests are provided as appendices to this document:

- Appendix A—In-Package Chemistry Environment (Response to CLST 3.02 AIN-1, ENFE 3.03, TSPAI 3.14, and GEN 1.01 (Comments 116 and 126))
- Appendix B—Effects of Radiolysis and Engineered Materials on In-Package Chemistry (Response to CLST 3.03 AIN-1 and CLST 3.04 AIN-1)

- Appendix C—Demonstration of the Adequacy of the In-Package Chemistry Model Results (Response to ENFE 3.04 and CLST 3.05)

- Appendix D—Localized Corrosion and Stress Corrosion Cracking in Cladding (Response to CLST 3.06 AIN-1, CLST 3.07, CLST 3.08 AIN-1, CLST 3.09 AIN-1, and GEN 1.01 (Comment 124))

- Appendix E—Total System Performance Assessment Implementation of In-Package Chemistry (Response to TSPAI 3.08).

1.1 UNDERSTANDING OF IN-PACKAGE CHEMISTRY, WASTE FORM DEGRADATION, AND RADIONUCLIDE MOBILIZATION

As the starting point for all potential radionuclide releases to the biosphere, the source term for radionuclides within the EBS is an important submodel in the total system performance assessment (TSPA) for LA. For radionuclides to be transported through the EBS, the waste form must first degrade and the radionuclides mobilized. The degradation of the waste form and the mobilization of radionuclides within the waste package are herein jointly called the waste form degradation model. The function of the waste form degradation model is to estimate the availability and mobilization of radionuclides that are used as input by the EBS transport model.

Although radioactive waste can degrade by oxidation without water, radionuclides cannot be transported in the absence of water, and water must be present for the chemistry in the package to be modeled. Therefore, the models presented in this document assume that water will be present in the waste package. In some cases (e.g., in-package chemistry), the quantity of water assumed to be present in the waste package is dictated by the needs of the submodel and may not be consistent with the quantity of water assumed to be available in other related models.

The waste form degradation model consists of eight components, shown in Figure 1-2. Five of those components determine the degradation rate of waste forms: (1) in-package chemistry; (2) degradation of commercial SNF cladding, (3) degradation of commercial SNF, (4) degradation of U.S. Department of Energy SNF, and (5) degradation of high-level radioactive waste (HLW) glass. The other three components determine the mobilization of radionuclides from the waste form into the waste package corrosion products: radionuclide inventory, radionuclide solubility, and colloid formation and stability.

Understanding the source term for radionuclides within the EBS begins with the model of the average radionuclide inventory for three generic waste forms: commercial SNF, DOE SNF, and HLW encapsulated in borosilicate glass. A fourth waste form, naval SNF, is represented by commercial SNF. The three waste forms are placed into two waste package configurations: a commercial SNF waste package with various numbers of assemblies of SNF, and a codisposal waste package with typically one canister of DOE SNF and five canisters of HLW glass. Of the more than 100 radionuclides that will be potentially present in the initial inventory, 28 radionuclides (from 14 elements) are identified as being important to the estimate of expected dose to the reasonable maximally exposed individual (RMEI) during the 10,000-year regulatory period.

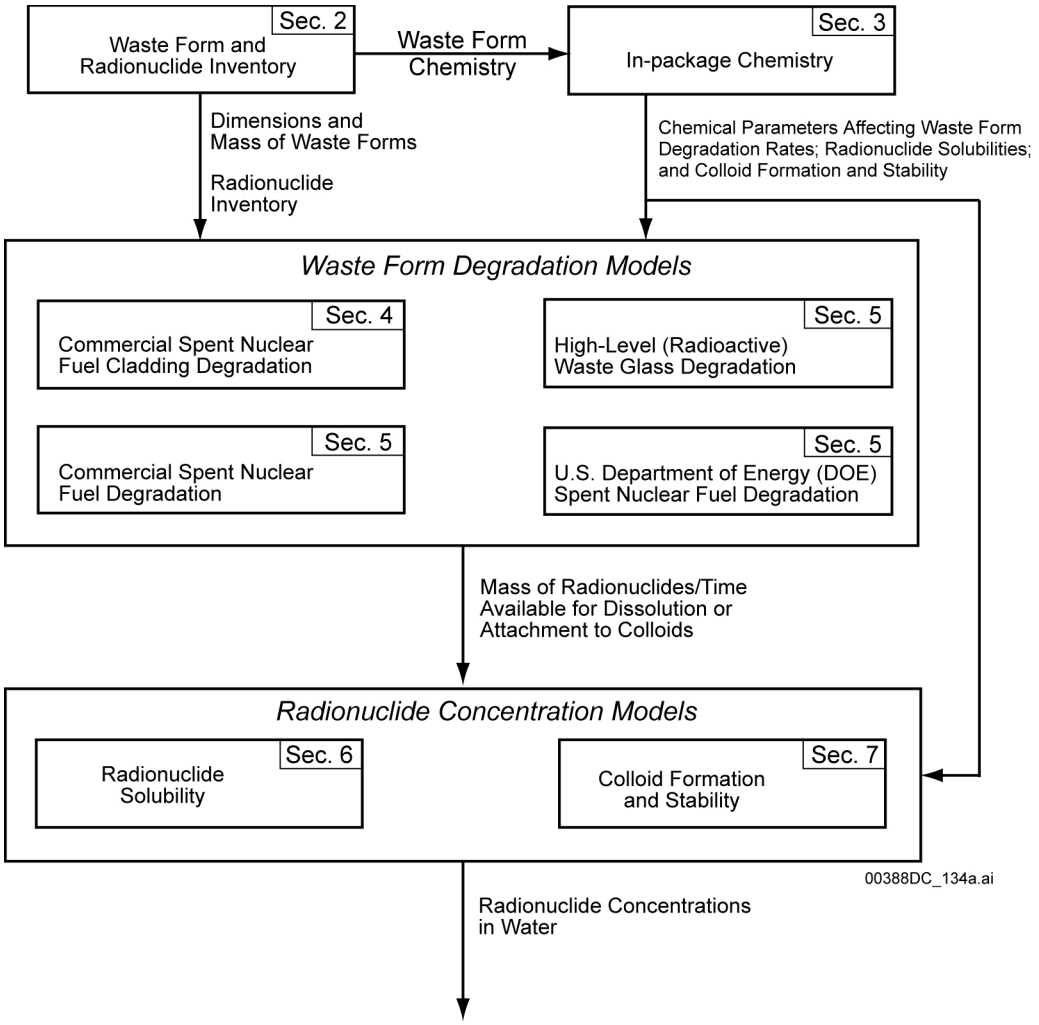

Figure 1-2. Components of the Waste Form Degradation Model

The evolution of water chemistry inside a breached waste package is controlled by the waste package corrosion rate, waste package type (commercial SNF versus codisposed), water inflow rate, cladding failure fraction, waste-form corrosion rate, and temperature. Water inflow rate will depend on whether seepage water drips onto the waste package. For nondripping conditions, water will enter a breached waste package as water vapor, whereas under dripping conditions, water will flow through a breached waste package. The pH of water within a waste package will be strongly influenced by the presence of corrosion products, primarily goethite. This phase will provide sufficient surface area for complexation reactions to buffer the pH below 8.1.

For commercial SNF, radionuclides can be released only from those fuel rods on which the cladding has failed. The rate of release of radionuclides from the fuel matrix is modeled as a function of four variables: temperature, pH, total carbonate concentration, and oxygen fugacity (or partial pressure). In addition, a small fraction of radionuclides resides in the grain boundaries of the fuel pellets and the gap between the fuel pellet and cladding of commercial SNF. Radionuclides (specifically ^{90}Sr, ^{137}Cs, ^{99}Tc, and ^{129}I) residing in the gap or grain boundary are available for dissolution as soon as water contacts the waste. The presence of a gap fraction and

the rapid degradation of the commercial SNF fuel matrix in an oxic environment, as is expected to exist in the repository, implies that the release of most radionuclides from a commercial SNF waste package is not limited by their availability (i.e., not limited by the waste form degradation rate) but by their solubility. The exceptions are ^{90}Sr, ^{137}Cs, ^{99}Tc, and ^{129}I. The solubilities of these four radionuclides are quite high under repository conditions; hence, the degradation rate of the commercial SNF fuel matrix and the initial inventory of these radionuclides in the gap and grain boundary influences their release rate.

Eleven DOE SNF groups have been used to categorize the several hundred distinct types of DOE SNF that will eventually be emplaced in the repository. A degradation rate model consisting of waste form degradation and radionuclide availability rapid enough to occur within the first TSPA-LA time step is used for all these waste groups, except naval SNF, which is assumed to behave as commercial SNF.

Many well-known processes contribute to HLW glass degradation, although there is some debate as to whether the dissolution process at high dissolved silica (H_4SiO_4) levels is controlled by surface reactions or by the diffusion of silica through alteration phases that form on the glass as it dissolves, as discussed further in Section 5.3. The glass dissolution process is controlled by the temperature and pH of the solution in contact with the glass. Under acidic and alkaline conditions, glass degradation rates increase with, respectively, decreasing and increasing pH. The degradation rate has an Arrhenius-type dependence on temperature.

The solubility of seven important elements (plutonium, americium, neptunium, thorium, uranium, protactinium, and actinium) depends on the water chemistry inside the waste package. The solubility exhibits a typical "U-shaped" dependence on pH with a minimum at approximately neutral to mildly basic pH values, which coincides with long-term in-package conditions. For an eighth element, radium, the solubility is defined solely as a function of pH. The solubilities of the remaining five important elements (i.e., carbon, cesium, strontium, iodine, and technetium) are high under expected repository conditions. Hence, the availability of these radionuclides for transport out of the waste form is determined by the fraction of cladding that fails, the degradation rate of the waste form, and the gap and grain boundary inventory.

Two sources of colloids are considered in the colloid model in the waste form: natural colloids in seepage groundwater and colloids generated from degradation of HLW glass, which exhibit a clay-like behavior. In addition, a third type of colloid, iron oxyhydroxide corrosion products, is assumed to form in the waste package as the waste form support structures corrode. Colloids formed from DOE HLW glass and naturally occurring groundwater colloids are both represented by smectite clay colloids, and can transport reversibly sorbed radionuclides. In addition, HLW glass colloids can transport embedded plutonium and americium. The stability of colloid suspensions is a function of ionic strength and pH. Dissolved cesium, americium, plutonium, protactinium, and thorium are partitioned (reversibly) between the water and groundwater colloids. Plutonium and americium embedded in HLW glass colloids are considered to be irreversibly sorbed and, thus, are not partitioned between the water and the HLW glass colloids. Corrosion product colloids are likely to be made up of some mixture of goethite, ferrihydrite, or hematite. Each solid has a high affinity for many radionuclides. Colloid suspensions are stable only when the ionic strength is less than 0.05 mol/L, and, at certain pH values, can be unstable at values of ionic strength lower than 0.05 mol/L. Colloid suspensions are believed to be stable

only for limited periods of time and under limited combinations of physical and chemical conditions during the 10,000-year regulatory compliance period. Moreover, in the nominal case scenario, when radionuclide transport within the EBS is expected to be diffusion-dominated, colloid-facilitated transport of radionuclides is physically impossible because the colloids will be too big to diffuse.

1.2 APPLICABILITY OF WASTE FORM DEGRADATION MODEL IN THE SCENARIO CLASSES

Waste form degradation is highly dependent on the amount of water entering the waste package. This dictates the in-package chemistry, which, in turn, influences waste form degradation rates, radionuclide solubility, and colloid stability. Water reaches the repository by infiltrating the mountain surface, percolating through the matrix and fractures above the repository, and seeping into the emplacement drift. Figure 1-3 shows the advective water flux pathways into and within the emplacement drifts, including the EBS and, hence, the potential sources of water for waste form degradation and radionuclide mobilization.

It is conservatively assumed that water will be present to dissolve and transport radionuclides even during periods of repository conditions that would inhibit such processes (i.e., when the waste package and waste form temperatures are higher than the surrounding surfaces and would otherwise drive moisture away). Water will be present in the repository environment, and if radionuclides are to leave the drift in large quantities, water must interact with fuel elements. To establish the limits of the water-borne dose, the broad features of waste form degradation by water must be modeled. If water never contacts the waste form, or if water contacts it in lower quantities than envisioned, TSPA predictions of dose will have been overestimated and, hence, conservative.

The waste form degradation model summarized in this document is intended to capture the expected chemical reactions induced when water enters a failed waste package either through advection (flow pathway 4 in Figure 1-3) or by diffusion and to estimate radionuclide release from waste packages into the invert either by advection (flow pathway 6 of Figure 1-3) or diffusion. The amount of water that enters a package is strongly dependent on the period of interest (i.e., whether temperatures in the repository are above the boiling point of water) and whether the engineered barriers have been disrupted. These two important aspects are used to define the three scenario classes considered in the TSPA-LA model (BSC 2002b, Section 4): nominal, seismic, and igneous scenario classes. A fourth scenario class, human intrusion, is a stylized analysis (BSC 2002b, Section 4) because of specific simplified assumptions imposed by the NRC in 10 CFR Part 63.

The models presented in this document are used in the nominal and seismic scenario classes. The igneous scenario class has two types of disruption: igneous intrusion of a dike into an emplacement drift and volcanic eruption through a waste emplacement drift. For waste packages that are destroyed by igneous intrusion, all the models discussed in this document are applicable and are used in the TSPA-LA model. For both the volcanic eruption scenario and the human intrusion calculations, only the radionuclide inventory model (Section 2) is used because neither set of calculations involves transport of radionuclides in groundwater. The scenario classes that

implement the models presented in this document and their relationship to waste package modeling are summarized in Table 1-1 and are discussed next.

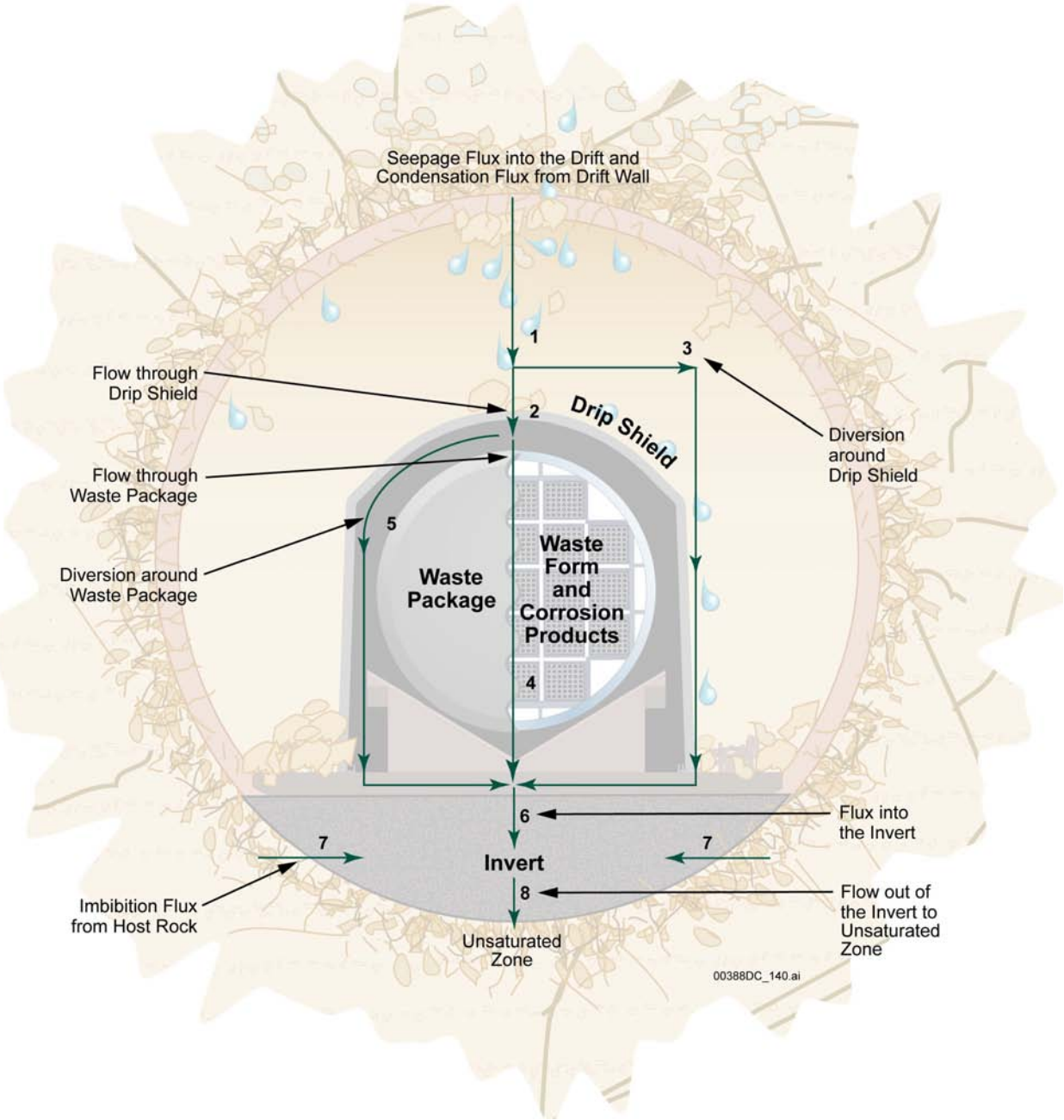

Figure 1-3. Potential Liquid Advective Pathways in the Engineered Barrier System

Table 1-1. Models Implemented in the Scenario Classes Included in the Total System Performance Assessment for the License Application

Scenario Class	Inventory	In-Package Chemistry	Cladding Failure	Waste Form Degradation	Radionuclide Solubility	Colloid Formation and Stability
Nominal scenario and waste packages unaffected by disruptive events in other scenario classes	X	X	X	X	X	X
Waste packages affected by seismic scenario	X	X	X	X	X	X
Waste packages affected by igneous intrusion	X	X	X	X	X	X
Waste packages affected by volcanic eruption	X					
Waste packages affected by human intrusion	X					

1.2.1 Degradation in the Nominal Scenario Class

The nominal scenario represents the collection of features, events, and processes (FEPs) most likely to occur during the 10,000-year regulatory period, such as climate change and heating of the repository (BSC 2002b, Section 4.1). Based on corrosion analysis (BSC 2003i, Section 6.7.1), the drip shield and waste package will remain intact for the 10,000-year regulatory period for all but a small fraction of the waste packages. As a result, water seeping into the emplacement drifts of the repository (flow pathway 1 of Figure 1-3) will be diverted away from all but a small fraction of the packages (flow pathway 3 of Figure 1-3). Hence, advective radionuclide transport through the vast majority of waste packages (flow pathway 4) cannot occur; only diffusive radionuclide transport through the waste package can occur in the 10,000 years after repository closure. Radionuclide transport by diffusion is possible only for dissolved species. In films thinner than the diameter of the colloids, transport is physically hindered. In thicker films, the substantially lower diffusion coefficients for colloids relative to dissolved species will tend to prevent appreciable colloid transport.

For the nominal scenario, only a small fraction of the waste packages (e.g., the probability of three or more failed waste packages is 0.026 (BSC 2003i, Table 46)) is expected to have small manufacturing weld defects near the waste package lid, allowing water vapor to diffuse into the package, saturate the contents of the package, and dissolve radionuclides, thereby establishing a pathway for diffusive radionuclide transport (Figure 1-4).

Only the small fraction of fuel rods that arrive at the repository with perforated cladding (about 0.1%) can lead to the release of radionuclides during the 10,000-year regulatory period. Additional cladding failures from other mechanisms (e.g., localized corrosion, static loading of rock) during the regulatory period are not anticipated. The cladding that is initially perforated is assumed to split along the entire length of the fuel rod. Subsequent degradation of exposed fuel is assumed to produce a water-saturated rind through which dissolved radionuclides diffuse, thereby leaving the waste matrix and entering into the corrosion products in the waste package.

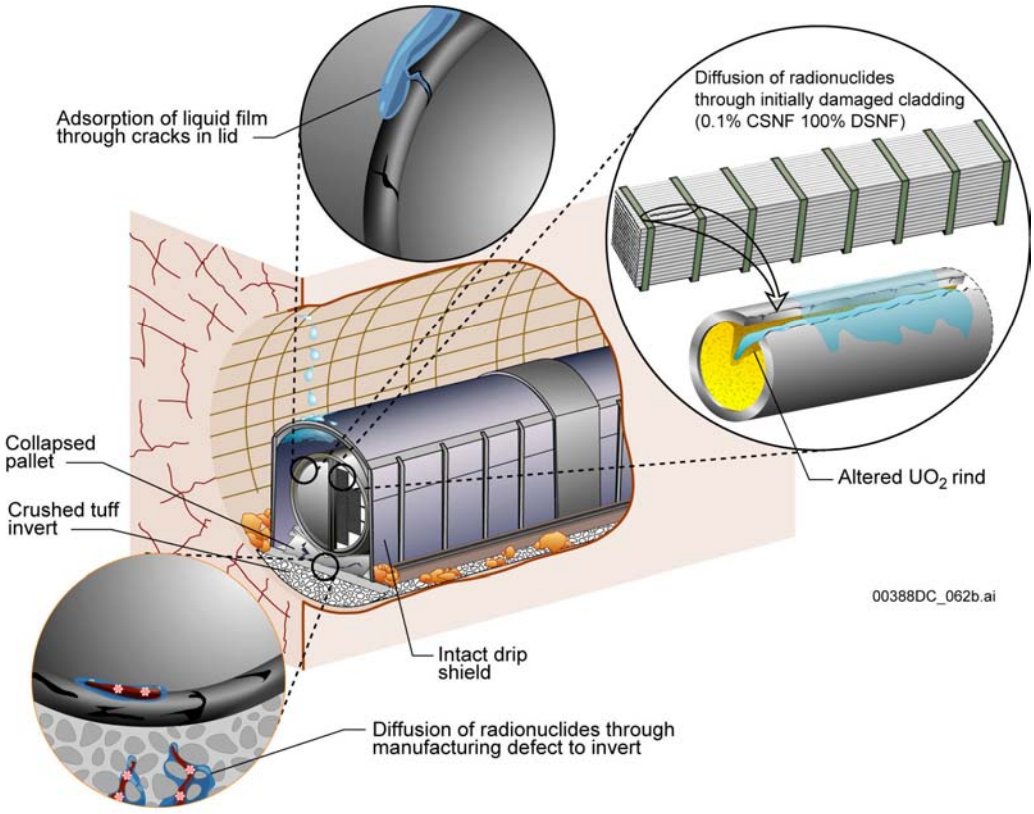

NOTE: For the nominal scenario, waste form degradation is limited and only diffusive release through manufacturing defects occurs because the drip shield and waste package remain intact for the first 10,000 years.

Figure 1-4. Degradation of Waste Form under Nominal Scenario Class

1.2.2 Degradation in the Seismic Disruptive Scenario

For the seismic disruptive scenario class (BSC 2002b, Section 4.3), the drip shields, waste packages, and cladding can be disrupted due to vibratory ground motion, fault displacement, and rockfall, as discussed in *Seismic Consequence Abstraction* (BSC 2003c, Table 31). The most likely waste package failure mechanism from a seismic event is accelerated stress corrosion cracking in areas that exceed the residual stress threshold for Alloy 22. It is postulated that a dense network of stress corrosion cracks would form, and the effective area of these cracks, which is much less than the overall affected surface area of the waste package, is the area through which flow and transport occur (Figure 1-5). The percentage of cladding that is perforated is a function of the peak ground velocity associated with the seismic event. The models of how the cladding splits once it is perforated and how radionuclides are transported through the rind are the same in the seismic scenario as they are in the nominal scenario. For those waste packages associated with undamaged drip shields or not encountering dripping water, radionuclide releases will be due to diffusion, similar to conditions in the nominal scenario.

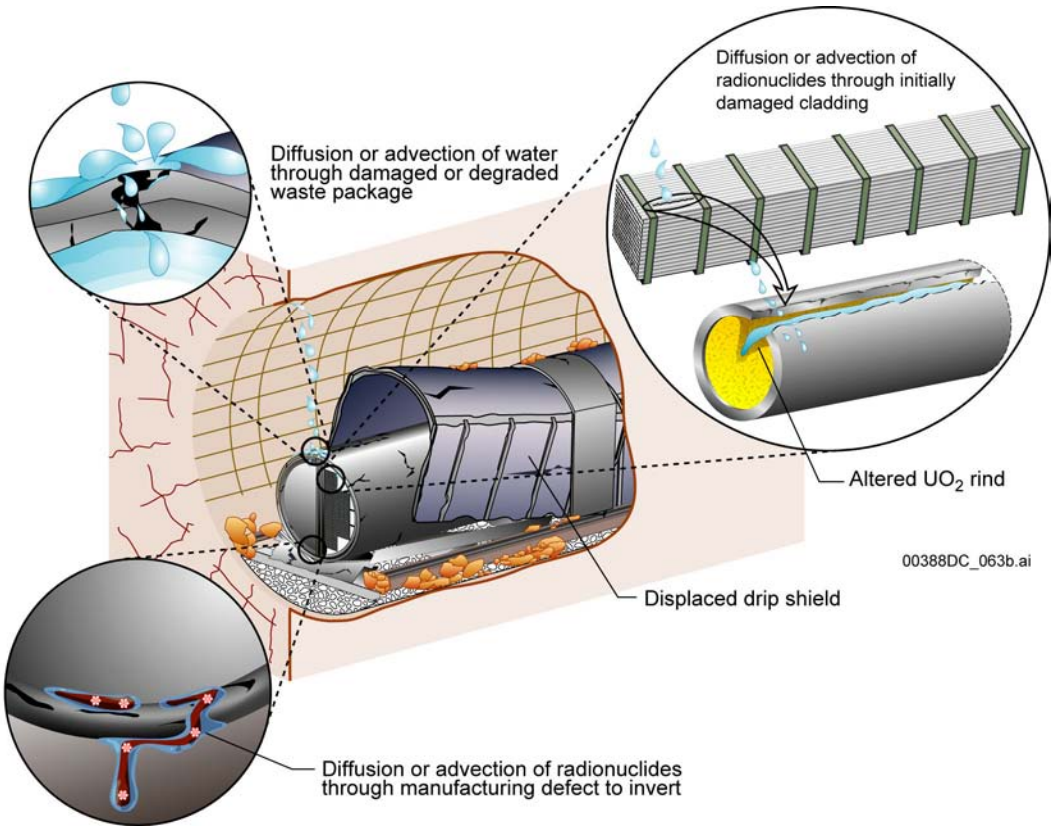

Figure 1-5. Degradation of Waste Form under the Seismic Disruptive Scenario

1.2.3 Degradation in the Igneous Intrusion Scenario

In the igneous intrusion scenario, a basalt dike is envisioned to intersect the repository (BSC 2002b, Section 4.2). Damage to waste packages and waste forms is conceptually divided into two distinct zones. In Zone 1 (where the emplacement drifts are intersected by the basaltic dike), the drip shields, waste packages, and commercial SNF cladding are disrupted and breached from the shock wave and heat. As a result, the waste form is distributed throughout the cooled magma but is chemically unchanged from the nominal scenario model. The latter is a reasonable assumption because the melting temperatures of fuel components are typically higher than the expected maximum temperature of the magma. Therefore, the waste degradation rates and dissolved concentration of radionuclides in water in the basalt would have the same dependence on water chemistry as does waste not affected by the intrusion (BSC 2004d, Section 6.5.1.2). In Zone 2, no damage is assumed, and thus, conditions are expected to be the same as in the nominal scenario (BSC 2004d, Section 8.1).

Degradation and dissolution of the waste form in breached waste packages in Zone 1 and degradation of the waste in Zone 2 occur once the drift cools (nominally, within roughly 100 years). In Zone 1, the drift is assumed to be completely filled with basalt. This scenario is most reasonably modeled as a uniform percolation of basalt-equilibrated fluid contacting bare fuel components (Figure 1-6) (BSC 2004d, Section 6.3).

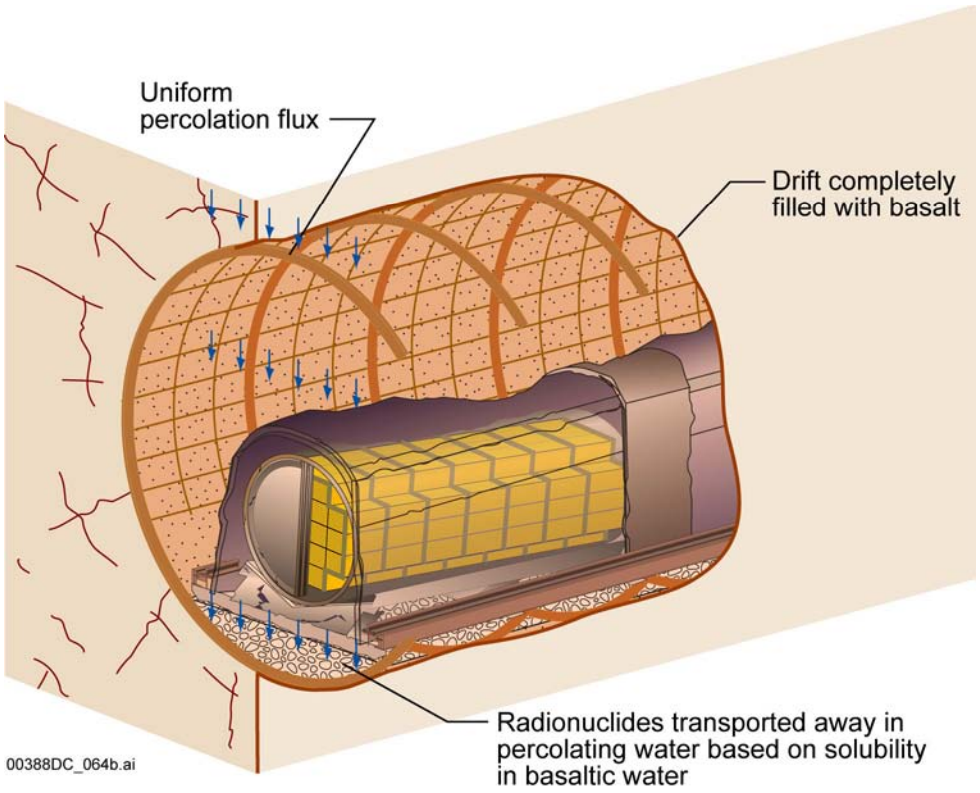

Figure 1-6. Degradation under the Igneous Intrusion Scenario

1.3 NOTE REGARDING THE STATUS OF SUPPORTING TECHNICAL INFORMATION

This document was prepared using the most current information available at the time of its development. This technical basis document and appendices providing KTI agreement and AIN request responses prepared using preliminary or draft information reflect the status of Yucca Mountain Project scientific and design bases at the time of submittal. In some cases, this involved the use of draft analysis model reports and other draft references whose contents may change with time. Information that evolves through subsequent revisions of the analysis model reports and other references will be reflected in the LA as the approved analyses of record at the time of LA submittal. Consequently, the project will not routinely update either this technical basis document or its KTI agreement appendices to reflect changes in the supporting references prior to submittal of the LA.

INTENTIONALLY LEFT BLANK

2. RADIONUCLIDE INVENTORY

This section summarizes the various waste forms and waste package configurations planned for the repository, as well as the screening process used to select the radionuclides included in the source term and the quantities of those radionuclides.

The sources of data are presented, as are the uncertainties, limitations, and confidence in the source term model. The information in this section is drawn primarily from *Radionuclide Screening* (BSC 2002a) and *Initial Radionuclide Inventories* (BSC 2003d). The information presented in this section serves as input to the in-package chemistry model (Section 3), the commercial SNF cladding degradation model (Section 4), and the waste form degradation models (Section 5), as shown in Figure 1-2.

2.1 TYPICAL WASTE PACKAGES, RELEVANT PROCESSES, AND MODELING ASSUMPTIONS

2.1.1 Waste Packages

Four types of waste are to be placed in the repository: commercial SNF, naval SNF, DOE SNF (not including naval SNF), and high-level radioactive waste (HLW) glass. Three packaging schemes will be used for these waste types. One waste package type will contain only commercial SNF. The second will contain only naval SNF but will be modeled as a commercial SNF waste package. The third waste package type, designated as a codisposal waste package, will contain DOE SNF and HLW in the same waste package. Figure 2-1 illustrates how waste in these categories will be combined and placed into waste packages.

Commercial SNF is classified into two broad categories based on the design of the reactor that produced the fuel: pressurized water reactor (PWR) or boiling water reactor (BWR). Commercial nuclear power plants use a variety of fuels and fuel configurations in their reactor cores to generate power. The predominant nuclear fuel is enriched uranium dioxide. Fuel pellets are packed into long cylindrical fuel rods that vary in size depending on reactor design, and these fuel rods, which are clad in Zircaloy or stainless steel, are bundled into assemblies. The number of fuel rods per assembly and the number of assemblies in a reactor core vary, depending on the core and reactor design (i.e., PWRs or BWRs).

DOE SNF consists of more than 250 distinct types of SNF, and, much like commercial SNF, radionuclide inventories vary widely depending on the history of the fuel. The large quantity of DOE SNF is indicative of the large number and variety of different research reactors within the DOE complex. The DOE fuel assemblies have been categorized by the size, shape, composition, and condition of the assemblies, and the size and corrosion resistance of the canister into which they may be loaded (DOE 2003a). The DOE SNF waste forms will be packaged in stainless steel canisters that will be loaded into the waste packages.

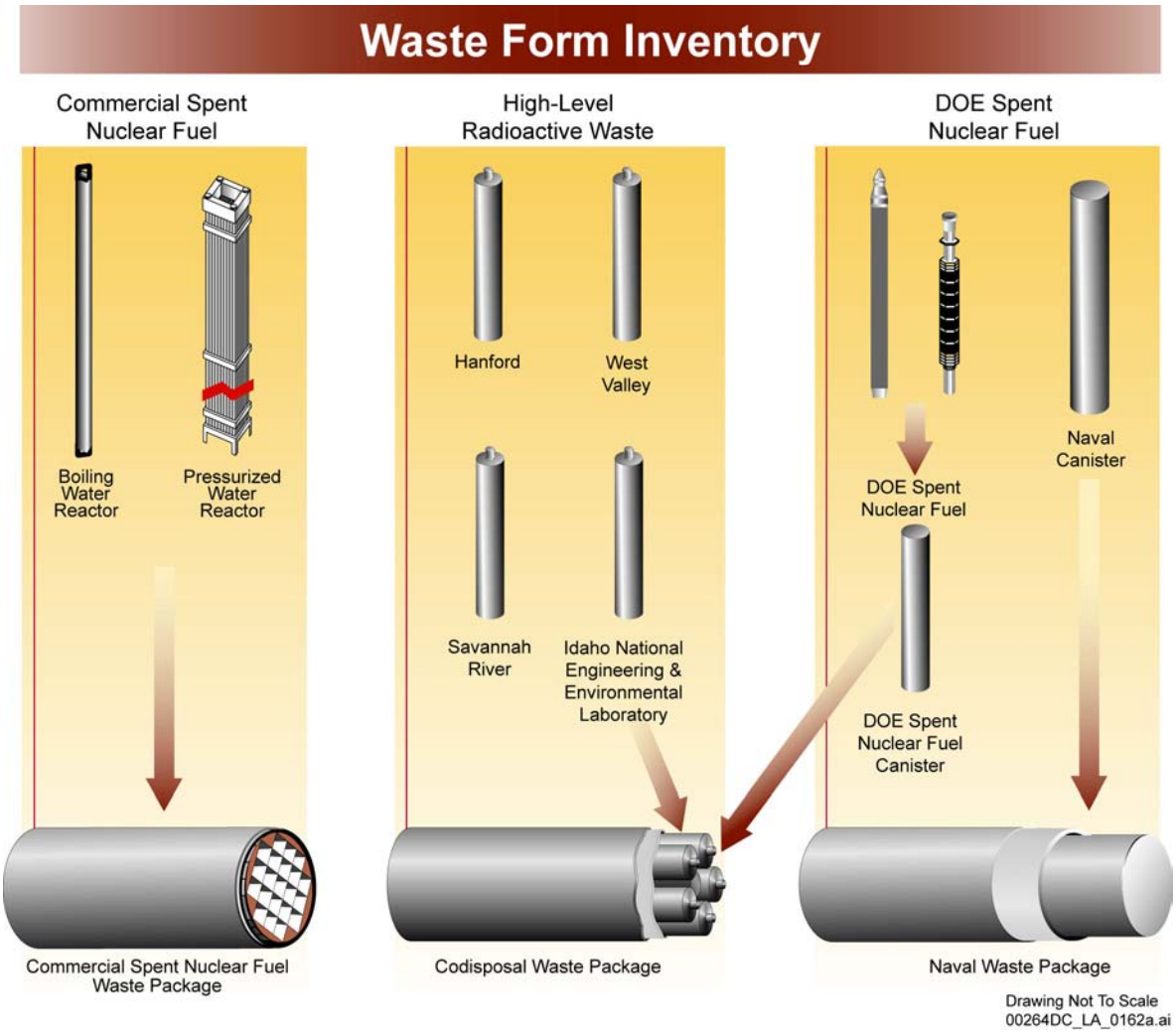

Source: BSC 2003d, Figure 1.

Figure 2-1. An Overview of Various Waste Package Types Containing Different Wastes

The HLW in storage at DOE sites is produced by treatment of waste from weapons production and by the reprocessing of SNF (mostly DOE SNF). The technology for immobilization of HLW is vitrification in a borosilicate glass. HLW glass will come from four DOE sites and will be delivered to the repository in either short (about 10 ft long) or long (about 15 ft long) pour-canisters. The Hanford Site will produce long canisters while the Savannah River Site and Idaho National Engineering and Environmental Laboratory will produce short canisters. Additionally, a small amount of HLW glass has been produced in short canisters at the West Valley Demonstration Project in New York State. Because the fuels reprocessed at each of these sites differ, the radionuclide inventory of the HLW and resultant glass product will vary among the sites.

Details regarding the design and long-term performance of naval SNF are provided in a separate report that has limited distribution for security purposes. Naval SNF is conservatively treated as commercial SNF in the TSPA-LA.

Based on design criteria such as structural integrity, thermal performance, criticality safety, and shielding properties, 10 waste packages were designed to accommodate the numerous waste types (DOE 2002a, Section 3.1). Five waste package designs are used to dispose of the two types of commercial SNF (BWR and PWR), three waste package designs are used to dispose of high-level radioactive waste glass from the four different sources (Hanford, West Valley, Savannah River, and Idaho National Engineering and Environmental Laboratory) as well as DOE SNF, and two waste package designs are used to dispose of naval SNF. Table 2-1 lists the contents of each of the 10 different waste packages and Figure 2-2 illustrates these waste package designs.

Table 2-1. Waste Package Designs

Waste Package Design	Description	Approximate Percentage of Waste Packages/Approximate Percentage of MTHM
21-PWR Absorber Plate	Capacity: 21 commercial pressurized water reactor assemblies and an absorber plate for preventing criticality	38%/55%
21-PWR Control Rod	Capacity: 21 commercial pressurized water reactor assemblies with higher reactivity, requiring additional criticality control that is provided by the placement of control rods in all assemblies	1%/1%
12-PWR Long	Capacity: 12 commercial pressurized water reactor assemblies and an absorber plate for preventing criticality; longer than the fuel assemblies placed in the 21-PWR packages. Because of its smaller capacity, it may also be used for fuel with higher reactivity or thermal output.	2%/2%
44-BWR	Capacity: 44 commercial boiling water reactor assemblies and an absorber plate for preventing criticality.	25%/32%
24-BWR	Capacity: 24 commercial boiling water reactor assemblies with higher reactivity, requiring a thicker absorber plate to prevent criticality than that used in the 44-BWR design	1%/<1%
5-DHLW/DOE SNF Short	Capacity: 5 short high-level radioactive waste canisters and 1 short DOE SNF canister.	14%/3%
5-DHLW/DOE SNF Long	Capacity: 5 long high-level radioactive waste canisters and 1 long DOE SNF canister	15%/4%
2-MCO/2-DHLW Long	Capacity: 2 DOE multicanister overpacks and 2 long high-level radioactive waste canisters.	1%/<1%
Naval SNF Short	Capacity: 1 short naval SNF canister	2%/<1%
Naval SNF Long	Capacity: 1 long naval SNF canister	1%/<1%

Source: DOE 2002a, Tables 3-2 and 3-3.

For purposes of modeling in the TSPA-LA, two representative waste package types are considered: (1) a representative commercial SNF waste package and (2) a representative codisposal waste package designed to hold both DOE SNF and HLW glass. As shown in Table 2-1, the number of commercial SNF configurations dominates the number of codisposal waste package configurations. Both waste package designs consist of a waste package with an outer corrosion resistant layer of Alloy 22 and an inner layer of stainless steel for structural strength (BSC 2003i, Section 1).

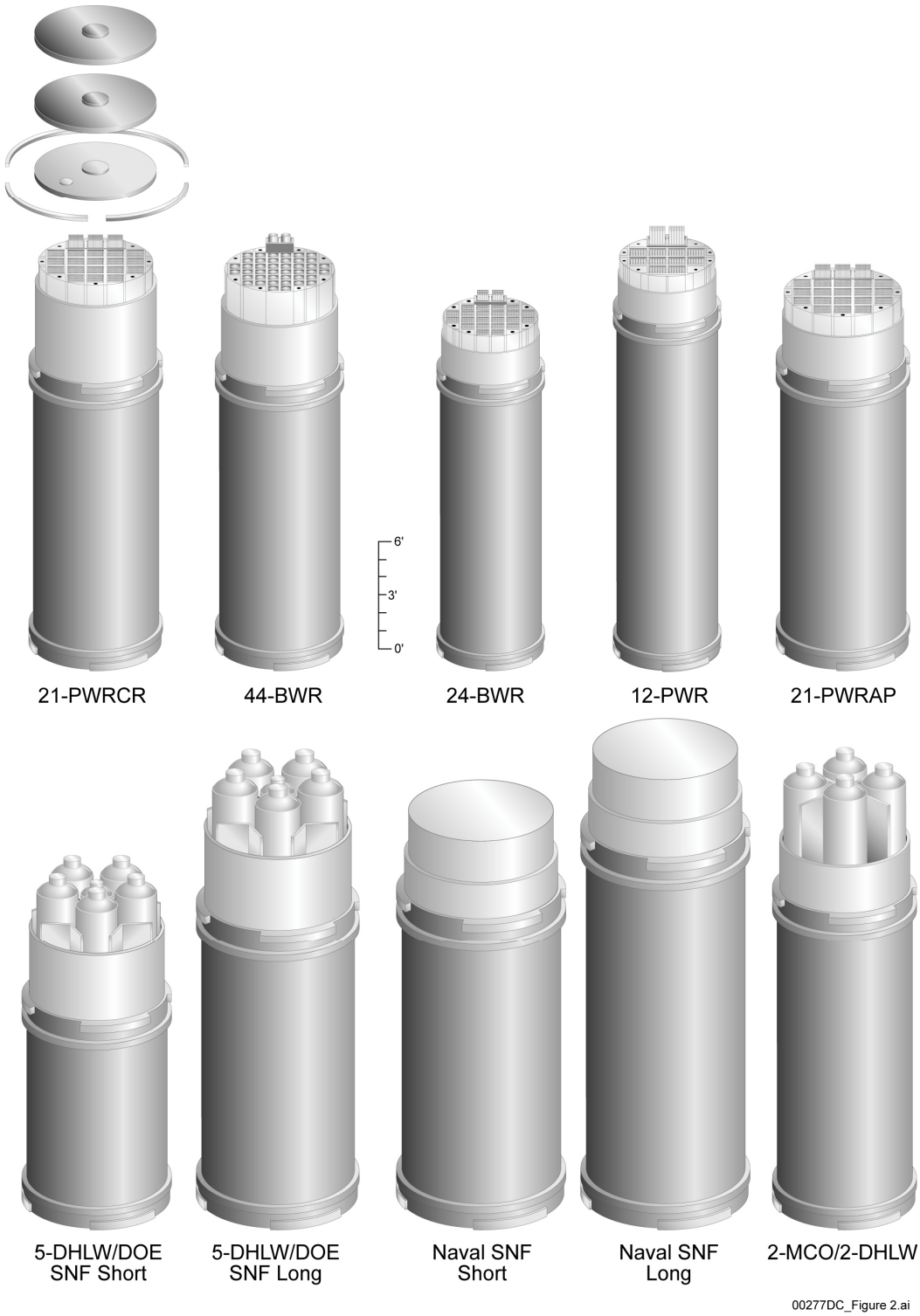

Source: DOE 2002a, Figure 3-5.

Figure 2-2. Waste Package Configurations for Commercial Spent Nuclear Fuel, U.S. Department of Energy Spent Nuclear Fuel, N Reactor Fuel, and High-Level Radioactive Waste Glass

2.1.2 Radionuclide Screening

Determining the initial radionuclide inventory is the foundation for estimating the radionuclide source term for all transport processes in the TSPA-LA model. This determination involves two steps. First, a screening process is used to determine those radionuclides with the highest contribution to expected dose.[1] Those radionuclides shown not to contribute significantly to expected dose can be eliminated from further consideration; in practice, this involved separating the radionuclides that make up roughly 95% of the dose (see below) from the remainder. Second, the initial inventory of radionuclides is estimated for each waste form type and each waste package type.

Radionuclides contained in the waste packages include fission products from reactor operations, actinides from neutron capture in uranium and plutonium, and activation products from neutron irradiation of structural materials and trace elements. Altogether, these fission products, actinides, and activation products include more than 100 radionuclides that may be collectively present in the waste packages at the time of repository closure. Many of the radionuclides are present in small quantities or have intrinsic physical and chemical properties that limit the quantities that can reach the RMEI (e.g., short half-life, low solubility, or strongly sorbing characteristics). Such nuclides will not be significant contributors to expected dose and will not pose a radiological risk to a RMEI at the point of compliance. The remaining nuclides represent only a small set of the total and need to be considered in the evaluation of repository postclosure performance.

Radionuclides with half-lives less than 10 years that are not decay products of other radionuclides in the waste inventory will not contribute significantly to the dose in the groundwater scenarios (BSC 2002a, Assumption 5.9). As an additional constraint, radionuclides that are most important to expected dose were determined using the screening process of the National Council on Radiation Protection and Measurement. This screening was based on dose calculations, which in turn consider consumption of locally produced vegetables, fish, meat, and milk; water consumption; inadvertent ingestion of soil; gardening and shoreline activities; inhalation; and exposure to contaminated ground. Two screening factors were calculated for each radionuclide, one for scenario classes involving groundwater transport (nominal, seismic, and igneous intrusion), and one for the volcanic eruption scenario, which does not involve groundwater transport. Screening factors for groundwater transport scenario classes accounted for radionuclide sorption and solubility characteristics. The screening factors are described in *Screening Models for Releases of Radionuclides to Atmosphere, Surface Water, and Ground* (NCRP 1996) and were adjusted to reflect the local biosphere, as described in Attachments I and II of *Radionuclide Screening* (BSC 2002a).

Radionuclides were screened by calculating a radionuclide-screening product for each radionuclide. The radionuclide-screening product, which is meant to be roughly proportional to dose, is obtained by multiplying the screening factor for each radionuclide by the activity of that radionuclide in the inventory. These screening products were ranked from largest to smallest,

[1] Some radionuclides that are not directly important to expected dose are still included because (1) regulatory requirements mandate their inclusion (40 CFR 197.30, 10 CFR 63.331), or (2) they are parents to radionuclides that are important to dose.

and were then summed, starting with the largest and adding the next largest until all of the screening products of each contributing radionuclide were included in the sum. Radionuclides were then screened based on their contribution to the summed radionuclide-screening product. The screening was at the 95% level, meaning that ranked radionuclides that contributed up to 95% of the summed radionuclide-screening product were considered potentially important and were retained for analysis (BSC 2002a, Section 5.5).

The relative importance of individual radionuclides to expected dose was evaluated for several waste types, time frames, and release scenarios. Those scenarios that require groundwater transport (e.g., nominal, seismic, and igneous intrusion) were evaluated together as "groundwater scenarios." The eruptive igneous scenario, which does not involve groundwater transport, was analyzed separately. Because radionuclide transport mechanisms differ between the scenarios that involve groundwater transport and the eruptive igneous scenario, the set of radionuclides identified as being important also differs between the groundwater-transport and no-groundwater-transport scenarios. The effects of inventory abundance, radionuclide longevity, element solubility, and element transport affinity were considered. To evaluate the effects of inventory abundance, eight waste types were examined (i.e., BWR, PWR, HLW, and DOE SNF for both average and bounding waste forms of each type). For the 10,000-year regulatory period, the screening times were at 100, 200, 300, 500, 1,000, 2,000, 5,000, and 10,000 years after emplacement. These sets of screening times capture the main features of the changing dominant radionuclides and their relative activities (BSC 2002a, Section 6.2.3). To evaluate the effects of element solubility and transport affinity, the elements were evaluated in three solubility groups (highly soluble, moderately soluble, and slightly soluble to nonsoluble) and in three transport affinity groups (highly sorbing, moderately sorbing, and slightly sorbing to nonsorbing). The isotopes in each group were compared to one another for relative importance.

The results of the screening process at the 95% level are shown in Table 2-2. The table also includes eight radionuclides (^{241}Pu, ^{245}Cm, ^{228}Ra, ^{235}U, ^{230}Th, ^{232}Th, ^{242}Pu, and ^{236}U) that were not important to expected dose but that must be included in the inventory because of regulatory requirements or because they are parents to radionuclides that are important to expected dose (BSC 2003d, Section 6.1). The rationale for inclusion of these eight radionuclides is as follows:

- The U.S. Environmental Protection Agency and NRC regulations require consideration of the combined activity of ^{226}Ra and ^{228}Ra in groundwater (40 CFR 197.30, 10 CFR 63.331). Therefore, ^{228}Ra must be added to the list of radionuclides. Because ^{228}Ra is produced by the decay of ^{236}U and ^{232}Th, both ^{236}U and ^{232}Th must be included in the inventory. ^{230}Th must be included because it decays into ^{226}Ra.

- ^{241}Pu and ^{245}Cm must be included because they decay to ^{241}Am, which is one of the screened-in radionuclides.

- ^{235}U must be included because it decays (via short-lived ^{231}Th) to ^{231}Pa, which is one of the screened-in radionuclides.

- ^{242}Pu must be included because it decays into ^{238}U, which is one of the screened-in radionuclides.

As shown in column 2 of Table 2-2, 28 isotopes of 14 elements must be included in the TSPA-LA model during the 10,000-year regulatory period for scenario classes involving groundwater transport. A subset of these 28 isotopes and 14 elements (i.e., 14 isotopes of eight elements, as shown in column 3 of Table 2-2) must be included in 10,000-year TSPA-LA model for volcanic eruption. Therefore, 28 isotopes of 14 elements are included in the initial inventory for TSPA-LA calculations.

Table 2-2. Radionuclides Included in Inventory for the 10,000-Year Regulatory Period

Radionuclide	Groundwater Scenario Classes	Volcanic Eruption (No Groundwater Transport)
^{227}Ac	X	X
^{241}Am	X	X
^{243}Am	X	X
^{14}C	X	
^{245}Cm	X	X
^{135}Cs	X	
^{137}Cs	X	X
^{129}I	X	
^{237}Np	X	
^{231}Pa	X	
^{238}Pu	X	X
^{239}Pu	X	X
^{240}Pu	X	X
^{241}Pu[a]	X	X
^{242}Pu[b]	X	
^{226}Ra	X	
^{228}Ra[c]	X	
^{90}Sr	X	X
^{99}Tc	X	
^{229}Th	X	X
^{230}Th[d]	X	
^{232}Th[e]	X	
^{232}U	X	X
^{233}U	X	X
^{234}U	X	X
^{235}U[f]	X	
^{236}U[e]	X	
^{238}U	X	
Isotopes	**28**	**14**
Elements	**14**	**8**

Source: BSC 2002a, Table 10; BSC 2003d, Table 16 and Section 6.1.

NOTE: [a] Included because precursor to ^{241}Am.
[b] Included because precursor to ^{238}U.
[c] Included for groundwater protection requirements.
[d] Included because precursor to ^{226}Ra.
[e] Included because precursor to ^{228}Ra.
[f] Included because precursor to ^{231}Pa.

2.2 MODEL OF RADIONUCLIDE INVENTORY

The nominal repository is designed to accommodate a total waste inventory of 70,000 MTHM. As designed, approximately 63,000 MTHM of the total inventory is commercial SNF and approximately 7,000 MTHM is DOE SNF and HLW. The radionuclide inventory for a representative commercial SNF and a representative codisposal waste package was derived by averaging the radionuclide inventories in each of the commercial SNF and codisposal waste package configurations over the number of waste packages per configuration.

Approximately 221,000 commercial SNF assemblies will be disposed of in the five proposed commercial SNF waste package designs (see first five entries of Table 2-1). These configurations are designed to accommodate each assembly based on its criticality safety needs. Each assembly, depending on the reactor configuration, initial fuel enrichment, burnup, and the age of the waste (time in storage), will have a unique isotopic composition. The total number of commercial SNF waste packages is 7,472 (BSC 2003d, Table 17).

Naval SNF is a robust fuel, more robust than commercial SNF and much more robust than DOE SNF. Releases from naval SNF waste packages are expected to be lower than those for commercial SNF waste packages (BSC 2001, Section 6.5). As such, naval fuel is not treated as DOE SNF in the codisposal waste package. For the TSPA-LA analysis, the 300 naval SNF waste packages have been treated as if they were commercial SNF waste packages with respect to their waste form degradation mechanisms and effects, as well as their initial radionuclide inventory (BSC 2003d, Section 6.2 and Attachment II). Naval SNF will be disposed of in two different waste package configurations, as shown in Figure 2-2.

Approximately 16,000 HLW glass logs and 3,600 DOE SNF canisters will be disposed of in the codisposal waste package configurations. The total number of codisposal waste packages is 3,412 (BSC 2003d, Table 17).

The result of the radionuclide screening analysis and the initial radionuclide inventory analysis is the initial radionuclide inventory (in terms of mass) of those radionuclides determined to be important to expected dose for a representative commercial SNF waste package and a representative codisposal waste package. The nominal initial radionuclide inventory for each waste form is given in Table 2-3; uncertainty in the radionuclide inventory is discussed in Section 2.4.

For certain radionuclides, the activity decreases with time as a result of simple radioactive decay; for others, the activity increases with time because of in-growth. For those radionuclides in the fission product category, the model abstraction calculates the variation of activity with time in accordance with the first order decay law. The inventory of short-lived fission products, such as ^{90}Sr and ^{137}Cs, decreases substantially over the 10,000-year compliance period. In contrast, the inventories of long-lived fission products such as ^{14}C, ^{99}Tc, and ^{129}I decrease only slightly over the compliance period.

Table 2-3. Nominal Initial Radionuclide Inventory for Each Waste Form

Radionuclide	Commercial SNF (g per waste package)	DOE SNF (g per waste package)	HLW (g per waste package)
^{227}Ac	2.50×10^{-6}	1.2×10^{-3}	2.07×10^{-4}
^{241}Am	8.28×10^{3}	2.15×10^{2}	4.07×10^{1}
^{243}Am	1.26×10^{3}	6.63×10^{0}	6.24×10^{-1}
^{14}C[a]	1.37×10^{0}	1.78×10^{0}	–[b]
^{245}Cm	1.77×10^{1}	9.11×10^{-2}	5.89×10^{-2}
^{135}Cs	4.41×10^{3}	9.59×10^{1}	1.38×10^{2}
^{137}Cs	5.97×10^{3}	9.57×10^{1}	3.28×10^{2}
^{129}I	1.75×10^{3}	3.51×10^{1}	7.89×10^{1}
^{237}Np	4.63×10^{3}	8.02×10^{1}	1.08×10^{2}
^{231}Pa	9.28×10^{-3}	2.11×10^{0}	1.66×10^{0}
^{238}Pu	1.54×10^{3}	1.23×10^{1}	4.24×10^{1}
^{239}Pu	4.37×10^{4}	2.18×10^{3}	6.06×10^{2}
^{240}Pu	2.08×10^{4}	4.28×10^{2}	5.01×10^{1}
^{241}Pu	2.69×10^{3}	2.88×10^{1}	1.32×10^{0}
^{242}Pu	5.34×10^{3}	2.97×10^{1}	4.22×10^{0}
^{226}Ra	–[b]	4.50×10^{-5}	2.63×10^{-5}
^{228}Ra	–[b]	1.49×10^{-5}	6.51×10^{-6}
^{90}Sr	2.52×10^{3}	5.14×10^{1}	1.89×10^{2}
^{99}Tc	7.64×10^{3}	1.56×10^{2}	1.10×10^{3}
^{229}Th	–[b]	3.19×10^{-1}	3.58×10^{-3}
^{230}Th	1.54×10^{-1}	1.16×10^{-1}	8.81×10^{-4}
^{232}Th	–[b]	2.14×10^{4}	3.23×10^{4}
^{232}U	1.03×10^{-2}	1.26×10^{0}	4.43×10^{-4}
^{233}U	5.83×10^{-2}	5.30×10^{2}	2.11×10^{1}
^{234}U	1.77×10^{3}	4.66×10^{2}	2.53×10^{1}
^{235}U	6.34×10^{4}	2.47×10^{4}	1.53×10^{3}
^{236}U	3.89×10^{4}	1.23×10^{3}	6.50×10^{1}
^{238}U	7.92×10^{6}	6.74×10^{5}	2.57×10^{5}

Source: BSC 2003d, Section 7.1, Table 21.

NOTE: Year of inventory projection: Commercial SNF, 2033; DOE SNF, 2030; and HLW, 2030. Total number of waste packages is 11,184 (7,772 commercial SNF and 3,412 codisposed).
[a] 18% of ^{14}C for commercial SNF resides in the hardware outside of the cladding.
[b] For these radionuclides, the inventory is an unknown small number.

For the radionuclides of actinide elements, the model abstraction accounts for the decay sequence and calculates the activity of each radionuclide as a function of decay and in-growth. Many of the actinide elements in Table 2-3 are daughter products.

If the nuclear waste remains contained in the waste packages, the decay history of each radionuclide can be analytically calculated in accordance with its decay sequence and half-life (Figure 2-3).

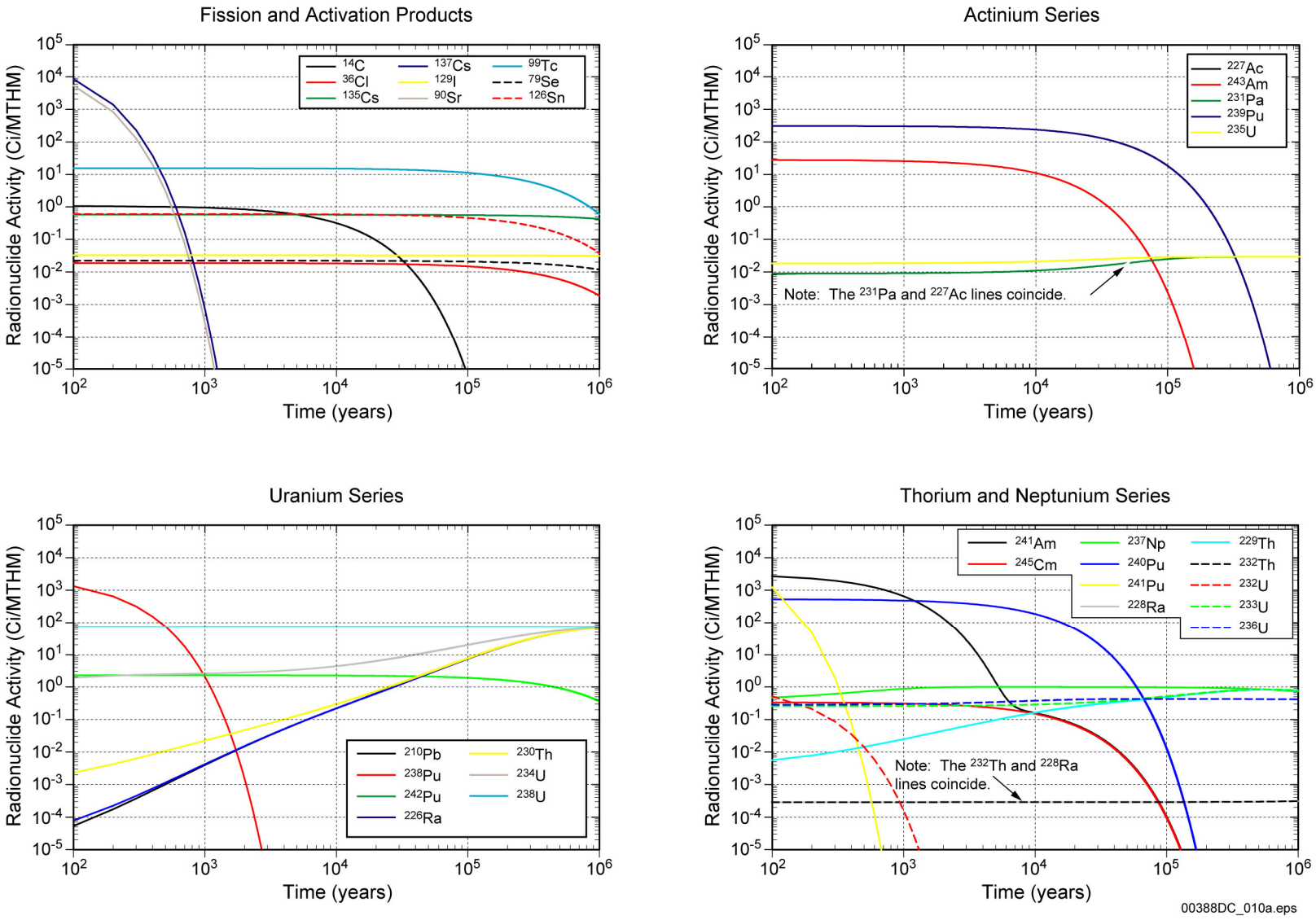

Source: BSC 2002a, Table 2; Figure adapted from CRWMS M&O 2000a, Figure 3.5-6.

Figure 2-3. Decay Histories for Radionuclides Modeled in Total System Performance Assessment for License Application

2.3 SOURCE OF DATA AND SUPPORTING DOCUMENTS

A 1995 data submittal from the commercial utilities provided the basic information from which the TSPA for the site recommendation (TSPA-SR) analysis inventory for commercial SNF was developed. At that time, the utilities supplied historical information about reactor assembly discharges up through December 1995, and they provided forecasts for the next five assembly discharges from their reactors. With this information, a design basis waste stream was developed in *1999 Design Basis Waste Input Report for Commercial Spent Nuclear Fuel* (CRWMS M&O 1999a), as well as forecasts for assembly discharges over the lifetime of each commercial power reactor. This same information is also used for the TSPA-LA analysis to arrive at the nominal values in Table 2-4. In addition, *2002 Waste Stream Projections Report* (Williams 2003) was used in conjunction with the 1995 data to develop the uncertainty bounds for the nominal commercial SNF inventory values. *2002 Waste Stream Projections Report* (Williams 2003) provides bounding waste stream information to capture probable limits of what might occur in the future with regard to fuel selection by utilities.

Table 2-4. Uncertainty Multipliers for the Initial Radionuclide Inventory for Each Waste Form Type

Parameter	Commercial SNF	DOE SNF	High-Level Radioactive Waste
Isotopes	All except ^{238}U	All except ^{238}U	All
Distribution	Uniform	Triangular	Triangular
Minimum	0.85	0.45	0.70
Most Likely	N/A	0.62	1
Maximum	1.4	2.9	1.5

Source: BSC 2003d, Section 7.1, Table 22.

NOTE: See Section 2.4 for a discussion on how uncertainty multipliers were developed.

DOE SNF information was collected from *Source Term Estimates for DOE Spent Nuclear Fuels* (DOE 2003a). This report provided information for the 28 radionuclides of interest and provided the basis for the modification to the codisposal waste package configurations by the addition of the wide canisters.

The HLW radionuclide inventory (in curies per canister for each radionuclide) has been evaluated for the borosilicate glass to be produced at the four sites that will be supplying HLW to the repository: Hanford Site (14,500 canisters), Savannah River Site (5,978 canisters), Idaho National Engineering and Environmental Laboratory (1,190 canisters), and West Valley Demonstration Project (300 canisters) for a total of approximately 22,000 HLW canisters (CRWMS M&O 2000b, Section 5.0). As this total exceeds the approximately 16,000 HLW canisters that will be disposed of in the mountain, each site's total radionuclide inventory was proportionally assigned in accordance with its total production.

2.4 UNCERTAINTIES, LIMITATIONS, AND MODEL CONFIDENCE

An important source of uncertainty in the model of radionuclide inventory stems from the assumption that screening radionuclides at the 95% level is appropriate for TSPA-LA (see Section 2.1.2). To address this uncertainty, an additional screening was performed at the 99% level. At the 99% level, an additional 10 radionuclides were identified as important to dose in the

groundwater scenarios, and an additional nine radionuclides were identified as important to dose in the volcanic eruption scenario. Of the 10 marginally important radionuclides identified at the 99% level for the groundwater scenarios, five are included in TSPA-LA because they are precursors to radionuclides identified as important at the 95% screening level (^{241}Pu, ^{242}Pu, ^{232}Th, ^{235}U, and ^{236}U); five are not included in the TSPA-LA (^{36}Cl, ^{244}Cm, ^{63}Ni, ^{210}Pb, and ^{126}Sn). Of the nine marginally important radionuclides identified as important to dose in the volcanic eruption scenario, six are included in the TSPA-LA modeling of the volcanic eruption scenario (^{237}Np, ^{231}Pa, ^{242}Pu, ^{126}Sn, ^{99}Tc, and ^{228}Th), while three are not included in TSPA-LA modeling of the volcanic eruption scenario (^{225}Ac, ^{244}Cm, and ^{225}Ra).

There are three sources of uncertainty in the radionuclide inventory common to all waste types. The first is due to the computational method and nuclear data used in predicting future radionuclide inventories (e.g., isotopic neutron cross section or decay half-life). The second source of uncertainty is the completeness of records kept for SNF burnup history and HLW batch compositions. The third source of uncertainty, which is the most difficult to quantify, is the uncertainty about future decisions that may influence the creation, packaging, or shipment of waste (BSC 2003d, Section 6.6). An analysis of these sources of uncertainty yielded the uncertainty multipliers shown in Table 2-4.

2.4.1 Commercial Spent Nuclear Fuel

An analysis of the potential error associated with the computational method and nuclear data, which also includes error in burnup history, has provided correction factors (i.e., ratios) to represent the minimum and maximum errors of 0.89 and 1.08 for the inventory of commercial SNF (BSC 2003d, Section 6.6.1).

The uncertainty due to heterogeneity of waste in the repository average inventories was investigated by comparing average burnups of three 1999 arrival forecasts and four 2002 arrival forecasts (BSC 2003d, Section 6.6.1). The minimum and maximum ratios of the projected average burnups for these cases over those given in Table 2-4 are 0.95 and 1.3. When multiplied by the minimum and maximum correction factors of 0.89 and 1.08 for the computational method, a range of 0.85 to about 1.4 is obtained (BSC 2003d, Section 6.6.1). Since all the radionuclide inventory, except ^{238}U, is highly burnup-dependent, they should not be sampled independently. Therefore, an uncertainty multiplier is chosen, which is sampled and then applied to all radionuclide inventories except ^{238}U. In defining the probability distribution of this multiplier, the end points are known, but the shape of the uncertainty distribution is not. In the absence of further information, a uniform distribution is the distribution of choice because it equally weighs all possible values. In the TSPA-LA model, a uniform distribution from 0.85 to 1.4 for an uncertainty multiplier is applied to the nominal values (provided in Table 2-3) for all radionuclides except ^{238}U. The ^{238}U uncertainty is very small and not modeled in TSPA-LA (BSC 2003d, Section 6.6.1).

2.4.2 U.S. Department of Energy Spent Nuclear Fuel

The fuel information currently available at DOE storage sites is often determined by the records requirements and the intended disposition path at the time the fuel was placed into storage. These requirements and disposition paths were often unique to each of the sites and evolved over

time. As a result, the availability and completeness of the radionuclide inventories and associated documentation varies considerably for DOE SNF. Detailed characterization of these fuels is not necessary because the conservative source term estimate for these fuels is used for repository design, analyses, and licensing activities.

A conservative estimate of this SNF inventory was developed for each of the DOE SNF storage sites. The inventory was generated using calculational techniques described in *Methodologies for Calculating DOE Spent Nuclear Fuel Source Terms* (DOE 2000), which uses relevant experimental data and confirmatory studies. Additional studies that demonstrate the validity of the model and underlying codes have been performed (DOE 2003a, p. 14). The result of this work is a database with over 500 DOE SNF types. Each DOE SNF type has entries that include the radionuclide inventory, number of assemblies, and number and type of canisters that will contain the DOE SNF.

The inventory estimates given in *Source Term Estimates for DOE Spent Nuclear Fuels* (DOE 2003a) provide both a nominal and a bounding radionuclide inventory estimate for each type of DOE SNF. Even though the bounding radionuclide inventory estimates were provided for the purpose of assessing preclosure risk associated with handling a worst-case canister, the values are used to represent a bounding inventory for assessing postclosure risk as well (BSC 2003d, Section 6.6.2). The nominal and bounding inventories per waste package for the weighted average of all DOE SNF waste reported by *Source Term Estimates for DOE Spent Nuclear Fuels* (DOE 2003a) were analyzed.

A range of total DOE SNF inventory (0.62 to 2 times the nominal inventory) was established on the following basis:

- The nominal inventory includes extremely conservative assumptions applied to the small percentage of fuel (0.31%) for which little information is available. These assumptions result in 38% of the total inventory in 0.31% of the fuel, resulting in a potential overestimation of the total curie inventory by about 38% (DOE 2003a, p. 39).

- The best estimate inventory has a ratio of 0.62 to the nominal inventory (BSC 2003d, Section 6.6.2). The best estimate inventory is lower than the nominal through removal of the extreme conservatism applied to the small percentage of fuel (0.31%) with little information and in effect replacing these assumptions with the approximation that the 0.31% of the fuel has the same inventory as the average of the remaining fuel (DOE 2003a).

- The bounding radionuclide inventory is 1 to 2 times the nominal inventory per waste package (BSC 2003d, Section 6.6.2).

Taking the total DOE SNF inventory, including uncertainty, the inventory was applied across the expected number of DOE SNF canisters.

Because of uncertainty in the loading of fuel into the DOE SNF canisters, the DOE SNF canister count range is between 2,500 and 5,000, with a best estimate of 3,607 (DOE 2003a; Luptak 2003). Applying a factor of 3,607/5,000 (0.72) to the best estimate inventory (0.62 times the

nominal) and a factor of 3,607/2,500 (1.44) to the maximum DOE SNF inventory (2 times the nominal) and 3,607/5,000 to the reasonable canister inventories results in a per canister inventory range of 0.45 to 2.9 times the nominal, with a best estimate of 0.62 times the nominal. This range is shown in Table 2-4.

Like commercial SNF, the uncertainties of the DOE SNF radionuclide inventories are correlated, and an uncertainty multiplier is defined to capture the uncertainty for all radionuclides except ^{238}U. The inventory of ^{238}U has much less relative uncertainty than the other radionuclides because it is present in the initial fuel and generally changes little during reactor operation. Only three points are available to define a probability distribution for the DOE SNF multiplier, a minimum value, a most likely value, and a maximum value. In this situation, the choice of a triangular distribution is reasonable. Thus the DOE SNF multiplier is defined as a triangular distribution, with a minimum of 0.45, most likely value of 0.62, and a maximum of 2.9. It is to be applied to the nominal values for DOE SNF grams per waste package in Table 2-3 for all isotopes except ^{238}U.

2.4.3 High-Level Radioactive Waste Glass

The uncertainty in the repository average inventories was investigated by comparing three radionuclide loadings and three canister-filling cases (BSC 2003d, Section 6.6.3). As was the case with commercial SNF and DOE SNF, the uncertainties in HLW radionuclide inventories are dependent on the same factors for HLW, in this case radionuclide loading per canister. Therefore, an uncertainty multiplier is again used to represent the uncertainty in the HLW inventory. With the current information, the nominal values reported in Table 2-4 are the most likely values, and thus the most likely value for the uncertainty multiplier is 1 (BSC 2003d, Section 6.6.3). The minimum number of waste packages is 0.70 times the central value, and the maximum number of canisters is 1.3 times the central value. Because of the uncertainty in possible new vitrified waste forms at the Savannah River Site with loading up to 50% higher, it is prudent to overestimate the upper limit. A maximum loading of 55% was chosen to provide margin, which corresponds to a ratio of 1.5 (BSC 2003d, Section 6.6.3). With the most likely maximum and minimum defined, a triangular distribution is chosen for the HLW uncertainty multiplier for use by the TSPA-LA model. This multiplier is to be applied to the nominal HLW inventories shown in Table 2-3 for all isotopes (including ^{238}U). The uncertainty multiplier has a triangular distribution with a minimum of 0.70, most likely value of 1, and a maximum of 1.5 as shown in Table 2-4.

2.5 SUMMARY AND CONCLUSIONS

The radionuclide inventory component defines the four waste forms (commercial SNF; naval spent fuel (which is modeled as commercial SNF); DOE SNF; and HLW glass) and the two representative types of waste packages (commercial SNF waste packages and the codisposal waste packages containing both DOE SNF and HLW glass) planned for disposal in the repository. In addition, of the more than 100 radionuclides potentially present in the repository, 28 radionuclides have been identified as being important to dose during the 10,000-year regulatory period. The initial inventory of these 28 radionuclides for the three waste forms modeled in TSPA-LA is given, as is the uncertainty associated with that inventory. The inventory of commercial SNF, which is the most abundant waste type to be disposed of in the

repository, has the least uncertainty while the inventory of DOE SNF, which is the least abundant waste type to be disposed of in the repository, has the most uncertainty. Because the TSPA-LA model can simulate the degradation and failure of individual waste packages, the radionuclide inventories are provided on a grams-per-package basis.

INTENTIONALLY LEFT BLANK

3. IN-PACKAGE CHEMISTRY

Two sets of calculations were performed to estimate the chemistry of fluids reacting with SNF: one set represents conditions expected under the nominal and seismic scenario classes; the other set represents conditions expected under the igneous intrusion scenario. The bulk of this section describes the in-package chemistry model for the nominal and seismic scenario classes. Section 3.6 presents the in-package chemistry model for the igneous intrusion scenario.

The in-package chemistry model simulates the chemistry of water as it reacts with waste package components and waste forms inside failed waste packages. The primary input parameters for the in-package chemistry model include the chemistry of seepage waters, the compositions of waste package materials and waste forms, and the corrosion rates of waste package components. The outputs of the model (which include pH, ionic strength, fluoride concentration, and total carbonate) are used, either directly or indirectly, as inputs to the models that evaluate dissolved concentrations of radionuclides, commercial SNF matrix degradation, HLW glass degradation, and colloid stability in the TSPA-LA calculations. The material presented in this section is primarily drawn from *In-Package Chemistry Abstraction* (BSC 2004b).

3.1 ASSUMPTIONS

As discussed in Section 2, two general types of waste packages are considered as representative of all waste packages: commercial SNF and codisposal waste packages containing both DOE SNF and HLW glass. For purposes of modeling in-package chemistry, the latter is represented by a waste package containing two N Reactor SNF canisters and two HLW canisters (BSC 2004b, Section 6.3.3). N Reactor SNF was selected to represent the DOE SNF in the codisposal waste package because examination of the dissolution rate literature for other DOE SNF waste forms (DOE 2002b, Section 6) indicates that the degradation rate of N Reactor fuel generally exceeds that of the other types of DOE SNF and because N Reactor SNF comprises approximately 85% of the total metric tons of heavy metal of DOE SNF (DOE 2002b, Appendix D).

The in-package chemistry model simulates chemical interactions of water with the waste package materials and waste forms for both types of waste packages under different physical, hydrologic, and chemical conditions. The simulations are performed with the reaction-path code EQ3/6 (Wolery 1992; Wolery and Daveler 1992), with the assumption that the water will always maintain equilibrium with precipitated secondary mineral phases as waste package components slowly dissolve. The outer shell of the waste package (Alloy 22) is assumed to be inert because of its extremely slow corrosion rate (CRWMS M&O 2000c, p. 109, Section 6.9.1). The calculation also assumes that oxygen is in equilibrium with the ambient atmosphere outside of the waste package. Therefore, the fugacity of O_2 is set to the atmospheric value, 0.2 atm (BSC 2004b, Section 6.3.1). Localized reducing conditions may occur as corrosion products limit the access of oxygen to metal surfaces. However, lower redox conditions would favor substantially lower radionuclide solubilities.

Two different water ingress models are considered (BSC 2004b, Section 1): the no-drip model, which represents scenarios in which advection through the waste package does not occur, and the seepage-dripping model, which represents scenarios in which water can flow through the waste

package. In the no-drip model, water enters a failed waste package by vapor diffusion and subsequently reacts with the package materials and waste forms. The solutes exit the package by diffusion only. The evolution and the uncertainty range of in-package chemistry were simulated using individual waste package components or the combinations of these components as reactants, based on the consideration that water mixing may not fully occur in the waste package due to lack of advective flow. In the seepage-dripping model, seepage water drips into a waste package and continuously exits the package by advection after reacting with the package contents. In this case, the in-package chemistry is simulated by assuming that solutions reacting with various waste package components will be well mixed during the percolation inside a waste package.

One of the model boundary conditions is that a continuous water film forms over the waste package components. The thickness of the film is fixed to be 1 mm for commercial SNF and 2 mm for codisposal waste packages in the no-drip model, and 2.5 mm for commercial SNF and 3.5 mm for codisposal waste packages in the seepage-dripping model. The basis for these thicknesses is that they represent the minimum values required by the EQ3/6 code to complete the entire suite of simulations. They are also reasonable separation half-distances for the situation being modeled; with degradation and collapse of basket materials, the interior of the waste form will consist of loosely compacted fuel and basket elements separated by millimeter- to centimeter-size apertures.

In the current model, no water evaporation is allowed to occur inside the waste package (BSC 2004b, Section 6.3.2). This assumption may lead to a lower ionic strength of in-package water. As discussed in Section 7, a high ionic strength decreases colloid stability; thus, a lower ionic strength could allow more radionuclides to escape from the waste package in colloidal form (BSC 2003h, Figures 4 and 7).

3.2 RELEVANT PROCESSES

3.2.1 Water Fluxes

In the no-drip model, it is assumed that water will form a continuous water film on waste package components. However, in reality, this may not occur because water condensation can only be possible when the waste package temperature is equal to or below the ambient temperature. Given the fact that the interior of a waste package is the source of heat and the waste package temperature after closure is maintained above 40°C during the 10,000-year regulatory period (BSC 2004e, Figure 6.5-3), the formation of a water film over waste package materials seems unlikely. As a simplifying assumption, this thermal effect is not considered in the in-package chemistry model. The diffusive flux of water vapor is calculated to be 0.8 L/yr (43.88 mol/yr) per waste package for isothermal conditions (BSC 2004f, Section 6.3.1). The no-drip model is simulated in EQ3/6 as a titration (Wolery and Daveler 1992). That is, water and the reactants are added to a reaction vessel at their respective kinetic rates or diffusion flux for water; products form and may redissolve, but no water exits the system (Wolery and Daveler 1992, p. 42, Figure 3).

In the seepage-dripping model, seepage drips onto the upper surface of the waste package and penetrates the waste package through an opening. The solution then flows through the waste

package, forming a film on the interior waste package components, reacting, mixing, and transporting the dissolved material out of the waste package. There is no accumulation of water in the waste package. The water flux through the waste package is varied from 0.15 to 15.0 L/yr, representing low to moderate seepage rates (BSC 2003j, Figure 6.8-3). Use of a lower water flux increases the contact time of water with waste package components and thus allows the chemical reactions to progress further. For sensitivity analyses, a few simulations were performed with flux rates as high as 1,000 L/yr. In the seepage-dripping model, the solid-centered flow-through option in EQ6 is used. This option simulates a single-cell batch reactor. Seepage water "flows" into the cell at a specified rate while reactants are added to the cell at rates dictated by the degradation rates of their source materials. Water exits the cell at the same rate as it enters.

3.2.2 Kinetic Degradation of Package Components

The rate at which waste package components degrade, together with the rate of water influx, determine the evolution of in-package water chemistry. The degradation rate of commercial SNF is formulated as a function of pH and dissolved carbonate concentration, while the rate of HLW dissolution is described as a function of pH only, based on transition state theory and experimental measurements (see Section 5). For the corrosion of the codisposed N Reactor SNF and the metal alloys in the waste package, constant reaction rates are used. The reaction rates also depend on the surface areas of waste package components exposed, which have been estimated based on the configurations and dimensions of waste packages (BSC 2004b, Sections 6.5.2 to 6.5.4). The surface areas are assumed to remain constant during degradation. This assumption is reasonable because the surface area would decrease as the quantity of a remaining reactant decreases while, on the other hand, it could also increase due to grain disaggregation. For the no-drip model, the calculations have been performed for the following percentages of surface area exposure: 10% for commercial SNF, 100% for HLW glass, and 50% for N Reactor SNF. For the seepage-dripping model, the following percentages are considered: 1%, 10%, and 100% for commercial SNF, and 100% for both HLW and N Reactor SNF. These values were chosen only to parameterize the impact of coverage on effluent chemistry. The time-dependent percentage of commercial SNF surface area exposed as cladding splits (discussed in Section 4) and the surface areas of commercial SNF and high-level radioactive waste used in the waste form degradation models (discussed in Section 5) are not input to the in-package chemistry model when the model is implemented in TSPA-LA.

3.2.3 Potential Generation of Alkaline or Acid Waters

The waste package components could have a significant impact on the predicted in-package pH. The dissolution of high-level radioactive waste glass, which contains high concentrations of sodium and potassium, could generate an alkaline condition by releasing alkalis (Na^+, K^+, or Ca^{2+}) into solution:

$$\text{Glass}{-}\text{Na}^+ + \text{H}^+ \rightarrow \text{Na}^+ + \text{Glass}{-}\text{H}^+ \qquad \text{(Eq. 3-1)}$$

In contrast, the Carbon Steel Type A516, which contains elemental sulfur, is a strong acid generator:

$$\text{Metal}{-}\text{S} + \text{H}_2\text{O} + 3/2\text{O}_2 \rightarrow \text{SO}_4^{2-} + 2\text{H}^+ + \text{Metal}^+ \qquad \text{(Eq. 3-2)}$$

Similarly, the Stainless Steel Type 304L, also containing elemental sulfur, could also potentially generate an acid solution. However, its effect is expected to be much smaller than Carbon Steel Type A516, because of its very slow corrosion rate. The pH resulting from these two reactions will be altered by other chemical reactions such as surface complexation on corrosion products, leading to a near neutral pH range.

3.2.4 Surface Complexation

Steel corrosion, which is rapid relative to fuel oxidation, will result in a large accumulation of ferric (hydr)oxide corrosion products inside the waste package. It is estimated that 10 to 40 moles of ferric (hydr)oxides (ferrihydrite, goethite, or hematite) are potentially able to form per liter of void space due to the degradation of low carbon and stainless steel (BSC 2004b, Section 6.3.3). Roughly half appears in the first 100 years after package failure due to the degradation of Carbon Steel Type A516. From 0.2% to 90% of precipitated iron(III) is able to react with solutions. This is equivalent to 0.02 to 40 moles of pH-buffering sites available per liter of water. Such a large buffering capacity will be a dominant factor controlling in-package chemistry. Given the fact that Carbon Steel Type A516 contains only trace amounts of sulfur (approximately 0.035 wt %) (Table 3-1), the proton release from reaction (Equation 3-2) will be overwhelmed by surface complexation on the corrosion products. Since the isoelectric point of ferric (hydr)oxides is approximately pH 7 to 8 (Davis and Kent 1990, Table 4, p. 210), the surfaces of these solids will acquire protons at pH less than 7 and lose them to solution at pH greater than 8, in effect limiting the pH range to near neutral.

Table 3-1. Composition of Steel and Aluminum Alloys

Element	Carbon Steel Type A516 (wt %)	Neutronit[a] (wt %)	Al-6061 (wt %)	SS31600 (wt %)	Al-1100 (wt %)	Stainless Steel Type 304L (wt %)
Carbon	0.28	0.04	—	0.02	—	0.03
Manganese	1.045	—	0.15	2.00	—	2.00
Phosphorus	0.035	—	—	0.045	—	0.05
Sulfur	0.035	—	—	0.03	—	0.03
Silicon	0.29	—	0.60	0.75	0.45	0.75
Chromium	—	18.5	0.195	17.00	—	19.00
Nickel	—	13	—	12.00	—	10.00
Cobalt	—	0.2	—	—	—	—
Molybdenum	—	2.2	—	2.50	—	—
Nitrogen	—	—	—	0.08	—	0.10
Iron	98.3	64.82	0.7	65.58	0.50	68.05
Boron	—	1.245	—	—	—	—
Zinc	—	—	0.25	—	—	—
Copper	—	—	0.275	—	0.05	—
Magnesium	—	—	1.0	—	—	—
Titanium	—	—	0.15	—	—	—
Aluminum	—	—	96.68	—	99.00	—
Total	**100.00**	**100.00**	**100.00**	**100.00**	**100.00**	**100.00**

Source: BSC 2004b, Table 8.

NOTE: [a] A nickel alloy interspersed with gadolinium (UNS N06464) is recommended to replace Neutronit as the absorber material. The effects of this change on in-package chemistry should be negligible because deleting the Neutronit does not significantly change the quantity of available stainless steel; the low corrosion rates of the nickel alloy relative to stainless steel will result in slightly higher in-package pH (i.e., less aggressive), and gadolinium will form phosphates that are fairly insoluble (Loros and Williams 2004).

3.2.5 Precipitation and Dissolution of Uranium Minerals

The uranium mineral, schoepite, together with iron corrosion products, dominates the composition of the alteration products from 500 years and beyond (BSC 2004b, Section 6.8.2). Whether schoepite dissolution produces or consumes hydrogen ions depends on the pH of the solution:

$$UO_3 \cdot 2H_2O + 2H^+ \leftrightarrow UO_2^{+2} + 3H_2O \text{ for pH} \leq 5.5 \qquad \text{(Eq. 3-3)}$$

$$UO_3 \cdot 2H_2O + 3HCO_3^- \leftrightarrow UO_2(CO_3)_3^{-4} + H^+ + 3H_2O \text{ for pH} > 7\text{-}7.5 \qquad \text{(Eq. 3-4)}$$

These two reactions constitute a negative feedback that resists pH excursions to high or low pH, and ultimately constrains pH values near the schoepite solubility minimum pH 6.5 to 7,

depending on the ambient carbon dioxide fugacity. The carbon dioxide fugacity determines the total concentration of aqueous carbonate species (see Section 3.5.3).

3.2.6 Effect of Radiolysis

When radiation passes through a material, some energy is deposited in the medium and chemical reactions can occur from the local deposition of energy (radiolysis). When gamma and fast neutron energy pass through moist air, nitric acid is produced. Hydrogen peroxide is generated from the radiolysis of water. Thus, radiolysis could potentially influence the results of the in-package chemistry model. However, EQ3/6 simulations show that the amount of acid produced from radiolysis has an insignificant effect on in-package chemistry (BSC 2004b, Attachment III).

3.2.7 Effect of Temperature

Most EQ3/6 simulations were run at either 25°C or 50°C. However, a few simulations were run at higher temperatures to investigate the effect of temperature on pH and ionic strength (BSC 2004b, Section 6.7.5). The results show that as temperature increases, pH tends to decrease and ionic strength remains largely unaffected. The reason for the decrease in pH is related to the increased dissociation of the water molecule as temperature rises. The effect of temperature was included in the pH abstraction used in TSPA-LA, as described in Section 3.5.1.

3.3 SOURCE OF DATA

The primary input parameters for the in-package chemistry model include the chemistry of seepage waters, the compositions of waste package materials and waste forms, and the corrosion rates of waste package components (BSC 2004b, Section 4). For reference, some of these parameters are listed in Tables 3-1 through 3-4. Table 3-4 gives experimental corrosion rates of the metal alloys in the waste package. The corrosion rate data in Table 3-4 were collected under a variety of conditions and provide the basis for the metal alloy corrosion rates used in the in-package chemistry abstraction and shown in the last column of Table 3-4.

Table 3-2. Input Water Composition for Model Calculation

Parameter	Units	Calcium Pore Water ECRB-SYS-CS1000/ 7.3-7.7/UC[a]	Sodium Pore Water ECRB-SYS-CS2000/ 16.3-16.5/UC[b]	Well J-13[c]
Ca	mg/L	94	81	13.0
Mg	mg/L	18.1	3.3	2.01
Na	mg/L	39	120	45.8
K	mg/L	7.6	6.1	5.04
Si	mg/L	N/A	N/A	28.5
SiO_2	mg/L	42	42	N/A
NO_3	mg/L	2.6	0.41	8.78
HCO_3	mg/L	397	362	Calculated from charge balance
Cl	mg/L	21	24	7.14
F	mg/L	3.4	6	2.18
SO_4	mg/L	36	31	18.4
pH	pH	7.6	7.4	7[d]

Source: BSC 2004b, Table 2.

NOTE: [a] Sample: ECRB-SYS-CS1000/7.3-7.7/UC; DTN: GS020408312272.003.
[b] Sample: ECRB-SYS-CS2000/16.3-16.5/UC; DTN: GS020408312272.003.
[c] DTN: MO0006J13WTRCM.000.
[d] Harrar et al. 1990, pp. 4–9.

Table 3-3. Chemical Composition of Commercial Spent Nuclear Fuel, N Reactor Fuel, and High-Level Radioactive Waste Glass

Element	Commercial SNF (mol/100 g)	N Reactor Fuel (mol/100 g)	High-Level Radioactive Waste Glass (mol/100 g)
Uranium	0.3617	0.42	0.00782
Neptunium	0.0009	N/A	0
Plutonium	0.0027	N/A	0
Zirconium	0.0005	N/A	0
Molybdenum	0.0009	N/A	0
Technetium	0.0008	N/A	0
Ruthenium	0.0020	N/A	0
Cesium	0.0013	N/A	0
Barium	0.0010	N/A	0.00108
Gadolinium	0.0035	N/A	0
Oxygen	0.7385	N/A	2.70
Aluminum	0	N/A	0.0863
Sulfur	0	N/A	0.00401
Calcium	0	N/A	0.0162
Phosphorus	0	N/A	0.000489
Silicon	0	N/A	0.776
Boron	0	N/A	0.291
Fluorine	0	N/A	0.00166
Iron	0	N/A	0.172
Potassium	0	N/A	0.0751
Magnesium	0	N/A	0.0333
Sodium	0	N/A	0.577

Source: BSC 2004b, Tables 10 and 11.

Table 3-4. Metal Alloy Corrosion Rates

Metal	Condition	Corrosion rate (μm/yr)					Rate Used in the In-Package Chemistry Model (μm/yr)
		Min.	Max.	Median	Mean	σ	
Carbon Steel Type A516 (times less than 0.53 years)	SDW (60°C)	78.71	130.70	101.95	102.71	12.37	72
	SDW (90°C)	58.08	130.02	77.05	81.14	15.13	
	SCW (60°C)	50.25	104.20	62.77	68.08	14.17	
	SCW (90°C)	7.39	22.06	12.42	12.78	3.77	
Carbon Steel Type A516 (times greater than 1.0 years)	SDW (60°C)	65.77	106.93	74.56	77.43	8.83	
	SDW (90°C)	29.53	88.68	48.70	51.80	12.99	
	SCW (90°C)	6.77	14.36	10.83	10.61	2.02	
	SCW (90°C)	3.69	9.35	6.75	6.84	1.25	
Neutronit	Freshwater (29.5°C)	0.001	0.011	0.003	0.004	0.004	0.1
	Freshwater (50°C to 100°C)	0.025	0.330	0.203	0.206	0.088	
	Saltwater (26.7°C)	1.810	29.220	7.38	11.060	10.190	
Aluminum Alloy	Freshwater	0.40	36.93	9.50	12.95	10.84	3.0
	Saltwater	0.12	110.91	4.76	9.69	15.34	
Stainless Steel Type 316	Freshwater (29.5°C)	0.0007	0.0475	0.003	0.0083	0.0136	0.1
	Freshwater (50°C to 100°C)	0.037	0.51	0.229	0.248	0.146	
	Saltwater (26.7°C)	0.0014	14.787	0.7362	1.939	3.346	
Stainless Steel Type 304L	Freshwater (25°C to 100°C)	0.001	1.570	0.1285	0.214	0.298	0.1
	Saltwater (26.7°C)	1.588	39.147	5.08	11.441	11.134	
	Saltwater (90°C)	0.660	15.900	2.03	5.816	5.953	

Source: BSC 2004b, Table 9; BSC 2004g, Table 7-4.

NOTE: σ = standard deviation; SDW = simulated dilute water; SCW = simulated concentrated water. See note in Table 3-1.

3.3.1 Initial Water Compositions

For the seepage-dripping model, three water compositions have been used for the initial conditions (BSC 2004b, Table 2), as shown in Table 3-2: (1) a calcium-dominated pore water, (2) a sodium-dominated pore water, and (3) a J-13 well water. The calcium- and sodium-dominated pore water compositions were used because they were obtained from core samples near the repository. The decision to use these water compositions was based on several lines of reasoning. The J-13 well water composition was used for comparison purposes (i.e., to maintain continuity between the current work and past in-package chemistry analyses). The calcium and sodium pore water compositions, corresponding to pore waters "W5" and "W4," respectively in *Drift-Scale Coupled Processes (DST and THC Seepage) Models* (BSC 2004e), are used because they were obtained from core samples proximal to the repository. These two pore waters represent possible in situ water compositions in the unsaturated repository horizon. Pore water compositions can also be perturbed thermally during the postclosure time period. However, a sensitivity analysis has shown that this perturbation is negligible (BSC 2004b,

Figure 14). For the no-drip model, the initial water is assumed to be pure water in equilibrium with the ambient fugacities of CO_2 and O_2 (BSC 2004b, Section 6.3).

3.3.2 Compositions of Waste Package Components

The chemical composition of each component is listed in Table 3-3. Table 3-3 summarizes the composition of commercial SNF, N Reactor fuel, and HLW glass. As discussed in Section 2, the commercial SNF is an oxide fuel while the N Reactor SNF is a uranium metal fuel.

3.3.3 Corrosion Rates

Metal corrosion rates are used to estimate the mean lifetime of the waste form internals and allow prediction of the time needed for structural collapse to occur. Metal corrosion proceeds initially by the direct oxidation of reduced constituents (iron, aluminum, chromium, etc.) to form a coating of metal hydroxides that can slow the further access of water and oxygen to the dissolving metal surface. Consequently, absolute rates of corrosion depend on both the oxidation step and the stability and chemical reactivity of the corrosion product layer. Solution chemistries that solubilize the latter, for example, can accelerate corrosion. Corrosion rates are important to the in-package chemistry model because they allow some predictions to be made of the rate of metal hydroxide accumulation, which is important for pH control, radionuclide sorption, and potential colloid formation. The corrosion rates of metal alloys are given in Table 3-4. These rates will encompass various aqueous parameters such as temperature (up to 100°C), water type (i.e., fresh versus saline), and pH. The corrosion rates of the different waste forms can be found in Section 5 of this document. Note that the corrosion rate of Carbon Steel Type A516 is about 3 orders of magnitude higher than that of Stainless Steel Type 304L. Therefore, even though both materials contain a similar sulfur content, their impacts on in-package pH will be quite different, as discussed in Section 3.2.3.

3.4 EVOLUTION OF IN-PACKAGE CHEMISTRY

The temporal evolution of in-package chemistry is calculated by assigning kinetic rates to waste package component degradation. Note that the starting time for the in-package chemistry model refers to the time at which waste packages are breached and sufficient water becomes available for chemical reactions. As discussed in Section 3.2, the in-package chemistry is controlled not only by waste and waste package corrosion and the associated mineral precipitation or dissolution, but also by surface complexation on corrosion products. The EQ3/6 code does not model interfacial chemical processes such as surface complexation. Thus, in-package conditions have been modeled in two steps. First, EQ3/6 calculations were made simulating the evolution of these conditions without considering the effects of surface complexation reactions for 20,000 years following the start of reactions in the package (which is significantly beyond the 10,000-year regulatory period). Second, the effects of surface complexation reactions on the in-package pH are modeled. The surface sites on which these reactions take place will be available for at least several hundred years, as long as a significant amount of steel degradation is occurring. During this period, surface complexation rather than the reactions modeled by EQ3/6 will likely control the in-package pH (BSC 2004b, Section 6.3.3).

The pHs predicted inside the waste form tend to be near neutral indicating that the pH-buffering ability of corrosion product surface complexation and schoepite dissolution will limit pH excursions. The isoelectric point of ferric corrosion products and the solubility minimum of schoepite are both near neutral. Equilibration of acidic or alkaline fluids with ferric corrosion products and schoepite consequently limits pHs to between approximately 4.5 and 8. Increasing carbon dioxide levels causes a slight shift of pHs to lower values while favoring the formation of carbonate-containing surface complexes at the corrosion product-solution interface and dissolved uranyl-carbonate species. The pH abstractions capture the net effect of these processes (BSC 2004b, Section 6.8.2).

3.4.1 Commercial Spent Nuclear Fuel Waste Packages

3.4.1.1 No-Drip Model

Figure 3-1 displays the EQ3/6 simulation results for individual commercial SNF components at 25°C (BSC 2004b, Figure 1). The figure provides information on how each waste package component contributes to the in-package pH and shows the upper and lower pH limits for a commercial SNF package without considering the effects of surface complexation reactions. Note that the horizontal axis is in terms of moles of material dissolved independent of time. The low pH resulting from Carbon Steel Type A516 corrosion is due to the combination of oxidation of elemental sulfur, the large quantity of Carbon Steel Type A516, and its high corrosion rate relative to the other waste package components. Both the Al-6061 and the commercial SNF have neutral to slightly basic pH profiles, while the S31600 and Neutronit (borated Carbon Steel Type 316) have slightly acidic pH profiles.

The simulations have also been performed for multicomponent ensembles and resulted in a similar pH range (BSC 2004b, Figure 2). The simulations show that if it were not for the surface complexation reactions, the early-time pH (less than 100 years) will be controlled by Carbon Steel Type A516 dissolution, and for 100 to 500 or 1,000 years the pH would be controlled by Al-6061 dissolution. At times greater than 500 to 1,000 years, when surface complexation reactions may no longer be effective, the pH will be controlled by equilibrium with the corrosion products.

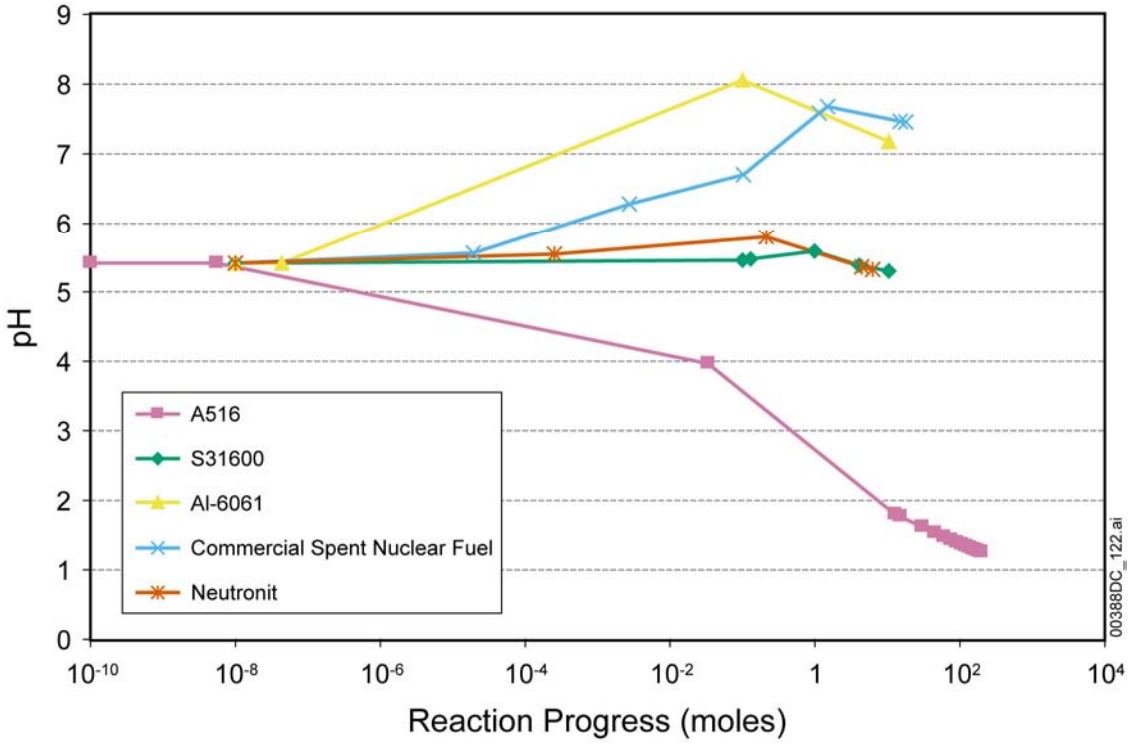

Source: DTN: MO0403SPAIPCHM.004, CSNF_singlereact_NDM.xls.

Figure 3-1. pH Calculated as a Function of Moles of Reactant Dissolved in Kilograms of Water for Commercial Spent Nuclear Fuel Single Component Degradation under No-Drip Conditions

3.4.1.2 Seepage-Dripping Model

The evolution of in-package chemistry for the median water flux and 10% fuel exposure at 25°C predicted by EQ3/6 is shown in Figure 3-2. Although nominal temperatures in the repository will exceed 40°C for the first 10,000 years, 25°C runs were used initially to identify the relevant chemical processes and trends as thermodynamic and kinetic data are better known at the slightly lower temperature. It can be seen that the compositions of seepage water have virtually no effect on the pH evolution. The solution pH will be quickly overwhelmed by waste package corrosion over the first 10 years. Low pH values modeled without considering the effects of surface complexation reactions result from the relatively fast corrosion of a large quantity of Carbon Steel Type A516 corrosion (Figure 3-2). As shown in the figure, however, this pH will be buffered by the corrosion of other waste package components after a few hundred years. The commercial SNF is predicted to completely degrade over approximately 5,000 years.

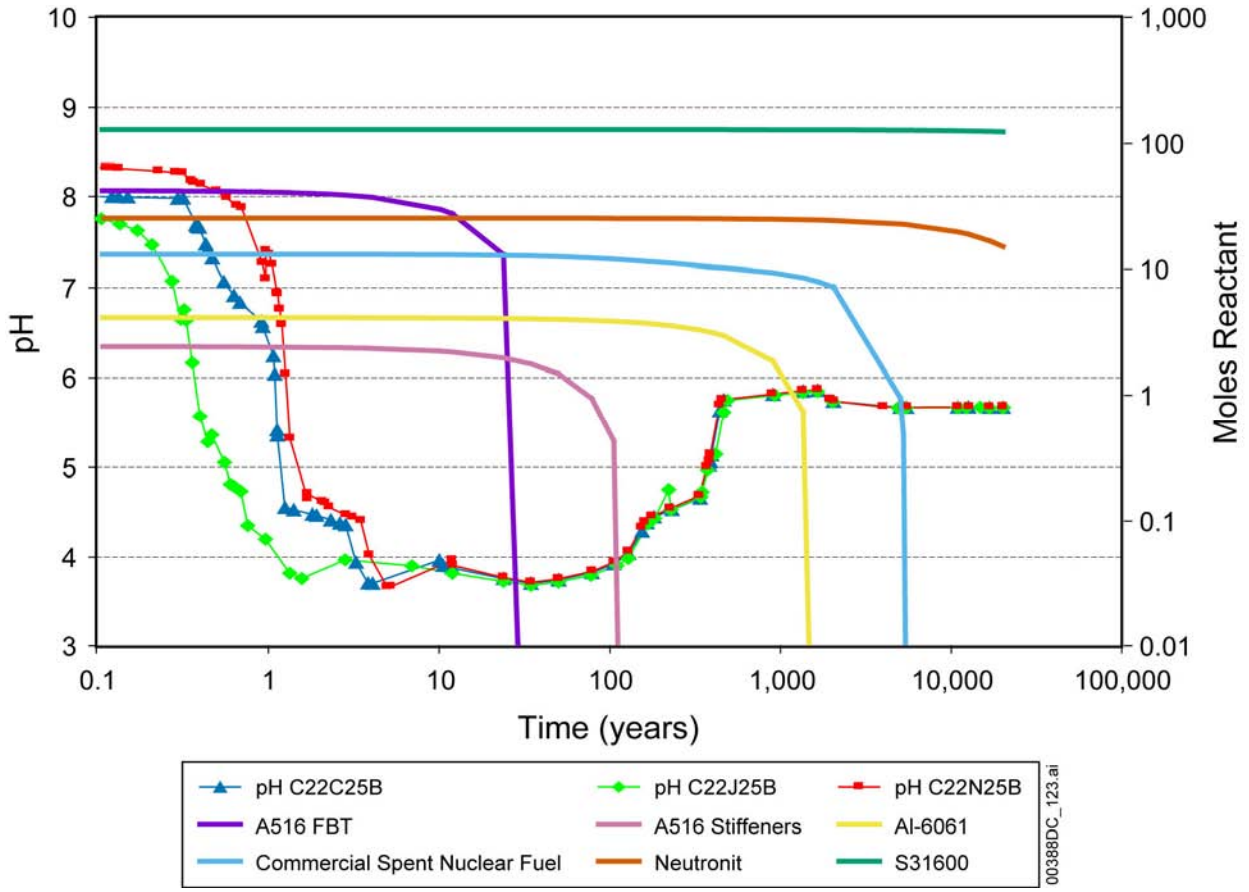

Source: DTN: MO0403SPAIPCHM.004, CSNF_SDM_25_rev03.xls.

NOTE: C22C25B = Ca-pore water, C22J25B = J-13 pore water, and C22N25B = Na-pore water.

Figure 3-2. Evolution of pH and Reactants for Commercial Spent Nuclear Fuel Waste Packages under 1.5-L/yr Seepage-Dripping Conditions and 10% Fuel Exposure at 25°C

3.4.2 Codisposal Waste Packages

3.4.2.1 No-Drip Model

Figure 3-3 displays the 25°C pH profiles for individual codisposal waste package components as calculated by EQ3/6. Again, note that the horizontal axis is in terms of moles of material dissolved independent of time. The codisposal waste package displays a much wider variation in pH compared to the commercial SNF package (Figure 3-1). This is because the HLW generates high pH conditions due to its high concentrations of sodium and potassium. The Al-1100, S31600, and N Reactor fall in the middle of the pH range at approximately 5.7 to 6.2. The corrosion of Carbon Steel Type A516 and Stainless Steel Type 304L corrosion leads to pH values of 1.5 to 2, as shown in Figure 3-3. However, over the first few hundred years this low pH will be buffered by surface complexation reactions of the corrosion products (BSC 2004b, Section 6.8.2). Furthermore, over longer time periods, results of the codisposal waste package multicomponent ensemble runs show that this low pH will be buffered by either HLW glass or N Reactor fuel, since the TSPA-LA model does not take cladding credit for N Reactor fuel or the glass pour canisters (BSC 2004b, Section 6.6.2.1, Figure 9).

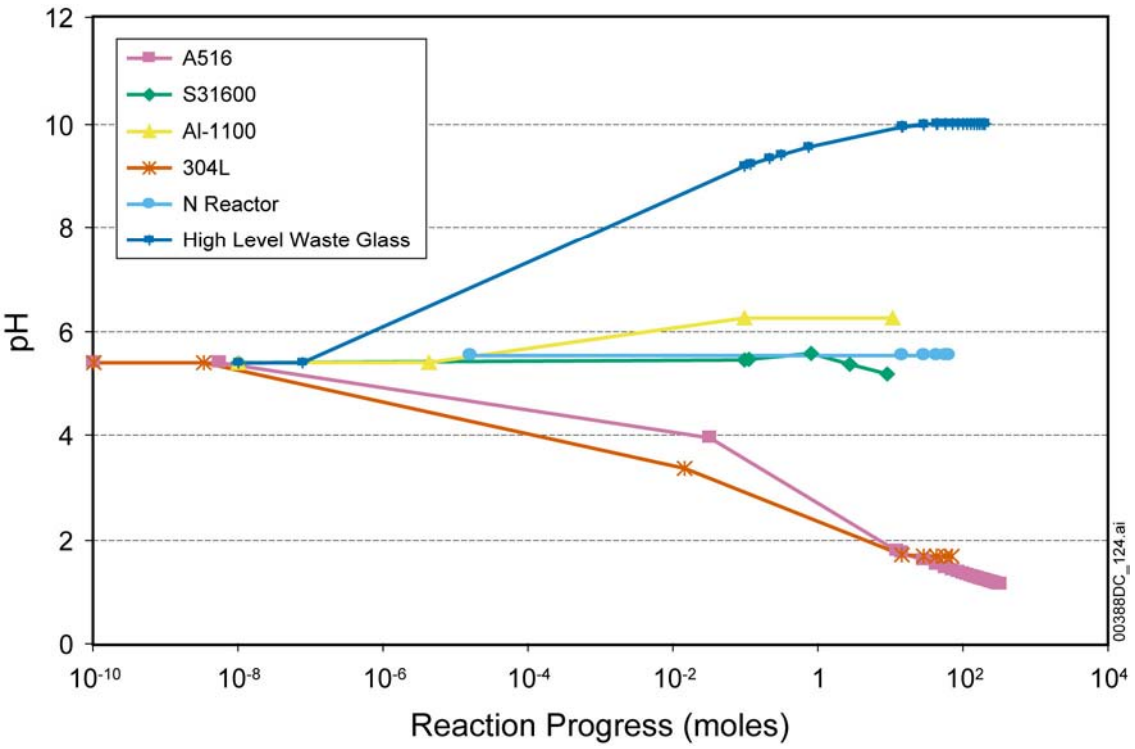

Source: DTN: MO0403SPAIPCHM.004, CD_singlereact_NDM.xls.

Figure 3-3. pH Calculated as a Function of Moles of Reactant Dissolved in Kilograms of Water for Codisposed Single Component Degradation under No-Drip Conditions

3.4.2.2 Seepage-Dripping Model

Figure 3-4 displays the 25°C evolution of pH and reactants for codisposal waste packages under seepage conditions. The pH profiles converge early in the simulations indicating that the model pH response is insensitive to starting water composition, which is similar to the pH profile behavior of the commercial SNF seepage-dripping model (Figure 3-2). The figure shows that the N Reactor fuel dissolves in just a few years. The rapid dissolution of the N Reactor fuel diminishes its contribution to the overall in-package chemistry. However, the resulting large quantity of schoepite may have the capacity to influence the in-package chemistry for an extended duration. The minimum pH for codisposal waste packages is approximately one unit higher that for commercial SNF under the same chemical and physical conditions (Figure 3-2).

Another important feature of the pH profiles in Figure 3-4 is the absence of a period of sustained high pH (greater than 9) that might be expected from the dissolution of the HLW glass. The codisposed no-drip models, single reactant and ensemble, both predicted that high pH conditions are possible in the absence of an acid-producing reactant (i.e., steel alloy) (Figure 3-3). However, in the seepage-dripping model, seepage is allowed to "stream" through the waste package reacting with waste package components, and it is unlikely that seepage, which has reacted with HLW glass could exit a waste package without contacting a steel component along its flow path.

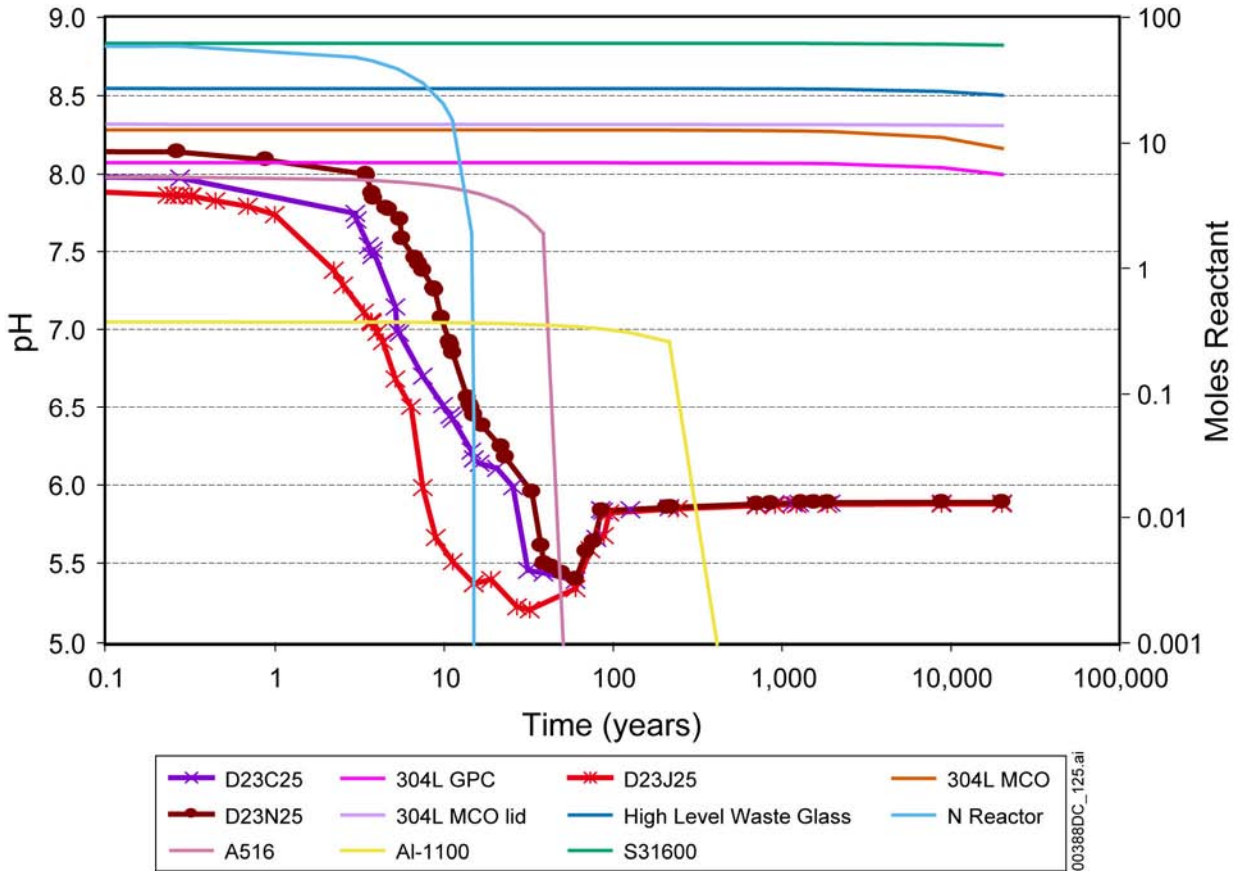

Source: DTN: MO0403SPAIPCHM.004, CDNR_SDM_25_rev03.xls.

Figure 3-4. Evolution of pH and Reactants for Codisposal Waste Packages under 1.5-L/yr Seepage-Dripping Conditions and 10% Fuel Exposure at 25°C

3.4.3 pH Regulated by Surface Complexation

As discussed in Section 3.2.4 (also see BSC 2004b, Section 6.3), a large quantity of Fe oxyhydroxides formed from steel corrosion will be available for surface complexation reactions. The surface protonation and deprotonation reactions as described by (Dzombak and Morel 1990; Appelo et al. 2002) are:

$$>\text{Fe-OH}_2^+ \leftrightarrow >\text{Fe-O-H} + \text{H}^+ \quad K_1 = [>\text{Fe-O-H}][\text{H}^+]/[>\text{Fe-O-H}_2^+] = 10^{-7.29} \qquad \text{(Eq. 3-5)}$$

$$>\text{Fe-OH} \leftrightarrow >\text{Fe-O}^- + \text{H}^+ \quad K_2 = [>\text{Fe-O}^-][\text{H}^+]/[>\text{Fe-O-H}] = 10^{-8.93} \qquad \text{(Eq. 3-6)}$$

where >Fe denotes sites exposed at the FeOOH-solution interface. Sorption of bicarbonate ions may also occur:

$$>\text{Fe-O-H} + \text{H}^+ + \text{CO}_3^{2-} \leftrightarrow >\text{Fe-HCO}_3^- + \text{H}_2\text{O} \qquad \text{(Eq. 3-7)}$$

$$K_{CO3} = [>\text{Fe-HCO}_3^-]a_{H_2O}/[>\text{Fe-OH}][\text{H}^+][\ \text{CO}_3^{2-}] = 10^{12.78} \qquad \text{(Eq. 3-8)}$$

By accounting for the surface complexation effect, the Carbon Steel Type A516 dissolution reaction can be written as:

$$\begin{aligned} &Fe_{1.76}Mn_{0.019}C_{0.0233}Si_{0.0103}P_{0.00113}S_{0.00109} + mH_2O + fO_2 \rightarrow \\ &0.00109SO_4^{2-} + 0.00113(H_3PO_4 + H_2PO_4^- + HPO_4^{2-}) + 0.0103H_4SiO_4 + \\ &0.0233(H_2CO_3 + HCO_3^-) + 0.019MnO_2 + (1.76 - X)\,FeOOH + \\ &X(>Fe\text{-}O\text{-}H + >Fe\text{-}O\text{-}H_2^+ + >Fe\text{-}O^- + >Fe\text{-}O\text{-}CO_3^-) + nH^+. \end{aligned} \quad \text{(Eq. 3-9)}$$

where X is the amount of Fe in FeOOH (moles) that is exposed to solution, mH_2O is moles of water, and fO_2 is fugacity of oxygen.

Given a value of $X = 0.176$ (10% of Fe sites, a reasonable value for goethite) for dissolution of 1 mol of Carbon Steel Type A516 into a near neutral solution:

$$\begin{aligned} n\ &= 2[SO_4^{2-}] + [H_2PO_4^-] + 2[HPO_4^{2-}] + [HCO_3^-] + \\ &[>Fe\text{-}O^-] + [>Fe\text{-}O\text{-}HCO_3^-] - [>Fe\text{-}O\text{-}H_2^+]. \end{aligned} \quad \text{(Eq. 3-10)}$$

Similarly, charge balance for a solution in contact with carbon dioxide gas at 0.001 atm and into which 1 mol of Carbon Steel Type A516 were dissolved would be:

$$\begin{aligned} &(H^+) + (>Fe\text{-}O\text{-}H_2^+) = 2[SO_4^{2-}] + [H_2PO_4^-] + 2[HPO_4^{2-}] + \\ &(OH^-) + (HCO_3^-) + (>Fe\text{-}O^-) + (>Fe\text{-}O\text{-}HCO_3^-). \end{aligned} \quad \text{(Eq. 3-11)}$$

The two phosphate terms can be manipulated with the equilibrium constant for their conversion to give:

$$\begin{aligned} &[H_2PO_4^-] = 0.00113/(1 + 10^{-7.2}/[H^+]) \text{ and } [HPO_4^{2-}] = \\ &0.00113(1 - 1/(1 + 10^{-7.2}/[H^+])). \end{aligned} \quad \text{(Eq. 3-12)}$$

Substituting these expressions, carbonate equilibrium constants, the surface equilibria above, and rearranging to solve for pH:

$$\begin{aligned} &(H^+) = 0.00218 + 0.00113/(1 + 10^{-7.2}/[H^+]) + \\ &0.00226(1 - 1/(1 + 10^{-7.2}/[H^+])) + 0.176[10^{-8.93}/(H^+) + \\ &pCO_2 10^{-5.28}/(H^+) - 10^{7.29}(H^+)] + 10^{-14}/(H^+) + 10^{-7.82}\,fCO_2/(H^+) \end{aligned} \quad \text{(Eq. 3-13)}$$

The equation above can be solved for pH as a function of fixed fugacity of CO_2. For the relevant fugacity of CO_2, the calculation shows that the surface complexation on the corrosion products of Carbon Steel Type A516 can sufficiently neutralize the acidic solution generated by sulfur oxidation and that the solution's pH will be buffered at 7.3 to 8.1. This will occur immediately after onset of A516 corrosion (that is within the first several decades after waste package breach). The effect of increasing carbon dioxide levels in the waste form is to lower the ambient pH.

3.4.4 Upper pH Limit

As discussed in Section 3.2.5, schoepite together with iron corrosion products dominates the composition of the alteration products from time periods of 500 years and beyond. Schoepite

dissolves at pH values below about 5.5 to consume protons and at pH values above about 7 to produce protons (Equations 3-1 to 3-2). These two reactions constitute a negative feedback that will constrain pH at 5.5 to 7.5. As Figure 3-3 shows, HLW glass reaction by itself could lead to pH values from 8 to 10. For such high pH values to develop, it would require an unlikely scenario in which water reacts with the glass without also reacting with schoepite inside the waste package. Thus, a "HLW glass only, no steel, no fuel" scenario that produces high pH values is highly unlikely to occur. The most reasonable high-end pH for waste packages containing HLW glass is therefore 6.5 to 7.

3.5 IMPLEMENTATION FOR NOMINAL AND SEISMIC SCENARIOS

3.5.1 Abstraction of pH

3.5.1.1 Commercial Spent Nuclear Fuel Waste Package pH Abstraction

During the period when surface complexation is implemented (0 to 600 years) and based on the results of the surface complexation analyses, the pH for a commercial SNF waste package for both the nondripping and the dripping models is constrained by the ranges defined as a function of the fugacity of carbon dioxide gas, as shown in Table 3-5.

The minimum pH value, pH 4.5, was set based on a simulation at 90°C, indicating that at times greater than 600 years the pH stabilizes around 4.5. This simulation is shown in Figure 3-5 and represents a minimum pH based on the EQ6 results that do not include surface complexation to account for the possibility of localized areas of low pH due to the potential of heterogeneous flow through the waste package internals. The maximum pH values for the 0-to-600-year period are calculated from Equation 3-13.

Table 3-5. Commercial Spent Nuclear Fuel Lookup Table of pH as a Function of Carbon Dioxide Fugacity

Period (years)	log(fCO_2)	minimum pH	maximum pH
0 to 600	−5.0	4.5	8.1
	−4.5	4.5	8.1
	−4.0	4.5	8.0
	−3.5	4.5	7.9
	−3.0	4.5	7.7
	−2.5	4.5	7.5
	−2.0	4.5	7.3
	−1.5	4.5	7.0
600 to 20,000	N/A	4.5	7.0

Source: BSC 2004b, Table 66; DTN: MO0404SPAIPCHM.005.

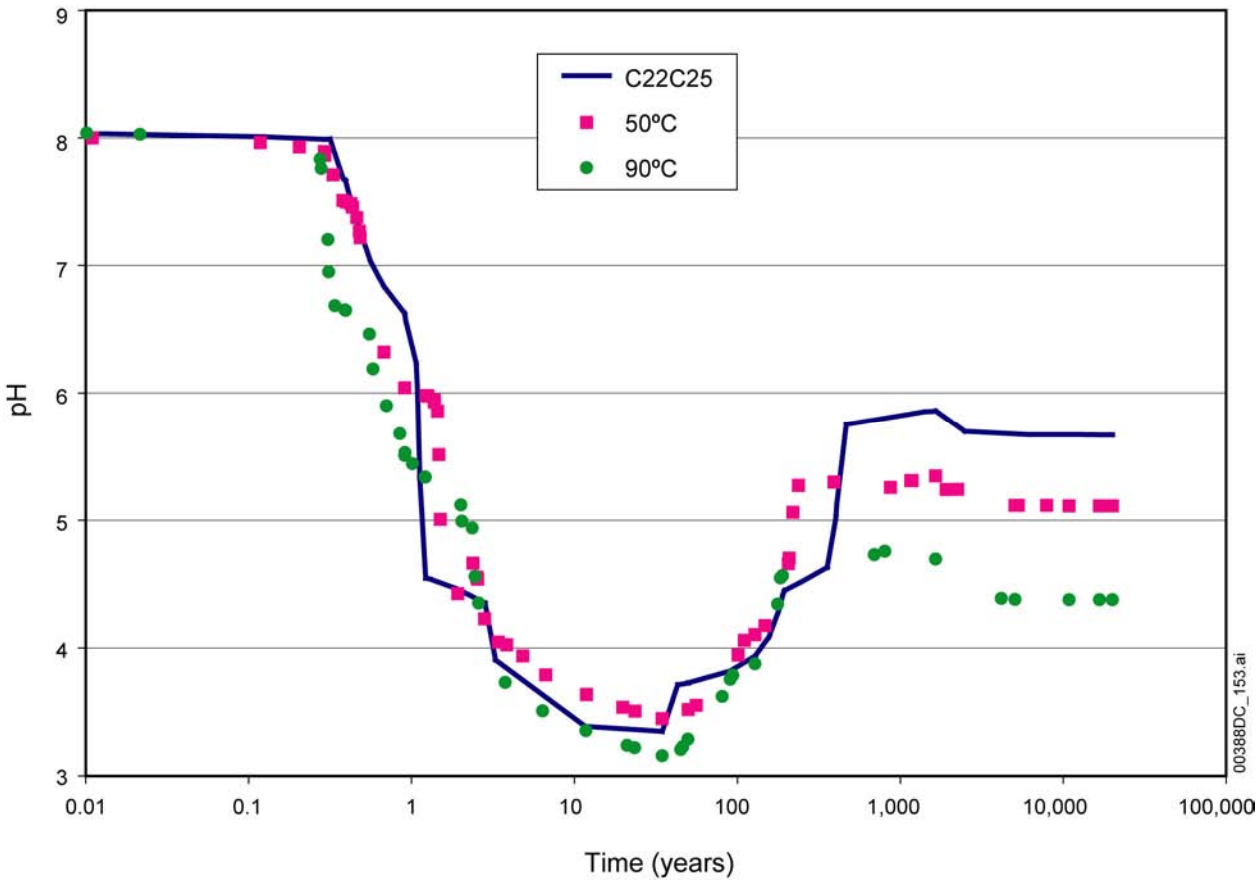

Source: BSC 2004b, Figure 24.

NOTE: C22C25 = 1.5-L/yr seepage dripping conditions, 10% fuel exposure, and calcium pore water at 25°C

Figure 3-5. Effect of Increasing Temperature on the pH Profile for Commercial Spent Nuclear Fuel Waste Package

During the period from 600 to 20,000 years, the minimum pH is set by the high temperature results shown in Figure 3-5 and the maximum by the 50-L/yr results shown in Figure 3-6. These values provide the maximum plausible range of pH.

For implementation in TSPA, the 0- to 600-year pH distributions are set using the minimum and maximum pH values (Table 3-5) for each $\log(fCO_2)$. Values for the latter are taken from the EBS physical and chemical environment model (BSC 2004h). Each distribution is uniform, and pHs for intermediate values of $\log(fCO_2)$ are linearly interpolated between nearest neighbor values. No uncertainty term is added to the sampled value. The abstracted pH values are independent of both time and temperature, and are not correlated to the pH in codisposal waste packages.

For the period from 600 to 20,000 years the pH should be uniformly sampled between pH 4.5 and pH 7 with no additional uncertainty term added. There is no correlation between this pH abstraction and that for codisposal waste packages.

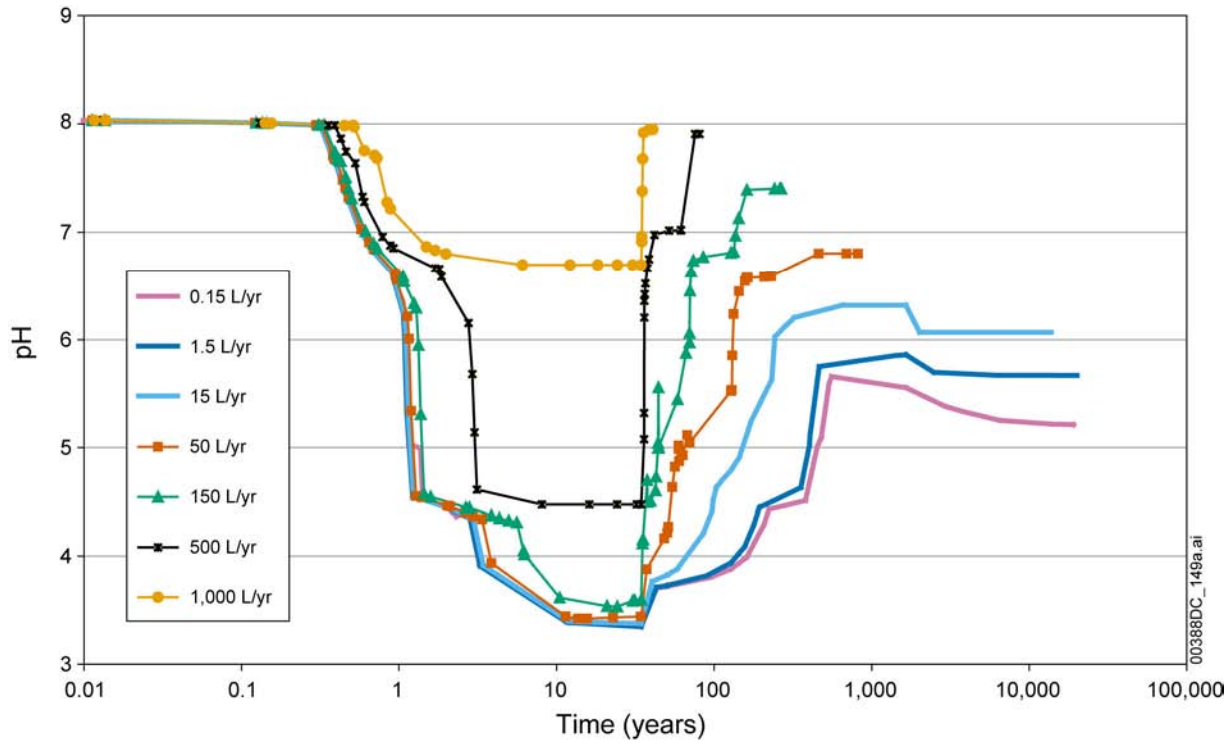

Source: BSC 2004c, Figure 20.

NOTE: Cases run using calcium–pore water, 10% fuel exposure, at 25°C.

Figure 3-6. Effect of Water Flux on pH for a Commercial Spent Nuclear Fuel Waste Package

3.5.1.2 Codisposal Waste Package Abstractions

The abstraction for pH inside a failed codisposal waste package, for both the dripping and nondripping models, is given in Table 3-6, and the basis for the minimum and maximum values are as follows. When the water flux is less than 150 L/yr per waste package, the maximum pH inside a codisposal waste package will not exceed 7 independent of temperature and CO_2 fugacity due to a variety of buffering reactions, for example, schoepite dissolution (BSC 2004b, Section 6.8.2). For water flux values greater than 150 L/yr per waste package, the maximum pH is 8 (BSC 2004b, Figure 22). The lower pH bound, pH = 4.5, was set by the high temperature analysis for both flux conditions (BSC 2004b, Figure 25).

For the purposes of implementation in TSPA, a uniform sampling of the ranges given in Table 3-6 with no additional uncertainty will capture the proper pH behavior for nondripping and seepage dripping scenarios in a codisposal waste package.

Table 3-6. Codisposal pH Abstraction

Period (years)	Flux Condition (L/yr per waste package)	Minimum pH	Maximum pH
0 to 20,000	Q<150	4.5	7.0
	Q>150	4.5	8.0

Source: BSC 2004b, Table 67.

3.5.2 Ionic Strength Abstraction

The ionic strength results predicted using the EQ6 model were based on layer thickness values adjusted to avoid exceeding the ionic strength limit of the aqueous model. Thus, the ionic strength boundary condition was set by the model itself. Ionic strength data are used by the colloid submodel to determine if the colloid stability threshold, 0.05 mol/kg ionic strength, has been exceeded. This threshold value is much below the upper limits of the aqueous model (not less than 1 mol/kg) so that use of the higher EQ6 calculated ionic strengths is acceptable.

The ionic strengths predicted by EQ6 may be high because the underlying calculations do not account for removal of dissolved salts from solution by corrosion product sorption. However, the inability to predict the identities and abundances (hence site densities) of the corrosion products over long periods of time prevents estimation of the magnitude of this effect. For example, complete conversion of corrosion products to low site density hematite over time would minimize any change in the ionic strengths predicted by EQ6. The possibility of ionic strength lowering by sorption reactions is dealt with by setting the uncertainty range to favor lower ionic strengths.

3.5.2.1 Ionic Strength for Commercial Spent Nuclear Fuel Waste Packages

The ionic strength distribution for commercial SNF no-drip conditions is constrained from the ensemble calculations (BSC 2004b, Figure 28). In the TSPA-LA model, it is sampled from 0.085 to 0.75 mol/kg with a loguniform probability distribution function. A loguniform distribution is used to envelop calculated ionic strengths that themselves vary by orders of magnitude. The uncertainty in ionic strength described below should be added to the sampled value.

For a seepage-dripping condition, the ionic strength is calculated as

$$y = ae^{b \log f} \qquad \text{(Eq. 3-14)}$$

where

y = ionic strength (mol/L)
a = constant (unitless)
b = constant (unitless)
f = seepage flux (L/yr).

The values of a and b used in Equation 3-14 were calculated from a curve-fitting procedure and are shown in Table 3-7, along with the appropriate temperature, flux limits, and regression coefficient for the curve fit. Values of ionic strength are either interpolated or linearly extrapolated from the 25°C and 50°C values to other temperatures from 25°C to 99°C (the limits of the in-package chemistry abstraction). As the seepage rate increases, the ionic strength inside the package will approach the values of initial waters. If the flux is less than the minimum, then the ionic strength should be evaluated using the lower flux limit. Likewise, if the flux is greater than the upper limit, then the ionic strength should be evaluated using the upper limit value.

Table 3-7. Commercial Spent Nuclear Fuel Seepage Dripping Model Ionic Strength Abstraction

Temperature (°C)	a (unitless)	b (unitless)	Flux Limits Per Waste Package (L/yr)	R^2
25	0.4755	−2.1652	Lower: 0.20 Upper: 185	0.9979
50	0.4472	−2.2424	Lower: 0.16 Upper: 145	0.9971

Source: BSC 2004b, Tables 70 to 73.

3.5.2.2 Ionic Strength for Codisposal Waste Packages

The ionic strength distribution for codisposal waste packages under no-drip conditions is constrained from the ensemble calculations (BSC 2004b, Figure 32). In the TSPA-LA model, it is sampled from 0.0032 to 0.75 mol/kg with a cumulative probability distribution shown in Table 3-8. The distribution in Table 3-8 is derived from the distribution of ionic strengths calculated in the reaction path runs.

Table 3-8. Codisposal Waste Package No-Drip Model Ionic Strength Cumulative Distribution

Time Period after Waste Package Breach (years)	Ionic Strength (mol/kg)	Probability
0 to 20,000	3.2×10^{-3}	0.0
	0.05	0.13
	0.75	1.0

Source: BSC 2004b, Table 74. DTN: MO0404SPAIPCHM.005.

For dripping conditions, the ionic strength is a function of seepage rate as shown in Equation 3-14, as it is for commercial SNF waste packages. The values of *a* and *b* used in Equation 3-14 were calculated from a curve-fitting procedure and are shown in Table 3-9, along with the appropriate temperature, flux limits, and regression coefficient for the curve fit. Values of ionic strength are either interpolated or extrapolated to other temperatures. For example, while 90°C values are not shown, they can be readily extrapolated from the 25°C and 50°C values. As the seepage rate increases, the ionic strength inside the package will approach the values of initial waters. If the flux is less than the minimum, then the ionic strength should be evaluated using the lower flux limit. Likewise, if the flux is greater than the upper limit, then the ionic strength should be evaluated using the upper limit value.

Table 3-9. Codisposal Waste Package Seepage Dripping Model Ionic Strength Abstraction

Temperature (°C)	a	b	Flux Limits Per Waste Package (L/yr)	R^2
25	0.5201	-2.1306	Lower: 0.25 Upper: 180	0.9993
50	0.4324	-2.1369	Lower: 0.18 Upper: 180	0.9993

Source: BSC 2004b, Tables 75 through 78.

3.5.2.3 Uncertainty in Ionic Strength

The variability of ionic strength is illustrated in Figure 3-7. For both the commercial SNF and codisposal waste package seepage-dripping models and no-dripping models at temperatures ranging from 25°C to 99°C (i.e., the temperature boundaries of the in-package chemistry abstraction) a uniformly sampled uncertainty value from the range of −0.8 to 0.4 multiplied by the sampled value is added to the sampled value. This range accounts for uncertainties in carbon dioxide levels as well as the possibility of lower ionic strengths as a result of surface complexation effects. Mathematically, the uncertainty for dripping and nondripping cases is implemented as follows:

$$\text{Ionic strength} = IS_{sampled} + (Uncertainty_{sampled} \times IS_{sampled}) \qquad \text{(Eq. 3-15)}$$

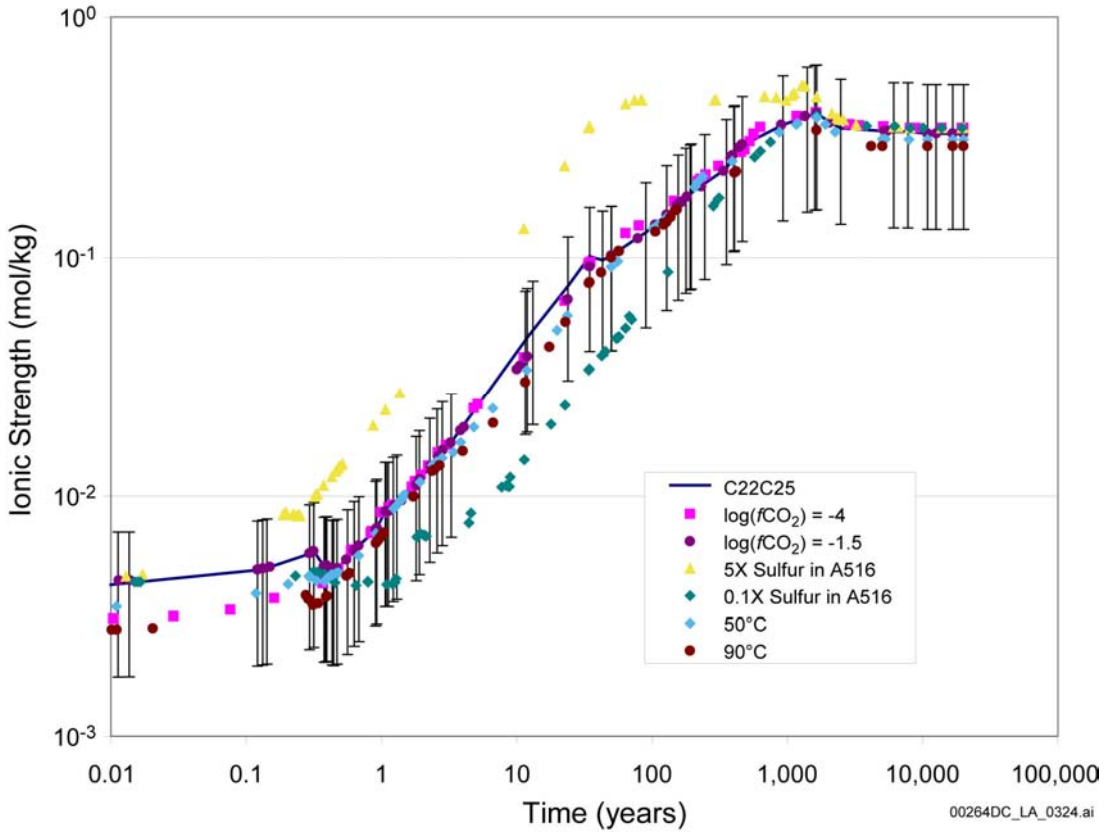

Source: DTN: MO0403SPAIPCHM.004.

NOTE: C22C25 represents commercial SNF, 1.5-L/yr water flux, calcium–pore water, 10% fuel exposure, at 25°C.

Figure 3-7. Commercial Spent Nuclear Fuel Ionic Strength Profile with Error Bars

3.5.3 Abstraction of Carbonate and Fluoride Concentrations

Total carbonate is used in the kinetic rate expression for the dissolution of commercial SNF; therefore, abstracted values are needed for the TSPA-LA model. In a system where the fugacity

of carbon dioxide (fCO_2) is constant over the modeled period and the pH and temperature are known, the total carbonate can be calculated using the equilibrium mass action expressions:

$$\text{Total C} = fCO_2 \left(10^{K_1} + 10^{(\text{pH} + K_1 + K_2)} + 10^{(2\text{pH} + K_1 + K_2 + K_3)}\right) \qquad \text{(Eq. 3-16)}$$

where

K_1 = log K for $CO_2(g) \leftrightarrow CO_2(aq)$;
K_2 = log K for $CO_2(aq) \leftrightarrow H^+ + HCO_3^-$; and
K_3 = log K for $HCO_3^- \leftrightarrow H^+ + CO_3^{2-}$.

The values of log K for the above reactions are shown in Table 3-10.

Table 3-10. Log K Temperature Interpolation Functions for Use in the Total Carbonate Abstraction

Log K	Log K expression[a]	R^2
K_1	Log $K_1 = 7 \times 10^{-5}T^2 - 0.0159T - 1.1023$	0.9992
K_2	Log $K_2 = 5 \times 10^{-7}T^3 - 0.0002T^2 + 0.0132T - 6.5804$	1.0
K_3	Log $K_3 = -8 \times 10^{-5}T^2 + 0.0128T - 10.618$	0.9977

Source: BSC 2004b, Table 86. DTN: MO0404SPAIPCHM.005.

NOTE: [a]T = temperature in degrees Celsius

The effect of fluoride concentration in the in-package solution is not a direct input parameter in TSPA-LA. However, actinide element solubilities are sensitive to fluoride concentrations so the ranges of fluoride concentrations were necessary in developing the dissolved concentration model (Section 6.2, below). Commercial SNF does not contain fluoride; therefore, the sole source of fluoride in commercial SNF waste packages is from the initial seepage waters, which is typically low. In contrast, the HLW contains a trace amount of fluoride, which will contribute the dissolved fluoride concentration. Based on the EQ3/6 simulations, the upper limit of fluoride concentration for codisposal waste packages can be as high as 0.011 mol/kg.

3.6 IMPLEMENTATION FOR IGNEOUS INTRUSION SCENARIO: POSTINTRUSIVE CHEMICAL ENVIRONMENT

For an igneous intrusion scenario, waste packages in a drift intersected by intrusion will be completely damaged and encapsulated by basaltic magma, which will cool and solidify, forming a fractured basaltic rock. It is assumed that the postintrusive chemical environment will be dominated by the interaction of seepage water percolating through the rock fractures and the basaltic rock matrix. In this sense, the chemical environment discussed in this section is no longer in-package chemistry per se.

The chemical interaction of seepage with the basalt is simulated with EQ3/6 for typical seepage water and basaltic rock compositions and flow rates (BSC 2004d, Section 6.5.3). The simulation results are summarized in Table 3-11.

Table 3-11. Value of pH and Ionic Strength for Use in the Igneous Intrusion Scenario

log(fCO_2)	Time Period*	pH		Ionic Strength (mol/kg)	
		Maximum	Minimum	Maximum	Minimum
−2 bar	$x \leq 25$ years	7.9	7.6	1.87×10^{-2}	9.64×10^{-3}
	$25 > x \leq 250$ years	8.1	7.8	3.59×10^{-2}	1.23×10^{-2}
	$250 > x \leq 2500$ years	8.1	7.8	4.00×10^{-2}	1.22×10^{-2}
	$2500 > x \leq 20000$ years	8.1	7.7	3.58×10^{-2}	1.15×10^{-2}
−2.5 bar	$x \leq 25$ years	8.4	8.1	2.09×10^{-2}	9.23×10^{-3}
	$25 > x \leq 250$ years	8.6	8.3	4.33×10^{-2}	1.31×10^{-2}
	$250 > x \leq 2500$ years	8.6	8.3	5.00×10^{-2}	1.29×10^{-2}
	$2500 > x \leq 20000$ years	8.6	8.2	4.22×10^{-2}	1.18×10^{-2}
−3 bar	$x \leq 25$ years	8.9	8.6	2.43×10^{-2}	9.14×10^{-3}
	$25 > x \leq 250$ years	9.0	8.8	5.00×10^{-2}	1.40×10^{-2}
	$250 > x \leq 2500$ years	9.1	8.8	5.00×10^{-2}	1.37×10^{-2}
	$2500 > x \leq 20000$ years	9.1	8.7	5.00×10^{-2}	1.19×10^{-2}
−3.5 bar	$x \leq 25$ years	9.4	9.0	3.00×10^{-2}	9.44×10^{-3}
	$25 > x \leq 250$ years	9.5	9.2	5.00×10^{-2}	1.67×10^{-2}
	$250 > x \leq 2500$ years	9.6	9.2	5.00×10^{-2}	1.62×10^{-2}
	$2500 > x \leq 20000$ years	9.5	9.1	5.00×10^{-2}	1.30×10^{-2}
−4 bar	$x \leq 25$ years	9.7	9.4	3.42×10^{-2}	1.02×10^{-3}
	$25 > x \leq 250$ years	9.9	9.6	5.00×10^{-2}	1.97×10^{-2}
	$250 > x \leq 2500$ years	9.9	9.6	5.00×10^{-2}	1.89×10^{-2}
	$2500 > x \leq 20000$ years	9.9	9.6	5.00×10^{-2}	1.43×10^{-2}

Source: BSC 2004d, Table 8-2.

NOTE: Time period represents time after re-establishment of seepage flow. Values archived in output DTN: MO0402SPAHWCIG.002.

Maximum and minimum pHs were taken from individual EQ3/6 runs. It can be seen from Table 3-11 that the pH of the reacted seepage waters will be maintained at a neutral to mildly basic range and the ionic strength will remain less than 0.2 mol/kg. EQ3/6 simulations also show either no changes or decrease in dissolved fluoride concentration during seepage–basalt interactions. Therefore, for the TSPA implementation, the fluoride concentration, if needed, should be set to the initial seepage water concentration.

3.7 UNCERTAINTIES, LIMITATIONS, AND MODEL CONFIDENCE

When water comes into contact with the materials inside a waste form, the reactions that ensue will be the same as, or very similar to, ones that occur naturally in soils and in other man-made materials. Reduced metals, metal oxides, and glass will dissolve and secondary corrosion products will form, all in the presence of ambient oxygen and carbon dioxide. In soils, the balance between proton production and consumption maintains the pHs to roughly neutral values. Only in highly unlikely scenarios do soil pHs fall below 4 (in essence, when high levels of reduced sulfur are present). Soil pHs exceed 8 to 9 only when the soil fluids are out of contact with the atmosphere and low carbon dioxide fugacities prevail. The in-package chemistry model faithfully reproduces these trends and limits.

The in-package chemistry model combines two approaches to model uncertainty: (1) application of a factorial design approach to account for known large potential variations in model input (reactant combinations, water flux, fuel exposure, temperature, and seepage composition); and (2) sensitivity analysis of lesser known, not as well defined input variations (carbon dioxide fugacity, Carbon Steel Type A516 sulfur content, corrosion rates, extreme temperatures and flux values). Where the first approach provided the functional basis of the in-package chemistry model abstraction, the second approach provided the uncertainty ranges of the abstracted parameters. Thus, the information to be used in TSPA-LA directly incorporates uncertainty exterior to the in-package environment and interior to the in-package environment in a form that can be readily implemented in TSPA-LA (i.e., model uncertainty is propagated through the abstractions). Thus, the only restrictions on the subsequent use of the in-package chemistry model abstraction in TSPA-LA are that all of the abstractions must be applied within the stated limits (flux, temperature, fCO_2, and fuel exposure) as specified in *In-Package Chemistry Abstraction* (BSC 2004b).

The in-package chemistry model was validated in two parts. The general output of EQ3/6 was validated by comparison with field observations (BSC 2004b, Section 7). Specifically, the buffering capacity of the in-package environment was considered quantitatively and shown to be reasonable relative to similar natural cases. The reactions that cause long-term shifts from neutral pH in natural systems (e.g., acid generation from metal sulfide oxidation, alkalinity production by base silicate dissolution in the absence of atmospheric carbon dioxide) were shown to be absent in the in-package environment. The modeling of corrosion product surface chemistry was validated through expert review, which concurs that the surface effect approach is reasonable (BSC 2004b, Section 7).

3.8 SUMMARY

Based on the modeling results presented in *In-Package Chemistry Abstraction* (BSC 2004b), in-package chemistry is insensitive to initial water composition, fCO_2, decreased corrosion rate of the waste package alloys, and minor modifications to waste package design configuration. The major controlling factors include waste package type (commercial SNF versus codisposal waste package), water flux, fuel exposure (cladding failure) and temperature. The EQ3/6 calculations establish the range of in-package chemical compositions as dictated by dissolution and reprecipitation of solids. Effluent chemistries will be strongly affected by the presence of the surfaces of corrosion products (primarily iron oxides and hydroxides). Corrected for the effect of surface complexation on corrosion products, the in-package pH ranges from 4.5 to 8.1 for the nominal and seismic scenario classes. For the igneous intrusion scenario class, the pH is neutral to slightly basic (7.6 to 9.9). The ionic strength inside a waste package increases with time and can reach a value above 1 mol/L. Increasing temperature and carbon dioxide levels would favor decreased pH and vice versa. Higher temperatures cause a general shift in acid-base equilibria towards lower pHs. Carbon dioxide levels greater than ambient lower pH as well (both inside the waste form and in a basalt-dominated fluid).

INTENTIONALLY LEFT BLANK

4. COMMERCIAL SPENT NUCLEAR FUEL CLADDING DEGRADATION

Most commercial SNF is encased in Zircaloy cladding. Therefore, degradation of commercial SNF considers degradation of the Zircaloy cladding, which can fail either before or after emplacement at the repository. The cladding degradation model is implemented in all three scenario classes, although in the igneous intrusion modeling case of the igneous scenario, the cladding in the impacted drifts is assumed to provide no protection for the fuel. Hence, the only aspect of the cladding degradation model implemented in the igneous intrusion modeling case is calculating the surface area available for radionuclide diffusion from the waste form to the corrosion products in the waste package. The fuel rod cladding contained in drifts that are not affected by an igneous intrusion event are treated as those in the nominal scenario. A small fraction (1.04%) of fuel rods is encased in stainless steel cladding rather than Zircaloy cladding. The cladding model for these fuel rods is bounding in that the cladding is assumed to split along the entire length of the fuel rod when the waste package fails.

The relevant processes and assumptions supporting the cladding degradation model are presented below, followed by the cladding degradation model abstraction. A discussion of the sources of data, uncertainty, and model confidence building activities concludes this section. The primary sources of information for this section are *Clad Degradation–Summary and Abstraction for LA* (BSC 2003b), *Clad Degradation–FEPs Screening Arguments* (BSC 2004a), and *Seismic Consequence Abstraction* (BSC 2003c).

4.1 RELEVANT PROCESSES AND ASSUMPTIONS

Zircaloy cladding degradation due to general corrosion, localized corrosion (radiolysis-enhanced, pitting, crevice, and fluoride-enhanced), the presence of dissolved silica, creep rupture, internal pressurization, mechanical impact, diffusion-controlled cavity growth, rockfall, electrochemical effects, chemical effects, thermal expansion or stress of in-package components, stress corrosion cracking, and hydride embrittlement is not expected for repository conditions (BSC 2004a, Table 1-1). Some Zircaloy cladding will degrade before disposal, and those fuel rods that have degraded cladding will split when contacted by water as a result of the increased volume of corrosion products. Because naval SNF is considered to be commercial SNF for modeling purposes, naval SNF cladding is assumed to be affected by the same processes (BSC 2004a, Table 1-1).

The cladding degradation model consists of two phases: cladding failure (perforation) and the subsequent splitting of the cladding along the length of the fuel rod. The first phase, cladding perforation, is the formation of small cracks or holes in the cladding from various sources. In the absence of the cladding degradation mechanisms given above that are not expected for repository conditions, cladding perforations can occur (BSC 2003b, Section 5.2):

1. During reactor operation and subsequent storage (including other operations before being received at the repository)

2. In the repository by mechanical action resulting from seismic events that can occur at any time (i.e., the seismic scenario class)

3. In the repository from static loading of rock overburden once the drip shield and waste package have failed after the 10,000-year regulatory period.

In the nominal scenario, only the small fraction of Zircaloy cladding with preexisting defects (cause 1, above) is assumed to be perforated during the 10,000-year regulatory period. All stainless steel cladding is assumed to be perforated when the waste package fails. Perforation of cladding from seismic events (cause 2, above) is modeled exclusively in the seismic scenario class. Perforation of cladding from rockfall (cause 3, above) is part of the nominal scenario class but occurs after the 10,000-year regulatory period.

Once the cladding has been perforated and the waste package containing the perforated cladding has failed, the cladding is assumed to immediately split along the length of the fuel rod, exposing the fuel to corrosion. This is the second phase of cladding degradation and is shown in Figure 4-1. Corrosion of the fuel occurs primarily along the cladding-fuel interface and along fractures within the fuel matrix. In this phase, corrosion of the fuel forms secondary mineral phases composed of higher oxides of UO_2 (commonly called rind), causing the cladding split to widen further and creating a diffusion pathway for radionuclides and water. Perforation and splitting of cladding affects the diffusion of radionuclides from the rind into the corrosion products in the waste package.

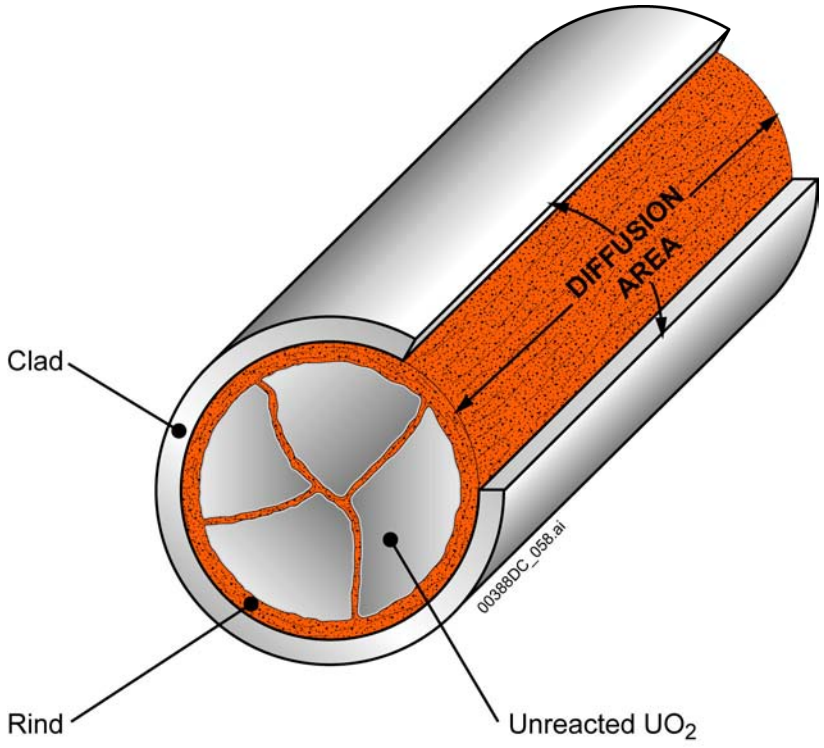

Figure 4-1. Fuel Rod Showing Cladding, Fractured Fuel, and Cladding Split

A small percentage (1.04%) of commercial SNF has stainless steel cladding instead of Zircaloy cladding. Stainless steel cladding was used in early core designs but is no longer used, so the quantity of stainless-steel-clad fuel is known and is unchanging. Stainless-steel-clad fuel rods are assumed to be perforated upon emplacement in the repository, making them immediately available for splitting lengthwise when the waste package fails (BSC 2003b, Section 6.2.2). It is assumed in this model that there is a finite probability that any delivery of fuel rods to the Yucca Mountain site containing stainless-steel-clad fuel rods will be loaded into two consecutive waste packages. This assumption is necessary because it addresses an absence of direct confirming evidence of how the waste packages are to be loaded. The basis of this assumption is that the stainless-steel-clad fuel is loaded into waste packages as it is received at the repository facilities to simplify surface facility operations. The model addresses the probability that for any stainless-steel-clad fuel delivery, the waste package being loaded could be near full and the remaining stainless-steel-clad fuel assemblies would then be loaded into a new waste package, increasing the number of waste packages containing stainless-steel-clad fuel assemblies. The shipments are not large enough to sequentially load three waste packages for a given delivery (BSC 2003b, Section 5.1).

Naval SNF cladding is modeled as commercial SNF cladding. Naval SNF has been found to be more robust than commercial SNF. Using a naval SNF source term developed by the Naval Nuclear Propulsion Program, the DOE estimated that the dose resulting from naval SNF is about four orders of magnitude less than that from an equivalent amount of commercial SNF (BSC 2001, Section 6). A planned classified Naval Nuclear Propulsion Program Addendum to the LA will provide details of this naval SNF source term. Therefore, using commercial SNF as a surrogate for naval SNF will overestimate radionuclide releases from naval SNF.

4.2 MODEL FOR DEGRADATION OF CLADDING

The model for degradation of commercial SNF cladding is presented in four parts:

- Fraction of cladding that is defective prior to placement in the repository
- Number of waste packages containing stainless steel cladding
- Mechanical failure of cladding after placement in the repository
- The area available for diffusion and volume of water available for UO_2 corrosion after the cladding has split.

The justification for the cladding degradation model used in TSPA-LA is based in large part on the exclusion of a number of processes considered unlikely to occur in the repository or to have an insignificant impact on repository performance. Some of the processes excluded from the cladding degradation model are general corrosion of cladding, localized corrosion from radiolysis, localized corrosion in pits and in crevices, creep rupture of cladding, stress corrosion cracking, and fluoride-enhanced localized corrosion of cladding. The basis for excluding these processes is given in *Clad Degradation—FEPs Screening Arguments* (BSC 2004a, Section 6).

4.2.1 Fraction of Cladding Perforated Prior to Placement in the Repository

The percent of fuel rods with cladding that has perforations prior to placement in the repository is given by a loguniform distribution with a range of 0.01% to 1% and a median value of 0.1. The loguniform distribution was selected because it gives equal weight to each decade of the full distribution. This failure rate is based on an analysis of reactor historical data by S. Cohen & Associates (1999, p. 2-31). It also includes defects from wet and dry storage at reactor sites and from handling of the waste packages. The as-received perforated fuel rods are available to undergo clad splitting and fuel-pellet corrosion once the waste package fails.

S. Cohen & Associates (1999, p. 2-31) concluded that damage of fuel during shipment, if any, will be minor. The rate of cladding perforation resulting from damage during handling at the repository surface facility is considered to be similar to that from damage during reactor operation and was estimated to be 0.0003% (S. Cohen & Associates 1999, p. 7-1) to 0.0005% (CRWMS M&O 2001a, Section 6.4.1).

4.2.2 Number of Waste Packages Containing Stainless-Steel Cladding

The fraction of fuel rods that have stainless steel cladding is 1.04% of the total commercial SNF inventory. Fuel with stainless steel cladding is placed into waste packages as it arrives at the repository. Assuming that deliveries of fuel with stainless steel cladding can be placed into either a single waste package or two consecutive waste packages results in 3.5% to 7% (uniformly distributed) of the waste packages containing stainless-steel-clad fuel rods (see Section 4.3). The percentage of stainless-steel-clad rods in a waste package is calculated in Equation 4-1 as:

$$\frac{\%\,\text{SS - clad rods in waste package} = (100\% \times 1.04\%)}{\%\ \text{of waste packages containing SS - clad fuel rods}} \qquad \text{(Eq. 4-1)}$$

Thus, waste packages containing stainless-steel-clad fuel rods will contain 15% to 30% stainless-steel-clad fuel rods, which are modeled as perforated and available for instantaneous splitting when the waste package fails.

4.2.3 Mechanical Failure of Cladding after Placement in the Repository

Once the fuel has been emplaced in the repository, intact cladding can be perforated as a result of seismic events that are modeled exclusively in the seismic scenario class (vibratory ground motion, fault displacement, and rockfall induced by ground motion) or as a result of the static load of a rock overburden. These two causes of mechanical failure are discussed below.

Seismic Events–The seismic events representing the seismic scenario class can occur at any time, and the effects of seismic activity on cladding integrity are developed and analyzed in *Seismic Consequence Abstraction* (BSC 2003c). Seismic events can damage fuel cladding in two ways: damage to the cladding from end-to-end impacts between adjacent waste packages and damage to the cladding from fault displacement. The end-to-end impact between two adjacent waste packages accounts for 87% of the mean damage to the waste package at the 10^{-6} per year ground motion level and 92% of the mean damage to the waste package at the 10^{-7} per

year ground motion level (BSC 2003c, Section 6.5.1.2). These results imply that the end-to-end impact of adjacent waste packages produces much more severe forces and accelerations than the side-on impact between a waste package and the emplacement pallet or drip shield.

In terms of peak ground velocity, the abstraction for damage to the cladding during a seismic event is a simple lookup table with a linear interpolation between the two points in Table 4-1, which shows that cladding is assumed to be 100% damaged if the peak ground velocity exceeds 1.067 m/s. The peak ground velocity values of 0.55 and 1.067 m/s correspond to mean annual exceedance frequencies of seismic events of 5×10^{-5} per year and 10^{-5} per year, respectively. There is no uncertainty in this abstraction because it represents a bounding estimate for cladding response at all values of peak ground velocity.

Table 4-1. Abstraction for Damage to the Cladding from Vibratory Ground Motion

Peak Ground Velocity Value (m/s)	Damage to Cladding (%)
0.55	0
1.067	100

Source: BSC 2003c, Table 18.

Static Load of Rock Overburden–Cladding perforation from the static load of rock overburden is modeled in two steps (BSC 2003b, Section 6.2.3):

1. Cladding perforation begins when both the fraction of drip shield patch openings (i.e., square areas of corrosion) and the fraction of waste package patch openings exceed the sampled uncertainty (0.2 to 0.5, uniform distribution).[2] Failure of the drip shield and the waste package from corrosion is not expected during the 10,000-year regulatory period and thus is not included in the cladding degradation model for this time period (BSC 2003b, Section 5.2).

2. After perforation commences, the fraction of cladding with perforations will depend linearly on only the fraction of waste package patches open (not the sum of waste package and drip shield patch fractions) until all the rods are perforated when an additional 50% of the waste package patches are open.

After there is no waste package or drip shield protection, a rubble bed of rocks from the collapse of the drift will mechanically load the bare fuel rods, which will perforate the cladding (CRWMS M&O 1999b, Section 6.2). Because there is epistemic uncertainty concerning how the waste package and drip shield will fail and when the weight of the rocks will be loaded onto the fuel, the equation describing the percent of rods with perforations in a waste package incorporates this uncertainty:

$$\% \text{ rods perforated} = 200 \times (PF - X) \qquad \text{(Eq. 4-2)}$$

[2] For the purpose of modeling spatial variability in waste package degradation, the surface of the waste package is divided into patches, each of which has an area of about 232 cm^2. The term "failure" means initial breach of the drip shield or waste package (BSC 2003i, Section 6.3.2 and Section 1).

where

PF = waste package patch fraction, in range $X \le PF \le X+0.5$
X = random number, uniformly distributed in range $0.2 \le X \le 0.5$

A submodel in the TSPA-LA model predicts when patches are corroded through, giving PF of Equation 4-2.

4.2.4 Split Cladding Geometry

Fuel rods whose cladding contained preexisting defects or has been damaged mechanically during a seismic event or from rock overburden are assumed to be instantly split (cladding splits down the length of the fuel rod) once the waste package has failed, leaving the fuel pellets exposed to the waste package internal environment and aqueous solutions (see Section 3). This assumption bounds the results of experimental observations, and has no uncertainty associated with it. It is based on fuel degradation tests performed at Argonne National Laboratory with two intentionally perforated fuel segments in steam at 175°C (Cunnane 2003). These test conditions are more severe than the repository conditions, where waste package surface temperatures are in the range of 105°C to 120°C at 500 years and the air is saturated with humidity but is not entirely steam. Both of the fuel segments split in less than two years, an extremely short time in terms of the postclosure repository time scale. As a result, in the TSPA-LA model the cladding instantly splits once it has been perforated and once the waste package has failed, leaving the fuel pellets exposed for corrosion.

After the cladding has split, the cladding still surrounds the fuel pellets and holds them into the original fuel geometry. Intact cladding is an engineered feature that prevents water from contacting and interacting with the fuel pellets. After the cladding has been perforated, it may still reduce radionuclide mobilization by limiting the exposed surface area of the fuel fragments and limiting the amount of water that can contact the pellet. The cladding degradation model abstraction considers the effect of cladding in reducing the exposed surface area through which radionuclides may be transported, but does not take credit for limiting the degree of corrosion or the amount of water that can contact the fuel (BSC 2003b, Section 6.1.1).

After the cladding splits, UO_2 in the fuel pellets along the complete length of the rod is available to corrode. The width of the split increases with time as the UO_2 corrodes to a secondary product, commonly called rind, which has an increased volume. The radionuclides diffuse through the split into the surrounding environment, as limited by the cladding.

The volume rind multiplier is the ratio of the rind volume to the UO_2 volume and accounts for the increase in volume from the formation of rind, which is schoepite ($UO_3 \cdot 2H_2O$). The volume rind multiplier is related to the porosity of schoepite, which is uncertain and assumed to be uniformly distributed between 0.05 and 0.3. Because of uncertainty in the porosity of schoepite, the value of the volume rind multiplier ranges from 2.8 to 3.8, with a mean value of 3.3, as given by Equation 4-3:

$$VRM = \frac{MW_{\text{sch}}}{D_{\text{sch}}} \times \frac{D_{\text{UO}_2}}{MW_{\text{UO}_2}} \times \frac{1}{1-\text{por}} \qquad \text{(Eq. 4-3)}$$

where

VRM = volume rind multiplier (unitless)
MW_{sch} = molecular weight of schoepite (322.1 g/mol)
D_{sch} = density of schoepite (4.9 g/cm^3)
MW_{UO_2} = molecular weight of UO_2 (270 g/mol)
D_{UO_2} = density of UO_2 (10.97 g/cm^3) and
por = porosity in schoepite (unitless).

The mass of the rind is increased from the UO_2 mass by the ratio of the molecular weights of the two minerals since water and oxygen are absorbed to form schoepite. Uncertainty in porosity is propagated through the model to uncertainty in diffusion parameters.

Both the corrosion rate of fuel (Section 5) and the amount of fuel corroded are calculated using the temperature and chemistry from the in-package chemistry model (Section 3).

The average distance for radionuclide diffusion from the rod to adjacent metallic corrosion products in the waste package is half of the rod diameter. The cross-sectional area for radionuclide diffusion from the rind in the failed rods to adjacent metallic corrosion products in the waste package is the product of rod length, split opening, and number of failed rods in a waste package.

For the igneous intrusion modeling case of the igneous scenario class, the cladding is destroyed by the intruding magma, and the radionuclides can diffuse through any place on the exposed fuel rod; thus, the average diffusion distance is one-fourth of the rind and UO_2 diameter. The diffusion area is the surface area of the rind and unreacted UO_2, although the split opening is now equivalent to the fuel and rind circumference.

After the waste package has failed and the relative humidity in the drift approaches 100%, water vapor will condense on the fuel and collect in the pores of the rind. The volume of water in the rind is used to calculate the mass of solubility-limited radionuclides released from the waste form, as discussed in Sections 5 and 6. The split continues to widen until all of the UO_2 in the rod corrodes, reaching a steady-state geometry. The time for complete corrosion of the rod depends on the waste package temperature and chemistry but generally takes less than 2,000 years (BSC 2003e, Section 6.4.3). Diffusion through the cladding split continues until all of the radionuclides are released.

4.3 SOURCES OF DATA AND PARAMETERS

There are many sources for data on cladding failure during reactor operation. Table 4-2 gives failure rates reported by various sources. Fuel reliability is reported every three years in the American Nuclear Society and International Atomic Energy Agency-sponsored International Topical Meeting on Light Water Reactor Fuel Performance. The Electric Power Research Institute also maintains data on fuel reliability during reactor operation as part of their Robust Fuels Program.

The model of the number of waste packages containing stainless-steel cladding was developed as follows. From *Stainless Steel in Waste Package for TSPA-SR* (DTN: *No. 7: In-Package*

Environment 4-8 June 2004 SN0001T0810599.008), 3.49% of the commercial SNF waste packages are modeled to contain 29.9% stainless-steel-clad fuel rods and 70.1% Zircaloy-clad fuel rods. The product of these two numbers is 1.04% and represents the total inventory of the commercial SNF with stainless steel cladding. However, *Stainless Steel in Waste Package for TSPA-SR* did not consider uncertainty associated with loading stainless-steel-clad fuel into waste packages. For the TSPA-LA model, uncertainty in loading of stainless steel-clad fuel into waste packages is accounted for by assuming that deliveries to the repository are always timed so that all deliveries require partial loading into a new waste package. With this assumption, the number of waste packages containing stainless-steel-clad fuel assemblies doubles to 7% and the stainless-steel-clad fuel rod content of these waste packages halves to 15%, yielding the (rounded) values given in Section 4.2.2.

Table 4-2. Comparison of Fuel Reliability from Various Sources

Fuel	Period	Reference	Failure Rate (%)
GE-8 × 8	1983	Andrews and Matzie 1985, p. 1-3	0.007
PWR-French	1979 to 1984 1984	Dehon et al. 1985, p. 2-24	0.001 to 0.01 0.005
BWR-Japan PWR-Japan	To 1997	Sasaki and Kuwabara 1997, pp. 13, 14	0.01 0.002
PWR-CE	To 11/1984	Andrews and Matzie 1985, p. 2-42, Table 2	0.011
All	Through 1984	EPRI 1997, p. 4-1	0.02 to 0.07
All	After 1984	EPRI 1997, p. 4-2	0.006 to 0.03
BWR PWR	To 1986	Sanders et al. 1992, p. I-36	0.10 to 0.73 0.07 to 0.48
PWR-Westinghouse	1 core, debris damage after steam generator replacement	McDonald and Kaiser 1985, p. 2-5	0.26
All	1969 to 1976	Manaktala 1993, pp. 3-2 and 3-3, Figure 3-1	0.01 to 2+
PWR-Mark B-B&W	1986 to 1996	Ravier et al. 1997, p. 34, Figure 4	0 to 0.055
BWR	2000	Edsinger 2000, p. 162	0.0005
BWR, GE Fuel	1995 to 1999	Potts 2000, p. 502, Figure 1	0.00058
PWR, Mitsubishi Fuel	1992 to 1999	Doi et al. 2000, p. 443	0 rod failures

NOTE: Failure rates are on a rod basis unless noted as assembly-based. The assembly value represents the percentage of assemblies that contain at least one failed rod. GE = General Electric.

The model of mechanical failure of the cladding during a seismic event is based on a study by Chun et al. (1987) that calculated g-loads for axial buckling and for yielding due to side drops. This data was used in Section 6.7 of *Seismic Consequence Abstraction* (BSC 2003c) to develop the abstraction of waste package perforation as a function of peak ground velocity.

The model of the split cladding geometry is based on simple geometric principles and constants (e.g., fuel pellet diameter, rod length, number of rods in an assembly) and physical constants (e.g., molecular weight and density of schoepite and UO_2). The porosity of schoepite is also used to calculate the split geometry as the pellet corrodes, and ultimately the amount of water used in the TSPA calculation. The porosity is uncertain with a range 0.05 to 0.3, uniformly distributed (DTN: LL010902212241.026).

4.4 UNCERTAINTIES, LIMITATIONS, AND MODEL CONFIDENCE

4.4.1 Uncertainties

The uncertainty in the fraction of fuel that is perforated as-received at the repository is based on observed fuel reliability from reactor operations and conservative predictions for other activities after removal from the reactor (BSC 2003b, Section 6.2.1). The fraction of commercial SNF that is clad in stainless steel is fixed and known, and no uncertainty in that fraction was considered. The input-loading pattern for the stainless-steel-clad fuel into waste packages is treated with uncertainty as described in Section 4.2.2.

Uncertainty in rind porosity and UO_2 corrosion rates, and chemical and temperature environments inside the waste package are treated in the TSPA calculations and produce an uncertainty in the rind geometry and diffusion of radionuclides from the fuel rind (BSC 2003b), Section 6.2.4). Since a bounding model (instantaneous splitting) is used, no uncertainty is used in the TSPA-LA model for clad splitting.

4.4.2 Limitations

The cladding degradation model has constraints and limitations (BSC 2003b, Section 1):

- The model is based on commercial water reactor fuel with Zircaloy cladding. Commercial gas-cooled reactor fuel from Fort St. Vrain is included in the inventory of DOE SNF and is, thus, not considered in the cladding degradation model.[3] (See Section 5.2.) Naval SNF is included in the cladding degradation model.

- Fuel reliability from reactor operation is determined for both PWRs and BWRs.

- The model is also limited to fuel exposed to normal operations and anticipated operational occurrences (i.e., events anticipated to occur within a reactor lifetime) and is not applicable to fuel exposed to severe accidents.

- The model applies to a repository design with the waste package surface temperature always less than 350°C. For higher waste package temperatures, cladding creep needs to be considered.

4.4.3 Confidence-Building

This section discusses the activities performed to generate confidence in the model during development. Confidence in the cladding degradation model is accomplished by corroborating model predictions with results of alternative mathematical models and (or) experimental data developed independently and available in the published literature and industry reports. This is done independently for each part of the cladding degradation model.

Confidence in Model of Fraction of Cladding Perforated Prior to Placement in the Repository–Model validation of the as-received cladding perforations is accomplished by

[3] DOE SNF is not considered in the cladding degradation model because it has no cladding.

validating model predictions with results of an alternative mathematical model and experimental data developed independently and available in the published literature and industry reports (BSC 2003b), Section 7.4.1). The alternative mathematical model (CRWMS M&O 2001a, p. 65) independently produced very similar results (median 0.095%; range 0.0155% to 1.29%) for the rod perforation rate for all causes. This is close to the model presented above (median 0.1%; range 0.01% to 1%), and builds confidence in the model of as-received cladding perforation. There also is justification of the use of technical information (as-received perforation rates) from S. Cohen and Associates (1999).

Confidence in the Model of Stainless Steel Clad Fuel–Assuming that all of the stainless steel clad fuel rods are perforated when placed in the waste packages is an upper limit. S. Cohen & Associates (1999, p. 2-22) estimated that only 0.005% to 1.4% of the stainless-steel-clad fuel rods actually had perforations. This reliability is close to that of the Zircaloy cladding and much less than the 100% perforation rate used in this model, thereby substantially overestimating the availability of UO_2 for corrosion.

The fraction of stainless steel cladding is well known, and since no current fuel manufacturer is using stainless steel, the quantity is fixed. An earlier alternative conceptual model (CRWMS M&O 1998a, Section 6.3.1.1) had the stainless-steel-clad fuel distribution mixed equally into all the waste packages. This is unlikely since the current surface design facility calls for loading waste packages as the fuel arrives on the site, and blending the stainless-steel-clad fuel is not planned. Assuming that a shipment of stainless-steel-clad fuel rods could be placed in two consecutive waste packages increases the percentage of waste packages containing stainless steel clad fuel from 3.5% to 7%, with a content ranging from 30% to 15%, respectively. The fraction of stainless-steel-clad fuel in a waste package represents a conservation-of-mass calculation and needs no validation.

Confidence in the Model of Mechanical Failure of Cladding in the Repository–Commercial SNF that was emplaced in the repository with intact cladding can be perforated only by mechanical failure, either from seismic events or from static loading of rocks once the drip shield and waste package have degraded. The model for cladding perforation from seismically induced ground motion is bounding and does not require further confidence building.

Confidence in the model for cladding perforation from static loading of rocks once the drip shield and waste package have degraded is obtained by comparison with experimental data. Wilmot (1981, Table VII) recommends the use of 71-g accelerations for the failure threshold for fuel rods experiencing side impacts and references an experimental threshold of 122 g for SNF. He notes that, in drop tests, rods were bent with end impacts of 38 g but did not fail. He references experimental thresholds for end impacts of 234 g. Fischer et al. (1987, Figure 8-3) suggested that 10% of the rods might fail with a 40-g end impact, and 100% might fail with a 100-g end impact. Witte et al. (1989, Table 3) report that the acceleration needed to perforate rods from side impact varies from 63 g to 211 g, depending on the fuel design. Sanders et al. (1992, Attachment III) present detailed structural analysis of various assemblies under impacts and give the probability of rod perforation from 9-m drops of transportation casks (Sanders et al. 1992, Attachment III, Table III-10). All these references show the robustness of spent fuel rods, thereby building confidence in the model that the rods break only from a significant amount of rock overburden.

The TSPA-LA model contains a submodel that predicts when square areas of the waste package surface will corrode through. It is intuitive that the waste package will offer some protection when the first patch opens and very little after the last one opens. The present model has the perforation of cladding start when 20% to 50% of the patches are open, which is reasonable. However, in the nominal case the waste package and drip shield will not fail from corrosion until after the 10,000-year regulatory period (BSC 2003b, Section 5.2). In the igneous case, all cladding is assumed to fail.

Confidence in the Split Cladding Model–The cladding instantaneously splits when both waste package and cladding perforations exist, leaving bare fuel pellets to react with the in-package environment. Model validation of the cladding splitting model is accomplished by a corroborating model. The cladding splitting model has predictions that bound results of experimental data developed independently and available in the published literature and industry reports (BSC 2003b, Section 7.4.3).

The rind model describes the release of radionuclides through the split opening along the cladding and accounts for the reduced radionuclide release compared to completely exposed fuel by simulating diffusion through a growing split. In this model, diffusion through a growing width of the split is modeled. The split diffusion surface area is treated as increasing with time as the split continues to open. Model validation of the rind model is accomplished by corroborating model predictions with results of experimental data developed independently and available in the published literature and industry reports (BSC 2003b, Section 7.4.3).

4.5 CONCLUSIONS

Most commercial SNF will be disposed of with Zircaloy cladding. Naval SNF is modeled in the TSPA-LA as Zircaloy-clad commercial SNF. At some time after emplacement, waste packages breach and the cladding on commercial SNF will be exposed to water or water vapor. Stainless steel cladding is assumed to split immediately upon exposure to water, while Zircaloy cladding is assumed to split if it had perforations prior to disposal, if it has been damaged by rockfall (following corrosion of the drip shield and waste package), or if it has been damaged by seismic events (for the seismic scenario class). The amount of UO_2 in any water inside the package influences the water chemistry to some extent. The percent of fuel exposed as a result of cladding failure was included in in-package chemistry calculations, as described in Section 3. For the nominal scenario, waste packages are expected to remain intact for at least 10,000 years except for those packages with cracks from manufacturing defects. Hence, only the fraction of fuel rods with cladding perforated prior to disposal can release radionuclides from those waste packages that have manufacturing defects during the 10,000-year regulatory period. That is, commercial SNF placed into the repository with unperforated cladding will remain intact for the 10,000-year regulatory period. Because the waste package and drip shield will not corrode significantly for more than 10,000 years, damage from rockfall following corrosion of the drip shield and waste package will not occur during the 10,000-year regulatory period.

For the seismic scenario, cladding is susceptible to mechanical failure from seismic events, depending on the nature and probability of the event, which can increase the number of perforated fuel rods. For the igneous intrusion scenario, the cladding is assumed to fail, allowing radionuclides to diffuse through the entire surface area of the failed fuel rod.

Once the cladding is perforated and water comes into contact with the underlying fuel, oxidation of the latter results in the formation of a fuel alteration product assemblage. This leads to further splitting of clad, followed by further fuel exposure, and so on until all the fuel is available for reaction. The cladding model assumes rapid splitting along the fuel rod. Degradation of the exposed fuel produces a rind whose volume, cross-sectional area for diffusion, diffusion distance, and width of split are estimated by the commercial SNF cladding degradation component. These parameters are used by the engineered barrier system transport submodel to determine the rate of diffusion of radionuclides into the corrosion products in the interior of the waste package.

5. WASTE FORM DEGRADATION MODELS

This section discusses the degradation processes for commercial SNF, DOE SNF and HLW glass, and presents a degradation model for each waste form. Commercial SNF will be disposed of in one of five different waste packages, as shown in Figure 2-2. DOE SNF (with the exception of naval SNF) and HLW will be disposed of together in codisposal waste packages, as discussed in Section 2. Relevant processes and modeling assumptions; data and supporting documents; and uncertainties, limitations, and model confidence regarding the waste form degradation models are discussed in this section. The primary sources of information for this section are *CSNF Waste Form Degradation: Summary Abstraction* (BSC 2003e), *DSNF and Other Waste Form Degradation Abstraction* (BSC 2003f) and *Defense HLW Glass Degradation Model* (BSC 2003g).

The degradation models for commercial SNF, DOE SNF and HLW glass calculate rates of radionuclide release from the waste form using input from other models (e.g., pH from in-package chemistry model discussed in Section 3). The output from these degradation models is used in other models (e.g., EBS transport) to estimate rates of radionuclide transport away from the waste form. The commercial SNF degradation model is discussed first, followed by the DOE SNF degradation model, and the HLW glass degradation model.

5.1 COMMERCIAL SPENT NUCLEAR FUEL DEGRADATION

PWR and BWR spent fuel assemblies will be placed in waste packages, with 12, 21, 24, or 44 assemblies per package, as indicated in Table 2-1. Such a packaging arrangement results in 7,472 packages containing PWR and BWR spent fuel assemblies. In addition, 300 packages of naval SNF are treated as if they were commercial SNF packages (see Section 5.2), yielding a total of 7,772 commercial SNF waste packages for the TSPA-LA model.

Once these waste packages are breached, the spent fuel will be exposed to either water or water vapor, and the commercial SNF rods with breached cladding will begin to degrade. The following model provides the commercial SNF degradation rate under conditions expected in the repository after the waste package and fuel cladding have been breached; degradation of cladding was discussed in Section 4.

When combined with the output from other models giving temperature, pH, total carbonate concentration and oxygen fugacity, this degradation model is used to calculate radionuclide release rates from commercial SNF in TSPA-LA calculations. The model is used to estimate radionuclide release rates from commercial SNF in scenarios that involve degradation of commercial SNF as a result of contact with water (see Section 1.2).

5.1.1 Degradation Processes

The following discussion of the degradation processes that are expected to affect commercial SNF in the repository is summarized from *CSNF Waste Form Degradation: Summary Abstraction* (BSC 2003e). The availability of individual radionuclides for dissolution, once the waste package and fuel cladding are breached, is limited by the structure, microstructure, and physiochemical properties of the irradiated fuel, as well as the distribution of fission products in the fuel rods. Most radionuclides, and essentially all of the rare earth and actinide radionuclides,

are retained in the fluorite structure of the fuel matrix. Transition metals are partly partitioned into metallic phases embedded in fuel grains and at the fuel grain boundaries. This part of the radionuclide inventory (present either as a solid solution in the fuel matrix or embedded as discrete phases in the fuel grains) is not available for dissolution until the fuel matrix is dissolved or otherwise altered, and is referred to as the matrix inventory. On the other hand, some fission gasses and more volatile radionuclides (i.e., cesium, strontium, iodine, and technetium) migrate out of the matrix during in-reactor operations. These accumulate in locations collectively referred to as the gap region (i.e., the interface between the pellets and the cladding, the rod plenum regions, and pellet fracture surfaces), while some accumulate at grain boundaries. The radionuclide inventory that is not a part of the matrix is called the gap and grain boundary inventory, and can be released rapidly once the cladding is breached (BSC 2003e).

Once the waste package and cladding have been breached, oxidation and degradation of the commercial SNF matrix will proceed. If the temperature exceeds approximately 230°C to 250°C, the degradation will proceed via solid-state reactions (CRWMS M&O 2000d). As the temperature decreases below this range, the relative humidity to which the commercial SNF matrix is exposed increases. The presence of water vapor complicates the oxidation process by facilitating formation of hydrated oxidation products (see Figure 5-1). Not only are the reaction products different in the presence of water vapor, but the rates and mechanisms for reaction differ as well (Aronson 1958, p. 94; Taylor et al. 1989); McEachern and Taylor 1998, Section 2.2). While high-temperature steam does not oxidize UO_2, humidity can influence air oxidation by forming hydrated uranyl phases (e.g., by hydrous disproportionation of U_3O_8), by supporting oxidative dissolution in water films that form on the surface at higher relative humidities, by enhancing grain-boundary oxidation in spent fuel, and by supporting radiolytic processes at grain boundaries. Because gas phase diffusion is rapid along the connected porosity at grain boundaries in spent fuel the oxidation of spent fuel can be considered to proceed simultaneously at grain boundaries throughout the fuel when it is exposed to humid air. This grain-boundary corrosion and associated decohesion of the fuel grains is likely to occur rapidly if commercial SNF pellets are exposed to humid air at temperatures greater than 100°C. The effects on the fuel are some bulk oxidation of the commercial SNF fuel grains and a very large increase in the specific surface area of the fuel as it disaggregates into grain-sized powders.

The commercial SNF corrosion process in humid air at temperatures less than 100°C is best characterized as an oxidative dissolution process in a film of water at the fuel surface, rather than an interaction between water vapor and oxygen in the air that accelerates the solid-state oxidation process. Thus, the commercial SNF degradation model discussed below assumes that oxidation followed by dissolution of commercial SNF in water or humid air at temperatures below 100°C is the degradation process relevant to repository conditions (BSC 2003e, Section 6.2.2).

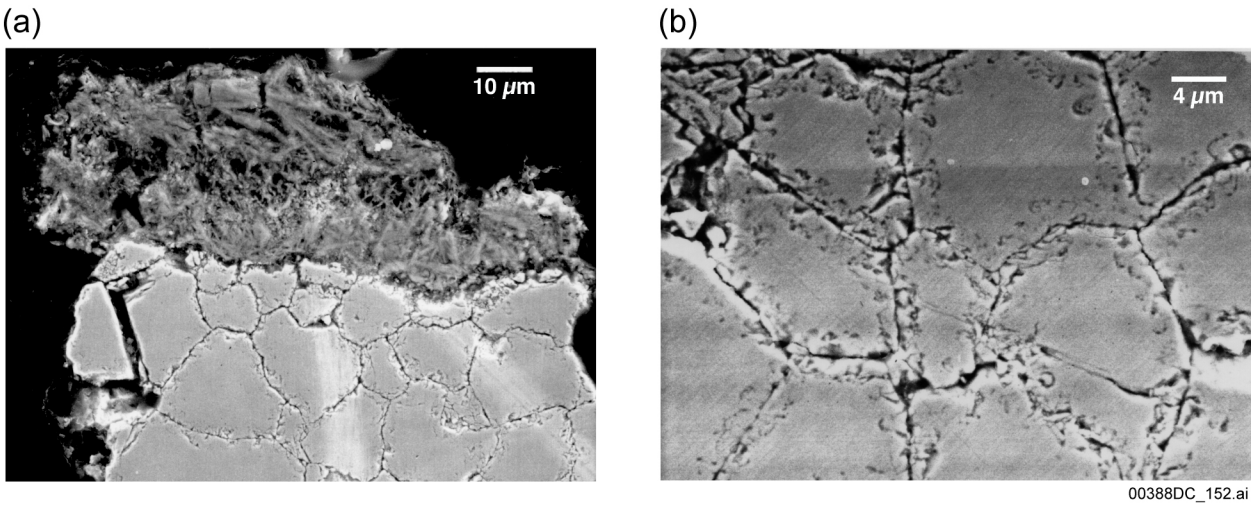

Source: BSC 2003e, Figure 6.2-2.

NOTE: (a) Backscattered-electron image of a polished section through a fuel particle (bright contrast) from a high drip rate experiment with a corrosion layer (intermediate contrast) predominantly composed of Na-boltwoodite (ATM-103 high drip rate 3.7 years). (b) Backscattered-electron image of a section showing curvilinear features at fuel-grain boundaries, which may result from dissolution along defects. The darkest contrast (black) is epoxy.

Figure 5-1. Scanning Electron Microscopy Images of Corroded Commercial SNF Fuel

5.1.2 Commercial Spent Nuclear Fuel Degradation Model

For modeling purposes, the radionuclide inventory in commercial SNF rods is divided into two fractions: (1) the combined gap and grain boundary inventory and (2) the matrix inventory. Separate models are developed for estimating radionuclide releases from the gap and grain boundary and from the matrix because the processes that control these releases are different.

5.1.2.1 Model for Release of Gap and Grain Boundary Inventory

The gap inventory is available for immediate dissolution when the cladding is breached. Therefore, release of the gap inventory is instantaneous upon contact of the breached fuel with water or water vapor. There is some uncertainty regarding the applicable degradation and release mechanisms for the grain boundary inventory. However, the grain boundary inventory is combined with the gap inventory in estimating the instantaneous release fraction.

The inventory available for instantaneous release of the gap and grain boundary inventory is expressed as a fraction of the total inventory of radionuclide *i* in the fuel (BSC 2003e, Section 1):

$$I_i^G = f_i \times I_i \qquad \text{(Eq. 5-1)}$$

where

I_i^G = gap and grain boundary inventory of radionuclide *i* available for instantaneous release (g)
f_i = instantaneous release fraction
I_i = total inventory of radionuclide *i* in the fuel (g)

The total inventory of each radionuclide *i* in the fuel (I_i) is given in Table 2-3; uncertainty in these inventories is given in Table 2-4. Instantaneous release fractions of these radionuclides are also uncertain; empirical probability distributions for instantaneous release fractions of ^{137}Cs, ^{129}I, ^{99}Tc, and ^{90}Sr are shown in Table 5-1 and were derived from measured gap and grain boundary inventories (Gray et al. 1992; DTN: LL000107951021.107).

Table 5-1. Triangular Probability Distribution Functions of Instantaneous Release Fraction

	^{137}Cs (%)	^{129}I (%)	^{99}Tc (%)	^{90}Sr (%)
Apex	3.63	11.24	0.10[a]	0.09
Minimum	0.39	2.04	0.01[b]	0.02
Maximum	11.06	26.75	0.26	0.25

Source: BSC 2003e, Table 8.1-1.

NOTE: [a] Rounded up from 0.06.
[b] Changed from zero to provide a nonzero minimum.

Table 5-1 shows that most of the inventory of fission gasses and volatile radionuclides remains in the matrix. This is especially true for ^{99}Tc and ^{90}Sr, where, at most, 0.26% and 0.25% of the inventory is in the gap and grain boundary, respectively. The radionuclide with the highest fraction of inventory in the gap and grain boundary is ^{129}I, where a maximum of 26.75% of the inventory can reside in the gap and grain boundary.

5.1.2.2 Model of Radionuclide Release from Matrix

The matrix radionuclide inventory cannot be released into the water until the matrix degrades. The key assumption in the matrix degradation model is that it results from oxidative dissolution of the fuel matrix in a film of water on the fuel surfaces (BSC 2003e, Section 6.2.2). The process of oxidative dissolution begins with the oxidation of uranium in the +4 oxidation state, uranium(IV), to uranium in the +6 oxidation state, uranium(VI), followed by the dissolution of uranium(VI) in the film of water. The likely electrochemical reaction sequence for this process is:

$$UO_2 \rightarrow UO_{2+x} \rightarrow UO_{2.33} \xrightarrow{\text{surface oxidation}} \{UO_2^{2+}\}_{surface} \xrightarrow{\text{bulk oxidation}} [UO_2^{2+}]_{bulk} \xrightarrow{\text{dissolution}} [UO_2^{2+}]_{soln} \rightarrow \text{Secondary Phases}$$

Three types of dissolution measurements have been made; flow-through, static (batch), and drip tests. The purpose of the flow-through dissolution studies was to examine the systematic effects of temperature and water chemistry on the forward dissolution rates of the UO_2 matrix in both unirradiated UO_2 and spent fuel. The forward reaction rate entails UO_2 corrosion/oxidation and detachment of uranium(VI) from the mineral lattice. The intrinsic dissolution rates of UO_{2+x} and spent fuel were determined by using a single-pass flow-through reactor that allows UO_2 dissolution to be measured far from solution saturation (no precipitation of dissolved products). Note that the forward dissolution rate bounds the release rate, the latter being the material loss rate from the fuel plus alteration products.

Another key assumption is that the fractional rate of radionuclide release from the commercial SNF matrix is equal to the fractional rate of oxidative dissolution of the matrix. The rate of radionuclide release from the matrix is expressed as (BSC 2003e, Section 1):

$$R_i = I_i^M \times F \qquad \text{(Eq. 5-2)}$$

where

R_i = rate of release of radionuclide i from the matrix (g/day)
I_i^M = matrix inventory of radionuclide i (g)
F = fractional dissolution rate of the fuel (per day)

The radionuclide release rate given in Equation 5-2 is used in the TSPA-LA model to provide the mass of a particular radionuclide available for dissolution into the volume of water available for radionuclide dissolution in the rind during a particular period of time (e.g., during a time step in a simulation). The concentration of a given radionuclide in water exiting the waste form is equal to the dissolved concentration of that radionuclide plus the concentration of that radionuclide attached to or embedded in colloids. The dissolved concentration of a given radionuclide is equal to its elemental solubility limit if one exists (see Section 6), as apportioned among the various isotopes of that element, if sufficient quantities of the radionuclide are available for dissolution. If sufficient quantities are not available, then the concentration in solution is equal to the mass available from waste form degradation divided by the water volume (i.e., the volume of the rind times the porosity of the rind). The dissolved concentration of a radionuclide that does not have an elemental solubility limit is equal to the mass released from the waste form during a given time step divided by the water volume. Commercial SNF is not a source of colloids although radionuclides released from the commercial SNF can attach to colloids generated elsewhere, as discussed in Section 7.

The following model for radionuclide release from the fuel matrix calculates F; the matrix inventory of radionuclides (I_i^M) is given by subtracting the gap and grain inventory calculated above from the commercial SNF inventory given in Table 2-3. The equation describing the model for radionuclide release from the fuel matrix is given as a piecewise-continuous function over the acidic and basic pH regimes (BSC 2003e, Sections 1 and 6.4.1.2):

$$\log(F) = \log(A) + a_0 + a_1 \times IT + a_2 \times p\mathrm{CO_3} + a_3 \times p\mathrm{O_2} + a_4 \times \mathrm{pH} \qquad \text{(Eq. 5-3)}$$

where

F = fractional dissolution rate of the fuel (1/day)
a_0, a_1, a_2, a_3, and a_4= model parameters determined from experimental data
A = effective specific surface area of the fuel (m^2/mg)
IT = inverse temperature (K^{-1})
$p\mathrm{CO_3}$ = negative log of the total carbonate molar concentration
$p\mathrm{O_2}$ = negative log of the oxygen fugacity
pH = negative log of the hydrogen ion molar concentration

The degradation of commercial SNF is thus a function of temperature, pH, $p\mathrm{CO_3}$, and $p\mathrm{O_2}$ and is valid for ranges of experimental conditions under which data were collected. The burnup of the

fuels used for the experiments ranged from 15 to 65 MWd/kgU for burnup, and the experimental conditions from 2 to 10 for pH, 0.002 to 0.2 atm for oxygen fugacity, 2×10^{-4} to 2×10^{-2} mol/L for carbonate/bicarbonate concentrations, and 23°C to 90°C for temperatures (BSC 2003e, Section 1). Results of tests conducted on commercial SNF (summarized in Section 5.1.3) were used to determine the values of the model parameters (A, a_0, a_1, a_2, a_3, and a_4) for both alkaline conditions and acidic conditions (BSC 2003e, Section 6.4.1), reflecting the functional dependence of the commercial SNF degradation rate on these environmental factors. The parameter values for both alkaline and acidic conditions are given in Tables 5-2 and 5-3, respectively.

Table 5-2. Parameter Values and Associated Characteristic Values of the Uncertainty Distributions for the Alkaline Conditions Model

Model Parameter	Parameter Value	Uncertainty Distribution Characteristic Values
log(A)	−6.50	Triangular distribution: Minimum = −7.3 Apex = −6.5 Maximum = −5.4
a_0	4.705	0.601[a]
a_1	−1093.826	186.829[a]
a_2	−0.102	0.0471[a]
a_3	−0.338	0.0506[a]

Source: BSC 2003e, Table 8.1-2.

NOTE: [a] Estimated standard errors from regression analyses performed using Excel.

Table 5-3. Parameter Values and Associated Characteristic Values of the Uncertainty Distributions for the Acidic Conditions Model

Model Parameter	Parameter Value	Uncertainty Distribution Characteristic Values
log(A)	−6.50	Triangular distribution: Minimum = −7.3 Apex = −6.5 Maximum = −5.4
a_0	6.60	0.67[a]
a_1	−1093.826	NA[b]
a_3	−0.338	NA[b]
a_4	−0.340	0.110[a]

Source: BSC 2003e, Table 8.1-3.

NOTE: [a] Estimated standard errors.
[b] Values for these estimated standard errors were taken from the alkaline conditions model and have no associated standard errors in the context of the acidic conditions analysis.

The acidic-conditions model is used when the pH is less than 6.8, and the alkaline-conditions model is used when the pH is equal to or greater than 6.8. Note that pH is not included in the model under alkaline conditions (i.e., $a_4 = 0$ in the alkaline-conditions model). The regression analyses indicated that pH was not a significant factor in the dissolution rate in a pH range of 8 to 10; therefore, it was removed from the alkaline-conditions model. In addition, carbonate concentrations are very low under acidic conditions (see Section 3). Therefore, total carbonate concentration was removed from the acidic-conditions model (i.e., $a_2 = 0$ in the acidic-conditions model).

The commercial SNF degradation rates and model dependencies on temperature and pO_2 are shown in Figure 5-2 for a fixed pCO_3 of 2.7. pH and temperature dependencies of the model are illustrated in Figure 5-3, which shows how long it takes for the commercial SNF matrix to degrade completely once the cladding is breached. For all curves in Figure 5-3, the fO_2 is 0.2 atm, the total carbonate concentration is 2×10^{-2} mol/L, and the value of log(A) is −6.50. As shown in this figure, for these nominal values, it will take between 90 and 1,800 years for the commercial SNF matrix to degrade completely. Under the acidic conditions expected in waste packages containing commercial SNF (see Chapter 3), the degradation rate is most sensitive to pH. Above a pH of 6.8, where the alkaline model parameter values are used, the degradation rate is most sensitive to oxygen fugacity and temperature (BSC 2003e, Section 6.4.1.2).

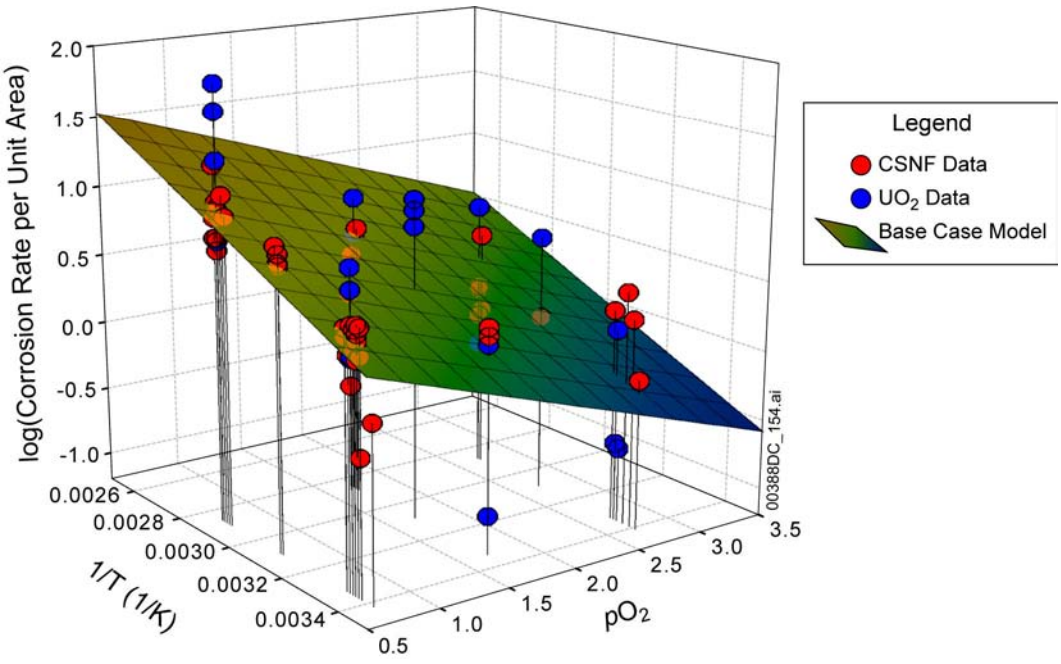

Source: BSC 2003e, Figure 6.4-1.

Figure 5-2. Base Case Model Plotted against Commercial SNF Degradation Data and UO_2 Data

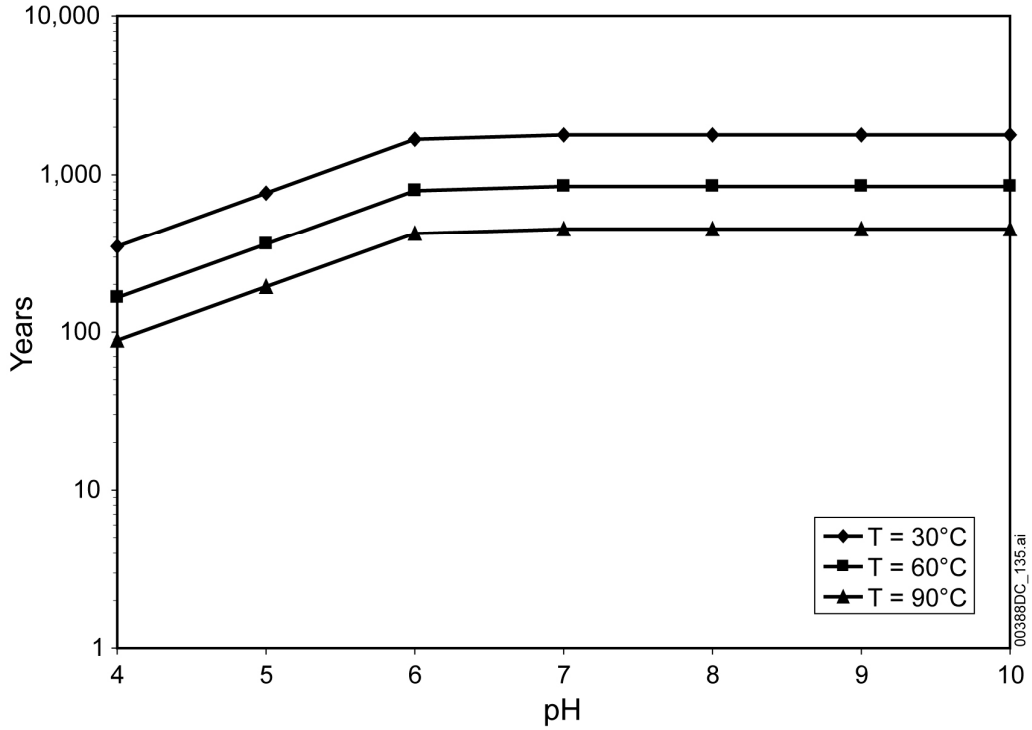

Source: Equation 5-3 and Tables 5-2 and 5-3.

NOTE: fO_2= 0.2 atm, $[CO_2]= 2 \times 10^{-2}$ mol/L, and log(A) = −6.50

Figure 5-3. Time after Cladding Breach until Commercial Spent Nuclear Fuel Matrix Degradation Complete as a Function of pH

5.1.3 Tests Conducted on Commercial Spent Nuclear Fuel

Several different tests were conducted on commercial SNF by various researchers to provide data that form the basis for the commercial SNF degradation model (Gray et al. 1992; Gray and Wilson 1995; Stout and Leider 1998; CRWMS M&O 2000e; Thomas 2003; Goldberg 2003). These tests are summarized next and are described in more detail in *CSNF Waste Form Degradation: Summary Abstraction* (BSC 2003e, Sections 4.1 and 6.3).

Gray et al. (1992) measured the gap and grain boundary inventories of cesium, strontium, iodine, and technetium (DTN: LL000107951021.107). Tests were run on light water reactor spent fuel, and results were given in terms of percentage of total inventory of these four radionuclides in the gap region and percentage of total inventory in the grain boundaries. These data were used to develop the model for release of the gap and grain boundary inventory.

Commercial SNF, in the form of grain-sized powders, was tested in single-pass, flow-through dissolution studies to provide the parametric dependence of the matrix dissolution rate over a range of conditions that span anticipated conditions at the repository (DTNs: MO0302PNLDUFTD.000; MO0304PNLLPHDD.000; Gray and Wilson 1995; Stout and Leider 1998). In these studies, the principal test response was the specific oxidative dissolution rate of the matrix. The data set spans a wide range of dissolution conditions, with pH ranging from 2 to 10, the pO_2 ranging from 0.002 to 0.2 atm, the temperature ranging from 23°C to 78°C, and carbonate/bicarbonate concentrations ranging from 2×10^{-4} to 2×10^{-2} mol/L.

In addition to commercial SNF, unirradiated UO_2 was also tested in these flow-through dissolution studies under alkaline conditions (DTN: LL030300112241.027). The UO_2 data are pertinent because the dissolution behavior of unirradiated UO_2 may be similar to the behavior of commercial SNF after the ^{137}Cs and ^{90}Sr have decayed and the associated radiolysis effects are no longer present (BSC 2003e, Section 6.4.1.1). The data are suitable for determining the functional dependence of the oxidative dissolution rate of the commercial SNF matrix on environmental factors.

Another set of tests examined fractional radionuclide release rates from fuel fragments from which cladding had been removed (DTNs: LL991001251021.090 and MO0301ANLSF001.451; CRWMS M&O 2000e; Thomas 2003). These fragments were exposed to one of two unsaturated test conditions, either the "high drip rate" or the "low drip rate," with water that had been equilibrated with tuff at 90°C (i.e., EJ-13 water). All tests were run at 90°C, and some tests have been run for more than eight years and are still underway. In these tests, the sources of oxygen for oxidative dissolution were as follows: air was dissolved in the water and introduced into the test vessel; air was present in the vessel void volume; and air was injected into the vessel as part of each twice-weekly injection cycle. These tests were designed to emulate a scenario in which dripping water in a failed waste package reacts with the fuel, dissolves soluble components and forms solid corrosion products. The data produced by these tests were used to estimate the effective surface area scaling factor.

In addition, five tests were conducted on short segments of fuel rods (1.4 to 3.7 inches long) (DTN: MO0301ANLSF001.450). In the tests, conducted at 90°C, EJ-13 water (evaporated J-13 water) was allowed to percolate under a low-hydraulic head through the fuel rod segment, with the effluent used to determine radionuclide release. The test configuration, matrix, and methodology are described in the data report (Goldberg 2003), together with the data. The tests began in February 1999 and are still underway. The data produced by these tests were also used to estimate the effective surface area scaling factor. The drip tests provide an effective means for identifying the reaction paths that may be relevant to long-term corrosion of spent fuel. They also broaden the conceptual understanding of the general controls over fuel degradation. One primary conclusion of the drip tests is that the secondary phase assemblages seen in the laboratory are broadly similar to the ones seen at natural analogs (see Section 5.1.4.3).

In summary, the following components of the commercial SNF degradation model are based on the following tests.

- Gap and grain boundary inventory is based on laboratory measurements of light water reactor SNF gap inventory and grain boundary inventory (Gray et al. 1992).

- The parametric dependence of the matrix dissolution rate on environmental conditions is based on single-pass, flow-through dissolution studies performed on commercial SNF in the form of grain-sized powders (Gray and Wilson 1995; Stout and Leider 1998) and on unirradiated UO_2 (DTN: LL030300112241.027).

- The effective surface area scaling factor is based on unsaturated drip tests run on fuel fragments from which cladding had been removed (CRWMS M&O 2000e, Thomas

2003) and on rod segment tests through which water percolated under a low hydraulic head (Goldberg 2003).

5.1.4 Uncertainties, Limitations, and Model Confidence

The commercial SNF degradation model is valid for the pH, pO_2, and pCO_3 ranges expected in the waste package (see Section 3) and for temperatures between 23°C and 90°C (BSC 2003e, Sections 1 and 4.1). The model is also valid for exposure to humid air and exposure to dripping water. Uncertainties associated with the model and model confidence building are summarized next.

5.1.4.1 Uncertainty in Release of Gap and Grain Boundary Inventory

The gap and grain boundary inventory of ^{137}Cs, ^{129}I, ^{99}Tc, and ^{90}Sr is uncertain, thus, the instantaneous release fractions for these radionuclides are uncertain parameters. The uncertainty is believed to be mostly aleatory and associated with factors such as linear power history, grain size and burnup that influence fission product migration during in-reactor operation, thereby affecting the gap and grain-boundary inventories of the above isotopes. The available data, shown in Table 5-4, were analyzed to determine ranges, and plausible probability distribution functions in these ranges, for the gap and grain-boundary inventory fractions (f_i). A triangular probability distribution function is used to represent uncertainty in the instantaneous release fractions. This distribution function spans the available data set, as shown in Table 5-1.

5.1.4.2 Uncertainty in Release of Matrix Inventory

Uncertainties in the mathematical form of the matrix degradation model and its validity over the extended time domain of application were addressed by examining model consistency with the current understanding of the oxidative dissolution mechanism that degrades the fuel under the range of plausible repository conditions. Comparison of the model with mechanistically based alternative models provided confidence that this empirically based modeling approach is appropriate for use in long-term predictions of commercial SNF matrix degradation. Graphically, Figure 5-2 gives an idea of the uncertainty associated with the model.

Uncertainties in parameter values (i.e., a_0, a_1, a_2, a_3, and a_4) are expressed as standard errors obtained from regression analyses and summarized in Tables 5-2 and 5-3. Propagating the standard errors in each of these terms through the model results in a standard error in R_i (from Equation 5-2) of plus or minus 6.4 (i.e., a factor of 6.4) for the alkaline-conditions model, and of plus or minus 4.0 (i.e., a factor of 4.0) for the acidic-conditions model. Uncertainty in the effective specific surface area of the fuel (A) is expressed as a triangular distribution, as shown in Tables 5-2 and 5-3.

In addition, uncertainties in the parameter values are correlated with each other, as defined in the covariance matrix given in Attachment II of *CSNF Waste Form Degradation: Summary Abstraction* (BSC 2003e). The Cholesky decomposition of the covariance matrix is used to generate uncertain regression coefficients, which are used in TSPA-LA to produce uncertain values of the parameters a_0, a_1, a_2, a_3, and a_4.

Table 5-4. Summary of the Gap and Grain Boundary Inventory Data

	Cesium		Technetium		Strontium		Iodine	
FGR(%)	GI(%)	GBI(%)	GI(%)	GBI(%)	GI(%)	GBI(%)	GI(%)	GBI(%)
1.1	1.2	0.2	-2.3×10^{-4}	5.00×10^{-2}	4.10×10^{-4}	2.00×10^{-2}		
7.85	0.72	1.16	0.00	7.70×10^{-2}	8.70×10^{-5}	2.00×10^{-2}		
7.85	0.85	0.39	-1.90×10^{-4}	5.40×10^{-2}	3.90×10^{-4}	6.30×10^{-2}		
7.85	2.23						1.55	5.3
7.85	1.55						3.34	
7.85		0.62						
0.59	0.21	0.l8		6.60×10^{-2}	2.00×10^{-4}	7.80×10^{-2}	0.03	
0.59	0.28						0.12	
0.59		0.74						2.01
7.4	1.92						0.1	8.5
7.4	3.25	0.56	0.139	−0.190	0.116	0.035		
7.4		0.74						
7.4		0.72						8.87
11	2.49	1	0.015	0.011	0.0229	0.13		
11	2.32		8.2×10^{-3}		1.22×10^{-2}			
11	3.25						1.48	7.65
11	3.04						1.1	
11		0.77						
11		0.83						9.35
18	4.11	0.88	0.0527	0.115	0.0939	0.069		
18	4.84		0.0245		0.0391			
18	7.11						17.4	7.35
18	9.9						11.8	
18		1.05						
18		1.15						8.1
Average	2.90	0.73	0.03	0.03	0.03	0.06	4.10	7.14
Maximum	9.90	1.16	0.14	0.12	0.12	0.13	17.40	9.35
Minimum	0.21	0.18	0.00	0.00	0.00	0.02	0.03	2.01

Source: BSC 2003e, Table 6.3-1. DTN: LL000107951021.107.

Notes: FGR = fission gas release; GBI = grain-boundary inventory; GI = gap inventory.

There are several sources of uncertainty in the data used to develop the matrix degradation model: measurement uncertainties, uncertainties in the test conditions, and uncertainties in the extent to which the test conditions and test configuration are relevant to in-service scenarios likely to occur in the repository. *CSNF Waste Form Degradation: Summary Abstraction* (BSC 2003e, Section 6.4.1.4) discusses these uncertainties and how they affect the matrix degradation model. Uncertainties that can be quantified are addressed by incorporating them into the uncertainty distribution of effective specific surface area (Tables 5-2 and 5-3). Uncertainties associated with the extent to which the input data may cause the model to be systematically biased are addressed by comparison against other models. Such a comparison is discussed in Section 5.1.4.3.

The degradation rates for commercial SNF may be biased high because all tests have been performed on fresh fuel (i.e., fuel out of the reactor for less than 20 years), although the magnitude of this bias is uncertain (BSC 2003e, Section 6.4.1.1). As reported by Tait and Luht

(1997, Figure 16 and p. 23), the associated β- and γ-radiation fields for this fuel may increase the dissolution rate in air-saturated water.

5.1.4.3 Model Confidence

Building confidence in the commercial SNF degradation model involves presenting technical evidence that the model predicts the commercial SNF degradation rate and the associated radionuclide release rate at an adequate level of confidence. To build confidence in the model, it was compared to data published in referred journals and industrial literature, alternative mathematical models, and natural analogs. These comparisons are summarized next.

Fractional radionuclide release rates estimated by the commercial SNF degradation model were compared to multiple sets of published literature on the fractional release rates of radionuclides measured under air-saturated dissolution conditions (Wilson 1990a; Forsyth 1997; Tait and Luht 1997; de Pablo et al. 1999; Torrero et al. 1997). To facilitate comparison of calculated radionuclide release rates and measured radionuclide release rates, an error metric was used. The error metric equals $\log(F_c/F_m)$ where F_c is the calculated fractional release rate (or calculated dissolution rate per unit area) and F_m is the measured fractional release rate (or measured dissolution rate per unit area). The absence of systematic modeling bias is indicated by values of the error metric centered at zero, with most values of the error metric expected to be between −1 and 1. The average error metric is 0.17, indicating a systematic modeling bias that slightly overestimates radionuclide release rates, although the mix of positive and negative values of the error metric indicates that this bias is slight. These results show overall good agreement between the experimental data and the model-calculated results.

Two alternative conceptual models for the dissolution of commercial SNF under alkaline conditions have been developed: the electrochemical model (Shoesmith 2000; Johnson et al. 1996; Grambow et al. 2000; Dehaudt 2001a; Dehaudt 2001b; Jégou et al. 2001; Pelletier 2001; Piron 2001) and the surface complexation model (de Pablo et al. 1999). The alkaline model was compared to these alternative models by evaluating the dissolution rates calculated by each model for a set of nominal repository conditions: a fO_2 of 0.2 atm, a total carbonate concentration of 2.00×10^{-3} mol/L, and a temperature of 30°C. The details of this comparison are given in *CSNF Waste Form Degradation: Summary Abstraction* (BSC 2003e, Section 7.2), and the results are shown in Table 5-5.

Table 5-5. Comparison of Commercial Spent Nuclear Fuel Dissolution Model to Alternative Models

Model	Calculated Dissolution Rate (mg/m^2·day)
Alkaline Commercial SNF Dissolution Model	3.8
Surface Complexation Model	2.4
Electrochemical Model	12.1

Source: BSC 2003e, Table 7.2-1.

The results in Table 5-5 show good agreement between the commercial SNF dissolution model and the surface complexation model. The dissolution rates calculated by the electrochemical model are about a factor of five larger than the rates calculated by the other two models. This is

well within the standard error range of the alkaline-conditions model (plus or minus 6.4 times the calculated dissolution rate).

To establish confidence that experimental commercial SNF alteration pathways effectively represent likely natural processes, it is useful to compare the alteration mineralogy observed in experiments with natural occurrences of altered uranium oxides. Uranium dioxide occurs in nature as the mineral uraninite, which is structurally similar to commercial SNF. Nopal I, a uranium mining site at Peña Blanca, Mexico, contains substantial quantities of uraninite and is arguably one of the best natural analogs for commercial SNF degradation in Yucca Mountain, as it possesses geologic, geochemical, and hydrogeologic characteristics most similar to those at Yucca Mountain (Murphy 1995). The volcanic (tuffaceous) host rock at Nopal I, the youngest of the studied sites, has been relatively oxidizing for tens of thousands of years, though uraninite, containing U^{4+}, was originally formed several million years ago. The uranium minerals found at Nopal I are listed in Table 5-6 (Pearcy et al. 1994).

Table 5-6. Paragenesis of Uranium Minerals at Nopal I

Mineral	Nominal Chemical Formula
Oxide Uraninite	UO_{2+x}
Oxyhydroxides Lanthinite	$U^{4+}(U^{6+}O_2)_5(OH)_{14}\cdot 3H_20$
Schoepite/ Dehydrated Schoepite	$UO_3\cdot 2H_20$ $UO_3\cdot nH_2O(n< 2)$
Becquerelite	$Ca(UO_2)_6O_4(OH)_6\cdot 8H_2O$
Billietite(?)/ Abernathyite(?)	$Ba(UO_2)_6O_4(OH)_6\cdot nH_2O(n=4\text{-}8)$ $K(UO_2)(AsO_4)\cdot 4H_2O$
Silicates Soddyite	$(UO_2)_2SiO_4\cdot 2H_2O$
Weeksite Boltwoodite	$K_2(UO_2)_2Si_6O_{15}\cdot 4H_2O$ $KH(UO_2)SiO_4\cdot 1.5H_2O$
Uranophane β-Uranophane	$Ca(UO_2)_2Si_2O_7\cdot 6H_2O$

Source: Pearcy et al. 1994.

In general, uraninite has been oxidized and hydrated at Nopal I. Silicate carried by groundwater has occasionally combined with oxidized U to form soddyite. Silicate in combination with alkali ions (e.g., calcium and sodium) form various alkaline uranyl silicate hydrates, such as Na-boltwoodite and β-uranophane. β-uranophane dominates alteration mineralogy at long times.

In the vapor tests a relatively simple combination of uranyl oxy-hydroxide alteration phases is observed, dehydrated schoepite $(UO_2)O_{0.25-x}(OH)_{1.5+2x}$ $(0 \le x \le 0.15)$ and metaschoepite (a minor phase is Cs-Ba-Mo-uranate, which incorporates two fission products, cesium and molybdenum). The most abundant elements in J-13 water are Na and Si, and, not surprisingly, the most abundant alteration products in the high-drip rate tests are Na- and Si-bearing U^{6+} phases. Other U^{6+} phases are also present, including metaschoepite and β-uranophane. The higher drip-rate tests exhibit two uranophane-group silicates, β-uranophane $[Ca(UO_2)_2(SiO_3OH)_2(H_2O)_5]$ and

Na-boltwoodite (Na,K)(UO_2)(SiO_3OH)(H_2O). Samples from low-drip-rate tests include metaschoepite, an unidentified Na-uranyl oxy-hydroxide tentatively identified as Na-compreignacite, and soddyite (Again, Cs-Ba-Mo-uranate is a minor constituent). In one sample, soddyite appears to replace Na-compreignacite. Also, a few isolated crystals of Na-boltwoodite were first detected in one low-drip-rate test. The groundwater at Nopal I is richer in calcium than J-13 (Pearcy et al. 1994) but poorer in sodium and potassium. This composition could explain the dominance of β-uranophane at the natural site, as well as the limited soddyite and weeksite occurrence. There is substantial calcite at Yucca Mountain. In time this may make repository alteration products conform more to the Nopal I sequence than that seen in the laboratory, which produces β-uranophane at long times. A summary of the corrosion products found in the course of the commercial SNF alteration experiments is shown in Table 5-7. A comparison of Tables 5-6 and 5-7 shows that the phase assemblage observed at Nopal I is similar to that derived experimentally in the commercial SNF degradation tests. This similarity builds confidence in the commercial SNF degradation model.

Table 5-7. Summary of UO_2 Alteration Phases Observed in Commercial Spent Nuclear Fuel Degradation Tests

Uranyl Oxide Hydrates	Formula
Schoepite (meta-schoepite)	$UO_3 \cdot 2H_2O$
Dehydrated Schoepite	$UO_3 \cdot (0.8\text{-}1.0H_2O)$
Compreignacite	$(Na,K)_2[(UO_2)_6O_4(OH)_6] \cdot 8H_2O$
Becquerelite	$Ca[(UO_2)_6O_4(OH)_6] \cdot 8H_2O$
Uranyl Silicate Hydrate	
Soddyite	$(UO_2)_2SiO_4 \cdot 2H_2O$
Uranyl Alkaline Silicate Hydrates	
β-Uranophane	$Ca(UO_2)_2 (SiO_3OH)_2 (H_2O)_5$
Boltwoodite	$K_2(UO_2)(SiO_3OH)(H_2O)$
Na-Boltwoodite	$(Na,K)(UO_2)(SiO_3OH)(H_2O)$
Sklodowskite	$Mg(UO_2)_2(SiO_3OH)(H_2O)_4$
Non-Uranyl Phases	
Palygorskite	$(Mg,Al_{0.12\text{-}0.66})_5(Si,Al_{0.12\text{-}0.66})_8O_{20}(OH)_5 \cdot 4H_2O$
Fe-Oxides	FeO_xOH_y
Ti-Oxides	TiO_x
Amorphous Silica	SiO_2

Source: Stout and Leider 1998, Table 2.1.3.5-10, p. 2-237.

5.2 U.S. DEPARTMENT OF ENERGY SPENT NUCLEAR FUEL DEGRADATION

DOE SNF will be placed in codisposal waste packages together with HLW, as discussed in Section 2. Eventually the waste packages will be breached, the DOE SNF will be exposed to water or water vapor, and the DOE SNF waste forms will begin to degrade. The following model provides the DOE SNF degradation rate as input to TSPA-LA for all applicable scenario classes (see Section 1.2).

More than 250 distinct types of DOE SNF may eventually be stored in the repository. Because it is not practical to model the degradation of each individual type of DOE SNF, 11 general groups were established to represent the entire inventory for TSPA-LA and TSPA-SR. The DOE and the National Spent Nuclear Fuel Program, centered at the Idaho National Engineering and Environmental Laboratory, collaborated to identify the groups, as documented in *DOE Spent Nuclear Fuel Information in Support of TSPA-SR* (DOE 2002b), which contains postclosure performance characteristics of the groups and suggests models for waste-form dissolution. That report was subsequently augmented by *Review of DOE Spent Nuclear Fuel Release Rate Test Results* (DOE 2003b), which summarizes available release-rate test data for DOE SNF.

The 11 DOE SNF groups identified in the National Spent Nuclear Fuel Program documents, along with a typical type of SNF for each group, are:

1. Zircaloy-clad naval SNF (represented by surface ship/submarine assemblies)
2. Plutonium/uranium alloy (represented by Fermi 1 SNF)
3. Plutonium/uranium carbide (represented by Fast Flux Test Facility-Test Fuel Assembly SNF)
4. Mixed oxide and plutonium oxide (represented by Fast Flux Test Facility-Demonstration Fuel Assembly and Fast Flux Test Facility—Test Demonstration Fuel Assembly SNF)
5. Thorium/uranium carbide (Fort St. Vrain SNF)
6. Thorium/uranium oxide (Shippingport light-water breeder reactor SNF)
7. Uranium metal (N Reactor SNF)
8. Uranium oxide (Three Mile Island-2 core debris)
9. Aluminum-based SNF (foreign research reactor SNF)
10. Miscellaneous fuel
11. Uranium-zirconium hydride (training research isotopes-General Atomics SNF)

In TSPA-SR, a 12th DOE SNF group, the immobilized plutonium waste form, was evaluated. This waste form was projected to consist of disks of a plutonium-containing titanium-based

ceramic enclosed in stainless steel cans encased in a borosilicate high-level radioactive waste glass matrix (CRWMS M&O 1998b). However, there is no current plan to dispose of this waste form in the repository, thus, it is not considered further in this report.

The degradation model for all DOE SNF groups (except naval SNF) is not a function of in-package chemistry and is considered to be very conservative: instantaneous degradation or dissolution of the waste form and complete release of radionuclides upon exposure to water (i.e., if a codisposal waste package is breached at the beginning of or during a time step, all radionuclides in the DOE SNF in that waste package (see Section 2) are available for dissolution into the available water during that time step). The dissolved concentration of each radionuclide is determined by its elemental solubility limit if one exists (see Section 6) and the availability/stability of radioactive colloids (see Section 7). The dissolved concentration of a radionuclide that does not have an elemental solubility limit is equal to the mass released from the waste form during a given time step divided by the water volume available in the codisposal waste package. DOE SNF is not a source of colloids, although radionuclides released from the DOE SNF can attach to colloids generated elsewhere, as discussed in Section 7. This model is used in the TSPA-LA model for all applicable scenarios because other models developed for DOE SNF degradation (BSC 2003f, Section 7.2) are not currently fully validated.

The degradation of naval SNF is modeled using the degradation model for commercial SNF given in Section 5.1 and the radionuclide inventory for commercial SNF given in Section 2. Using a naval SNF source term developed by the Naval Nuclear Propulsion Program, the DOE estimated that the dose resulting from naval SNF is about four orders of magnitude less than that from an equivalent amount of commercial SNF (BSC 2001, Section 6). A planned classified Naval Nuclear Propulsion Program Addendum to the LA will provide details of this naval SNF source term. Therefore, using commercial SNF as a surrogate for naval SNF will overestimate radionuclide releases from naval SNF.

5.3 HIGH-LEVEL RADIOACTIVE WASTE GLASS DEGRADATION

High-level radioactive waste immobilized in glass logs and encapsulated in stainless steel canisters will be placed in codisposal waste packages together with DOE SNF. Eventually the waste packages will be breached, the glass will be exposed to water or water vapor, and the glass waste forms will begin to degrade. The following model provides the source term for radionuclides released as the glass degrades as a result of contacting water (see Section 1.2).

5.3.1 Degradation Processes

The words “degradation” and “dissolution” are not interchangeable while discussing degradation of HLW glass. Dissolution is the process of a solid material entering solution, while degradation may also include transformation of a solid material to another solid phase. The glass degradation model accounts for both dissolution and solid-to-solid reactions that can occur when glass is exposed to humid air or dripping water or is immersed in water.

Most researchers agree that the dissolution rate of a borosilicate glass is controlled by the solution concentration of orthosilicic acid that is produced when glass logs contact water (e.g., Advocat et al. 1999; Bourcier 1994; Grambow et al. 1986; Knauss et al. 1990; McGrail

et al. 1998). Dissolution occurs through a hydrolysis reaction to break a silicon oxygen bond at the glass surface and release a unit of orthosilicic acid. The dissolution reaction is written as:

$$\text{glass} \equiv \text{Si-O-Si(OH)}_3 + \text{H}_2\text{O} \rightarrow \text{glass} \equiv \text{Si-OH} + \text{H}_4\text{SiO}_4\text{(aq)} \qquad \text{(Eq. 5-4a)}$$

where the last term is orthosilicic acid and the reverse reaction as:

$$\text{glass} \equiv \text{Si-OH} + \text{H}_4\text{SiO}_4\text{(aq)} \rightarrow \text{glass} \equiv \text{Si-O-Si(OH)}_3 + \text{H}_2\text{O} \qquad \text{(Eq. 5-4b)}$$

The net dissolution rate is the difference between the rates of the forward (dissolution) reaction in Equation 5-4a and the reverse (condensation) reaction in Equation 5-4b. The net dissolution rate depends on the activity (concentration) of orthosilicic acid and decreases as that activity increases. The glass cannot reach true equilibrium with the solution because glass is thermodynamically unstable (i.e., the net rate cannot decrease to zero). For the purposes of modeling glass dissolution, the solution is considered to have attained an apparent saturation limit when the net dissolution rate becomes immeasurably low (Grambow 1985). Glass degradation is experimentally observed to occur in three steps: Stage 1, early dissolution unaffected by low concentrations of orthosilicic acid; Stage II, dissolution decreases in the presence of orthosilicic acid; and Stage III, dissolution accelerates to rates approaching Stage I.

Two different conceptual models have been proposed to describe glass degradation under apparent saturation conditions. One assumes that diffusion of orthosilicic acid through the chemically and physically altered layer of glass that forms when glass degrades (i.e., rind) controls the glass degradation rate, while the other assumes that solution chemistry provides the primary control on dissolution rates. The conceptual model underlying the glass dissolution model presented here is based on the assumption that the glass dissolution rate is determined by the temperature and chemistry (i.e., pH) of the aqueous solution in contact with the glass. Thus, limiting effects of water transport to the reacting glass surface or transport of species released from the glass are not explicitly modeled. However, because experimentally measured dissolution and degradation rates are used to determine model parameter values, any transport limitations in the experimental system are included implicitly in the rate expression. A discussion of the alternative conceptual model (i.e., glass degradation as a diffusion-limited process) is provided in *Defense HLW Glass Degradation Model* (BSC 2003g, Section 6.4).

While transport through the alteration rind of species released from the glass is not modeled as part of the glass degradation rate, radionuclides that have been released from the glass must still diffuse through the rind to reach the surface of the rind so that they can be transported away from the waste form (see Figure 5-4). Release of a specific element into solution depends on its solubility and rate of diffusion through the rind. The role of the alteration layer as a diffusion barrier is discussed in Attachment IV of *Defense HLW Glass Degradation Model* (BSC 2003g). The model presented below calculates the volume of the rind, the volume of water in the rind, and thickness of the rind; a separate model is used to calculate the transport of radionuclides released from glass based on their diffusion coefficients, solubility limits, sorption behavior, etc. for the TSPA.

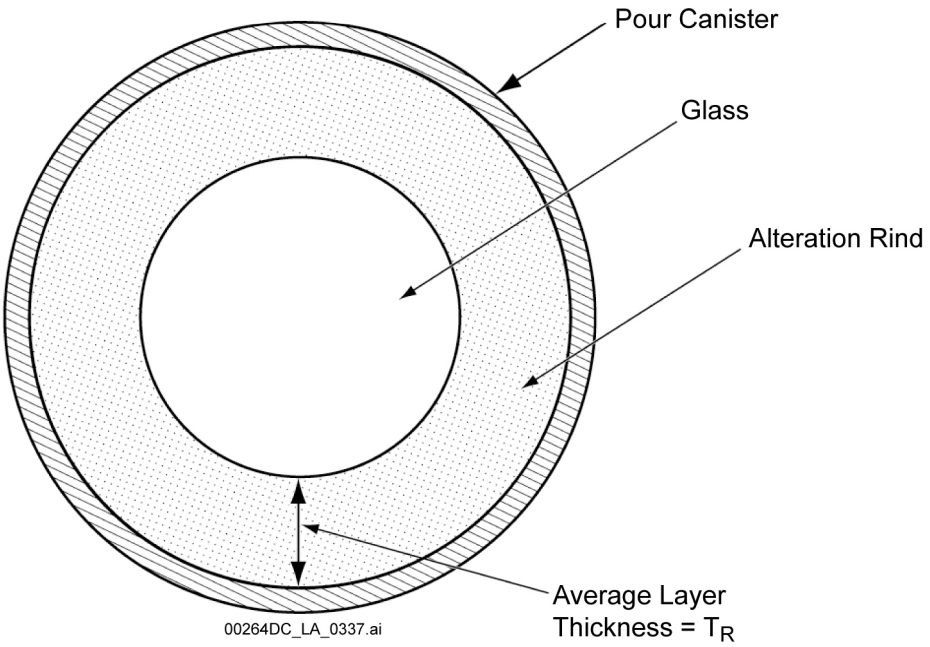

Source: BSC 2003g, Figure IV-1.

Figure 5-4. Canister Cross Section Showing Conceptual Model of Degradation of HLW Glass Logs

5.3.2 High-Level Radioactive Waste Glass Degradation Model

The release rate of radionuclides resulting from the degradation of HLW glass is calculated as the product of three terms (BSC 2003g, Section 6.5). These are:

$$R_i = \text{rate}_G \times S \times I_i \qquad \text{(Eq. 5-5)}$$

where

R_i = release rate of radionuclide *i* from HLW glass (g *i*/day)
rate_G = specific degradation rate of the glass (g glass/(m^2 day))
S = surface area of glass contacted by water (m^2)
I_i = inventory of radionuclide *i* in the glass (g *i*/g glass).

The radionuclide release rate given in Equation 5-5 is used in the TSPA-LA model to estimate the mass of a particular radionuclide *i* available for dissolution into water in the codisposed package during a particular period of time (e.g., during a time step). The concentration of a given radionuclide *i* in water exiting the waste form is equal to the dissolved concentration of that radionuclide in solution plus the concentration of that radionuclide attached to or embedded in colloids. The dissolved concentration of a given radionuclide in solution is equal to its elemental solubility limit if one exists (see Section 6), as apportioned among the various isotopes of that element, if sufficient quantities of the radionuclide are available for dissolution. If sufficient quantities are not available, then the concentration in solution is equal to the mass available divided by the water volume. The dissolved concentration of a radionuclide that does not have an elemental solubility limit is equal to the mass released from the waste form during a

given time step divided by the water volume available in the codisposed package. The water volume available for dissolution is equal to the volume of water contained in the glass alteration layer (rind). HLW glass is considered to be a source of colloids; radionuclides can be embedded in these HLW colloids as the colloids form or can attach to colloids generated by other sources. Colloid generation in the waste form is discussed in Section 7. Spallation of radionuclide-bearing colloidal sized glass shards has been observed in drip tests. When these colloids move into waters containing dissolved radionuclides, they can be expected to sorb and subsequently carry additional radionuclides in the colloidal state.

Mathematical expressions for the specific degradation rate of the glass and the surface area of the glass contacted by water are given in Equations 5-6 and 5-7, respectively (BSC 2003g). The inventory of radionuclides in HLW glass logs is presented in Table 2-3.

The specific degradation rate of the glass is given as (BSC 2003g, Section 6.5.2):

$$\text{rate}_G = k_E \times 10^{\eta \cdot \text{pH}} \times \exp(-E_a/RT) \qquad \text{(Eq. 5-6)}$$

where

k_E = glass degradation rate coefficient (g glass/(m^2 day))
η = the pH dependence coefficient
pH = $-\log[H^+]$
E_a = the effective activation energy (kJ/mol)
R = the gas constant (8.314 J/mol·K)
T = the temperature (K)

The value of k_E accounts for the effects of glass composition, including heterogeneity of the waste inventory, as well as the effects of solution composition (except pH). While solution composition will be considered below, the assumption of little compositional impact on dissolution must be considered further. The mean plus or minus one standard deviation of the values of $\log(k_E)$ calculated for the nine glasses having different compositions is $\log(k_E) = 5.14 \pm 0.17$ g/(m^2·d). The mean and standard deviation for a subset of reference HLW glasses (Hanford-D, WV ref 6, SRL 51S, SRL 165U, SRL 202U, and SRL 131U) is $\log(k_E) = 5.07 \pm 0.13$ g/(m^2·d). The percent relative standard deviation is small in both cases ($100 \times 0.17/5.14 = 3.31\%$ and $100 \times 0.13/5.07 = 2.56\%$, respectively). This suggests that compositional differences within the waste inventory will have little effect on overall glass degradation rates.

The model requires specification of three parameter values (k_E, η, and E_a) and is a function of pH and temperature. Values of the three parameters were determined as described in *Defense HLW Glass Degradation Model* (BSC 2003g, Section 6.5.3).

Figure 5-5 shows the functional form of the rate law and rates measured at 70°C and 90°C.

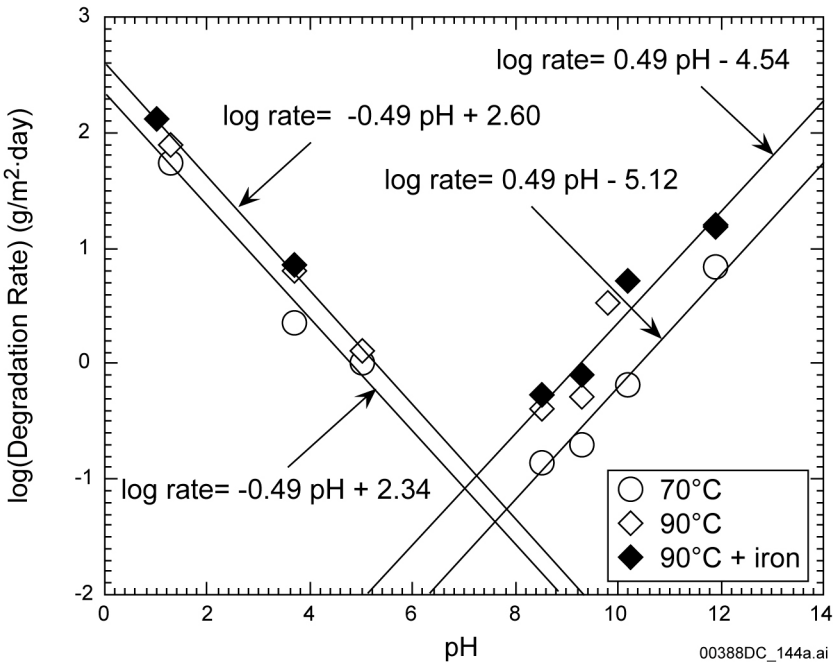

Source: BSC 2003g, Figure 6.5-2.

NOTE: The filled symbols represent results from a series of measurements of the effect of iron on degradation rates.

Figure 5-5. HLW Glass Degradation Rates at 70°C and 90°C

The equation used to calculate the glass surface area contacted by water as glass dissolves during each time step accounts for an increase in surface area from cracking and loss in surface area due to dissolution (BSC 2003g, Section 6.5.6):

$$S = f_{\text{exposure}} \times S_{sp} \times (M_0 - \sum M) \qquad \text{(Eq. 5-7)}$$

where

S = surface area of glass log available for reaction in the current time step (m^2)
f_{exposure} = exposure factor (dimensionless)
S_{sp} = specific surface area of a glass log (m^2/kg)
M_0 = initial mass of glass log (kg)
$\sum M$ = total mass of glass degraded in all previous time steps (kg)

The surface area is greater than the geometric surface area of the glass cylinder because waste logs crack from handling and from thermal and mechanical stresses generated as glass cools in the pour canisters. These cracks result in surfaces deep in the log that may be open to water or humid air. To account for the increase in surface area resulting from cracking and the uncertainties associated with cracking, the geometric surface area of the glass log (as determined by the dimensions of a pour canister and its fill height) is multiplied by a water exposure factor, f_{exposure}. The latter value is assumed to have a triangular distribution with a maximum at 17, a minimum at 4, and a most probable value of 4, as well.

Three key simplifications were made in developing this model. The first is that variability in orthosilicic acid activity resulting from variations in the glass degradation rate and the exposure conditions over time can be accounted for by using a range of rate coefficient values (k_Es) (BSC 2003g, Section 6.3.2). Minimum values of the rate coefficients represent exposure to small volumes of water in which high orthosilicic acid activities are expected; maximum values represent exposure to large volumes of water maintaining low orthosilicic acid activities. Because only small volumes of water are expected to contact waste glass, the minimum values of the rate coefficient are the most expected values.

The second key simplification is that degradation rates of all waste glasses increase as the pH decreases from neutral to lower values (i.e., the acidic leg) and as the pH increases from neutral to higher values (i.e., the alkaline leg). This simplification is based on tests with several different waste glasses (BSC 2003g, Section 6.3.2). To model this, parameters for Equation 5-6 were developed for both the acidic leg and the alkaline leg. The higher of the two rates calculated (i.e., the rate calculated using the parameters for the acidic leg and the rate calculated using the parameters for the alkaline leg) is used as the degradation rate of the glass. Again, this pH-dependent behavior is shown in Figure 5-5.

The third simplification is that all glass compositions have the same dependence on pH and temperature (BSC 2003g, Section 6.3.2). As discussed above, the effect of composition on the dissolution rate at fixed pH and temperature has been found to be small, so all glasses are modeled to have the same pH and temperature dependencies for the acidic and alkaline legs.

Degradation rates for most silicates tend to decrease over time. Glass degradation rates derived from long-term field measurements likewise tend to be much lower than rates measured over the space of weeks to months in laboratories. The glass degradation model is based largely on laboratory measurements. To adequately reflect the generally lower field rates, the most probable degradation rates are weighted toward the lowest laboratory rates.

A description of the alteration rind as a diffusion barrier is given in Attachment IV of *Defense HLW Glass Degradation Model* (BSC 2003g), including equations to calculate the volume, thickness, and water content of the rind, in terms of the mass of HLW glass that degrades in a canister. The volume of the alteration rind is calculated as:

$$V_L = 3.7 \times 10^{-4}\, \Sigma M \qquad \text{(Eq. 5-8)}$$

where

V_L = volume of the alteration rind (m^3).

The volume of pore water in the alteration rind is calculated as the product of the volume of the alteration rind and the porosity of the rind, which is 0.17, yielding (see discussion in *Defense HLW Glass Degradation Model* (BSC 2003g, Section 6.7 and Attachment II)):

$$V_W = 6.3 \times 10^{-5}\, \Sigma M \qquad \text{(Eq. 5-9)}$$

where

V_W = volume of pore water in the alteration rind (m^3).

The equation used to calculate the thickness of the rind through which radionuclides must diffuse (see Figure 5-4) after being dissolved is given as (BSC 2003g, Attachment II):

$$T_R = 0.30 - [0.090 - (3.0\times10^{-5}) \times \Sigma M]^{1/2} \qquad \text{(Eq. 5-10)}$$

where

T_R = thickness of the rind (m).

The parameter values to be used in the glass degradation model are shown in Table 5-8. These parameter values were calculated from glass dissolution test data as described in Section 6.5 of *Defense HLW Glass Degradation Model* (BSC 2003g) and as summarized below in Section 5.3.3. In addition, the results of vapor hydration tests indicated that a relative humidity of at least 44% is required for dissolution to occur. Therefore, the glass degradation rate is applied only when the relative humidity is above 44%.

Table 5-8. Glass Degradation Rate Parameters

Parameter Name	Parameter Description	Value	Distribution
η_{acidic}	pH coefficient for acidic solutions	−0.49	Single value
$\eta_{alkaline}$	pH coefficient for alkaline solutions	0.49	Single value
E_{a_acidic}	Temperature coefficient for acidic solutions	31 kJ/mol	Single value
$E_{a\_alkaline}$	Temperature coefficient for alkaline solutions	69 kJ/mol	Single value
K_{E_acidic}	Glass degradation rate coefficient for acidic solutions	Minimum: 8.41×10^3 g/(m^2 day) Maximum: 1.15×10^7 g/(m^2 day) Most probable: 8.41×10^3 g/(m^2 day)	Triangular
$K_{E\_alkaline}$	Glass degradation rate coefficient for alkaline solutions	Minimum: 2.82×10^1 g/(m^2 day) Maximum: 3.47×10^4 g/(m^2 day) Most probable: 2.82×10^1 g/(m^2 day)	Triangular
$f_{exposure}$	Glass exposure factor	Minimum: 4 Maximum: 17 Most probable: 4	Triangular
S_{sp}	Specific surface area of a glass log	2.70×10^{-3} m^2/kg	Single value
M_0	Initial mass of a glass log	2,710 kg	Single value
φ	Porosity of glass rind	0.17	Single value

Source: BSC 2003g, Table 8.1-1.

The glass degradation model dependencies on pH, temperature, and glass degradation rate coefficient are shown in Figure 5-6, which gives the percentage of glass remaining in a HLW glass log after 10,000 years of degradation. For all curves in Figure 5-6, the glass exposure factor used was the most probable value (i.e., 4). As this figure shows, the degradation rate is highly dependent on pH and the glass degradation rate coefficient (k_E), particularly at low pH values. Above a pH of about seven, most of the glass log is expected to be still intact after 10,000 years of degradation, regardless of the temperature or degradation rate coefficient.

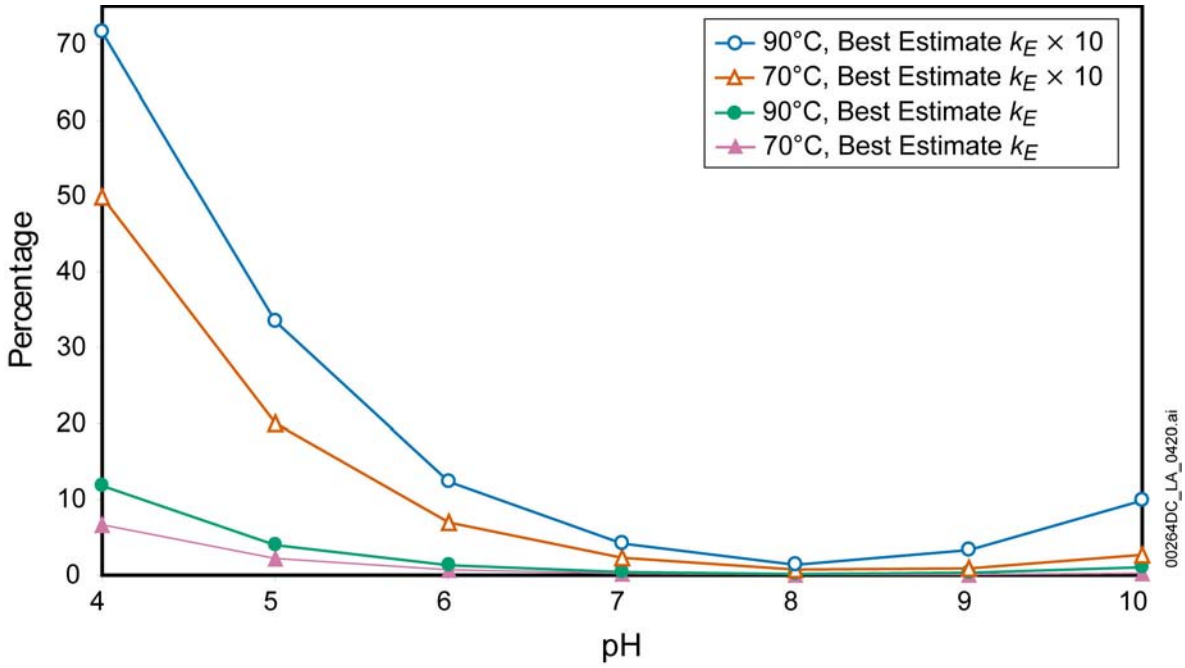

Source: Equations 5-6 and 5-7, and Table 5-8.

Figure 5-6. Percentage of Glass Log Degraded After 10,000 Years of Degradation with $f_{exposure}$ = 4

5.3.3 Tests Conducted on High-Level Radioactive Waste Glass

Several different tests on HLW glass were conducted by Argonne National Laboratory to provide data that form the basis for the glass degradation model (Ebert 2000, 2003a, 2003b, 2003c). These tests are summarized next.

One set of tests involved immersing a monolithic glass sample of known geometric surface area in a test solution within a sealed vessel for a predetermined duration (DTNs: MO0306ANLGIM01.525 and MO0306ANLGIM02.525; Ebert 2003a). At the end of the test, the solution was analyzed for dissolved glass components to measure the extent of glass dissolution. These measured concentrations were used to calculate the normalized boron mass, which was in turn used to calculate the forward glass dissolution rate as a function of pH and temperature. Tests were conducted at specific solution pH values (measured at room temperature) and at temperatures of 70°C, 90°C, and 90°C with added iron compounds. Thus, the collected data provide a measure of dissolution rates of glass immersed in water at different pHs, temperatures, and with and without iron corrosion products (see Figure 5-6). These tests and the data collected are described in more detail in Section 6.5.4 and Attachment I of *Defense HLW Glass Degradation Model* (BSC 2003g).

A second set of tests consisted of vapor hydration tests conducted specifically to measure the degradation rates of three glasses at 70°C, 90°C, 125°C, 150°C, 175°C, and 200°C in humid air (DTN: MO0306ANLGVH01.526; Ebert 2003b). The vapor hydration tests were conducted by suspending two monolithic glass samples in a sealed stainless steel vessel with a small amount of demineralized water, then heating at an elevated temperature for durations between a few hours and a few years. The extent of corrosion was quantified using the thickness of an alteration layer

that formed on the sample surfaces. Tests were conducted at several different values of relative humidity by varying the amount of water that was added, although the relative humidity was not measured directly. Tests were conducted with three glasses that were made at Argonne National Laboratory to be representative of Defense Waste Processing Facility waste glasses. At the end of the test, the vessel was opened and the pH of the water at the bottom of the vessel was measured. Thus, the collected data provide a measure of dissolution rates of glass exposed to water vapor at different pHs and temperatures. The data were used to calculate the near-neutral minimum glass degradation rate coefficient used in the model under alkaline conditions. These tests and the data collected are described in more detail in Section 6.5.5.3 and Attachment III of *Defense HLW Glass Degradation Model* (BSC 2003g).

A third set of tests examined the dissolution of two different glasses when periodically contacted by small amounts of a tuff groundwater dripping onto the glass (DTN: MO0301ANLGNN01.527; Ebert 2003a). The tests were conducted for more than 13 years at 90°C, and the injected tuff groundwater had a pH of about eight. About every six months, water that had first collected on the glass sample and corroded the sample, then dripped off the sample into the bottom of the test vessel and was removed and analyzed for boron. The amount of boron released was used as a measure of the extent of glass degradation. The data were used to calculate the near-neutral minimum glass degradation rate coefficient used in the model under acidic conditions. These tests and the data collected are described in more detail in Section 6.5.5.4 of *Defense HLW Glass Degradation Model* (BSC 2003g).

Another set of tests examined the effect of glass composition on the dissolution rate (DTN: MO0308ANLGPC01.528; Ebert 2000). Nine different glasses having compositions spanning the likely ranges of waste forms from Defense Waste Processing Facility, the West Valley Demonstration Project, and Hanford were subjected to Materials Characterization Center–Test Method 1 (MCC-1) tests at 90°C for durations between 1 and 15 days. These nine HLW glasses were also subjected to a 7-day product consistency test at 90°C. While both test methods involve immersion of a sample in water, the MCC-1 uses a large volume of water (to achieve a dilute solution) and the product consistency test uses a small volume of water (to achieve a concentrated solution). The pH was allowed to drift in both tests and was measured at the conclusion of the test. For both tests, the measured boron concentration was used to determine the glass dissolution rate. The data from the MCC-1 tests were used to calculate the maximum glass degradation rate coefficient under acidic conditions, while the data from the 7-day product consistency tests were used to calculate the maximum glass degradation rate coefficient under alkaline conditions. These tests and the data collected are described in more detail in Sections 6.5.4.2 and 6.5.4.5 of *Defense HLW Glass Degradation Model* (BSC 2003g).

Thus, the data used to develop the HLW glass degradation model were collected under conditions similar to the three water-contact modes anticipated in the monitored geologic repository (see discussion in Section 1): contact with humid air, contact with dripping water and immersion. In addition, the data were collected for a range of HLW glass compositions that meet the chemical durability requirement stipulated in *Waste Acceptance System Requirements Document* (DOE 2002c) and *Waste Acceptance Product Specifications for Vitrified High-Level Waste Forms* (DOE 1996). Applicability of the glass degradation model to HLW forms other than those compliant with this requirement must be determined separately.

5.3.4 Uncertainties, Limitations, and Model Confidence

The HLW glass degradation model is valid for the pH ranges expected in the waste package (see Section 3) and for the temperatures expected in the waste package (see Section 6). The model is also valid for exposure to humid air, exposure to dripping water, and immersion. Uncertainties associated with the model and model confidence building are discussed in the following section, which is summarized from *Defense HLW Glass Degradation Model* (BSC 2003g, Section 6.8).

5.3.4.1 Uncertainty in Glass Degradation Model

Uncertainty in the glass degradation model is represented by a range of values and distributions assigned to the degradation rate coefficients (k_E) for contact by acidic and alkaline solutions. Because the coefficients are based on results of laboratory tests conducted over a range of water contact modes (humid air, dripping water and immersion), glass compositions, and chemical affinities, the range accounts for uncertainty in the water contact mode, the glass composition, and the chemical affinity term. For acidic and alkaline solutions, the distributions of k_E assume the most likely environmental condition will be small amounts of condensed water vapor forming thin films on exposed glass, and the least likely environmental condition will be immersion in a large volume of water.

In laboratory tests, the release of boron is used to represent the glass degradation rate, thereby representing the release rates of all radionuclides, because boron is the most rapidly released structural element of borosilicate waste glass. Tests have shown that technetium, which bonds weakly to the glass, is released nearly stoichiometrically with boron (some tests show that technetium is released faster than boron, while other tests show that technetium is released slower than boron), while other radionuclides (e.g., plutonium and americium) are released much slower than boron. A radionuclide-specific factor could be included in the model to scale the release of individual radionuclides to the release of boron. However, such a scaling factor was not used because data were not available to reliably quantify the relative releases of all radionuclides. Using the release rate of boron to represent the release rate of all radionuclides is reasonable.

Uncertainty in the surface area is represented by a range of values and distributions assigned to the exposure factor, f_{exposure}. The area of glass that is accessible to water and the area that is contacted by water in a breached waste package are the most difficult model parameter values to measure. The maximum value of 17 represents a high estimate of the increase in surface area based on measurements of thermal cracking and impact cracking, combined with a high estimate of the fractions of glass logs that will be affected. A factor of 12 (Smith and Baxter 1981) is used to account for thermal cracking for all canisters, and a factor of 40 (Smith and Ross 1975) is used to account for impact cracking of 1% of the canisters (i.e., $(40 \times 12 \times 1\%) + (12 \times 99\%)$). The minimum value of four represents a subjective estimate of the accessibility of water to tight cracks within the glass log and the reduced reactivity of glass within tight cracks due to transport limitations, both for water entering cracks and radionuclides exiting cracks. This minimum value is rounded down from 4.25, which is obtained by starting with the maximum value of 17, and then assuming that 0.5 of the glass surfaces formed by fractures are freely accessible to water and that glass within cracks has one-half the reactivity of glass at free surfaces. Estimates of water accessibility and glass reactivity are based on qualitative experimental evidence.

Assignment of the distribution of values is based on experimental evidence that the dissolution of large samples with cracking representative of full-sized glass logs increases by less than a factor of four, compared to laboratory-sized samples without cracks. In addition, over time, the accumulation of alteration products is likely to decrease water accessibility.

The constant values used for the specific surface area of a glass log and the initial mass are based on the expected number of long and short canisters, and the estimated geometric surface area and mass of the glass logs. These values are intended to reflect uncertainty in whether a long or short waste package is breached in a simulation.

5.3.4.2 Model Confidence

The glass degradation model realistically estimates the glass degradation rate for waste glasses immersed in water, exposed to humid air, or contacted by dripping water. Building confidence in the model involved showing that the glass degradation rate equation and its associated range of parameter values adequately represent waste glass degradation and radionuclide release. This proof was obtained several ways, as discussed in *Defense HLW Glass Degradation Model* (BSC 2003g, Section 7) and summarized next. First, the general algebraic form of the proposed model is widely accepted and used in the literature of waste glass corrosion, and has also been applied to describe the alteration of basalt, a natural analog for waste glass, on the seabed. This wide acceptance substantially validates the basic algebraic form of the model, namely, a forward reaction rate, a dependence on the solution pH, an Arrhenius temperature dependence, and a term representing the feedback effects of solutes (BSC 2003g, Section 7.1).

Figure 5-7 shows the general consistency of the approach by demonstrating that long-term degradation rates (Stage III) can be adequately predicted by the model. In this figure, filled circles represent maximum rates calculated by the model and open circles represent minimum calculated rates. The vertical lines show the range of rates calculated with the range of values of k_E for that pH and 90°C. A diagonal line is drawn to indicate where the calculated and measured rates are equal. The maximum rates for all pH values lie above the diagonal line, which indicates that the model provides an upper bound estimate of the long-term rates for these glasses, and the minimum rates for all pH values lie below the diagonal line. This provides confidence that the upper limit of the base case model bounds the maximum degradation rate of a disposed waste glass.

Second, literature data were examined to build confidence in the model of exposed surface area, namely in the exposure factor, f_{exposure}. As shown in Table 5-9, the exposure factor was compared with results of fracturing tests conducted on full-scale samples of nonradioactive glass. The fracture ratios for the published tests were generally within the range of 4 to 17 that is used in the glass degradation model, providing confidence in the range of surface areas calculated in the TSPA-LA glass degradation model.

Table 5-9. Measured Surface Areas for Full-Scale Glass Logs of R7T7 Glass

	Sample 1	Sample 2
Ratio of measured surface area to geometric surface area as determined by 2-D tomography	7 ±2	15 ±4
Ratio of measured surface area to geometric surface area as determined by Soxhlet Method	3 ±2	37 ±24[a]

Notes: [a] Results not representative of a canistered waste glass because of excessive fracturing.

Source: BSC 2003g, Table 7.2-1.

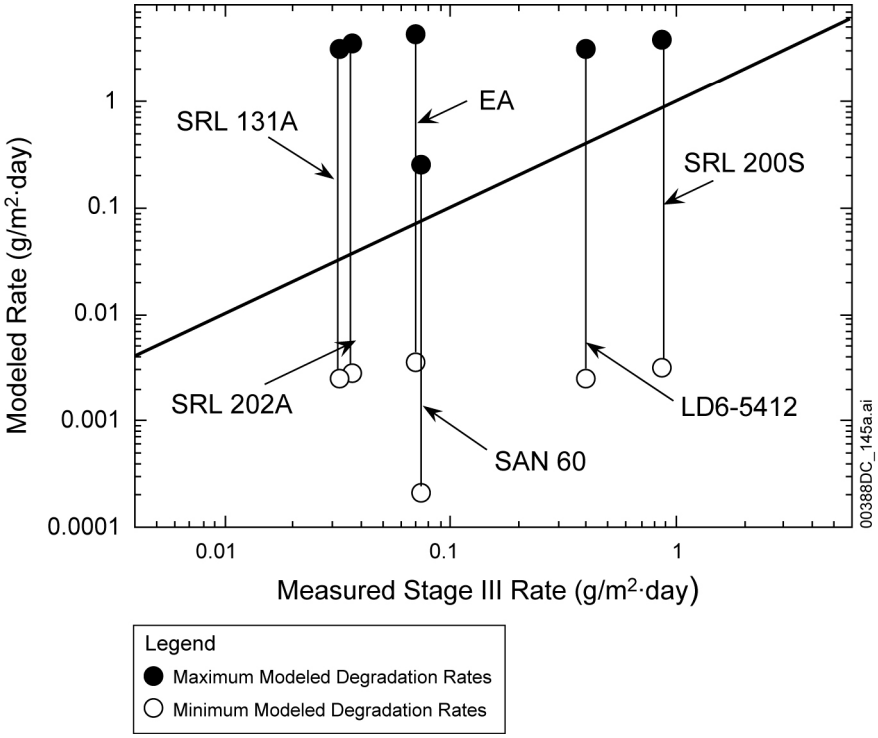

Source: BSC 2003g, Figure 7.1-1.

Figure 5-7. Comparison of Stage III and Model Output Rates for a Variety of Glasses

Third, the TSPA-LA glass degradation model was compared with basalts, which are used as natural analogs for waste glasses. The dissolution rates calculated using the model presented above with the minimum and maximum values of k_E were compared directly with the dissolution rate of basalts recovered from the seabed. The dissolution rates of several basalt samples were calculated based on the thickness of the layer of palagonite that forms as an alteration phase and the age of the basalt (Grambow et al 1986, pp. 268 to 269, Table 2, Figure 3). The dissolution rates for basalts covered in sediment and exposed to Si-saturated seawater at about 3°C are about 0.1×10^{-6} m per thousand years, which is equivalent to 6×10^{-7}g/(m^2 day). The typical pH range for seawater is seven to nine. The respective minimum and maximum dissolution rates calculated using the model presented above at 3°C are 6.62×10^{-9} and 1.16×10^{-5} g/(m^2 d) at pH 7, and 6.33×10^{-8} and 1.11×10^{-4} g/(m^2 d) at pH 9 (BSC 2003g, Attachment II, Table II-5). Thus, the rate expression given previously bounds the long-term dissolution rate of basalts, providing confidence in the model.

Finally, the glass degradation model parameters that account for pH and temperature dependencies (η and E_a) were compared with pH and temperature dependencies that were either determined previously for the dissolution rates of other alkali borosilicate glasses or determined from published test results. The comparison indicated that the pH and temperature dependence parameter values used in the TSPA-LA glass degradation model are either representative of a wide range of borosilicate waste glass compositions or provide an upper bound, thus building confidence in these values.

5.4 SUMMARY AND CONCLUSIONS

Once a commercial SNF waste package and some fraction of the cladding contained therein have failed, and the exposed fuel has been contacted by water, radionuclides in the gap and grain boundary (^{137}Cs, ^{129}I, ^{99}Tc, and ^{90}Sr) are released. Radionuclides in the fuel matrix are released more slowly as the matrix degrades. The degradation rate of the matrix is a function of the pH, pO_2, and pCO_3 in the waste package, the temperature in the package, and the surface area of the fuel. As the matrix degrades, radionuclides dissolve in and diffuse through the water in the rind formed by the dissolution of UO_2, making them available for transport away from the waste form. Degrading commercial SNF is not considered a source of colloids.

Once DOE SNF has been contacted by water, it is modeled to degrade in one time step, thereby making all radionuclides available for dissolution and transport away from the waste form. The HLW encapsulated in glass is released more slowly, with a release rate determined by the pH of water in the codisposed package, the temperature in the package, the surface area of the glass log, and sampled values of the degradation rate constant. As the glass degrades, radionuclides dissolve in and diffuse through the water in the alteration rind formed by the dissolution of glass, making them available for transport away from the waste form. Degrading HLW glass is a source of colloids, some of which contain embedded radionuclides and some of which have attached radionuclides, while DOE SNF is not considered a source of colloids.

6. DISSOLVED RADIONUCLIDE CONCENTRATIONS

This section summarizes an analysis of dissolved concentration limits (also referred to as solubility limits) of radioactive elements identified to be important under relevant repository conditions. When water comes into contact with spent fuel and waste glass, radionuclides will dissolve into solution up to a solubility limit that will depend on the particular radionuclide, solution chemistry, and the secondary phases likely to form in equilibrium with the fluid. For some radionuclides (e.g., ^{99}Tc in oxidizing solutions) there are no secondary phases likely to limit dissolved technetium levels appreciably. For others, such as uranium and many of the actinides, dissolved levels are controlled by secondary phases that tend to grow rapidly from natural waters. Estimating the dissolved concentrations of radionuclides in contact with solids containing them requires a thermodynamic database, a numerical means for calculating solution concentrations, a broad picture of the likely range in fluid chemistry (e.g., pH and fCO_2) and temperature, and an explicit choice of the likely solubility-limiting phases for the individual radionuclides.

Estimated dissolved concentrations as a function of solution chemistry are provided to TSPA-LA as lookup tables, distributions, or single values and, except for uranium, are applicable to all scenario classes that involve groundwater transport of radionuclides. There are two uranium solubility models: one for commercial SNF waste packages in the nominal and seismic scenarios and the other for commercial SNF waste packages for the igneous intrusion scenario and for the invert and for CDSP waste packages in all scenarios. The scenario-specific nature of the uranium solubility model accounts for the likely impact of dissolved silica on the identity of U-containing solids in glass-containing waste packages and in basalt.

The information in this section is drawn mainly from *Radionuclide Screening* (BSC 2002a), *Dissolved Concentration Limits of Radioactive Elements* (BSC 2004c), and *Drift-Scale Coupled Processes (DST and THC Seepage) Models* (BSC 2004e).

6.1 RELEVANT PROCESSES AND MODELING ASSUMPTIONS

6.1.1 Physical and Chemical Environment of the Engineered Barrier System

The general physical and chemical environment in the waste package is important for understanding dissolved radionuclide concentrations. In particular, temperature, pH, ionic strength, fCO_2, and water chemistry are important factors in calculating dissolved radionuclide concentrations in the waste package.

The peak temperature of a waste package varies from 115°C to 180°C, as shown in Figure 6-1. To estimate the effects of changing temperature on solubilities, solubility calculations were carried out at 100°C for a range of pH values at a single fCO_2 value. In all cases, the solubilities at 100°C were found to be lower than those at 25°C. Therefore, solubilities given in this report are for 25°C. Because of the lower solubilities at higher temperatures, this is a conservative approach (BSC 2004c, Section 6.3.3.3).

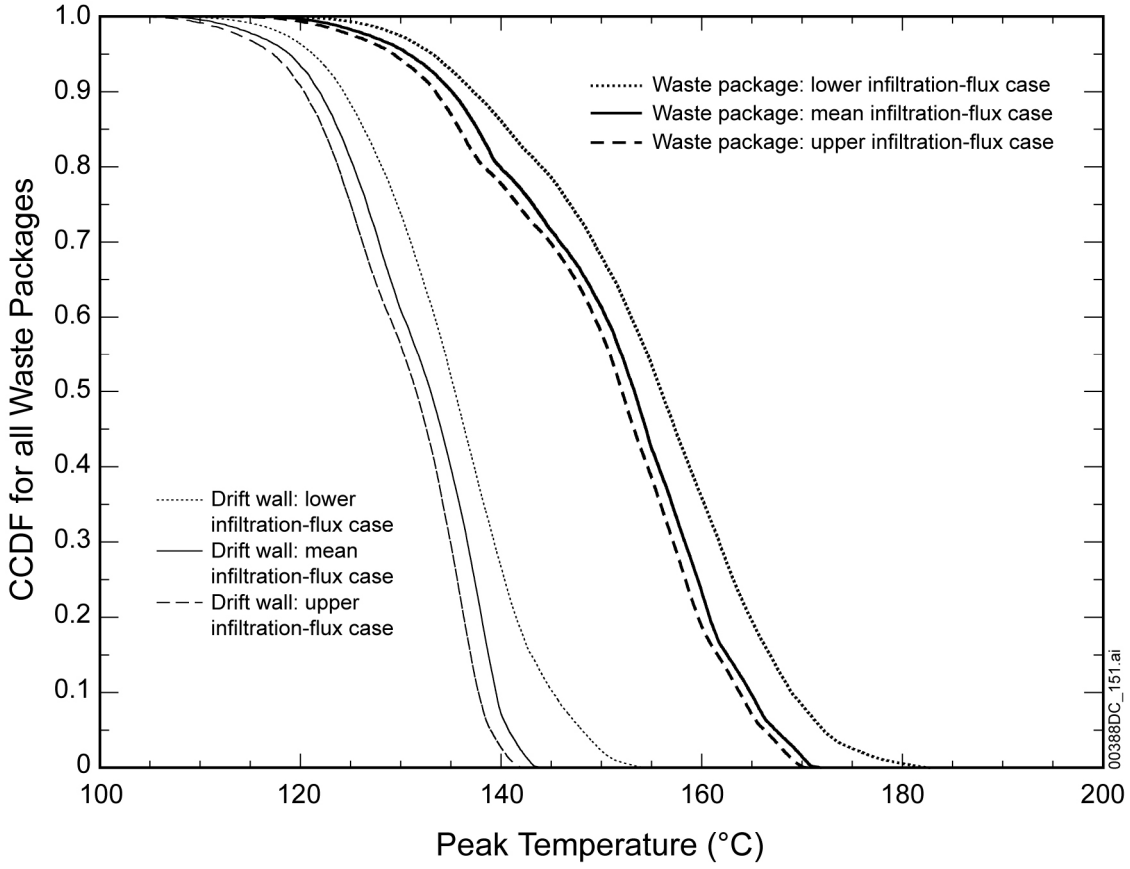

Source: BSC 2004i, Figure 6.3-2

Figure 6-1. The Complementary Cumulative Distribution Function (CCDF) for Peak Temperature on the Drift Wall and on the Waste Packages for Lower-Bound, Mean, and Upper-Bound Infiltration Flux Cases.

Solution pH and ionic strength are calculated by the in-package chemistry model, as presented in Section 3, and are used to calculate dissolved radionuclide concentrations, as shown below. The fugacity of carbon dioxide (fCO_2) is calculated by the model presented in *Engineered Barrier System: Physical and Chemical Environment Model* (BSC 2004h) and is also used to calculate dissolved radionuclide concentrations, as shown below.

Uncertainties in water chemistry were examined, and it was determined that solubilities of the actinide elements are sensitive to the fluoride content of the water because of actinide ion-fluoride solution complexes (BSC 2004c, Section 6.3.3.2). The effects of different fluoride concentrations are treated as a source of uncertainty in the actinide solubility calculations, as described below.

6.1.2 Selection of Radionuclides

Selection of an appropriate set of radionuclides for TSPA-LA is documented in *Radionuclide Screening* (BSC 2002a), and summarized in Section 2.2.2. As shown in Table 2-2, and described in Section 2.1.2. Fourteen elements have been identified to be important to total dose

calculations: actinium, americium, carbon, cesium, curium,[4] iodine, neptunium, plutonium, protactinium, radium, strontium, technetium, thorium, and uranium (BSC 2004c, Section 6.3.1). The solubility limits for these elements are discussed below.

6.1.3 Solubility Limit and Controlling Solid Phase

The term solubility used in repository performance assessments generally refers to elemental solubility. The selection of an appropriate set of controlling solid phases is crucial for evaluating dissolved radionuclide concentration limits. In the context of thermodynamics, the most stable solid is selected as the controlling phase because it ultimately replaces less stable phases. However, due to kinetic effects, the thermodynamically most stable solid may not appear under expected repository conditions. Therefore, the selection of the controlling solid purely from thermodynamic considerations may be not reliable. To obtain a reasonable but conservative concentration limit, a less stable solid phase may be chosen. Laboratory experiments and observations of natural systems provide the basis for such choices, which are shown in Table 6-1 (BSC 2004c, Section 6.3.2).

6.1.4 Water Chemistry and Aqueous Speciation

Table 6-2 gives the composition of the base-case water used as a starting point to develop the solubility models. The water composition given in this table does not represent the only conditions under which the solubility models are applicable. Water of this composition has been used as the benchmark for the repository for many years and, for that reason, was used instead of the Ca or Na-type waters listed in Section 3. A detailed rationale for using this water has been thoroughly discussed by a project committee (Harrar et al. 1990). In addition, a sensitivity analysis to evaluate the effect of various cation and anion concentrations on radionuclide solubilities was carried out as described in Section 6.4.2.5 of *Dissolved Concentration Limits of Radioactive Elements* (BSC 2004c). Because all of the solubility-affecting solution chemistry parameters (e.g., fluoride, carbon dioxide and proton activities) are varied by orders of magnitude from that of J-13, the solubility expressions themselves are largely independent of the choice of J-13 as the starting composition.

The dissolved concentration limits of radionuclides were calculated for a range of pH and fCO_2 values in water having the composition of J-13 water, modified by the addition of Na^+ or SO_4 as required for solution electroneutrality. The calculations were made using the speciation-solubility code EQ3NR (Wolery 1992) and the thermodynamic database "Data0.ymp.R2" (Steinborn et al. 2003) with updates described in Section 4.1 of *Dissolved Concentration Limits of Radioactive Elements* (BSC 2004c). Activity coefficients of aqueous species are estimated using the b-dot equation (Wolery 1992). The dominant species for each element under various modeled conditions are tabulated in Table 6-1. These species account for more than 95% of total dissolved concentration. The principal properties of the matrix water to which the solubilities show sensitivity are pH, fCO_2, and fluoride concentration. The effects of varying pH and fCO_2 are directly considered, and values of calculated radionuclide concentrations are presented in

[4] Curium is important only because ^{245}Cm decays through ^{241}Pu to ^{241}Am, which is an important radionuclide in terms of human dose. Rather than model curium explicitly in TSPA-LA, the inventory of ^{241}Am will be increased appropriately to account for the production of ^{241}Am by the decay of ^{245}Cm. Therefore, a model for curium solubility is not included in this section.

lookup tables for a range of pH and fCO_2 values. The effects of different fluoride concentrations are uncertain and are addressed through the use of uncertainty coefficients, as discussed below.

Table 6-1. Controlling Solid Phases and Dominant Aqueous Species in Solubility Modeling

Element(s)	Controlling Solid(s)	Dominant Aqueous Species	Comments
Plutonium	PuO_2 (hyd, aged): hydrated and aged amorphous PuO_2	PuO_2SO_4, PuO_2F^+, PuO_2^{2+}, PuO_2CO_3, PuO_2^+, $PuO_2(CO_3)^-$ and $PuO_2(CO_3)_3^{4-}$	
Neptunium	Np_2O_5 and $NaNpO_2CO_3$	NpO_2^+, NpO_2SO_4, $NpO_2(SO_4)_2^{2-}$, $NpO_2(CO_3)_2^{2-}$, $NpO_2CO_3^-$, and $NpO_2(CO_3)_3^{4-}$	Np_2O_5 is the phase identified in laboratory solubility experiments. See Section 6.4.3
Uranium	Schoepite, Na−boltwoodite, and $Na_4UO_2(CO_3)_3$	$UO_2(CO_3)_3^{4-}$, UO_2SO_4, $(UO_2)_2(OH)_2^{2+}$, UO_2F^+, UO_2CO_3, $(UO_2)_2CO_3(OH)_3^-$, $UO_2(CO_3)_2^{2-}$, UO_2F_2, UO_2OH^+, UO_2HPO_4, $UO_2PO_4^-$, $UO_2(OH)_3^-$, and HUO_4^-	
Thorium	ThO_2(am)	$Th(SO_4)_2$, $Th(OH)_3CO_3^-$, $Th(OH)_4$, $Th(CO_3)_5^{6-}$ & ThF_3^+	
Americium	$AmOHCO_3$	$Am(CO_3)_3^{3-}$, $Am(CO_3)^{2-}$, $AmCO_3^+$, $Am(OH)_2^+$, $AmOH_2^+$, $AmSO_4^+$, $Am(SO_4)_2^-$ and Am^{3+}	
Actinium			Americium is used as a chemical analog to actinium. Actinium solubility is assumed to be 10^6 times americium solubility (BSC 2004c, Section 6.10.4).
Protactinium			Based on considerations of chemical analogy, protactinium solubility should range from below that of thorium to below that of neptunium(V).
Radium	$RaSO_4$		Solubility is modeled as a piecewise function of pH for pH < 9.75. For pH > 9.75, the concentration of radium is assumed to be not limited by solubility.
Technetium, Carbon, Iodine, Cesium, and Strontium			Not limited by solubility; limited by inventory and dissolution rate.

Source: BSC 2004c, Section 6.

Table 6-2. Chemical Composition of Reference Water (from Well J-13)

Component	Concentration (mg/L)[a]	Uncertainty
Na^+	45.8	2.29
K^+	5.04	0.61
Ca^{2+}	13.0	0.99
Mg^{2+}	2.01	2.01
Si (SiO_2(aq))	28.5 (60.97)	1.85
Cl^-	7.14	0.61
F^-	2.18	0.29
NO_3^-	8.78	1.03
SO_4^{2-}	18.4	1.03

Source: BSC 2004c, Table 4-2.

NOTE: [a]DTN: MO0006J13WTRCM.000 contains recommended mean values of major constituents in well J-13 water. In the technical data management system database, the term "abundance" was used instead of concentration.

6.1.5 Redox Reactions

The design of the repository is such that it is under atmospheric conditions throughout. Thus, oxidizing conditions are assumed, and all solubilities were calculated at a redox potential corresponding to an fO_2 of 0.2 bars, the atmospheric value, with the exception of plutonium solubility. For plutonium, the solubility model using a redox potential calculated from $fO_2 = 0.2$ is inconsistent with experimentally determined plutonium solubilities. Therefore, for plutonium, solubilities were calculated with a modified Eh-pH relationship that provides a better fit of calculated solubilities to experimentally determined solubilities (BSC 2004c, Section 6.5).

6.2 SOLUBILITY MODEL

The solubility model has three different forms:

- Lookup tables as a function of pH and fCO_2 along with associated uncertainty terms
- A constant for specified pH intervals
- No solubility limit.

These three different forms of the model and the elements to which each form is applied are discussed below.

6.2.1 Lookup Tables

Results of the calculations for the solubilities of plutonium, neptunium, uranium, thorium, americium, actinium, and protactinium (without uncertainty) are shown in Figures 6-2 through 6-9 and are tabulated in Tables 6.5-3, 6.6-2, 6.7-3, 6.7-5, 6.7-6, 6.8-2, 6.9-2, 6.10-2, and 6.11-3 of *Dissolved Concentration Limits of Radioactive Elements* (BSC 2004c). The solubilities of these actinide elements increase with pH and fCO_2 under alkaline conditions, while under acid conditions they increase with decreasing pH values. This "U-shape" (or "V-shape") curve is typical for actinides. Minimum solubilities are attained at neutral to mildly basic pH values,

generally within the range of pH predicted by the in-package chemistry model (Section 3). The solubility of actinides increases with fCO_2. This dependence on fCO_2 can cause solubility to vary by several orders of magnitude for a given pH.

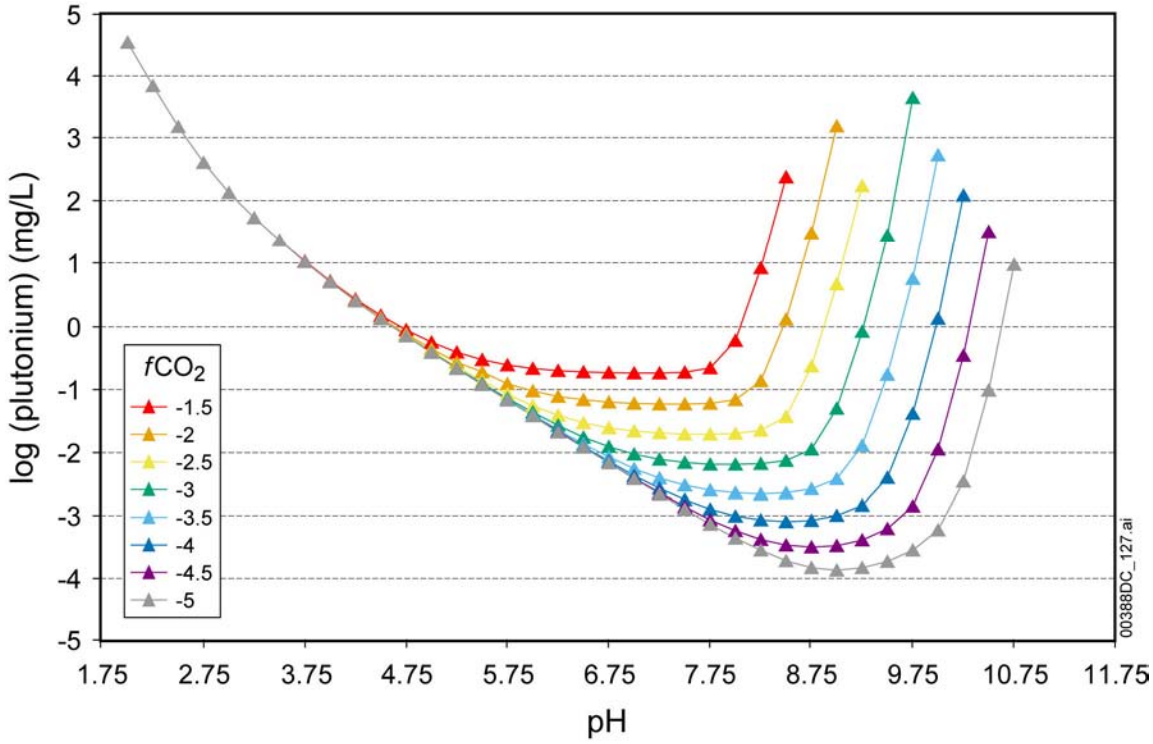

Source: BSC 2004c, Table 6.5-3.

Figure 6-2. Solubility of Plutonium Modeled as a Function of fCO_2 and pH

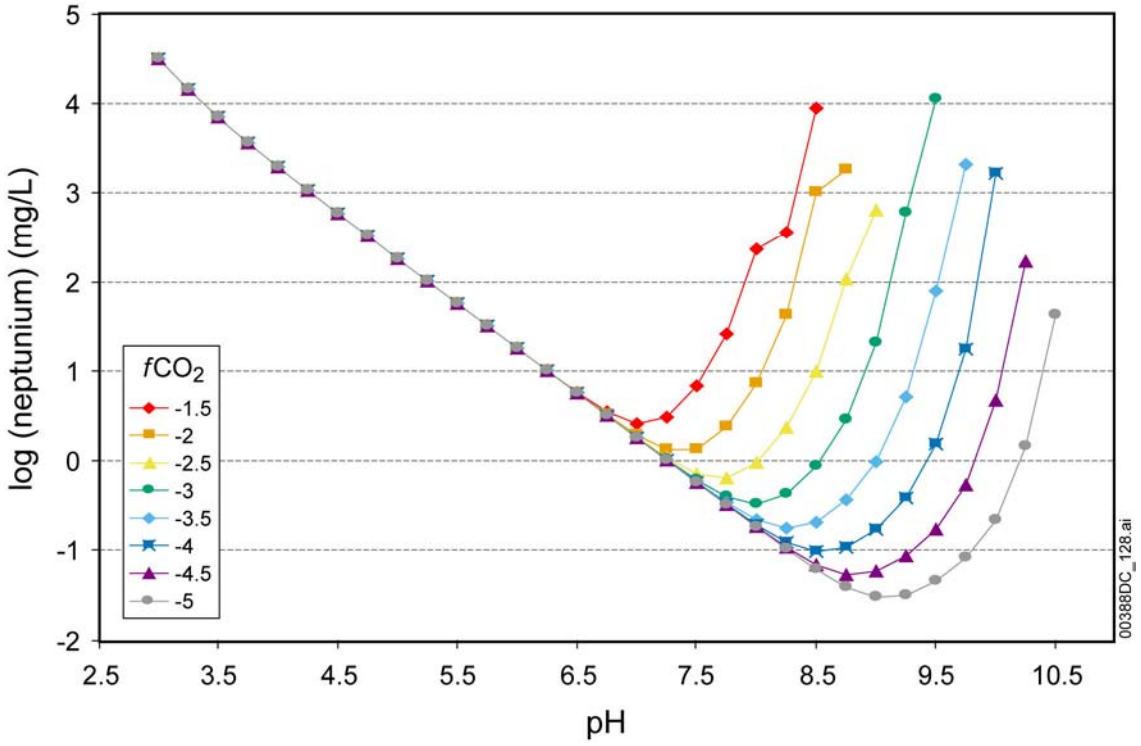

Source: BSC 2004c, Table 6.6-3.

Figure 6-3. Solubility of Neptunium Modeled as a Function of fCO_2 and pH

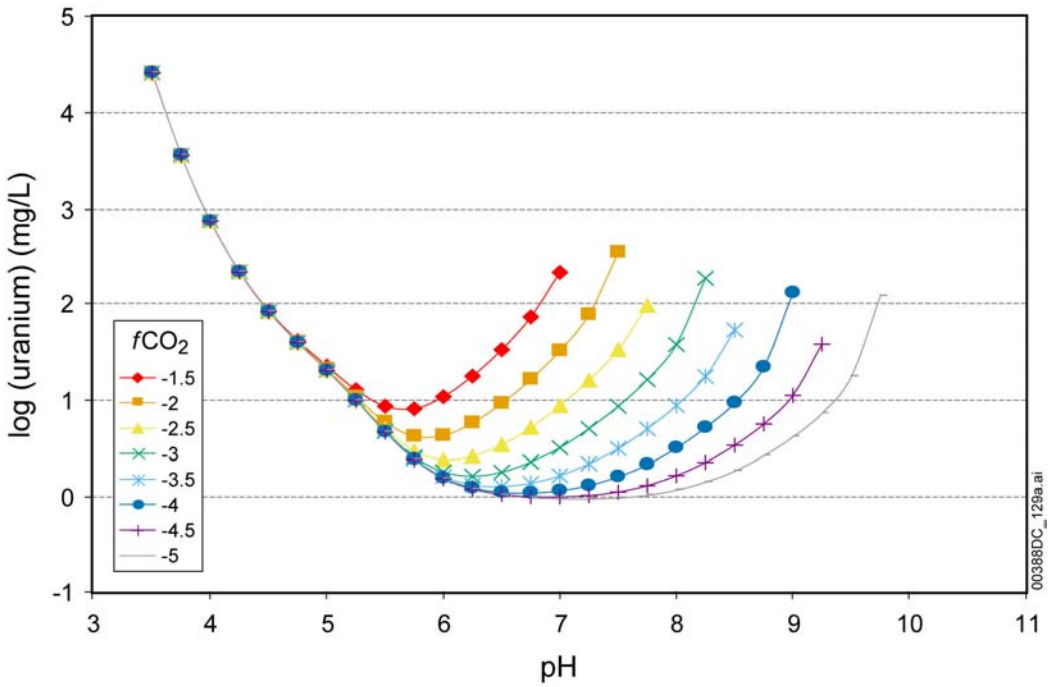

Source: BSC 2004c, Figure 6.7-1.

NOTE: Schoepite is the controlling mineral under all conditions of pH and fCO_2.

Figure 6-4. Uranium Solubility in Commercial SNF Packages Breached under Nominal and Seismic Scenarios

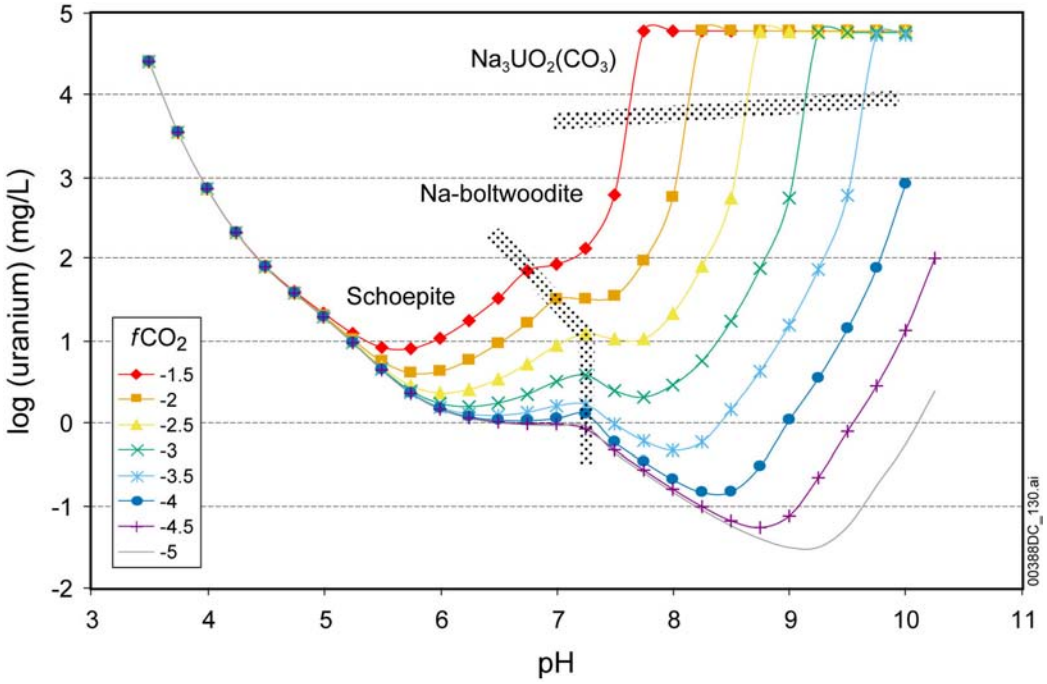

Source: BSC 2004c, Figure 6.7-2.

NOTE: Shaded areas are boundaries between pH – fCO_2 regions controlled by indicated minerals.

Figure 6-5. Uranium Solubility in Commercial SNF Packages Breached by an Igneous Event, Codisposal Waste Packages under Any Breach Scenario, and Waters in the Invert Modeled as a Function of pH and fCO_2

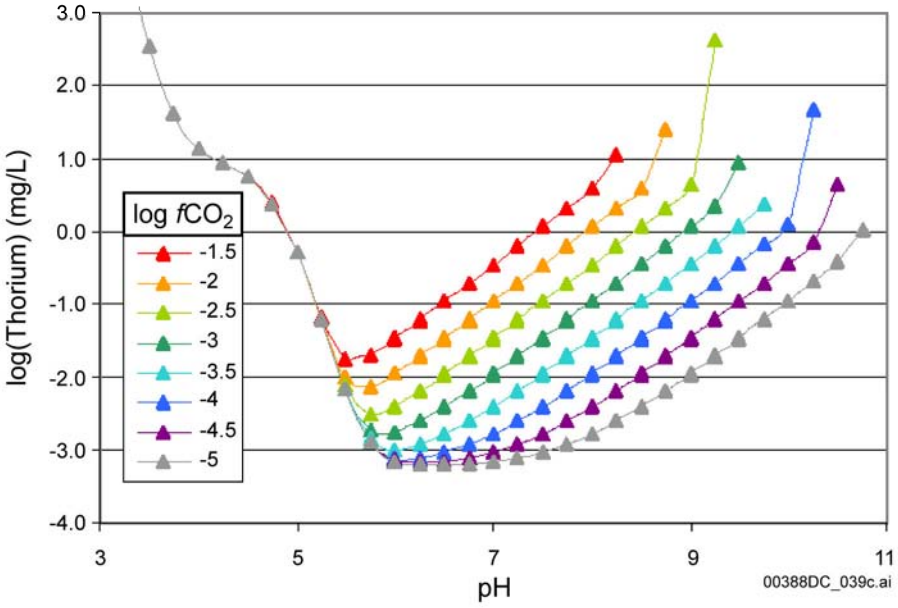

Source: BSC 2004c, Figure 6.8-1.

Figure 6-6. Solubility of Thorium Modeled as a Function of fCO_2 and pH

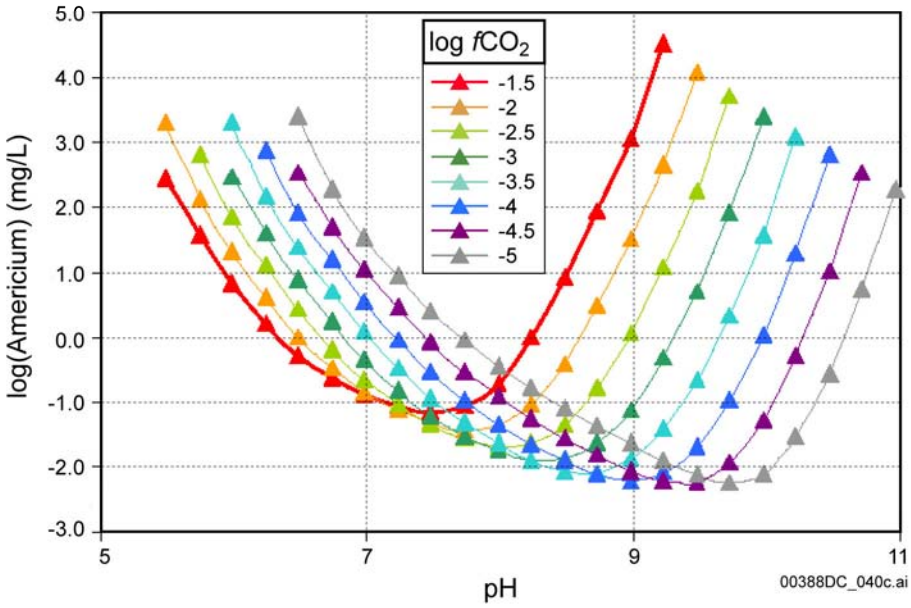

Source: BSC 2004c, Figure 6.9-1.

Figure 6-7. Solubility of Americium Modeled as a Function of fCO_2 and pH

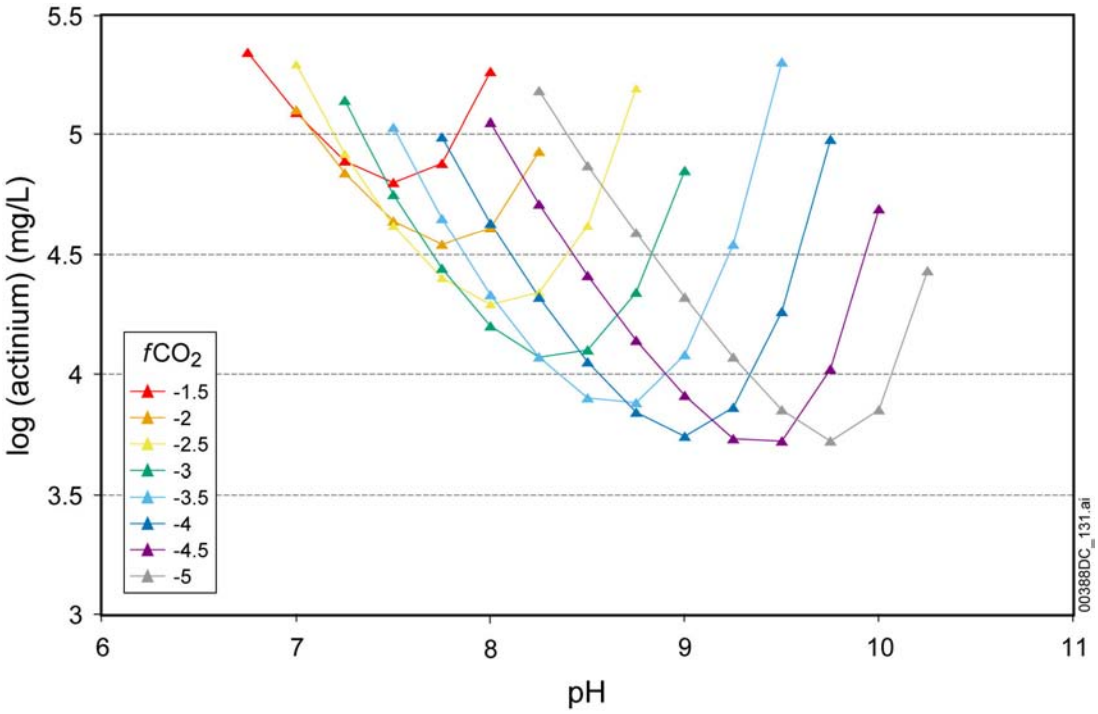

Source: BSC 2004c, Table 6.10-2.

Figure 6-8. Solubility of Actinium Modeled as a Function of fCO_2 and pH

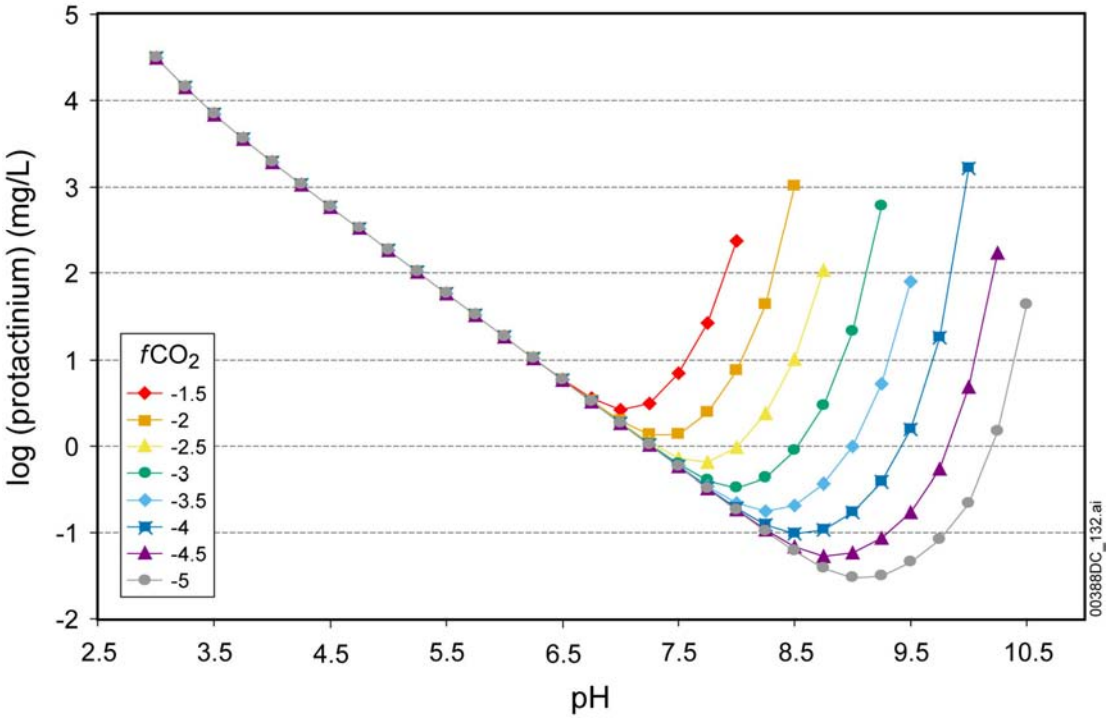

Source: BSC 2004c Table 6.11-3

Figure 6-9. Solubility of Protactinium Modeled as a Function of fCO_2 and pH

The solubility model for uranium requires some discussion because three lookup tables (BSC 2004c, Tables 6.7-3, 6.7-5, and 6.7-6) are used, rather than one. This reflects the fact that the conditions for mineral phase formation will be different. In the nominal and seismic scenarios, very little silica will exist in solution and will prevent the formation of otherwise insoluble uranium silicates. Instead, schoepite will likely form. The first lookup table provides uranium concentrations calculated assuming schoepite control of solubility in commercial SNF waste packages for the nominal and seismic scenario classes. Glass-containing packages will generate Si-rich solutions, as will interaction of groundwater with basalt in the igneous scenario. In Si-rich fluids, dissolved uranium levels will be controlled by either schoepite or Na-boltwoodite, a sodium uranyl silicate. The second two tables provide uranium concentrations in codisposal waste packages for all scenario classes, in commercial SNF waste packages for the igneous intrusion scenario, and in the invert. The second table gives concentrations for low and circum-neutral pH values and Si-rich fluids. The third table provides concentrations at circum-neutral to high pH values for Si-rich fluids. These correspond to Na-boltwoodite or to $Na_4UO_2(CO_3)_3$ solubility, although for part of the table it is uncertain whether schoepite or Na-boltwoodite is controlling uranium solubility.

Calculated uranium concentrations are summarized in Figures 6-4 and 6-5. At the lower pH values, schoepite is the least soluble phase. At pH values around 7, there is an inflection in the concentration curves where the solubility curves of Na-boltwoodite cross those of schoepite so that the controlling mineral phase changes. With increasing pH values, the uranium concentrations increase steeply. The pH values corresponding to this increase vary with fCO_2, being lowest at the highest fCO_2 values. This is due to the increasing carbonate content of the

water with increasing pH and fCO_2, which leads to the formation of high concentrations of uranyl carbonate solution complexes. When the carbonate content reaches sufficiently high values, the uranyl carbonate solid, $Na_4UO_2(CO_3)_3$, becomes stable, thus limiting further increases in the uranium concentration.

The concentrations used in TSPA-LA consist of the solubilities calculated by EQ3NR, which are found in a lookup table (the values of which were shown in Figures 6-2 through 6-9), plus uncertainty terms. The concentration (except for plutonium and uranium) is expressed as (BSC 2004c, Section 6):

$$\log(RN) = S(pH, \log fCO_2) + \varepsilon_1 + \varepsilon_2^i \quad \text{(Eq. 6-1)}$$

where

RN = solubility limit of the element used in TSPA-LA (mg/L)
S = logarithmic value of the solubility calculated with the speciation code, EQ3NR (tabulated in lookup tables and shown in figures above)
ε_1 = uncertainty associated with the equilibrium constant
ε_2^i = uncertainty associated with the effect of the dissolved F^- concentration
i = either the commercial SNF or codisposal waste package.

For plutonium and uranium, the concentration is expressed as (BSC 2004c, Sections 6.5.8.5 and 6.7.6):

$$\log(RN) = S(\text{pH}, \log fCO_2) + \varepsilon_1 + \varepsilon_2^i * N(\text{pH}) \quad \text{(Eq. 6-2)}$$

where

N(pH) = normalized pH dependence of fluoride uncertainty factor ε_2^i.

Uncertainty associated with the equilibrium constant, *K*, of the reaction between controlling solids and aqueous species is captured by the uncertainty term ε_1. This uncertainty is derived from uncertainties in the standard state Gibbs free energy of formation ($\Delta_f G^0$) of the species involved in the dissolution reaction. Uncertainties in $\Delta_f G^0$ values are taken from various sources (BSC 2004c, Section 6.3.3.1) and correspond to the 95% confidence interval, which is taken to represent two standard deviations (2σ) in a normal distribution. Uncertainty in log *K* is calculated from the expression $\Sigma\Delta_f G^0_{\text{products}} - \Sigma\Delta_f G^0_{\text{reactants}} = -RT\ln K$. This expression is a simple algebraic sum, so uncertainties in the $\Delta_f G^0$ terms can be combined by the root-mean-square procedure to obtain $2\sigma \log K$. This calculation is performed for all dominant aqueous species of a given element, and the largest value of $2\sigma \log K$ is used to determine 1σ as the standard deviation of a normal distribution. These values are shown as the ε_1 uncertainty term in Table 6-3 for plutonium, neptunium, uranium, thorium, americium, actinium, and protactinium.

Table 6-3. Uncertainties Associated with Lookup Table Solubility Model

Radionuclide	Uncertainty Term			
	ε_1	ε_2^{CSNF}	$\varepsilon_2^{CDSP-INV}$	*N(pH)*
Plutonium	Normal distribution: $\mu = 0$ $\sigma = 1.0$	Triangular distribution: a = b = 0 c = 4.91×10^{-1}	Triangular distribution: a = b = 0 c = 2.15	BSC 2004c, Table 6.5-4.
Neptunium	Normal distribution: $\mu = 0$ $\sigma = 0.8$	Triangular distribution: a = b = 0 c = 1.59×10^{-2}	Triangular distribution: a =b = 0 c = 0.474	N/A
Uranium (Commercial SNF waste packages, nominal and seismic scenario classes)	Normal distribution: $\mu = 0$ $\sigma = 0.5$	Triangular distribution: a = b = 0 c = 1.03	N/A	BSC 2004c, Table 6.7-10.
Uranium (codisposal waste packages for all scenario classes and commercial SNF waste packages for igneous intrusion modeling case)	Normal distribution: $\mu = 0$ $\sigma = 0.6$ ($Na_4UO_2(CO_3)_3$) $\sigma = 0.5$ (schoepite and Na-boltwoodite)	Triangular distribution: a = b = 0 c = 1.65 (schoepite) c = 0.368 (Na-boltwoodite) c = 0 ($Na_4UO_2(CO_3)_3$)	Triangular distribution: a = b = 0 c = 2.40 (schoepite) c = 1.17 (Na-boltwoodite) c = 0 ($Na_4UO_2(CO_3)_3$)	BSC 2004c, Table 6.7-12.
Thorium	Normal distribution: $\mu = 0$ $\sigma = 0.7$	Triangular distribution: a = b = 0 c = 3.10	Triangular distribution: a = b = 0 c = 5.72	N/A
Americium	Normal distribution: $\mu = 0$ $\sigma = 1.0$	Triangular distribution: a = b = 0 c = 5.91×10^{-2}	Triangular distribution: a = b =0 c = 1.46	N/A
Actinium	Normal distribution: $\mu = 0$ $\sigma = 2.0$	Triangular distribution: a = b = 0 c = 0.04	Triangular distribution: a = b = 0 c = 1.46	N/A
Protactinium	Uniform distribution: $\alpha = -1.02$ $\beta = 3.04$	Triangular distribution: a = b = 0 c = 3.10	Triangular distribution: a = b = 0 c = 5.79	N/A

Source: BSC 2004c, Tables 6.5-5, 6.6-4, 6.7-11, 6.8-4, 6.9-5, 6.10-3, and 6.11-4; Section 6.7.6.

NOTE: Models and associated uncertainties for protactinium and actinium are based on their corresponding chemical analogs (neptunium and thorium for protactinium and americium for actinium).

Uncertainty associated with the effects of F^- concentration is captured by the uncertainty term ε_2^i where *i* refers to either the commercial SNF waste package or the codisposal waste package and the invert. The only source of fluoride for commercial SNF waste packages is the groundwater, whereas HLW glass releases fluoride as it dissolves. To evaluate the effects of fluoride content on solubilities, calculations for a range of pH values at a single fCO_2 value were performed at higher fluoride contents for each type of waste: 10 times the base-case (shown in Table 6-2) for commercial SNF and 200 times the base-case for codisposal waste packages and the invert (except for uranium). To evaluate the effects of fluoride content on uranium solubilities in codisposal waste packages and in the invert, calculations were performed with fluoride contents that were 96 times the base-case values (for the no-dripping case) and 27 times the base-case values (for dripping cases). In general, increased fluoride concentration is associated with increased actinide solubility, as illustrated for uranium in Figure 6-10. Table 6-3 gives the distributions of the uncertainty term ε_2^i for the seven actinide elements.

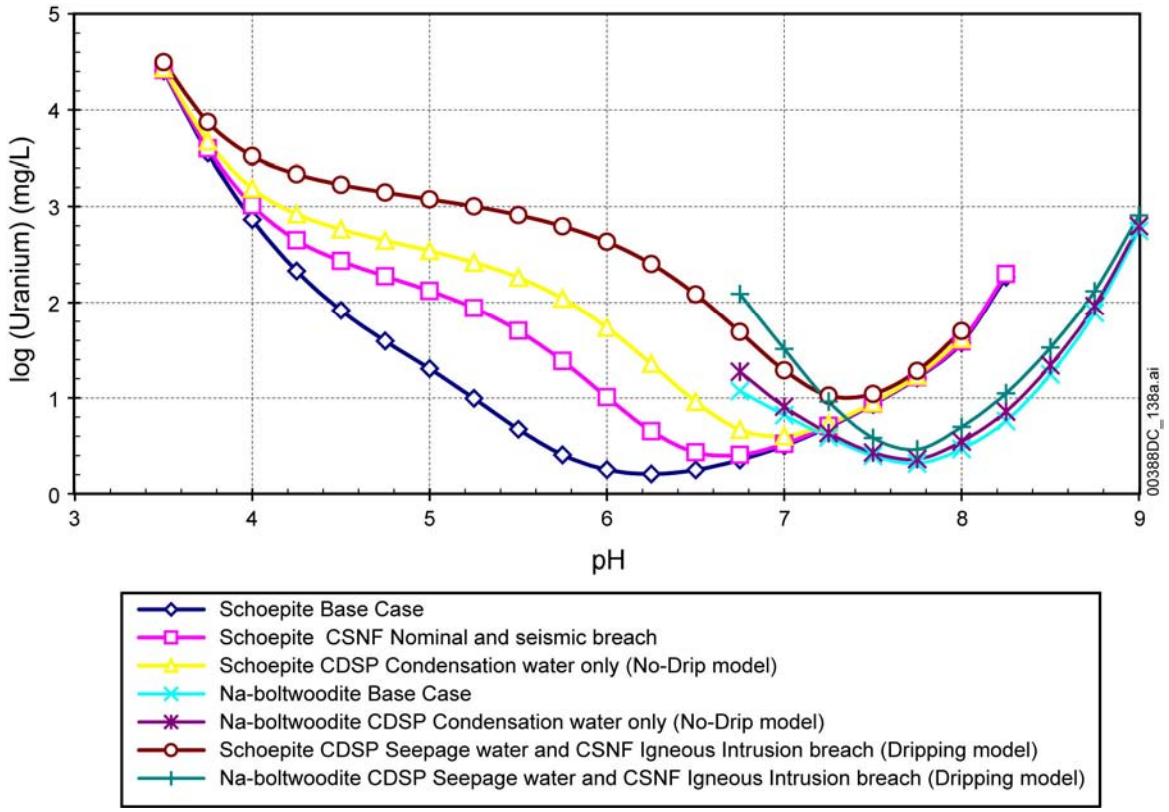

Source: BSC 2004c, Figure 6.7-3.

Figure 6-10. Effect of Scenario-Dependent Fluoride Concentration on the Solubilities of Schoepite and Na-Boltwoodite at $\log(fCO_2) = -3.0$

As Figure 6-10 shows, fluoride increases uranium (and plutonium) solubilities; the maximum impact at 25°C is around pH 6. Fluoride can appear inside the waste form inflow from groundwater or by dissolution out of HLW glass. No-drip models with commercial SNF will have no fluoride. Codisposed, seepage and igneous intrusion models will all involve fluids containing some fluoride. Absolute levels in the waste form are uncertain and must be modeled as such. Fluoride impacts on solubility are bounded as a function of pH and scenario as shown

in Figure 6-10. For plutonium and uranium, this variation has been captured explicitly by expressing the fluoride uncertainty as a function of pH (Equation 6-2). The maximum fluoride uncertainties are shown in Table 6-3 (parameter "c"). The factors modulating these maximum uncertainties as functions of pH are given in Tables 6.5-4 (for plutonium) and Tables 6.7-10 and 6.7-11 (for uranium) of *Dissolved Concentration Limits of Radioactive Elements* (BSC 2004c).

Under some conditions, the concentrations of certain radionuclides cannot be established by the above solubility calculations. This occurs for americium and actinium at low pH values (Figures 6-7 and 6-8), for plutonium, thorium, neptunium, and protactinium at high pH and fCO_2 values (Figures 6-2, 6-3, 6-6, and 6-9), and for all radionuclides at ionic strengths greater than three. In principle, concentrations are also limited by the rate of radionuclide release from the waste form and the available water volume. In some TSPA-LA realizations, calculated concentrations are higher than physically possible. In these cases, a solubility cap equal to the density of the solid metal is imposed.

6.2.2 Constant Solubility for Specified pH Intervals

The solubility of one element, radium, is constant for specified pH intervals. The solubility limit of radium is based on the solubility of pure $RaSO_4$ and is modeled as a piecewise function of pH (BSC 2004c, Table 6.12-1). For slightly alkaline (J-13 water) and acidified Yucca Mountain waters, the calculated radium solubility ranges from 9.1×10^{-3} to 1.9×10^{-2} mg/L. Thus, a constant solubility of 2.0×10^{-2} mg/L is recommended for radium for pH 7.75 or less. Under more alkaline conditions, pH from 7.75 to 9.75, the calculated solubility ranges from 7.1×10^{-2} to 1.2 mg/L. For this pH range a constant value of 1.2 mg/L is recommended. Above a pH of 9.75, there is no solubility limit. The solubility model for radium is summarized in Table 6-4.

Table 6-4. Radium Solubility Values

pH Range	Radium Solubility (mg/L)
3.0 to 7.75	2×10^{-2}
7.75 to 9.75	1.2
> 9.75	No Limit

Source: BSC 2004c, Table 6.12-1.

6.2.3 No Solubility Limit

For technetium, carbon, iodine, cesium, and strontium, it is assumed that no solubility-controlling solid exists. Therefore, solubility is undefined for these five elements. Release of these five elements should be controlled by the dissolution rate of waste forms rather than by solubility.

6.3 SOURCE OF DATA

Direct inputs for solubility calculations include the thermodynamic database "data0.ymp.R2" (Steinborn et al. 2003) with updates described in Section 4.1 of *Dissolved Concentration Limits of Radioactive Elements* (BSC 2004c) and representative J-13 water chemistry. Water chemistry data are shown in Table 6-2. The thermodynamic database was built from the experimental

measurements and theoretical analysis by a large number of international experts. The database specifically includes the most recent actinide solubility measurements and parameterizations of the Organization for Economic Cooperation and Development–Nuclear Energy Agency (OECD-NEA) and the Swiss radionuclide solubility effort (e.g., Grenthe et al. 1992; Silva et al. 1995; Lemire 2001; Hummel et al. 2002). As an example, the equilibrium constants for the dissolution and precipitation of solubility-controlling mineral phases from the database "data0.ymp.R2" in DTN: MO0302SPATHDYN.000 are listed in Table 6-5.

Table 6-5. Equilibrium Constants for the Dissolution and Precipitation of Solubility-Controlling Mineral Phases

Controlling Solid	Reaction	Log *K*
PuO_2(hyd,aged)	$PuO_2(hyd,aged) + 4H^+ = Pu^{4+} + 2H_2O$	-1.9803
Np_2O_5	$Np_2O_5 + 2H^+ = 2NpO_2^+ + H_2O$	3.7031
$UO_3 \cdot 2H_2O$ (schoepite)	$UO_3 \cdot 2H_2O + 2H^+ = UO_2^{2+} + 3H_2O$	4.8443
ThO_2(am)	$ThO_2(am) + 4H^+ = Th^{4+} + 2H_2O$	7.3100
$AmOHCO_3$	$AmOHCO_3 + 2H^+ = Am^{3+} + HCO_3^- + H_2O$	3.1520
$NaNpO_2CO_3$	$NaNpO_2CO_3 + H^+ = Na^+ + HCO_3^- + NpO_2^+$	-1.3265
Na-boltwoodite	Na-boltwoodite + $3H^+ = Na^+ + SiO_2 + UO_2^{2+} + 4H_2O$	5.82
$Na_4UO_2(CO_3)_3$	$Na_4UO_2(CO_3)_3 + 3H^+ = 4Na^+ + 3HCO_3^- + UO_2^{2+}$	4.0504

Source: DTN: MO0302SPATHDYN.000: database "data0.ymp.R2."

6.4 UNCERTAINTIES, LIMITATIONS, AND MODEL CONFIDENCE

6.4.1 Model Limitations

The solubility models presented above are valid only within certain ranges of pH, fCO_2, temperature, F^- concentration, and ionic strength. These limits are summarized in Table 6-6. It should be noted, however, that dissolved concentration limits could not be determined for all elements for all values of pH and fCO_2, as demonstrated in Figures 6-2 through 6-9.

Table 6-6. Valid Range of the Solubility Models

Variable	Value or Range
pH	Given by individual solubility table
log(fCO_2)	-5.0 to -1.5 bars
Temperature	25°C to 100°C
F^- concentration	1 to 10 times base-case value for commercial SNF waste packages 1 to 200 times base-case value for codisposal waste packages and the invert For uranium: 1 to 96 times base-case value for no-dripping commercial SNF waste packages and invert 1 to 27 times base-case value for dripping commercial SNF waste package and invert
Ionic strength	Less than 1 mol/kg. With additional uncertainty in solubility value, less than 3 mol/kg.

Source: BSC 2004c, Table 8-5.

6.4.2 Model Uncertainty

Uncertainty from various sources has been addressed in developing the models presented above. The primary sources of uncertainty are (1) uncertainty in log *K* of the solubility-controlling phase, (2) uncertainty associated with temperature variations, and (3) uncertainty associated with variations in fluoride concentrations. For elements with solubility limits that are taken from lookup tables, these uncertainties (except for uncertainties associated with temperature variations) are addressed through the use of uncertainty terms added to the solubility value taken from the lookup table (Equations 6-1 and 6-2, and Table 6-3). The uncertainty associated with temperature variations is addressed by performing calculations at 25°C. Because actinides have lower solubilities at 100°C than at 25°C, performing calculations at the lower temperature results in higher solubilities. For radium, uncertainty is not addressed, nor is it addressed for technetium, iodine, cesium, strontium, or carbon because solubility limits are not provided for these five elements.

6.4.3 Model Confidence

Developing solubility models involves:

1. A thermodynamic database and a modeling tool
2. The specification of environmental conditions
3. Construction of a conceptual model
4. The calculation of solubility limits using a geochemical modeling tool based on the conceptual model.

The thermodynamic database was composed of data developed to support general geochemical use of the EQ3/EQ6 package, augmented by data principally on actinides from the critical reviews carried out within the Chemical Thermodynamic Database project of the Organization for Economic Cooperation and Development–Nuclear Energy Agency (Grenthe et al. 1992; Lemire 2001; Silva et al. 1995). The specific database used received additional technical review and approval for project use (Steinborn et al. 2003; DTN: MO0302SPATHDYN.000) and so requires no additional confidence building. The geochemical modeling was carried out using the EQ3NR (Wolery 1992) code from the EQ3/EQ6 package. This group of codes is widely used and accepted for general geochemical modeling and in support of nuclear waste activities and required no additional confidence building for its application here. It has received approval for project use. Neither the code nor the database was used outside its range of validity. Thus, aspects 1 and 4 above are exempted from further model confidence building. Aspect 2 consists of inputs to this report; thus, no model confidence building is necessary. Therefore, model confidence building focuses on whether the conceptual model (i.e., the selection of solubility-controlling mechanism) is appropriate.

The selection of solubility-controlling solids was based on laboratory and/or field observations that were determined to be applicable to the expected range of conditions. Specifically, potential solubility-forming solids for specific radionuclides were eliminated from consideration if they were not observed to form in the laboratory or the field under the chemical conditions being

considered. In the absence of experimental or field evidence of appearance and solubility control the conservative approach of selecting less crystalline, more hydrated phases was followed. This results in prediction of higher solubilities relative to those resulting from control by more crystalline, less hydrated phases. The end result is that the outputs of the solubility model are either directly supported by experimental or field observations or, where observation is lacking, conservative.

In addition, the plutonium and neptunium solubility models were corroborated with laboratory measurements or relevant observations not previously used to develop the model. These corroborative activities are discussed below.

Plutonium–Figure 6-11 presents the model of plutonium solubility at $\log(f\mathrm{CO_2}) = -3.5$ bars, as well as several sets of experimental data. Experiments conducted by Rai (1984) and Rai et al. (2001) were open to air, while experiments conducted by Nitsche et al. (1993a, 1993b) and by Efurd et al. (1998) were conducted in an argon/CO_2 atmosphere. Other conditions were comparable to the modeled conditions. Four different types of solutions were used in the experiments conducted by Rai et al. (2001):

- 0.403 mol/L NaCl solution
- 0.408 mol/L $NaClO_4$ solution
- 4.36 mol/L NaCl solution
- 4.92 mol/L $NaClO_4$ solution.

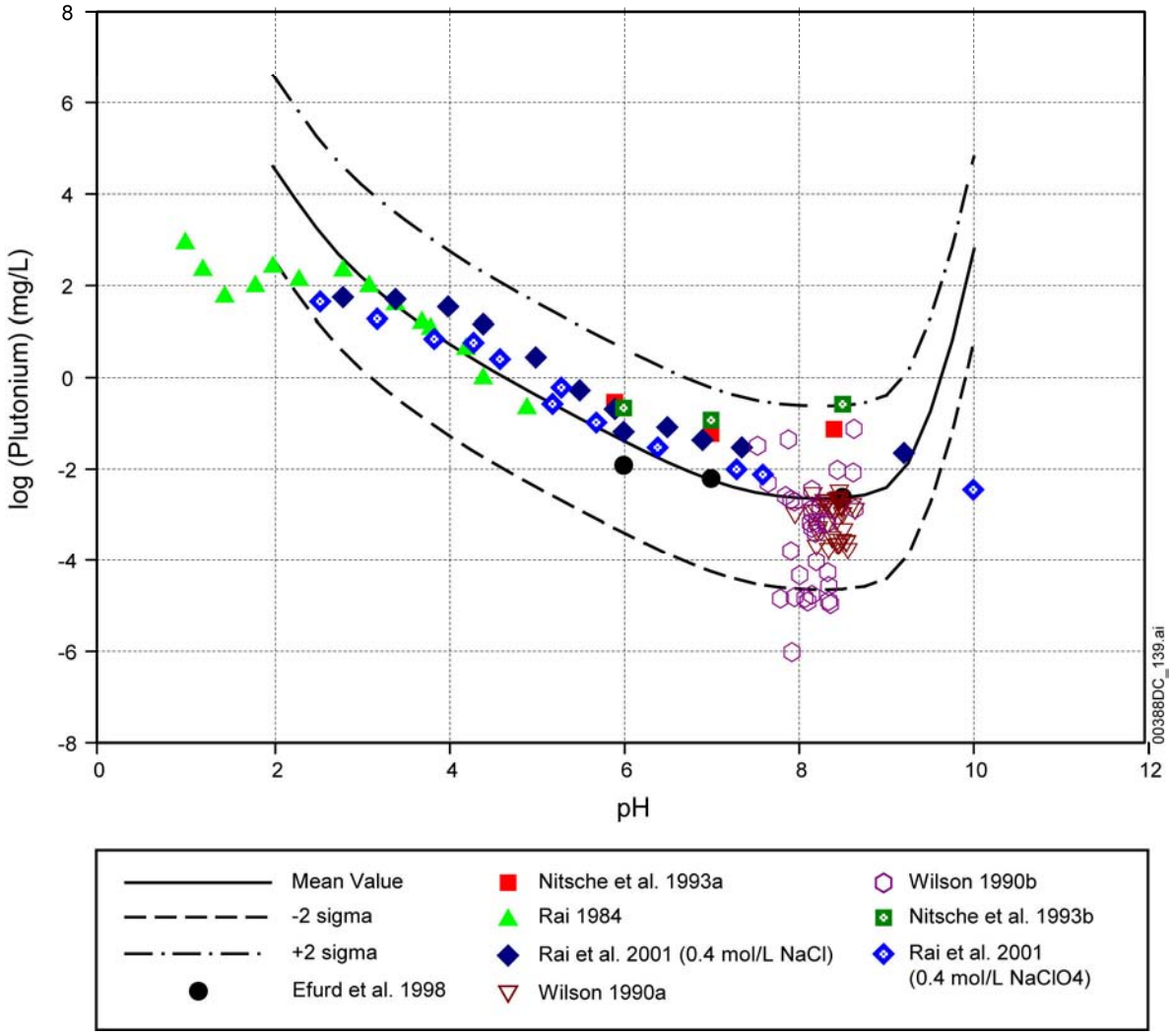

Source: BSC 2004c, Figure 7-1.

Figure 6-11. Comparison of Experimental Data with Predictions of Plutonium Solubility Model

Since the thermodynamic database used in this report is invalid for high ionic strength solutions, only the results of the lower ionic strength solutions reported by Rai et al. (2001) are shown in Figure 6-11. The other two data sets are plutonium concentrations measured in SNF leaching experiments by Wilson (1990a, 1990b).

Most of the data points from these seven experiments fall within the uncertainty range of the model. The good match between the model results and experimental results, which were not used in the model development, indicates that this proposed plutonium solubility model is representative of measured solubilities given the assumed controlling solid phase and assumed Eh conditions, and it enhances confidence in the plutonium solubility model.

Neptunium–Figure 6-12 presents Np_2O_5 solubility at 25°C and at $\log(fCO_2) = -3.5$ bars. The inputs for this model were derived from the thermodynamic analysis of experimental data reported in Lemire (2001) and elsewhere (see discussion in BSC 2004c, Section 6.6). To show that the model is conservative the Np_2O_5 solubility model predictions can be compared against

actual fuel leaching experiments. Figure 6-12 also presents measured neptunium concentrations in several SNF corrosion experiments. These experiments were conducted at Pacific Northwest National Laboratory (Wilson 1990a, 1990b) and at Argonne National Laboratory (Finn et al. 1994; CRWMS M&O 2000e; CRWMS M&O 2000f; DTN: LL991001251021.090). This comparison shows that the Np_2O_5 solubility model is conservative and thus is adequate for use in the TSPA-LA model. An alternative conceptual model using the high temperature phase NpO_2 as the controlling phase led to solubilities only about 1 order of magnitude lower than those from the Np_2O_5 model (BSC 2004c, Figure 6.6-2). The fact that the measured neptunium concentrations in spent fuel corrosion experiments are 4 to 6 orders of magnitude lower than the concentrations modeled using Np_2O_5 and 3 to 5 orders of magnitude lower than the concentrations modeled using NpO_2 indicates that neptunium may be controlled by different mechanisms than by pure phase solubility. Another alternative conceptual model for neptunium dissolved concentrations based on incorporation of neptunium into secondary uranium phases has also been investigated (BSC 2004c, Section 6.6). This model is based on incorporation of neptunium into secondary uranium phases, such as schoepite. However, this alternative model is not used in TSPA because the experimental data upon which the inputs to the model are based have been questioned (Adkins 2003).

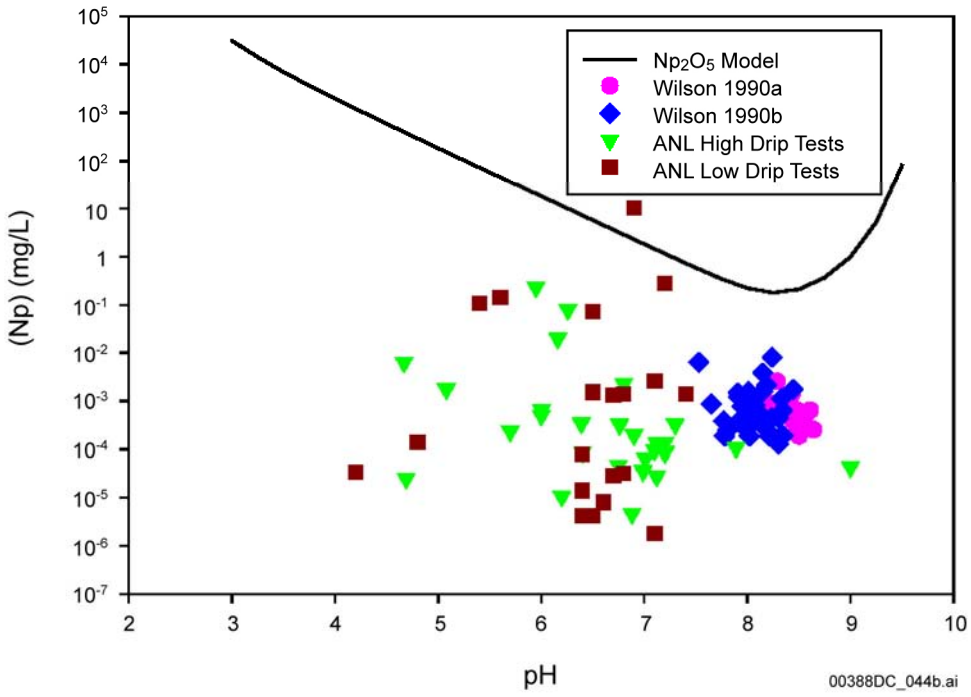

Source: BSC 2004c, Figure 7-2.

Figure 6-12. Comparison of Np_2O_5 Neptunium Solubility Model with Pacific Northwest National Laboratory and Argonne National Laboratory Measurements

Uranium–The uranium solubility model is based on calculations of the solubility of several uranium-bearing solids: schoepite ($UO_3 \cdot 2H_2O$), the controlling mineral at low to moderate pH and fCO_2 values; Na-boltwoodite ($NaUO_2SiO_3OH \cdot 1.5H_2O$), the controlling solid at moderate to high pH and fCO_2 values; and the solid $Na_4UO_2(CO_3)_3$, the controlling solid at high pH and fCO_2

values. In these calculations, dissolved silica concentration was fixed by saturation with the silica phase chalcedony. Evidence supporting the selection of these uranium- and silicon-controlling phases was presented in Section 5.1.4.3 and is summarized below. A more complete discussion can be found in Section 6.7 of *Dissolved Concentration Limits of Radioactive Elements* (BSC 2004c).

The selection of the solids used to model uranium concentrations was based on laboratory studies (Wronkiewicz et al. 1997; Pearcy et al. 1994) describe a natural analog study of uraninite alteration in the Nopal I deposit at Peña Blanca, Mexico, an environment similar in most respects to that of Yucca Mountain. The paragenesis of alteration products in the natural analog study is entirely consistent with that of the laboratory study; the differences that are evident are related to the chemistry of the alteration water in the two situations. These studies are described in more detail in Section 5.1.4.3, where they also provide confidence in the commercial SNF dissolution model.

The alteration paragenesis found in both the laboratory and natural analog study begins with uranyl-oxide hydrate minerals (principally of the schoepite group) and passes to alkali and alkaline earth uranyl silicates hydrates. In the natural analog, the principal silicate alteration product is uranophane. Weeksite and boltwoodite are also found, but they occur farther from the uraninite deposit itself and tend to form over earlier-formed phases. Pearcy et al. (1994, p. 726) conclude that "…the specific uranyl silicate formed in a given area depended on the local geochemical conditions rather than on the broad evolution of the oxidizing system." In the laboratory study, uranophane is also an important secondary silicate but it is more evident that the final silicate phase is Na-boltwoodite (Wronkiewicz et al. 1997, Section 4.2.1 and Figure 7).

Considering the phases for which data are available and the principal secondary phases observed in the laboratory study, schoepite and Na-boltwoodite were selected as the controlling phases for the uranium solubility model. Although uranophane is the most common uranyl silicate found in the natural analog study, calcium must be present in the degrading water for it to form. The groundwater at Peña Blanca has a considerably higher calcium and lower sodium content than J-13 water or the water used for the laboratory degradation experiments (Pearcy et al. 1994, Table 5). Furthermore, conditions of high pH and high fCO_2 that can occur in the drift should lead to high dissolved carbonate contents and, consequently, to low calcium concentrations because of the precipitation of carbonate minerals such as calcite. Thus, the natural analog study validates the selection of schoepite and Na-boltwoodite.

Schoepite saturation leads to the lowest uranium concentrations at low pH values. With increasing pH, Na-boltwoodite becomes the controlling phase. At still higher fCO_2 and pH values, the carbonate content of the solution increases strongly. The uranyl ion forms a series of strong complexes with the carbonate ion so increasing carbonate contents lead to increasing uranium concentrations. When the dissolved carbonate reaches a high enough concentration, modeling shows that the solid $Na_4UO_2(CO_3)_3$ will form, limiting further increase in dissolved uranium. This phase is not observed in the laboratory studies or natural analog site because the pH and fCO_2 conditions in these studies are too low for this solid to form.

Thorium–The minimum thorium concentration modeled is 6.36×10^{-4} mg/L (2.7×10^{-9} mol/L) at an fCO_2 of 10^{-5} bars and a pH of 6.25. At this pH and low fCO_2, the impact of F^-, SO_4^{2-}, and

CO_3^{2-} complexes is minimal and the hydroxyl complex $Th(OH)_4(aq)$ dominates. This solubility should therefore represent the experimental solubility of thorium dioxide in pure water at moderate to high pH values. Hummel et al. (2002, Section 5.21) have developed an internally consistent set of thermodynamic data for thorium. As part of their reported work they summarize the results of a number of studies of thorium solubility in pure water. From these data, they show that at pH values above 6 the solubility is $10^{-8.5\pm0.6}$ mol/L (Hummel et al. 2002, Figure 5.21.1). The minimum solubility modeled in this report (2.7×10^{-9}) equals $10^{-8.6}$, close to the mean and well within the uncertainty of the measured values. The above comparison demonstrates that the thorium solubility model compares favorably with test data; thus, it is adequate for use in TSPA-LA.

Americium–$AmOHCO_3$ was chosen as the controlling solid phase in all calculations of americium solubility. The choice of this mineral is based on the studies by Nitsche et al. (1993a; 1993b, p. 1494), which identify $AmOHCO_3$ as the solid phase precipitated from water corresponding to the water used in these calculations at a pH range from 5.9 to 8.4 and temperatures from 25°C to 90°C. This is the most likely controlling phase under the range of environmental variables of interest to this analysis. Thus, the model of americium solubility is consistent with experimental data generated for the Yucca Mountain Project and is adequate for use in TSPA-LA.

Actinium–Actinium is commonly considered to be directly analogous to americium (e.g., Berner 2002, p. 37). Only one set of actinium solubility measurements is known (Baes and Mesmer 1986, Table 7.2) and was used to develop the actinium solubility model in which actinium concentrations are 106 times those of americium. Thus, no direct validation is possible.

Protactinium–Thermodynamic data for protactinium are not available in the database, based on their similar positions in the periodic table, so protactinium was assumed to be an analog of neptunium for the purpose of solubility calculations. Protactinium solubility is, thus, taken to be equal to neptunium solubility. Experiments on protactinium behavior in solutions of several types at a range of pH values are described by Berry et al. (1989). The protactinium behavior was dominated by sorption, but the authors were able to develop a solubility limit of 10^{-10} mol/L (2.3×10^{-5} mg/L) at high pH values in waters typical of those emanating from cements. This is 4 orders of magnitude lower than the lowest neptunium solubility, indicating that the solubility model developed for protactinium is conservative.

Radium–The radium solubility given is based on the solubility of pure $RaSO_4$. Field studies have shown that radium concentrations in some natural waters are orders of magnitude below levels corresponding to $RaSO_4$ saturation. Radium concentrations more probably correspond to the solubilities of radium in solid solutions of more common sulfate solids such as $SrSO_4$ or $BaSO_4$ (Langmuir and Riese 1985). A radium concentration based on pure $RaSO_4$ solubility is therefore a conservative value and adequate for TSPA use.

Technetium, Carbon, Iodine, Cesium, and Strontium–These are more soluble radionuclides and their dissolved concentrations are determined from their inventory and waste degradation rates (BSC 2004c, Sections 6.14 to 6.18). Therefore, no solubility models are used for these elements in TSPA-LA and confidence building of the solubility models is not necessary.

6.5 SUMMARY AND CONCLUSIONS

A total of 14 radionuclides have been identified important to total dose calculations: plutonium, neptunium, uranium, thorium, americium, curium,[5] actinium, protactinium, radium, technetium, carbon, iodine, cesium, and strontium. The solubility-controlling solid phases for plutonium, neptunium, uranium, thorium, and americium have been carefully selected; concentration limits of these radionuclides are calculated as functions of pH and CO_2 fugacity and fed to TSPA-LA as lookup tables. Uncertainties associated with predicted limits are captured in two stochastic terms, representing uncertainties in the thermodynamic data and the effect of dissolved fluoride, respectively. All solubilities used in TSPA-LA are calculated at 25°C, because solubilities of relevant radionuclides decrease with temperature.

Concentration limits and the associated uncertainties of actinium and protactinium are estimated from their chemical analogs (americium for actinium, and neptunium and thorium for protactinium). The solubility of radium is chosen as a piecewise function of pH. The concentrations of other more soluble radionuclides (technetium, carbon, iodine, cesium, and strontium) are limited by their inventory and waste dissolution rates.

The implementation of the solubility limits of radionuclides in the waste form degradation model is shown in Figure 6-13. The radionuclide mass dissolved in the rind water, whether limited by a solubility limit, by inventory, or by the waste degradation rate, is used as input to the engineered barrier system flow and transport models to calculate radionuclide transport into the waste package corrosion products.

[5] Curium is important only because ^{245}Cm decays through ^{241}Pu to ^{241}Am, which is an important radionuclide in terms of human dose. Rather than model curium explicitly in TSPA-LA, the inventory of ^{241}Am will be increased appropriately to account for the production of ^{241}Am by the decay of ^{245}Cm. Therefore, a model for curium solubility is not included in this section.

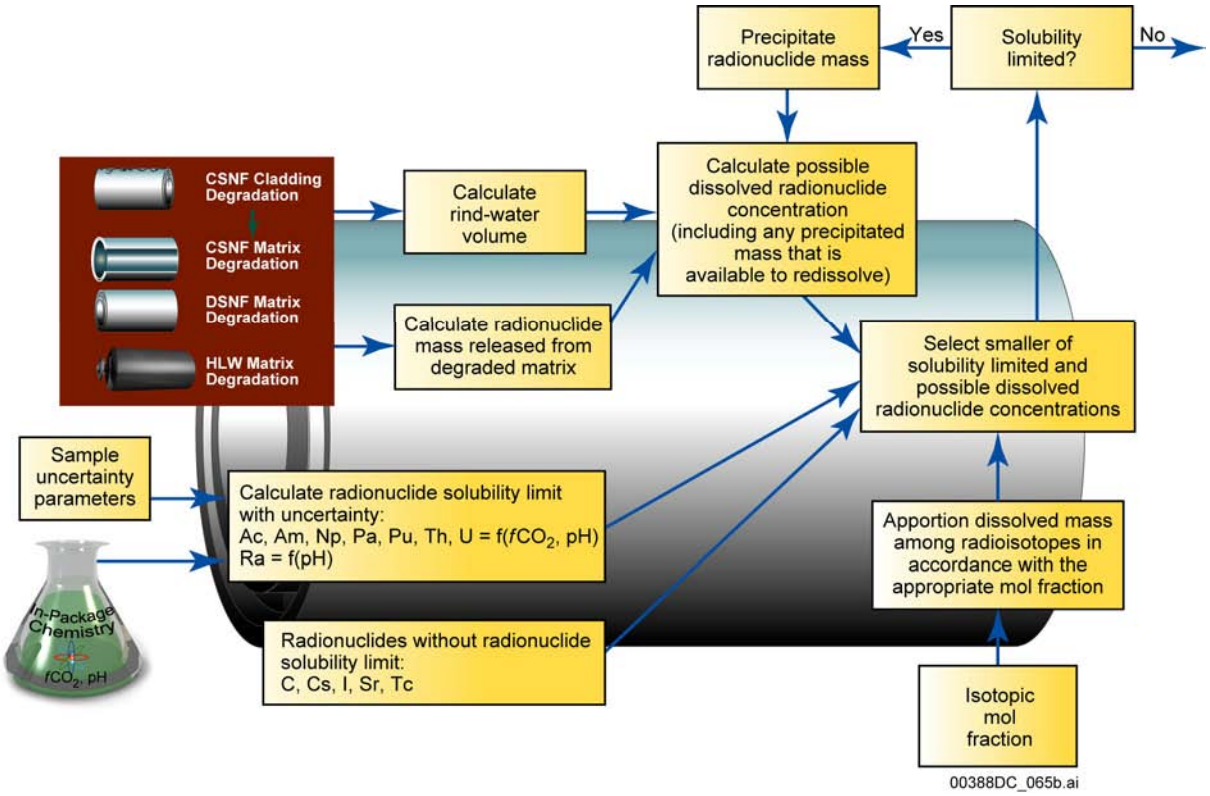

Figure 6-13. Implementation of Solubility Component in Waste Form Degradation Model in TSPA

INTENTIONALLY LEFT BLANK

7. COLLOIDAL RADIONUCLIDE AVAILABILITY

Colloids are very fine particles ranging in size from 1 nm to 10 μm in characteristic dimension. Colloids have been of concern because of the possibility that radionuclides attached to colloids may be transported faster than radionuclides dissolved in water. The primary source of information used in this section is *Waste Form and In-Drift Colloids-Associated Radionuclide Concentrations: Abstraction and Summary* (BSC 2003h).

This section discusses the formation, stability, and concentration of radioactive colloids in the waste package once water has contacted the waste and the waste has started to degrade. The discussion below describes processes occurring in the waste form that affect colloids; tests that have been performed on colloidal systems; the waste form colloid model; and uncertainties, limitations, and confidence in the model.

7.1 RELEVANT PROCESSES AND ASSUMPTIONS

The relevant processes and assumptions included in the model of colloids in the waste form are summarized below, organized by the major concepts considered: colloid formation and occurrence, colloid stability and concentration, and attachment of radionuclides to colloids. Some processes included in modeling colloid-facilitated transport in other parts of the repository are not included in the model of colloid generation in the waste form: colloid filtration, colloid sorption at the air-water interface, microbial effects, and the effects of elevated temperature. Reasons for not including these processes in the model of colloid generation in the waste form are given in *Waste Form and In-Drift Colloids-Associated Radionuclide Concentrations: Abstraction and Summary* (BSC 2003h, Sections 5.6 to 5.9).

7.1.1 Colloid Formation and Occurrence

Radioactive colloids (i.e., colloids that carry radionuclides) have been classified as either Type I colloids or Type II colloids. Type I colloids are also called true colloids, intrinsic colloids, real colloids, Eigenkolloide, and primary colloids, and are formed from the hydrolysis and polymerization of actinide ions dissolved in solution. Type I colloids are not likely to form in the waste form, and are not likely to be stable if they were to form, as discussed in Section 6.3.1 of *Waste Form and In-Drift Colloids-Associated Radionuclide Concentrations: Abstraction and Summary* (BSC 2003h). Therefore, they are not included in the model of colloids in the waste form. Type II colloids are formed when radionuclides adsorb onto colloids suspended in the water, and are the type of colloids included in the waste form colloid model.

Three sources of Type II colloids are included in the waste package colloid model: natural colloids, corrosion-produced colloids, and waste form colloids. Natural (or groundwater) colloids occur in seepage water entering the waste package and can be organic (microbes or humic substances) or inorganic (mineral fragments). As discussed in Section 6.3.1 of *Waste Form and In-Drift Colloids-Associated Radionuclide Concentrations: Abstraction and Summary* (BSC 2003h), organic colloids are not important at the repository; therefore, only inorganic natural colloids are considered, and these are modeled as smectite.

Corrosion-produced colloids are derived from the corrosion of waste package materials, and are modeled as iron oxyhydroxides. Under oxic (i.e., with oxygen) repository conditions, iron

oxyhydroxide colloids most likely consist of three species: goethite, hematite, and ferrihydrite (or hydrous ferric oxide) (Langmuir 1997, pp. 436 and 437). In addition to colloid-sized particles, the corrosion of waste package materials will produce iron oxyhydroxides that can form an immobile phase and large-scale particles that will settle out. Radionuclides can adsorb to the colloid-sized particle, the immobile phase, and the settled out particles.

Waste form colloids are formed from the corrosion of DOE HLW glass and are also modeled as smectite because experiments have shown that the degradation products of HLW glass are predominantly smectite clay (BSC 2003h, Section 4.1). Commercial SNF and DOE SNF are not considered to be sources of waste form colloids, as summarized in Section 7.3.1 and explained in Section 6.3.1.2 of *Waste Form and In-Drift Colloids-Associated Radionuclide Concentrations: Abstraction and Summary* (BSC 2003h). Colloids produced from glass waste forms contain measurable and irreversibly attached plutonium and americium. The radionuclides are modeled as embedded within the colloid, such that the properties of the smectite colloid govern the colloidal properties of the radionuclide-bearing phases.

7.1.2 Colloid Stability and Concentration

For radionuclide-bearing colloids to affect repository performance, the colloidal system must be stable during the transport period and must be able to transport significant quantities of radionuclides. The stability of colloidal suspensions against coagulation (also called agglomeration or flocculation) is controlled by electrostatic and chemical processes at colloid surfaces and by the attractive and repulsive forces between colloids. The attractive force is inversely proportional to the distance between the colloids and colloid size (Guzy et al. 1983). That is, the closer the colloids are to each other and the smaller they are, the higher the strength of the attractive force, and the more likely the colloids are to coagulate and become unstable. There are several factors that affect the strength of the repulsive force: the zeta potential (a measure of the surface charge), colloid size, ionic strength, pH, and temperature. The repulsive force is inversely proportional to the square root of temperature and to the square root of the ionic strength (Guzy et al. 1983, Equations 47 and 48). Thus, higher ionic strengths and higher temperatures lead to weaker repulsive forces between colloids, causing the colloids to coagulate and the colloidal suspensions to become unstable.

Ionic strength is one of the key factors in modeling the generation and stability of colloids inside the waste package. Initially, temperatures in the waste package will be well in excess of 100°C, which will cause dilute species in the water to become concentrated by evaporation, resulting in a high-ionic strength solution (greater than about 0.05 mol/L) that, in turn, will tend to destabilize colloid suspensions. Another key factor in colloid stability is pH. The pH at which the net surface charge of a colloid is zero is called the “zero point of charge.” Colloids become unstable and flocculate near the zero point of charge because of the reduced repulsive forces between colloids. Examples of the interaction between ionic strength and pH are given in Figures 7-1 and 7-2. Note that in these figures, the colloids are unstable above an ionic strength of 0.05 mol/L, regardless of the pH.

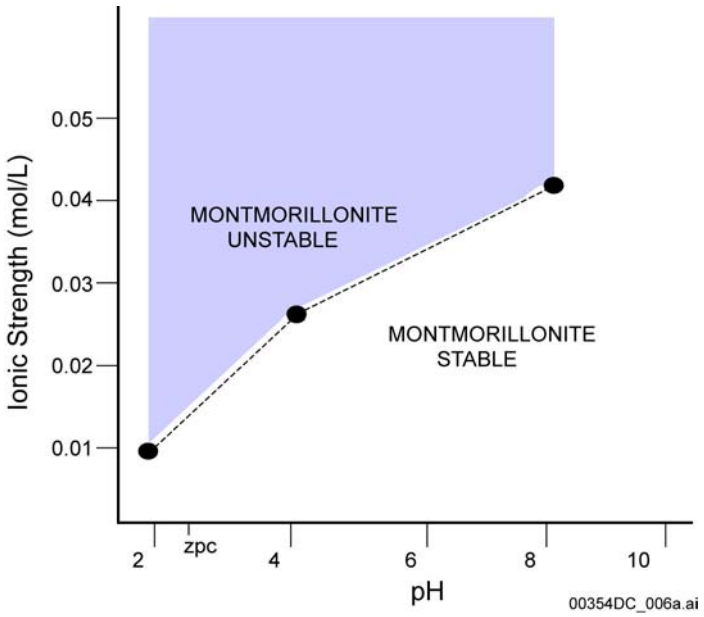

Source: BSC 2003h, Figure 4.

NOTE: zpc = zero point of charge.

Figure 7-1. Experimental Determination of Montmorillonite (a Variety of Smectite) Stability as a Function of pH and Ionic Strength

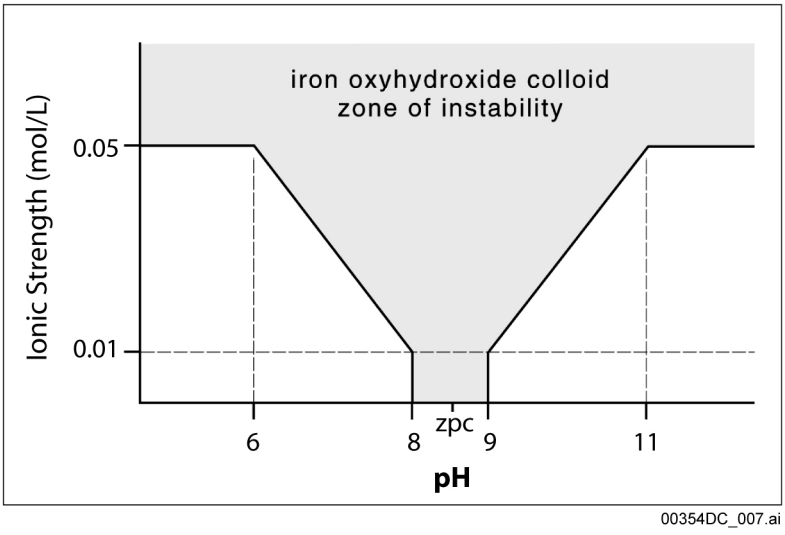

Source: BSC 2003h, Figure 7.

NOTE: zpc = zero point of charge.

Figure 7-2. Iron Oxyhydroxide Colloid Stability as a Function of pH and Ionic Strength

The ionic strength of solutions in the waste package is modeled in TSPA-LA, as described in *In-Package Chemistry Abstraction* (BSC 2004b) and summarized in Section 3, and is a complex function of waste form, flux of water through the waste package and temperature. The ionic

strength–colloid stability relations are applied to the nominal, seismic, and igneous intrusion scenarios.

Formation of stable colloid suspensions during much of the regulatory period is not likely because of the ionic strength of the solution in the waste package is likely to exceed 0.05 mol/L (e.g., see Sections 3.5.2.1 and 3.5.2.2). It is postulated, therefore, that colloid suspensions will be stable only for limited periods and limited combinations of physical and chemical conditions during the regulatory compliance period.

Colloid concentrations are related to the ionic strength and were obtained from a variety of experiments and tests, as described below in Section 7.3.

7.1.3 Radionuclide Sorption onto Colloids and Stationary Corrosion Products

Colloids become important to performance assessment only when radionuclides are attached to them. Three types of radionuclide attachment to colloids are modeled in the waste form:

- Embedded plutonium and americium from the formation of colloids from HLW glass
- Irreversible sorption of plutonium and americium on iron oxyhydroxide corrosion product colloids
- Reversible sorption of plutonium, americium, thorium, protactinium, and cesium onto HLW glass, groundwater colloids, and oxyhydroxide colloids.

These five radionuclides are included in the colloid model because they (1) have isotopes with long half-lives, (2) have low solubilities, (3) can attach to colloids, (4) represent a major portion of the inventory, and (5) have large biological dose conversion factors. The screening process by which these radionuclides were chosen is discussed in more detail in Section 6.3.3 of *Waste Form and In-Drift Colloids-Associated Radionuclide Concentrations: Abstraction and Summary* (BSC 2003h).

Plutonium and americium isotopes embedded in HLW glass degradation colloids are an intrinsic part of the colloid and are not in equilibrium with the aqueous system. These embedded radionuclides are, in effect, irreversibly attached to the colloid. Therefore, it is not necessary to model the attachment/detachment of these radionuclides (BSC 2003h, Section 6.3.3.3).

Plutonium and americium attach irreversibly to iron oxyhydroxide colloids and attach reversibly to all three kinds of colloids. The irreversibly sorbed fraction of these elements is modeled as a function of specific surface area, site density, mass of corrosion colloids, dissolved concentration of plutonium and americium, and other parameters internal to the TSPA-LA model. As a result, 90% to 99% of the plutonium and americium is irreversibly attached to iron oxyhydroxide colloids (BSC 2003h, Section 6.3.3.2).

Reversible attachment of the five elements on the three colloid types is modeled using the linear isotherm approach (Langmuir 1997), which results in radionuclide-specific distribution coefficients (K_ds) describing the partitioning of that radionuclide between the solute and the solid to which it is attached. Because both natural colloids and HLW glass colloids are modeled as

smectite, K_ds are needed for each element for smectite and iron oxyhydroxide colloids (BSC 2003h, Table 10).

To accurately represent both irreversible and reversible sorption of plutonium and americium, the upper bound of the K_d range for the reversibly sorbed fraction is reduced by a factor of 100. This results in solid/fluid partitioning that is consistent with partitioning in the unsaturated and saturated zone (BSC 2003h, Section 6.3.3.2).

Iron oxyhydroxide corrosion products form immobile phases, as well as colloids and the colloid model includes attachment of radionuclides (irreversibly for plutonium and americium, and reversibly for all five radionuclides) onto this immobile phase. A significant fraction of plutonium and americium attaches to immobile iron oxyhydroxide phases, which is more realistic than not allowing these elements to attach to immobile phases, but which also decreases the quantities of plutonium and americium available for transport.

7.2 MODEL OF COLLOIDS IN THE WASTE PACKAGE

The model of radioactive colloid generation in the waste form consists of executing two steps (BSC 2003h, Section 6.5.1) at each time step in the calculations: calculation of colloid stability and concentration, and calculation of radionuclide attachment. The two steps are presented below, along with the equations and parameters needed to execute the steps.

7.2.1 Colloid Stability and Concentration

In the first step, colloid stability and concentration are determined based on ionic strength and pH (as provided by the in-package chemistry model). The experimental data shown in Figure 7-1 were used to establish a relationship between ionic strength and pH to determine the stability of smectite colloids (BSC 2003h, Section 6.3.2.2) as follows.

- If the ionic strength exceeds pH/200, the smectite colloid suspension is not stable
- If the ionic strength is less than pH/200, the smectite colloid suspension is stable.

The pH/200 criterion represents a fit to experimental data that is discussed further in Section 7.3. If the smectite colloid suspension is stable, the concentration of groundwater colloids is sampled from the probability distribution function shown in Table 7-1. If the colloid suspension is not stable, the groundwater colloid concentration is not zero, but is set to a very small number, 1×10^{-6} mg/L.

The concentration of iron oxyhydroxides is based on experimental data discussed further in Section 7.3 and is given as a uniform distribution with a minimum concentration of 0.05 mg/L and a maximum concentration of 50 mg/L, for an ionic strength less than 0.05 mol/L (BSC 2003h, Section 6.3.2.3). This probability distribution is sampled to obtain the colloid concentration. For ionic strengths greater than 0.05 mol/L, the iron oxyhydroxide concentration is 10^{-3} mg/L, a small nonzero number (BSC 2003h, Section 6.3.2.3).

Table 7-1. Probability Distribution Function for Groundwater Colloid Concentrations Based on Ionic Strength of the Water

Ionic Strength	Groundwater Colloid Concentration (mg/L)	Probability of Occurrence
< 0.05 mol/L	0.001 to 0.1	50
	0.1 to 1.0	25
	1.0 to 10	15
	10 to 50	8
	50 to 200	2
≥ 0.05 mol/L	1×10^{-6}	100

Source: BSC 2003h, Table 5.

The concentration of waste form colloids is a function of ionic strength and is given in terms of the concentration of plutonium-bearing colloids determined by fitting experimental data (BSC 2003h, Section 6.3.2.4),

$$[\text{plutonium colloid}] = -2.5 \times 10^{-6} \times I + 1.25 \times 10^{-7}, \text{ for } 0.01 < I < 0.05 \qquad \text{(Eq. 7-1)}$$

where

[plutonium colloid] = concentration of plutonium-bearing waste form colloids (mol/L)
I = ionic strength (mol/L).

At ionic strengths less than 0.01 mol/L, the plutonium-bearing concentration of colloids is 10^{-7} mol/L, while at ionic strengths greater than 0.05 mol/L, the plutonium-bearing colloid concentration is stipulated to be 10^{-11} mol/L. The concentration of americium-bearing colloids is calculated by multiplying the plutonium-bearing concentration by the ratio of americium to plutonium in the radionuclide inventory of HLW glass at each TSPA-LA time step (BSC 2003h, Section 6.3.2.4). The concentration of colloids is obtained from the experimentally determined relationship that 1 ppm of colloids is equivalent to 2×10^{-8} mol/L of plutonium-bearing colloids (BSC 2003h, Section 6.3.1.1).

7.2.2 Radionuclide Attachment

Once colloid concentrations have been estimated, the available dissolved inventory of cesium, americium, plutonium, protactinium and thorium is partitioned between the solute and the colloids. For reversible sorption processes, a linear isotherm model is used to determine effective reversibility of the radionuclides on colloids (BSC 2003h, Section 6.5.1):

$$C_{\text{RN,adsorbed}} = C_{\text{RN,dissolved}} \times K_{d,\text{ RN}} \times M_{\text{colloid}} \times 10^{-6} \qquad \text{(Eq. 7-2)}$$

where

$C_{\text{RN, adsorbed}}$ = concentration of radionuclide reversibly attached to colloids (mg/L)
$C_{\text{RN, dissolved}}$ = concentration of dissolved radionuclide (mg/L)
$K_{d,\text{RN}}$ = distribution coefficient for radionuclides on colloids (mL/g)
M_{colloid} = colloid concentration (mg/L)
10^{-6} = correction factor to account for various units

The concentration of dissolved radionuclides is given by the model described in Section 6, while the colloid concentrations are given above. The probability distributions for the distribution coefficients used in Equation 7-2 are given in Table 7-2.

Table 7-2. K_d Values (mL/g) Used for Reversible Radionuclide Sorption on Colloids

Radionuclide	Colloid	K_d Value Intervals (mL/g)	K_d Value Interval Probabilities
Pu	Smectite	$<1 \times 10^3$ 1×10^3 to 5×10^3 5×10^3 to 1×10^4 1×10^4 to 5×10^4 5×10^4 to 1×10^5 1×10^5 to 5×10^5 5×10^5 to 1×10^6 $> 1 \times 10^6$	0 0.04 0.08 0.25 0.2 0.35 0.08 0
	Iron Oxyhydroxide	$<1 \times 10^4$ 1×10^4 to 5×10^4 5×10^4 to 1×10^5 1×10^5 to 5×10^5 5×10^5 to 1×10^6 $> 1 \times 10^6$	0 0.15 0.2 0.5 0.15 0
Am, Th, Pa	Smectite	$<1 \times 10^4$ 1×10^4 to 5×10^4 5×10^4 to 1×10^5 1×10^5 to 5×10^5 5×10^5 to 1×10^6 1×10^6 to 5×10^6 5×10^6 to 1×10^7 $> 1 \times 10^7$	0 0.07 0.1 0.23 0.2 0.32 0.08 0
	Iron Oxyhydroxide	$<1 \times 10^5$ 1×10^5 to 5×10^5 5×10^5 to 1×10^6 1×10^6 to 5×10^6 5×10^6 to 1×10^7 $> 1 \times 10^7$	0 0.15 0.2 0.55 0.10 0
Cs	Smectite	$<1 \times 10^2$ 1×10^2 to 5×10^2 5×10^2 to 1×10^3 1×10^3 to 5×10^3 5×10^3 to 1×10^4 $> 1 \times 10^4$	0 0.2 0.25 0.5 0.05 0
	Iron Oxyhydroxide	$<1 \times 10^1$ 1×10^1 to 5×10^1 5×10^1 to 1×10^2 1×10^2 to 5×10^2 5×10^2 to 1×10^3 $> 1 \times 10^3$	0 0.13 0.22 0.55 0.1 0

Source: BSC 2003h, Table 10

The distribution of plutonium and americium irreversibly attached to mobile and immobile iron oxyhydroxide colloids is calculated by a kinetic model that is described in Attachment II of *EBS Radionuclide Transport Abstraction* (BSC 2004f). It is a function of the specific surface area of iron oxyhydroxide colloids and corrosion products, the mass of iron oxyhydroxide colloids and corrosion products, the porosity of the iron oxyhydroxide matrix, and the reaction rate of the irreversible attachment reaction.

The distribution of plutonium and americium in embedded HLW glass colloids does not need to be calculated because it was calculated as a part of determining the colloid concentration (see Equation 7-1).

7.2.3 Output to Model of Corrosion Products in Waste Package

The waste form colloid source term model provides eight outputs to the model of the invert. They are:

- Mass concentration of waste form (HLW glass, modeled as smectite) colloids. This is calculated from stability requirements and Equation 7-1, as scaled by the relationship of 1 ppm colloids = 2×10^{-8} mol/L plutonium colloids.

- Mass concentration of iron oxyhydroxide colloids. This is calculated from stability requirements and sampled from iron oxyhydroxide colloid concentration distribution

- Mass concentration of groundwater colloids. This is calculated from stability requirements and sampled from the distribution shown in Table 7-1.

- Radionuclide (americium and plutonium) mass concentration embedded in waste form colloids. This is calculated from stability requirements and Equation 7-1.

- Radionuclide mass concentration reversibly attached to waste form colloids. This is calculated from stability requirements, Equation 7-1 as scaled by the relationship of 1 ppm colloids = 2×10^{-8} mol/L plutonium colloids, Equation 7-2, and K_d values given in Table 7-2.

- Radionuclide (americium and plutonium) mass concentration irreversibly attached to iron oxyhydroxide colloids. This is calculated from stability requirements, sampled iron oxyhydroxide colloid concentrations, and kinetic equations (BSC 2004f, Attachment II).

- Radionuclide mass concentration reversibly attached to iron oxyhydroxide colloids. This is calculated from stability requirements, sampled iron oxyhydroxide colloid concentrations, Equation 7-2, and K_d values given in Table 7-2.

- Radionuclide mass concentration reversibly attached to groundwater colloids. This is calculated from stability requirements, groundwater colloid concentrations sampled from the distribution given in Table 7-1, Equation 7-2, and K_d values sampled from the distributions given in Table 7-2.

7.3 SOURCES OF DATA AND EXPERIMENTAL PROGRAM

The data from many experiments and tests have been used in developing the colloid model. Results from tests and experiments on waste forms, tests to determine colloid concentrations, studies of colloid stability, and experiments to determine radionuclide sorption properties are discussed below.

7.3.1 Tests on Commercial Spent Nuclear Fuel, U.S. Department of Energy Spent Nuclear Fuel, and High-Level Radioactive Waste Glass to Examine Colloid Generation

Long-term corrosion testing of commercial SNF and DOE SNF under hydrologically unsaturated, oxidizing conditions have been performed at Argonne National Laboratory and Pacific Northwest National Laboratory to examine release of dissolved and colloid-associated radionuclides (Mertz et al. 2003, DTN: MO0306ANLSF001.459). This testing is described in some detail in Section 6.3.1.2 of *Waste Form and In-Drift Colloids-Associated Radionuclide Concentrations: Abstraction and Summary* (BSC 2003h). Testing was designed to simulate a variety of repository-relevant water-exposure conditions for several waste forms spanning a range of fuel burnups and compositions. Results from the unsaturated testing of commercial SNF indicated some spallation of alteration products containing low concentrations of uranium-based colloids as well as low concentrations of actinides. Data from DOE SNF tests are still preliminary but show rapid disintegration of uranium metal into particles, many of colloid size. Most of the colloids were uranium oxyhydroxides; the data suggest that over time some smectite colloids with associated plutonium formed. In separate tests designed to investigate the stability of schoepite colloids, it was observed that they became less stable over a period of a few months, and that they appeared to dissolve when introduced to well J-13 water.

Colloids formed from commercial SNF and DOE SNF degradation are not included in the colloid model and abstraction based on the Argonne National Laboratory and Pacific Northwest National Laboratory results. Additional information obtained at Argonne National Laboratory on the characterization of uranium-phase colloid suspensions, and results from natural analog studies (BSC 2003h, Section 6.3.1.2) substantiate this modeling approach.

Tests on HLW in borosilicate glass have been conducted at Argonne National Laboratory in which EJ-13 water or deionized water drips onto or immerses HLW glass waste forms (CRWMS M&O 2001b). Waste forms tested include Savannah River Laboratory and West Valley Demonstration Project glasses. Transmission electron microscopy and filtration were used to characterize colloids produced during the tests. The unsaturated drip tests are representative of drip conditions that may occur in a geologic repository with canisters exposed to groundwater and air. These tests allow the spallation of fragments (including colloids) to be investigated. Saturated tests appear to be suitable for simulating colloid formation from glass reaction (Buck and Bates 1999), where similar colloids (smectite clay and rhabdophane colloids) are formed in both unsaturated and saturated tests.

7.3.2 Tests to Determine Colloid Concentrations

Corrosion colloid concentration values are estimated based on experiments performed at the University of Nevada, Las Vegas. In these experiments, scaled-down miniature waste packages were exposed to Well J-13 groundwater in either a bathtub mode or a flow-through mode. Corrosion products released from the miniature waste packages were characterized by x-ray diffraction (DTN: MO0302UCC034JC.003), and the quantity of corrosion products transported out of the waste packages was measured by microfiltration (DTN: MO0212UCC034JC.002).

Recently acquired data from the Yucca Mountain area and the Nevada Test Site by Los Alamos National Laboratory show a wide range in natural (groundwater) colloid concentrations over a relatively narrow range of ionic strength. The colloid concentration data, as well as the probability distribution used in TSPA-LA, were collected from nine different sources, as described in Section 6.3.2.5 of *Waste Form and In-Drift Colloids-Associated Radionuclide Concentrations: Abstraction and Summary* (BSC 2003h). Literature data (Degueldre et al. 2000) and groundwater sampling at the Idaho National Engineering and Environmental Laboratory (BSC 2003h, Section 6.3.2.5) provided additional technical information that corroborated site-specific data.

The saturated tests on HLW glass performed at Argonne National Laboratory described above were also used to estimate the concentration of plutonium-bearing colloids resulting from the degradation of HLW glass (CRWMS M&O 2001b). Colloid concentration was observed to decrease as the ionic strength increased, and flocculation was observed at an ionic strength of approximately 0.05 mol/L.

7.3.3 Tests to Examine Colloid Stability

The DOE HLW tests conducted at Argonne National Laboratory resulted in measured pH ranging between approximately 9 and 11.5 (Buck and Bates 1999), which is part of the range at which smectite colloids exhibit the highest surface charge and, hence, are most stable. Tombacz et al. (1990) investigated the stability of smectite (referred to as montmorillonite by Tombacz et al.) suspensions as a function of pH and ionic strength in a NaCl solution. It was found that suspensions became unstable and flocculated at pH 2, 4, and 8 in 0.01 mol/L, 0.025 mol/L, and 0.04 mol/L NaCl solutions, respectively (see Figure 7-1). The abstracted relationship between ionic strength and smectite colloid stability as a function of pH (up to pH 10 and ionic strength of 0.05 mol/L) for use in TSPA-LA model is discussed in Section 7.2 (i.e., colloid suspension is stable if ionic strength is less than pH/200).

The stability of iron oxyhydroxide colloids has been investigated (Liang and Morgan 1990) with the results used to abstract the stability region as a function of pH and ionic strength. At and near the zero point of charge, colloid suspensions are not stable, even at low ionic strengths. For iron oxyhydroxide colloids, the zero point of charge ranges from about pH 5.5 to about 8.5, depending on colloid mineralogy and water chemistry. Colloids are stable at higher and lower pH values, similar to other mineral colloids, if the ionic strength is less than 0.05 mol/L. The result is a U-shaped stability curve (Liang and Morgan 1990).

7.3.4 Radionuclide Sorption

The K_d values used to model reversible radionuclide sorption onto colloids were obtained from various data sources and measurements including those from National Cooperative for the Disposal of Radioactive Waste, the U.S. Environmental Protection Agency, and Yucca Mountain-specific projects. These sources are discussed in Section 6.3.3.1 of *Waste Form and In-Drift Colloids-Associated Radionuclide Concentrations: Abstraction and Summary* (BSC 2003h). Based on these sources, professional judgment was used to develop the uncertainty distributions given in Table 7-2.

Sources of Yucca Mountain Project–specific sorption data from Los Alamos National Laboratory research provide valuable information on the sorption of plutonium onto colloidal dispersions of hematite, goethite, montmorillonite, and silica (Lu et al. 1998; Lu et al. 2000). Data on americium were generated for all but goethite. Sorption was measured as a function of time up to 4 or 10 days. Desorption was measured after 150 days because desorption tends to be much slower in these mineral-sorbate systems.

Two compendia of sorption data were considered in the development of K_d values. One is the compendium developed by the National Cooperative for the Disposal of Radioactive Waste (NAGRA, Switzerland) in which a set of K_d values was compiled (Stenhouse 1995). The second compendium was developed by the U.S. Environmental Protection Agency (EPA 1999). In that work, information on radionuclides including strontium, cesium, thorium, uranium, and plutonium is compiled. Predicted ranges of K_d values are presented for soils in shallow subsurface environments. The group of radionuclides covered does not provide analog elements for americium(III), protactinium(V), or neptunium(V).

In developing K_d values a modeling analysis was performed (Honeyman and Ranville 2002) that incorporated Yucca Mountain–vicinity groundwater chemistry and colloid size and concentration data (Kingston and Whitbeck 1991). K_d values were calculated by accounting for electrostatic forces and chemical reactions occurring at the surface of the colloids. Colloid concentrations of up to about 100 mg/L were included. In the system analyzed, approximate K_d value ranges for americium, neptunium, plutonium, thorium, and uranium were provided.

Plutonium and americium sorb strongly to iron oxyhydroxides, based on observations that plutonium binds strongly to soils, leaving very little, if any, soluble plutonium available for groundwater transport or plant uptake. The estimated exchangeable plutonium, which is the quantity of plutonium that may desorb after initial sorption, is less than 1% (Coughtrey et al. 1985; Litaor and Ibrahim 1996; Bunzl et al. 1995). Exchangeable americium ranges from 1.5% to 15% (Bunzl et al. 1995). Transport of colloidal plutonium over hundreds of meters was observed at the Nevada Test Site (Kersting et al. 1999). The laboratory experiments of plutonium sorption onto iron oxides cited above have shown that only approximately 1% of the initially sorbed plutonium can be desorbed into solution, even after months of time have elapsed (Lu et al. 2000), which is broadly consistent with field observations.

7.4 UNCERTAINTIES, LIMITATIONS, AND MODEL CONFIDENCE

The model for radioactive colloid generation, stability, and concentration in the waste form is valid for the ionic strengths and pH ranges expected in the waste package (see Section 3). Uncertainties associated with the model and model confidence building are discussed below.

7.4.1 Uncertainty in Colloid Model

There are several sources of uncertainty in the colloid model, mostly resulting from incomplete knowledge of the system and its properties (epistemic uncertainty): temporal scaling, spatial scaling, physical and chemical conditions of data acquisition, waste form colloid concentrations, groundwater colloid concentrations, colloid stability conditions, and colloid sorption parameters. The discussion of these uncertainties presented below is based on *Waste Form and In-Drift Colloids-Associated Radionuclide Concentrations: Abstraction and Summary* (BSC 2003h, Section 6.6.2). Many of the uncertainties in the model are treated by using parameter ranges and distributions rather than a single deterministic value in the model. These uncertainties are propagated through to the model results by using Monte Carlo simulation techniques.

Temporal Scaling–Data gathered over days to a few years, or perhaps decades, were used to develop a model of what is anticipated to occur over thousands of years. For fundamental parameters, such as radionuclide half-life, this extrapolation does not introduce uncertainty. For other parameters, such as those influenced by kinetic considerations, such an extrapolation can introduce significant uncertainty. This uncertainty is best accounted for by developing and using scientifically sound assumptions.

Spatial Scaling–Data collected in the laboratory on processes occurring on a small scale (centimeters) were used to develop a model of what is anticipated to occur on a much larger scale (kilometers). This uncertainty was accounted for by corroborating data obtained from small-scale processes with empirical field observations, to the extent possible. For example, empirical field observations of uranium mines and deposits showed low concentrations of uranium-bearing colloids and showed that uranium leaches from colloids as they migrate downgradient (BSC 2003h, Section 6.3.1.2.4).

Physical and Chemical Conditions of Data Acquisition–Data may have been collected under physical or chemical conditions that are not directly relevant to repository conditions (e.g., pH). In such cases, the experimental conditions and the expected repository conditions were compared in detail to determine the applicability of the data. For example, data on generation of waste form colloids was obtained at pHs ranging from 9 to 11.5. However, the pH in the codisposal waste package is expected to range from 4.5 to 8.1 under the nominal and seismic scenarios and from 7.6 to 9.9 in the igneous intrusion scenario. The experimental data were found to be applicable because smectite is stable in the pH range expected in the codisposal waste package (BSC 2003h, Sections 6.3.2.4 and 7.1).

Waste Form Colloids–Potentially significant uncertainty comes from basing modeled glass waste form colloid concentrations, as well as associated plutonium concentrations, on two data sets generated from glass-waste-form degradation testing. Additional uncertainty is introduced by using assumptions (spherical form, single density, etc.) for converting particle concentrations

to mass concentrations. Colloid and plutonium mass concentrations are predicted on the basis of these data, and ionic strength and pH obtained from in-package chemistry calculations.

Iron Oxyhydroxide Colloids–Three studies reported groundwater colloid concentrations dominated by iron oxyhydroxide colloids, and the colloid concentrations reported varied greatly (BSC 2003h, Section 6.3.1.3). As a result, the values and ranges developed for the corrosion colloid source-term parameters have a large degree of uncertainty. To reduce uncertainty and increase the defensibility of the developed parameters, the distribution of iron oxyhydroxide colloid concentrations was based on quantities of iron oxyhydroxide colloids observed in scaled-down miniature waste package degradation experiments by an ongoing DOE-funded research project at the University of Nevada, Las Vegas. The use of appropriately scaled-down waste package configurations (i.e., surface area to total waste package volume scaled-down proportionally to approximately 1/70 the size of actual repository waste packages) and the use of water of similar chemical composition to the groundwater found at Yucca Mountain render the experiments directly relevant to conditions anticipated in the repository. Additionally, bounding values have been established for corrosion product colloid parameters recommended for use in the model in order to propagate the uncertainty associated with these parameters throughout the TSPA-LA.

Groundwater Colloids–Uncertainties associated with the determination of colloid concentration in seepage or groundwater result from differences in field-sampling techniques (including differences in pumping rates at each well during extraction of the water samples; unknown factors affecting the quantities of particles suspended in water samples such as additives introduced to the wells during the drilling process), and errors inherent to the laboratory methods used to measure the quantities of colloids suspended in the water samples (e.g., filter ripening, and interference and detection limitations for dynamic light-scattering measurement techniques). In general, sampling perturbations may result in overestimation of colloid concentrations. To account for this uncertainty, a cumulative distribution function was developed based on groundwater samples extracted in the vicinity of Yucca Mountain and Idaho National Engineering and Environmental Laboratory (BSC 2003h, Table 5).

Uncertainty in Colloid Stability–Uncertainty in the stability of smectite colloids as a function of pH and ionic strength is associated mostly with the extrapolation of laboratory data reported in literature or project-supported experimental work solution chemistry in the repository environment over the regulatory compliance period. Establishing bounding values and ranges of parameter values accommodate much of this uncertainty, which is propagated in TSPA-LA model by stochastic sampling of distributions.

Uncertainty in Sorption Partition Coefficients–There is uncertainty associated with the development of sorption partition coefficients (K_d values) that describe the degree of sorption of specific radionuclides to colloids in TSPA-LA model. Values reported in literature are primarily the result of experimental work that establishes K_d values for contaminants sorbed onto rocks, soils and other minerals; literature specific to colloid-size minerals is not readily available. For this reason, the K_d value parameters established for smectite colloids largely rely on limited experimental work conducted at the Los Alamos National Laboratory (Lu et al. 1998; Lu et al. 2000). Corroborative data reported in the literature were evaluated to augment this work (BSC 2003h, Section 6.3.3.1, Table 10).

7.4.2 Model Confidence Building

To build confidence in the model, various aspects of the model were compared to data published in refereed journals or literature, and to data from natural analog sites, when possible. A summary of these comparisons is presented below, arranged by waste form, colloid concentration, and radionuclide attachment modeling. A more detailed discussion is in Section 7 of *Waste Form and In-Drift Colloids-Associated Radionuclide Concentrations: Abstraction and Summary* (BSC 2003h).

Waste Forms–The assumption that commercial SNF and DOE SNF are not a source of colloids has been corroborated by the observation of few colloids in the vicinity of uranium mines and deposits. HLW glass data were collected at pH values ranging from 9 to 11.5, but the pH range anticipated in the repository is from 4.5 to 8.1 for the nominal and seismic scenarios and from 7.6 to 9.9 for the igneous intrusion scenario. The applicability of the data from the tests to repository conditions was evaluated by considering the physicochemical properties of smectite colloids and similarities between test conditions and the probable microenvironment at the degrading glass surface. Uncertainty in plutonium concentration was accounted for by using a bounding value.

Colloid Concentrations–Smectite colloid concentrations obtained from HLW glass testing appear to conform to accepted scientific principles with respect to colloid suspensions, and they are reasonable with respect to observations of colloids of similar mineralogy in the literature. Groundwater colloid concentrations used in the model are site-specific, have been bounded realistically, are internally consistent, and are similar to colloid concentration data from disparate geologic terrain around the world. Iron oxyhydroxide colloid concentrations could not be compared with literature values because of the lack of peer-reviewed publications that present colloid concentrations as a function of aqueous chemistry (BSC 2003h, Section 7.2). However, they are reasonable and realistic, have been corroborated by laboratory-scale waste package corrosion tests, and perhaps overpredict colloid concentrations.

Radionuclide Attachment Modeling–The assumption that plutonium is embedded in HLW glass colloids is based on the results of HLW glass tests performed at Argonne National Laboratory. These are one-of-a-kind data and so cannot be compared to results in refereed journals, nor are there any analog sites. Some model confidence can be built, however, by noting that repeated sample analyses produced similar results. Furthermore, this assumption increases the potential mobility of plutonium. The K_d values chosen to model reversible attachment of radionuclides to colloids have a strong scientific basis because of good agreement between literature-based and observation-based values. The assumption that plutonium is irreversibly attached to iron oxyhydroxides has been corroborated in laboratory experiments, which show almost complete retention of plutonium onto iron oxyhydroxide colloids for up to 6 months and in field observations over periods up to 50 years.

7.5 SUMMARY AND CONCLUSIONS

Colloids come from the degradation of HLW glass and associated components in the repository or from water seeping into the waste package. The TSPA-LA model of colloids in the waste

package includes colloids from both HLW glass (smectite), steel (iron oxyhydroxides), and seepage water (smectite). Commercial SNF and DOE SNF are not sources of colloids.

Colloid stability and concentrations are determined in the TSPA-LA model and are based on ionic strength and pH. If chemical conditions are favorable for sustaining a colloidal suspension, colloid concentrations are estimated from equations or sampled from uncertainty distributions. If chemical conditions lead to an unstable colloidal suspension, colloid concentrations are assigned a very small (nonzero) value.

Two types of colloid attachment, reversible (using a linear isotherm) and irreversible, are modeled. Plutonium and americium are (irreversibly) embedded in HLW glass colloids and can also attach irreversibly to iron oxyhydroxide colloids and stationary iron oxyhydroxide corrosion products in the waste package. The reversible attachment of five elements is modeled: plutonium, americium, thorium, protactinium, and cesium. These five elements sorb reversibly onto the three different colloid types.

The model provides colloid mass concentrations (mass concentrations of HLW glass, iron oxyhydroxide, and natural colloids) and radionuclide mass concentrations (mass concentrations of embedded plutonium and americium; of plutonium and americium irreversibly attached to iron oxyhydroxide colloids; and of plutonium, americium, thorium, protactinium, and cesium reversibly attached to HLW glass, iron oxyhydroxide, and natural colloids) to the model of the invert. These concentrations are used to model radionuclide movement through the rest of the repository system.

As long as chemical conditions are favorable to colloid stability, stable colloid suspensions may form, and colloids may facilitate movement of radionuclides through the repository. However, colloid suspensions are not highly likely to be stable in the waste package because the chemical conditions are not highly likely to be favorable.

INTENTIONALLY LEFT BLANK

8. SUMMARY AND CONCLUSIONS

As the starting point for all potential radionuclide releases to the biosphere, the source term for radionuclides within the engineered barrier system is an important component model for the TSPA-LA. This document deals with an aspect of the source term component — the degradation of the waste form and the mobilization of radionuclides within the waste package — herein called the waste form degradation model. The function of the waste form degradation model is to estimate the availability and mobilization of radionuclides that are used as input by the engineered barrier system transport model. The engineered barrier system transport model discussed in *Technical Basis Document No. 9: Engineered Barrier System Radionuclide Transport* provides the radionuclide source term to the unsaturated zone transport model discussed in *Technical Basis Document No. 10: Unsaturated Zone Transport.*

8.1 COMPONENTS OF WASTE FORM DEGRADATION MODEL

The waste form degradation model consists of eight components. Five of those components determine the degradation rate of waste forms: in-package chemistry (Section 3); degradation of commercial SNF cladding (Section 4); and degradation of commercial SNF fuel pellets, DOE SNF, and HLW vitrified in borosilicate glass (Section 5).

Of the remaining three components—radionuclide inventory (Section 2), dissolved concentration of radionuclides (Section 6), and concentration of radionuclides attached to colloids (Section 7)—the latter two determine the mobilization of radionuclides from the degraded waste form into the waste package corrosion products.

All eight components are used in the nominal and seismic scenario classes and the igneous intrusion modeling case of the volcanic scenario class (Table 1-1). Only the radionuclide inventory component is used to model radionuclide release in those emplacement drifts of the repository that are disrupted by a volcanic eruption For the human intrusion analysis, only the radionuclide inventory component is used.

8.2 RADIONUCLIDE INVENTORY

An important input to the waste form degradation model is the average radionuclide inventory (expressed as grams of each radionuclide per package) for three generic waste forms: commercial SNF, DOE SNF and HLW encapsulated in borosilicate glass. A fourth waste form, naval SNF, is conservatively represented by commercial SNF. The three waste forms are placed into two waste package configurations: a commercial SNF waste package with various numbers of assemblies of SNF, and a codisposal waste package with typically one canister of DOE SNF and five canisters of HLW. As described in Section 2, 28 radionuclides (14 elements) were identified (BSC 2002a, Section 6.3.1) as being important to evaluating expected dose within the biosphere during the 10,000-year regulatory period. Of these 14 elements, curium was decayed and added into the inventory of americium in the TSPA-LA model.

8.3 IN-PACKAGE CHEMISTRY

The in-package chemistry component models the evolution of water chemistry inside the breached waste package for the nominal scenario class when only water vapor enters the waste

package, in the igneous intrusion scenario when bare fuel comes into contact with basalt-equilibrated groundwater, and for the seismic scenario class when dripping water enters several waste packages. Factors that control the in-package chemistry component are the waste package corrosion rate, waste package type (commercial SNF versus codisposed), water inflow rate, cladding failure fraction, waste-form corrosion rate, and temperature. The water inflow rate is modeled under two different situations: water vapor inflow and variable dripping water inflow. In the latter situation, in-package chemistry is a direct function of the dripping water rate and fraction of failed cladding on commercial SNF. In-package chemistry is insensitive to initial water composition, decreased corrosion rate of the waste package alloys and minor modifications to waste package design.

Primary outputs from the in-package chemistry component include time-dependent pH, ionic strength, total carbonate, and fluoride. Of these outputs, pH and ionic strength are the most important. Effluent chemistries will be strongly affected by the presence of the surfaces of corrosion products, primarily iron oxides and hydroxides. Corrected for the effect of surface complexation on corrosion products, the in-package pH ranges from 4.5 to 8.1 for the nominal and seismic scenario classes. For the igneous intrusion scenario class, the pH is neutral to slightly basic (7.6 to 9.9). The ionic strength inside a waste package increases with time and can reach a value above 1 mol/L.

This water chemistry information is used by five waste form degradation and radionuclide mobilization models: commercial SNF matrix degradation, HLW degradation, dissolved concentration of radionuclides, HLW colloidal concentration, and corrosion products and groundwater colloidal concentration. Some of these models are very sensitive to the pH in the waste package, particularly low values of pH that can lead to higher waste form degradation rates and higher radionuclide solubilities.

8.4 COMMERCIAL SPENT NUCLEAR FUEL CLADDING DEGRADATION COMPONENT

For the nominal scenario class, only the small fraction of fuel rods that arrive at the repository with perforated cladding (about 0.1%) can lead to the release of radionuclides during the 10,000-year regulatory period. Additional failures during the regulatory period from other mechanisms (e.g., hydride embrittlement, localized corrosion) are not anticipated. Once cladding is perforated, the cladding is assumed to rapidly split along the entire length of the fuel rod. Subsequent degradation of exposed fuel is assumed to produce a rind, the volume of which is estimated by the commercial SNF cladding degradation component. Radionuclides dissolved in available water must diffuse through the rind to escape from the waste matrix.

However, for the seismic scenario class, the cladding is susceptible to mechanical failure from seismic events, depending on their nature and probability, which can increase the number of failed fuel rods. Once the cladding is perforated, the progression of clad splitting, fuel dissolution, and radionuclide transport proceeds as in the nominal scenario.

In the igneous intrusion scenario, cladding is assumed to be destroyed, exposing the fuel pellets to water.

8.5 WASTE FORM DEGRADATION

8.5.1 Commercial Spent Nuclear Fuel Matrix Degradation

The radionuclide inventory in commercial SNF rods is divided into two fractions. The largest fraction of the inventory resides in the fuel matrix. A small fraction of the inventory resides in the grain boundaries of the fuel pellets and the gap between the fuel pellet and cladding. Radionuclides (specifically ^{90}Sr, ^{137}Cs, ^{99}Tc, and ^{129}I) residing in the gap or grain boundary are available for dissolution as soon as water contacts the waste. Uncertainty in the gap and grain boundary fractions is represented by triangular probability distributions.

The release of radionuclides from the fuel matrix is based on a statistical fit of experimental data using four variables: temperature, pH, total carbonate concentration and oxygen fugacity. Based on the experimental data, two models were developed, one for alkaline conditions and one for acidic conditions. The specific degradation rate is lowest at values of pH above 6.8. The fractional release rate of any radionuclide in the fuel matrix is obtained by multiplying the specific degradation rates of the fuel matrix by the estimated effective specific surface area of the fuel and the matrix inventory of that radionuclide. The uncertainty in specific surface area of the fuel has an important effect on radionuclide releases and was estimated from experimental fractional release data.

The presence of a gap fraction and the rapid degradation of the commercial SNF fuel matrix in an oxic environment, as expected to exist in the repository, implies that the release of most radionuclides from the waste package is not limited by their availability (i.e., not limited by the degradation rate) but by their solubility or by adsorption onto corrosion products. However, the solubilities of ^{99}Tc and ^{129}I are quite high in an oxic environment and are not readily adsorbed; hence, the degradation rate of the commercial SNF fuel matrix influences the release rate of these two radionuclides.

8.5.2 U.S. Department of Energy Spent Nuclear Fuel Degradation Component

Eleven DOE SNF groups have been used to categorize several hundred distinct types of DOE SNF that will eventually be emplaced in the repository. Although degradation models were developed for each DOE SNF group, their use is not recommended because they are based on currently unqualified data. Instead, a degradation rate model consisting of waste form degradation and radionuclide dissolution within the first time step in the TSPA model following waste package breach is applied for all waste groups except naval SNF. Naval SNF cladding is modeled as commercial SNF cladding. Naval SNF has been found to be more robust than commercial SNF. Using the naval SNF source term developed by the Naval Nuclear Propulsion Program, the DOE estimates that the dose resulting from naval SNF is significantly less than that from an equivalent amount of commercial SNF. A planned classified Naval Nuclear Propulsion Program Technical Support Document to the LA will provide details of this naval SNF source term. Therefore, using commercial SNF as a surrogate for naval SNF will overestimate radionuclide releases from naval SNF.

Because radionuclides from DOE SNF are considered to be available for transport once the waste form is contacted by water, the dissolved concentration of a particular radionuclide is

controlled either by radionuclide solubility (for those radionuclides with solubility limits) or by the waste form degradation rate (for those radionuclides that do not have solubility limits).

8.5.3 High-Level Radioactive Waste Degradation Component

The dissolution of HLW glass into water has been studied for many years, producing an extensive database of experimental results. Many processes contribute to glass degradation and these are well known, although there is some debate as to whether the rate of dissolution at high dissolved silica concentrations is controlled by surface reactions or by the diffusion of silica through alteration phases that form on the glass as it dissolves.

Glass degradation is controlled by the temperature and pH of the solution in contact with the glass. The degradation rate equation has an Arrhenius-type dependence on temperature, and uncertainty in the degradation rate is accounted for by an uncertain degradation rate coefficient. Experimental data obtained from experiments in which HLW glasses were exposed to water vapor and dripping water, and were immersed in water, were used to develop the degradation rates of the HLW glass logs. Because specific glass dissolution rates are lowest at a near-neutral pH and increase as the pH decreases from 7 or increases from 7, model parameters were developed for both acidic and alkaline conditions. The mass of a particular radionuclide released from the HLW glass per time is calculated by multiplying the specific glass degradation rate by the effective specific surface area of the glass log and the inventory of that radionuclide.

The specific surface area of the glass contacted by water changes as the glass dissolves and increases as a result of cracking. These surface-area effects are addressed by recalculating the amount of glass remaining after each time step, and by multiplying the surface area by an empirically determined uncertain exposure factor to account for cracking. The uncertainty in this exposure factor is described by a triangular probability distribution.

8.6 DISSOLVED RADIONUCLIDE CONCENTRATION COMPONENT

The dissolved radionuclide concentration component determines the availability of specific radionuclide species in the waste package. For all scenario classes involving transport of colloidal and dissolved radionuclides by groundwater, the solubility of seven important elements transported (plutonium, americium, neptunium, thorium, uranium, protactinium and actinium) depends on the water chemistry inside the waste package (specifically, pH and fugacity of carbon dioxide). The solubility of these actinides exhibits a typical U-shaped dependence on pH with a minimum at approximately neutral to mildly basic pH values, which coincides with long-term in-package conditions. For example, compare the solubility minima in Figures 6-2 to 6-10 with the pH range of 4.5 to 8.1 expected in the waste form. Error terms are added to the solubility value calculated by EQ3NR and used to characterize (1) the uncertainty in thermodynamic data, and (2) the uncertainty in the fluoride concentration. The latter term was added because the fluoride content of in-package water will vary depending on the source of the water (condensate or seepage) and the extent of dissolution of fluoride-containing HLW glass. The relationship of solubilities to pH and fCO_2 was based on numerous thermodynamic equilibrium calculations at 25°C. Actinide solubilities decrease with increasing temperature so the use of 25°C values for higher temperatures is conservative. The range of applicability for the functional relationships are an ionic strength less than 3 mol/L, a $\log(fCO_2)$ between −5 and

−1.5, and a pH between 2 and 11, depending on the element. The latter pH envelope is much larger than the expected pH range, 4.5 to 8.1 and allows functional dependencies in solubility to be highlighted.

For an eighth element, radium, the solubility is defined solely as a function of pH without any error terms. The solubilities of the remaining five important elements transported (i.e., carbon, cesium, strontium, iodine, and technetium) depend mostly on the oxygen state of the repository. Over the long-term, the repository is expected to be fairly oxic (i.e., in equilibrium with atmospheric oxygen); as a result, these radionuclides are highly soluble. Hence, the availability of these radionuclides for transport out of the waste form is determined by the fraction of cladding that fails and the degradation rate of the waste form.

8.7 COLLOID CONCENTRATION COMPONENT

The colloid model estimates the concentration and stability of colloids available for transporting radionuclides. Three sources of colloids are considered in the colloid model in the waste form: natural colloids in seepage groundwater, colloids generated from degradation of HLW glass, and colloids formed from corrosion products. Colloids formed from DOE HLW glass and naturally occurring groundwater colloids are represented by smectite clay colloids, and can transport reversibly sorbed radionuclides. In addition, HLW glass colloids can transport embedded plutonium and americium. Colloids formed from corrosion products are iron oxyhydroxide minerals such as goethite, hematite, and ferrihydrite.

The availability of colloids is evaluated in two steps executed at each time step. First, the groundwater colloid mass is sampled from a probability distribution function and the HLW glass colloid mass is determined as a function of ionic strength. The stability of these colloidal masses is determined as a function of ionic strength and pH. If the colloids are determined to be unstable, a low (but nonzero) value of colloid concentration is used. Second, dissolved cesium, americium, plutonium, protactinium, and thorium are partitioned (reversibly) between fluid, mobile colloids (both smectite and iron oxyhydroxide), and fixed corrosion products. Plutonium and americium embedded in HLW glass colloids are considered to be irreversibly sorbed and, thus, are not partitioned between the water and the HLW glass colloids. In addition, dissolved americium and plutonium are irreversibly partitioned between fluid, mobile colloids, and immobile corrosion products.

Colloid suspensions are stable only when the ionic strength is less than 0.05 mol/L, and, at certain pH values, can be unstable at values of ionic strength lower than 0.05 mol/L.

8.8 CONCLUSIONS

The models described in this technical basis document provide the mass of radionuclides, both as dissolved species and associated with colloids, in water that leaves the waste form. Therefore, these models provide the source term for all subsequent radionuclide transport analyses within TSPA-LA calculations. The estimation of total dose depends on the quantity and rate of radionuclides released from the waste form, regardless of other processes that affect radionuclide transport from the source to the receptor.

INTENTIONALLY LEFT BLANK

9. REFERENCES

9.1 DOCUMENTS CITED

Adkins, H.E. 2003. "Transmittal of Draft Version of Validation of Dissolved Concentrations, Argonne National Laboratory." Interoffice memorandum from H.E. Adkins (BSC) to Y. Chen, June 19, 2003, 0617037708, with attachment. ACC: MOL.20030619.0100.

Advocat, T.; Jollivet, P.; Minet, Y.; Luckscheiter, B.; Grambow, B.; Gens, R.; Lemmens, K.; Van Iseghem, P.; Aertsens, M.; Pirlet, V.; and Curti, E. 1999. *Experimental and Modelling Studies to Formulate a Nuclear Waste Glass Source Term in Representative Geological Disposal Conditions*. EUR 19120 EN. Luxembourg, Luxembourg: Commission of the European Communities. TIC: 254312.

Andrews, M.G. and Matzie, R.A. 1985. "A Report on the Reliability, Performance and Progress of Combustion Engineering's Fuel Assemblies Toward Extended Burnup." *Proceedings, American Nuclear Society Topical Meeting on Light Water Reactor Fuel Performance, Orlando, Florida, April 21–24, 1985.* DOE/NE/34130-1. Volume 1. La Grange Park, Illinois: American Nuclear Society. TIC: 226810.

Appelo, C.A.J; Van der Weiden, M.J.J.; Tournassat, C.; and Charlet, L. 2002. "Surface Complexation of Ferrous Iron and Carbonate on Ferrihydrite and the Mobilization of Arsenic." *Environmental Science and Technology, 36,* 3096–3103. Washington, D.C.: American Chemical Society. TIC: 255581.

Aronson, S. 1958. "Oxidation of UO_2 in Water Containing Oxygen." In *Bettis Technical Review, Reactor Metallurgy.* 14th Edition. WAPD-BT-10. TID-4500. Pittsburgh, Pennsylvania: Westinghouse Electric Corporation, Bettis Atomic Power Division. ACC: NNA.19911025.0062.

Baes, C.F., Jr. and Mesmer, R.E. 1986. *The Hydrolysis of Cations.* Malabar, Florida: Krieger Publishing Company. TIC: 223481.

Berner, U. 2002. *Project Opalinus Clay: Radionuclide Concentration Limits in the Near-Field of a Repository for Spent Fuel and Vitrified High-Level Waste.* PSI Bericht 02-22. Villigen, Switzerland: Paul Scherrer Institut. TIC: 253856.

Berry, J.A.; Hobley, J.; Lane, S.A.; Littleboy, A.K.; Nash, M.J.; Oliver, P.; Smith-Briggs, J.L.; and Williams, S.J. 1989. "Solubility and Sorption of Protactinium in the Near-Field and Far-Field Environments of a Radioactive Waste Repository." *Analyst*, *114*, 339-347. Cambridge, England: Royal Society of Chemistry. TIC: 247004.

Bourcier, W.L. 1994. *Critical Review of Glass Performance Modeling.* ANL-94/17. Argonne, Illinois: Argonne National Laboratory. TIC: 211862.

BSC (Bechtel SAIC Company) 2001. *Performance Assessment of U. S. Department of Energy Spent Fuels in Support of Site Recommendation.* CAL-WIS-PA-000002 REV 00. Las Vegas, Nevada: Bechtel SAIC Company. ACC: MOL.20010627.0026.

BSC 2002a. *Radionuclide Screening*. ANL-WIS-MD-000006 REV 01. Las Vegas, Nevada: Bechtel SAIC Company. ACC: MOL.20020923.0177.

BSC 2002b. *Total System Performance Assessment–License Application Methods and Approach*. TDR-WIS-PA-000006 REV 00. Las Vegas, Nevada: Bechtel SAIC Company. ACC: MOL.20020923.0175.

BSC 2003a. *Pitting Model for Zirconium-Alloyed Cladding at YMP*. MDL-WIS-MD-000001 REV 00. Las Vegas, Nevada: Bechtel SAIC Company. ACC: DOC.20031017.0003.

BSC 2003b. *Clad Degradation—Summary and Abstraction for LA*. ANL-WIS-MD-000021REV 00. Las Vegas, Nevada: Bechtel SAIC Company. ACC: DOC.20030626.0002.

BSC 2003c. *Seismic Consequence Abstraction*. MDL-WIS-PA-000003 REV 00. Las Vegas, Nevada: Bechtel SAIC Company. ACC: DOC.20030818.0006.

BSC 2003d. *Initial Radionuclide Inventories*. ANL-WIS-MD-000020 REV 00. Las Vegas, Nevada: Bechtel SAIC Company. ACC: DOC.20031110.0002.

BSC 2003e. *CSNF Waste Form Degradation: Summary Abstraction*. ANL-EBS-MD-000015 REV 01. Las Vegas, Nevada: Bechtel SAIC Company. ACC: DOC.20030708.0004.

BSC 2003f. *DSNF and Other Waste Form Degradation Abstraction*. ANL-WIS-MD-000004 REV 02. Las Vegas, Nevada: Bechtel SAIC Company. ACC: DOC.20030711.0002.

BSC 2003g. *Defense HLW Glass Degradation Model*. ANL-EBS-MD-000016 REV 01. Las Vegas, Nevada: Bechtel SAIC Company. ACC: DOC.20030821.0006.

BSC 2003h. *Waste Form and In-Drift Colloids—Associated Radionuclide Concentrations: Abstraction and Summary*. MDL-EBS-PA-000004 REV 00 ICN 01. Las Vegas, Nevada: Bechtel SAIC Company. ACC: DOC.20030626.0006.

BSC 2003i. *WAPDEG Analysis of Waste Package and Drip Shield Degradation*. ANL-EBS-PA-000001 REV 01. Las Vegas, Nevada: Bechtel SAIC Company. ACC: MOL.20031208.0004.

BSC 2003j. *Abstraction of Drift Seepage*. MDL-NBS-HS-000019 REV 00C. Las Vegas, Nevada: Bechtel SAIC Company. ACC: MOL.20030728.0198.

BSC 2004a. *Clad Degradation—FEPs Screening Arguments*. ANL-WIS-MD-000008 REV 01. Las Vegas, Nevada: Bechtel SAIC Company. ACC: MOL.20040327.001.

BSC 2004b. *In-Package Chemistry Abstraction.* ANL-EBS-MD-000037 REV 03B. Las Vegas, Nevada: Bechtel SAIC Company. ACC: MOL.20040609.0094.

BSC 2004c. *Dissolved Concentration Limits of Radioactive Elements.* ANL-WIS-MD-000010 REV 03B. Las Vegas, Nevada: Bechtel SAIC Company. ACC: MOL.20040609.0095.

BSC 2004d. *Igneous Intrusion Impacts on Waste Package and Waste Forms*. MDL-EBS-GS-000002 REV 01. Las Vegas, Nevada: Bechtel SAIC Company. ACC: DOC.20040421.0002.

BSC 2004e. *Drift-Scale Coupled Processes (DST and THC Seepage) Models.* MDL-NBS-HS-000001 REV 02, with errata. Las Vegas, Nevada: Bechtel SAIC Company. ACC: DOC.20030804.0004; DOC.20040219.0002; DOC.20040405.0005.

BSC 2004f. *EBS Radionuclide Transport Abstraction*. ANL-WIS-PA-000001 REV 01J. Las Vegas, Nevada: Bechtel SAIC Company. ACC: MOL.20040414.0096.

BSC 2004g. *Probability Analysis of Corrosion Rates for Waste Package Materials.* ANL-DSD-MD-000001 REV 00. Las Vegas, Nevada: Bechtel SAIC Company. ACC: DOC.20040506.0004.

BSC 2004h. *Engineered Barrier System: Physical and Chemical Environment*. ANL-EBS-MD-000033 REV 02, with errata. Las Vegas, Nevada: Bechtel SAIC Company. ACC: DOC.20040212.0004; DOC.20040426.0003.

BSC 2004i. *Multiscale Thermohydrologic Model*. ANL-EBS-MD-000049 REV 01. Las Vegas, Nevada: Bechtel SAIC Company. ACC: DOC.20040301.0004.

Buck, E.C. and Bates, J.K. 1999. "Microanalysis of Colloids and Suspended Particles from Nuclear Waste Glass Alteration." *Applied Geochemistry*, *14*, 635–653. New York, New York: Elsevier. TIC: 245946.

Bunzl, K.; Flessa, H.; Kracke, W.; and Schimmack, W. 1995. "Association of Fallout $^{239+240}$Pu and ^{241}Am with Various Soil Components in Successive Layers of a Grassland Soil." *Environmental Science & Technology*, *29*, (10), 2513–2518. Washington, D.C.: American Chemical Society. TIC: 234160.

Chun, R.; Witte, M.; and Schwartz, M. 1987. *Dynamic Impact Effects on Spent Fuel Assemblies.* UCID-21246. Livermore, California: Lawrence Livermore National Laboratory. ACC: HQX.19881020.0031.

Coughtrey, P.J.; Jackson, D.; Jones, C.H.; Kane, P.; and Thorne, M.C. 1985. *Radionuclide Distribution and Transport in Terrestrial and Aquatic Ecosystems, A Compendium of Data.* Volume 6. Rotterdam, The Netherlands: A.A. Balkema. TIC: 240299.

CRWMS M&O (Civilian Radioactive Waste Management System Management and Operating Contractor) 1998a. "Waste Form Degradation, Radionuclide Mobilization, and Transport Through the Engineered Barrier System." Chapter 6 of *Total System Performance Assessment-Viability Assessment (TSPA-VA) Analyses Technical Basis Document*. B00000000-01717-4301-00006 REV 01. Las Vegas, Nevada: CRWMS M&O. ACC: MOL.19981008.0006.

CRWMS M&O 1998b. *Immobilized in Ceramic.* Volume II of *Report on Intact and Degraded Criticality for Selected Plutonium Waste Forms in a Geologic Repository*. BBA000000-01717-5705-00020 REV 01. Las Vegas Nevada: CRWMS M&O. ACC: MOL.19981217.0112.

CRWMS M&O 1999a. *1999 Design Basis Waste Input Report for Commercial Spent Nuclear Fuel*. B00000000-01717-5700-00041 REV 00. Washington, D.C.: CRWMS M&O. ACC: MOV.19991006.0003.

CRWMS M&O 1999b. *Breakage of Commercial Spent Nuclear Fuel Cladding by Mechanical Loading.* CAL-EBS-MD-000001 REV 00. Las Vegas, Nevada: CRWMS M&O. ACC: MOL.19991213.0237.

CRWMS M&O 2000a. *Source Terms for HLW Glass Canisters.* CAL-MGR-NU-000002 REV 01. Las Vegas, Nevada: CRWMS M&O. ACC: MOL.20000823.0004.

CRWMS M&O 2000b. *Total System Performance Assessment for the Site Recommendation.* TDR-WIS-PA-000001 REV 00 ICN 01. Las Vegas, Nevada: CRWMS M&O. ACC: MOL.20001220.0045.

CRWMS M&O 2000c. *General Corrosion and Localized Corrosion of Waste Package Outer Barrier.* ANL-EBS-MD-000003 REV 00. Las Vegas, Nevada: CRWMS M&O. ACC: MOL.20000202.0172.

CRWMS M&O 2000d. *Clad Degradation—Dry Unzipping*. ANL-EBS-MD-000013 REV 00. Las Vegas, Nevada: CRWMS M&O. ACC: MOL.20000503.0200.

CRWMS M&O 2000e. *Commercial Spent Nuclear Fuel Degradation in Unsaturated Drip Tests.* Input Transmittal WP-WP-99432.T. Las Vegas, Nevada: CRWMS M&O. ACC: MOL.20000107.0209.

CRWMS M&O 2000f. *Measured Solubilities, Argonne National Lab High Drip Rate Tests.* Input Transmittal 00333.T. Las Vegas, Nevada: CRWMS M&O. ACC: MOL.20000919.0019.

CRWMS M&O 2001a. *Clad Degradation—Summary and Abstraction*. ANL-WIS-MD-000007 REV 00 ICN 01. Las Vegas, Nevada: CRWMS M&O. ACC: MOL.20010214.0229.

CRWMS M&O 2001b. *Colloid-Associated Radionuclide Concentration Limits: ANL.* ANL-EBS-MD-000020 REV 00 ICN 01. Las Vegas, Nevada: CRWMS M&O. ACC: MOL.20010216.0003.

Cunnane, J. 2003. "Observed Cladding Behavior in ANL Tests." Interoffice memorandum from J. Cunnane (BSC) to H.E. Adkins, January 21, 2003, 0121035737, with attachment. ACC: MOL.20030121.0180.

Davis, J.A. and Kent, D.B. 1990. "Surface Complexation Modeling in Aqueous Geochemistry." *Mineral-Water Interface Geochemistry.* Hochella, M.F., Jr. and White, A.F., eds. *Reviews in Mineralogy, 23*, 177–260. Washington, D.C.: Mineralogical Society of America. TIC: 224085.

Degueldre, C.; Triay, I.; Kim, J.-I; Vilks, P.; Laaksoharju, M.; and Miekeley, N. 2000. "Groundwater Colloid Properties: A Global Approach." *Applied Geochemistry, 15*, (7), 1043–5304. New York, New York: Pergamon Press. TIC: 249340.

Dehaudt, P. 2001a. "Physical and Chemical State of the Nuclear Spent Fuel after Irradiation." Section 5.2 of *Synthesis on the Long Term Behavior of the Spent Nuclear Fuel*. Poinssot, C., ed. CEA-R-5958(E). Volume I. Paris, France: Commissariat à l'Énergie Atomique. TIC: 253976.

Dehaudt, P. 2001b. "State of the Art of the Oxidation of Spent Nuclear Fuel." Section 7.2 of *Synthesis on the Long Term Behavior of the Spent Nuclear Fuel*. Poinssot, C., ed. CEA-R-5958(E). Volume II. Paris, France: Commissariat à l'Énergie Atomique. TIC: 253976.

Dehon, C.; Cambon, J.L.; Houdaille, B.; and Chagrot, M. 1985. "Main Results from FRAGEMA Fuel Performance in Power Reactors." *Proceedings, American Nuclear Society Topical Meeting on Light Water Reactor Fuel Performance, Orlando, Florida, April 21–24, 1985.* DOE/NE/34130-1. Volume 1. La Grange Park, Illinois: American Nuclear Society. TIC: 226810.

de Pablo, J.; Casas, I.; Giménez, J.; Molera, M.; Rovira, M.; Duro, L.; and Bruno, J. 1999. "The Oxidative Dissolution Mechanism of Uranium Dioxide. I. The Effect of Temperature in Hydrogen Carbonate Medium." *Geochimica et Cosmochimica Acta*, *63*, (19–20), 3097–3103. New York, New York: Pergamon. TIC: 254443.

DOE (U.S. Department of Energy) 1996. *Waste Acceptance Product Specifications for Vitrified High-Level Waste Forms*. DOE/EM-WAPS, Rev. 02. Washington, D.C.: U.S. Department of Energy. TIC: 234751.

DOE 2000. *Methodologies for Calculating DOE Spent Nuclear Fuel Source Terms.* DOE/SNF/REP-055, Rev. 0. Idaho Falls, Idaho: U.S. Department of Energy, Idaho Operations Office. TIC: 246937.

DOE 2002a. *Yucca Mountain Science and Engineering Report*. DOE/RW-0539, Rev. 1. Washington, D.C.: U.S. Department of Energy, Office of Civilian Radioactive Waste Management. ACC: MOL.20020404.0042.

DOE 2002b. *DOE Spent Nuclear Fuel Information in Support of TSPA-SR*. DOE/SNF/REP-047, Rev. 2. Idaho Falls, Idaho: U.S. Department of Energy, Idaho Operations Office. TIC: 252089.

DOE 2002c. *Waste Acceptance System Requirements Document*. DOE/RW-0351, Rev. 4. Washington, D.C.: U.S. Department of Energy, Office of Civilian Radioactive Waste Management. ACC: MOL.20020326.0056.

DOE 2003a. *Source Term Estimates for DOE Spent Nuclear Fuels*. DOE/SNF/REP-078, Rev. 0. Idaho Falls, Idaho: U.S. Department of Energy, Idaho Operations Office. TIC: 254275.

DOE 2003b. *Review of DOE Spent Nuclear Fuel Release Rate Test Results*. DOE/SNF/REP-073, Rev.0. Idaho Falls, Idaho: U.S. Department of Energy, Idaho Operations Office. ACC: DOC.20030905.0010.

Doi, S.; Suzuki, S.; Mori, M.; and Takahashi, T. 2000. "Advanced Fuel Design and Performance for Burnup Extension." *Proceedings of the 2000 International Topical Meeting on Light Water Reactor Fuel Performance, Park City, Utah, April 10–13, 2000*. La Grange Park, Illinois: American Nuclear Society. TIC: 248973.

Dzombak, D.A. and Morel, F.M.M. 1990. *Surface Complexation Modeling, Hydrous Ferric Oxide*. New York, New York: John Wiley & Sons. TIC: 224089.

Ebert, W. 2000. "Interpretation/Analysis of MCC-1 Test Results in Support of ANL-EBS-MD-000016." Memorandum from W. Ebert to File, February 18, 2000, with attachment. ACC: MOL.20000221.0327.

Ebert, W.L. 2003a. "Data Report for MCC-1 Tests and PCTs with SRL 202G Glass." Memo from W.L. Ebert to File, July 24, 2003, with attachment. ACC: MOL.20030728.0214; MOL.20030728.0215.

Ebert, W.L. 2003b. "Vapor Hydration Tests with DWPF Reference Glasses." Memo from W.L. Ebert to File, July 24, 2003, with attachment. ACC: MOL.20030728.0211; MOL.20030728.0212.

Ebert, W.L. 2003c. "Results from Unsaturated (Drip) Tests with Glass: The N2 & N3 Tests." Memo from W. Ebert to File, July 29, 2003, with attachment. ACC: MOL.20030730.0322; MOL.20030730.0323.

Edsinger, K. 2000. "A Review of Fuel Degradation in BWRs." *Proceedings of the 2000 International Topical Meeting on Light Water Reactor Fuel Performance, Park City, Utah, April 10–13, 2000.* La Grange Park, Illinois: American Nuclear Society. TIC: 248973.

Efurd, D.W.; Runde, W.; Banar, J.C.; Janecky, D.R.; Kaszuba, J.P.; Palmer, P.D.; Roensch, F.R.; and Tait, C.D. 1998. "Neptunium and Plutonium Solubilities in a Yucca Mountain Groundwater." *Environmental Science & Technology, 32*, (24), 3893–3900. Easton, Pennsylvania: American Chemical Society. TIC: 243857.

EPA (U.S. Environmental Protection Agency) 1999. *Understanding Variation in Partition Coefficient, K_d, Values.* EPA 402-R-99-004A&B Two volumes. Washington, D.C.: U.S. Environmental Protection Agency. TIC: 249201.

EPRI (Electric Power Research Institute) 1997. *The Technical Basis for the Classification of Failed Fuel in the Back-End of the Fuel Cycle.* EPRI TR-108237. Palo Alto, California: Electric Power Research Institute. TIC: 236839.

Finn, P.A.; Buck, E.C.; Gong, M.; Hoh, J.C.; Emery, J.W.; Hafenrichter, L.D.; and Bates, J.K. 1994. "Colloidal Products and Actinide Species in Leachate from Spent Nuclear Fuel." *Radiochimica Acta, 66/67,* 197–203. Munchen, Germany: R. Oldenbourg Verlag. TIC: 238493.

Fischer, L.E.; Chou, C.K.; Gerhard, M.A.; Kimura, C.Y.; Martin, R.W.; Mensing, R.W.; Mount, M.E.; and Witte, M.C. 1987. *Shipping Container Response to Severe Highway and Railway Accident Conditions.* NUREG/CR-4829. Volume 1. Washington, D.C.: U.S. Nuclear Regulatory Commission. ACC: NNA.19900827.0230.

Forsyth, R. 1997. *The SKB Spent Fuel Corrosion Program. An Evaluation of Results from the Experimental Programme Performed in the Studsvik Hot Cell Laboratory.* SKB TR-97-25. Stockholm, Sweden: Svensk Kärnbränsleförsörjning A.B. TIC: 246406.

Goldberg, M. 2003. *Rod Segment Test Data Report, CSNF Degradation Model: Q Data Input from ANL Testing*. Task Number: PAWC1M5. Argonne, Illinois: Argonne National Laboratory, Chemical Engineering Division. ACC: MOL.20030627.0221.

Grambow, B. 1985. "A General Rate Equation for Nuclear Waste Glass Corrosion." *Scientific Basis for Nuclear Waste Management VIII, Symposium held November 26–29, 1984. Boston, Massachusetts*. Jantzen, C.M.; Stone, J.A.; and Ewing, R.C.; eds. *44*, 15–27. Pittsburgh, Pennsylvania: Materials Research Society. TIC: 203665.

Grambow, B.; Jercinovic, M.J.; Ewing, R.C.; and Byers, C.D. 1986. "Weathered Basalt Glass: A Natural Analogue for the Effects of Reaction Progress on Nuclear Waste Glass Alteration." *Scientific Basis for Nuclear Waste Management IX, Symposium held September 9–11, 1985, Stockholm, Sweden*. Werme, L.O., ed. *50*, 263–272. Pittsburgh, Pennsylvania: Materials Research Society. TIC: 203664.

Grambow, B.; Loida, A.; Martinez-Esparza, A.; Diaz-Arocas, P.; de Pablo, J.; Paul, J.L.; Marx, G.; Glatz, J.P.; Lemmens, K.; Ollila, K.; and Christensen, H. 2000. "Long-Term Safety of Radioactive Waste Disposal: Source Term for Performance Assessment of Spent Fuel as a Waste Form, Final Report." *Forchungszentrum Karlsruhe, Technik und Umwelk, FZKA 6420*. Karlsruhe, Germany: Forschungszentrum Karlsruhe GmbH. TIC: 254058.

Gray, W.J.; Strachan, D.M.; and Wilson, C.N. 1992. "Gap and Grain-Boundary Inventories of Cs, Tc, and Sr in Spent LWR Fuel." *Scientific Basis for Nuclear Waste Management XV, Symposium held November 4–7, 1991, Strasbourg, France*. Sombret, C.G., ed. *257*, 353–360. Pittsburgh, Pennsylvania: Materials Research Society. TIC: 204618.

Gray, W.J. and Wilson, C.N. 1995. *Spent Fuel Dissolution Studies FY 1991–1994*. PNL-10450. Richland, Washington: Pacific Northwest Laboratory. ACC: MOL.19960802.0035.

Grenthe, I.; Fuger, J.; Konings, R.J.M.; Lemire, R.J.; Muller, A.B.; Nguyen-Trung, C.; and Wanner, H. 1992. *Chemical Thermodynamics of Uranium.* Volume 1 of *Chemical Thermodynamics.* Wanner, H. and Forest, I., eds. Amsterdam, The Netherlands: North-Holland Publishing Company. TIC: 224074.

Guzy, C.J.; Bonano, E.J.; and David, E.J. 1983. "The Analysis of Flow and Colloidal Particle Retention in Fibrous Porous Media." *Journal of Colloid and Interface Science*, *95*, (2), 523–543. New York, New York: Academic Press. TIC: 254741.

Harrar, J.E.; Carley, J.F.; Isherwood, W.F.; and Raber, E. 1990. *Report of the Committee to Review the Use of J-13 Well Water in Nevada Nuclear Waste Storage Investigations*. UCID-21867. Livermore, California: Lawrence Livermore National Laboratory. ACC: NNA.19910131.0274.

Honeyman, B.D. and Ranville, J.F. 2002. "Colloid Properties and their Effects on Radionuclide Transport through Soils and Groundwaters." Chapter 7 of *Geochemistry of Soil Radionuclides.* Zhang, P-C. and Brady, P.V., eds. SSSA Special Publication Number 59. Madison, Wisconsin: Soil Science Society of America. TIC: 253952.

Hummel, W.; Berner, U.; Curti, E.; Pearson, F.J.; and Thoenen, T. 2002. *Nagra/PSI Chemical Thermodynamic Data Base 01/01*. Parkland, Florida: Universal Publishers. TIC: 253421.

Jégou, C.; Paul, J.L.; and Lucchini, J.F. 2001. "State of the Art of the Leaching and RN Release from Spent Fuel." Section 8.2 of *Synthesis on the Long Term Behavior of the Spent Nuclear Fuel*. Poinssot, C., ed. CEA-R-5958(E). Volume 2. Paris, France: Commissariat à l'Énergie Atomique. TIC: 253976.

Johnson, L.H.; LeNeveu, D.M.; King, F.; Shoesmith, D.W.; Kolar, M.; Oscarson, D.W.; Sunder, S.; Onofrei, C.; and Crosthwaite, J.L. 1996. *Vault Model*. Volume 2 of *The Disposal of Canada's Nuclear Fuel Waste: A Study of Postclosure Safety of In-Room Emplacement of Used CANDU Fuel in Copper Containers in Permeable Plutonic Rock*. AECL-11494-2. Pinawa, Manitoba, Canada: Atomic Energy of Canada Limited. TIC: 226733.

Kersting, A.B.; Efurd, D.W.; Finnegan, D.L.; Rokop, D.J.; Smith, D.K.; and Thompson, J.L. 1999. "Migration of Plutonium in Ground Water at the Nevada Test Site." *Nature, 397*, (6714), 56–59. London, England: Macmillan Journals. TIC: 243597.

Kingston, W.L. and Whitbeck, M. 1991. *Characterization of Colloids Found in Various Groundwater Environments in Central and Southern Nevada.* DOE/NV/10384-36. Las Vegas, Nevada: Desert Research Institute, Water Resources Center. ACC: NNA.19930607.0073.

Knauss, K.G.; Bourcier, W.L.; McKeegan, K.D.; Merzbacher, C.I.; Nguyen, S.N.; Ryerson, F.J.; Smith, D.K.; Weed, H.C.; and Newton, L. 1990. "Dissolution Kinetics of a Simple Analogue Nuclear Waste Glass a Function of pH, Time and Temperature." *Scientific Basis for Nuclear Waste Management XIII, Symposium held November 27–30, 1989, Boston, Massachusetts*. Oversby, V.M. and Brown, P.W., eds. *176*, 371–381. Pittsburgh, Pennsylvania: Materials Research Society. TIC: 203658.

Langmuir, D. 1997. *Aqueous Environmental Geochemistry*. Upper Saddle River, New Jersey: Prentice Hall. TIC: 237107.

Langmuir, D. and Riese, A.C. 1985. "The Thermodynamic Properties of Radium." *Geochimica et Cosmochimica Acta, 49*, 1593–1601. New York, New York: Pergamon Press. TIC: 241035.

Lemire, R.J. 2001. *Chemical Thermodynamics of Neptunium and Plutonium.* Volume 4 of *Chemical Thermodynamics.* New York, New York: Elsevier. TIC: 209037.

Liang, L. and Morgan, J.J. 1990. "Chemical Aspects of Iron Oxide Coagulation in Water: Laboratory Studies and Implications for Natural Systems." *Aquatic Sciences, 52*, (1), 32–55. Basel, Switzerland: Birkhauser Verlag. TIC: 246125.

Litaor, M.I. and Ibrahim, S.A. 1996. "Plutonium Association with Selected Solid Phases in Soils of Rocky Flats, Colorado, Using Sequential Extraction Technique." *Journal of Environmental Quality, 25*, (5), 1144–1151. Madison, Wisconsin: American Society of Agronomy. TIC: 252783.

Loros, E. and Williams, N.H. 2004. Meeting Minutes, Bechtel SAIC Company, LLC, Technical Review Board (TMRB) Meeting, April 22, 2004. Las Vegas, Nevada: Bechtel SAIC Company. ACC: MOL.20040622.0297.

Lu, N.; Conca, J.; Parker, G.R.; Leonard, P.A.; Moore, B.; Strietelmeier, B.; and Triay, I.R. 2000. *Adsorption of Actinides Onto Colloids as a Function of Time, Temperature, Ionic Strength, and Colloid Concentration, Waste Form Colloids Report for Yucca Mountain Program (Colloid Data Summary from 1999 to 2000 Research).* LA-UR-00-5121. Los Alamos, New Mexico: Los Alamos National Laboratory. TIC: 249708.

Lu, N.; Triay, I.R.; Cotter, C.R.; Kitten, H.D.; and Bentley, J. 1998. *Reversibility of Sorption of Plutonium-239 onto Colloids of Hematite, Goethite, Smectite, and Silica*. LA-UR-98-3057. Los Alamos, New Mexico: Los Alamos National Laboratory. ACC: MOL.19981030.0202.

Luptak, A. 2003. "Canister Range." E-mail from A. Luptak (INEEL) to C. Stockman, September 23, 2003. ACC: MOL.20030929.0018.

Manaktala, H.K. 1993. *Characteristics of Spent Nuclear Fuel and Cladding Relevant to High-Level Waste Source Term.* CNWRA 93-006. San Antonio, Texas: Center for Nuclear Waste Regulatory Analyses. TIC: 208034

McDonald, S.G. and Kaiser, R.S. 1985. "The Impact of Metallic Debris on Fuel Performance—A Case History." *Proceedings, American Nuclear Society Topical Meeting on Light Water Reactor Fuel Performance, Orlando, Florida, April 21–24, 1985.* DOE/NE/34130-1. Volume 1. La Grange Park, Illinois: American Nuclear Society. TIC: 226810.

McEachern, R.J. and Taylor, P. 1998. "A Review of the Oxidation of Uranium Dioxide at Temperatures Below 400°C." *Journal of Nuclear Material, 254,* 87–121. Amsterdam, The Netherlands: Elsevier. TIC: 246427.

McGrail, B.P.; Ebert, W.L.; Bacon, D.H.; and Strachan, D.M. 1998. *A Strategy to Conduct an Analysis of the Long-Term Performance of Low-Activity Waste Glass in a Shallow Subsurface Disposal System at Hanford*. PNNL-11834. Richland, Washington: Pacific Northwest National Laboratory. TIC: 249433.

Mertz, C.J.; Finch, R.J.; Fortner, J.A.; Jerden, J.L., Jr.; Yifen, T.; Cunnane, J.C.; and Finn, P.A. 2003. *Characterization of Colloids Generated from Commercial Spent Nuclear Fuel Corrosion.* Activity Number: PAWTP30A. Argonne, Illinois: Argonne National Laboratory. ACC: MOL.20030422.0337.

Murphy, W.M. 1995. "Natural Analogs for Yucca Mountain." *Radwaste Magazine, 2,* (6), 44-50. La Grange Park, Illinois: American Nuclear Society. TIC: 237929.

NCRP (National Council on Radiation Protection and Measurements) 1996. *Screening Models for Releases of Radionuclides to Atmosphere, Surface Water, and Ground*. NCRP Report No. 123 I. Bethesda, Maryland: National Council on Radiation Protection and Measurements. TIC: 225158.

Nitsche, H.; Gatti, R.C.; Standifer, E.M.; Lee, S.C.; Müller, A.; Prussin, T.; Deinhammer, R.S.; Maurer, H.; Becraft, K.; Leung, S.; and Carpenter, S.A. 1993a. *Measured Solubilities and Speciations of Neptunium, Plutonium, and Americium in a Typical Groundwater (J-13) from the Yucca Mountain Region.* LA-12562-MS. Los Alamos, New Mexico: Los Alamos National Laboratory. ACC: NNA.19930507.0136.

Nitsche, H.; Roberts, K.; Prussin, T.; Kenney, D.; Carpenter, S.A.; Becraft, K.; and Gatti, R.C. 1993b. "Radionuclide Solubility and Speciation Studies for the Yucca Mountain Site Characterization Project." *High Level Radioactive Waste Management, Proceedings of the Fourth Annual International Conference, Las Vegas, Nevada, April 26–30, 1993. 2*, 1490–1495. La Grange Park, Illinois: American Nuclear Society. TIC: 208542.

Pearcy, E.C.; Prikryl, J.D.; Murphy, W.M.; and Leslie, B.W. 1994. "Alteration of Uraninite from the Nopal I Deposit, Peña Blanca District, Chihuahua, Mexico, Compared to Degradation of Spent Nuclear Fuel in the Proposed U.S. High-Level Nuclear Waste Repository at Yucca Mountain, Nevada." *Applied Geochemistry*, *9*, 713–732. New York, New York: Elsevier. TIC: 236934.

Pelletier, M. 2001. "State of the Art on the Potential Migration of Species." Section 5.4 of *Synthesis on the Long Term Behavior of the Spent Nuclear Fuel*. Poinssot, C., ed. CEA-R-5958(E). Volume 1. Paris, France: Commissariat à l'Énergie Atomique. TIC: 253976.

Piron, J.P. 2001. "Presentation of the Key Scientific Issues for the Spent Nuclear Fuel Evolution in a Closed System." Section 5.1 of *Synthesis on the Long Term Behavior of the Spent Nuclear Fuel*. Poinssot, C., ed. CEA-R-5958(E). Volume 1. Paris, France: Commissariat à l'Énergie Atomique. TIC: 253976.

Potts, G.A. 2000. "Recent GE BWR Fuel Experience." *Proceedings of the 2000 International Topical Meeting on Light Water Reactor Fuel Performance, Park City, Utah, April 10–13, 2000.* La Grange Park, Illinois: American Nuclear Society. TIC: 248973.

Rai, D 1984. "Solubility Product of Pu(IV) Hydrous Oxide and Equilibrium Constants of Pu(IV)/Pu(V), Pu(IV)/Pu(VI), and Pu(V)/Pu(VI) Couples." *Radiochimica Acta*, *35*, 97–106. Munchen, German: Oldenbourg Verlag. TIC: 219109.

Rai, D.; Moore, D.A.; Felmy, A.R.; Choppin, G.R.; and Moore, R.C. 2001. "Thermodynamics of the PuO_2^+-Na^+-$OH^-$$Cl^-$$ClO_4^-$-$H_2O$ System: Use of NpO_2^+ Pitzer Parameters for PuO_2^+." *Radiochimica Acta*, *89*, (8), 491–498. München, Germany: Oldenbourg Wissenschaftsverlag. TIC: 255398.

Ravier, G.; Masuy, G.; and Willse, J.T. 1997. "Framatome and FCF Recent Operating Experience and Advanced Features to Increase Performance and Reliability." *Proceedings of the 1997 International Topical Meeting on Light Water Reactor Fuel Performance, Portland, Oregon, March 2–6, 1997.* Pages 31–36. La Grange Park, Illinois: American Nuclear Society. TIC: 232556.

S. Cohen & Associates 1999. *Effectiveness of Fuel Rod Cladding as an Engineered Barrier in the Yucca Mountain Repository*. McLean, Virginia: S. Cohen & Associates. TIC: 246541.

Sanders, T.L.; Seager, K.D.; Rashid, Y.R.; Barrett, P.R.; Malinauskas, A.P.; Einziger, R.E.; Jordan, H.; Duffey, T.A.; Sutherland, S.H.; and Reardon, P.C. 1992. *A Method for Determining the Spent-Fuel Contribution to Transport Cask Containment Requirements*. SAND90-2406. Albuquerque, New Mexico: Sandia National Laboratories. ACC: MOV.19960802.0116.

Sasaki, S. and Kuwabara, S. 1997. "Utility Perspective on Commercial Light-Water Reactor Fuel in Japan." *Proceedings of the 1997 International Topical Meeting on Light Water Reactor Fuel Performance, Portland, Oregon, March 2–6, 1997*. Pages 11–20. La Grange Park, Illinois: American Nuclear Society. TIC: 232556.

Shoesmith, D.W. 2000. "Fuel Corrosion Processes under Waste Disposal Conditions." *Journal of Nuclear Materials, 282*, (1), 1–31. Amsterdam, The Netherlands: North-Holland. TIC: 254043.

Silva, R.J.; Bidoglio, G.; Rand, M.H.; Robouch, P.B.; Wanner, H.; and Puigdomenech, I. 1995. *Chemical Thermodynamics of Americium. Chemical Thermodynamics, 2.* Amsterdam, The Netherlands: Elsevier. TIC: 237106.

Smith, P.K. and Baxter, C.A. 1981. *Fracture During Cooling of Cast Borosilicate Glass Containing Nuclear Wastes*. DP-1602. Aiken, South Carolina: E.I. du Pont de Nemours & Company, Savannah River Laboratory. TIC: 238536.

Smith, T.H. and Ross, W.A. 1975. *Impact Testing of Vitreous Simulated High-Level Waste in Canisters*. BNWL-1903. Richland, Washington: Battelle Pacific Northwest Laboratories. TIC: 238924.

Steinborn, T.L.; Wolery, T.J.; Alcorn, S.R.; Arthur, S.E.; Bernot, P.A.; Brady, P.V.; Chen, Y.; Domski, P.S.; Jolley, D.M.; Metcalf, R.C.; and Thomas, E. 2003. *Data Qualification: Update and Revision of the Geochemical Thermodynamic Database, Data0.ymp.* TDR-EBS-MD-000022 REV 00. Las Vegas, Nevada: Bechtel SAIC Company. ACC: DOC.20030331.0003.

Stenhouse, M.J. 1995. *Sorption Databases for Crystalline, Marl and Bentonite for Performance Assessment.* NAGRA Technical Report 93-06. Wettingen, Switzerland: National Cooperative for the Disposal of Radioactive Waste. TIC: 247885.

Stout, R.B. and Leider, H.R. 1998. *Waste Form Characteristics Report*. CD-ROM Version. UCRL-ID-132375. Livermore, California: Lawrence Livermore National Laboratory. TIC: 246106.

Tait, J.C. and Luht, J.L. 1997. *Dissolution Rates of Uranium from Unirradiated UO_2 and Uranium and Radionuclides from Used CANDU Fuel Using the Single-Pass Flow-Through Apparatus*. 06819-REP-01200-0006 R00. Toronto, Ontario, Canada: Ontario Hydro. TIC: 243164.

Taylor, P.; Wood, D.D.; Duclos, A.M.; and Owen, D.G. 1989. "Formation of Uranium Trioxide Hydrates on UO_2 Fuel in Air-Steam Mixtures Near 200°C." *Journal of Nuclear Materials, 168*, (1–2), 70–75. Amsterdam, The Netherlands: Elsevier. TIC: 246601.

Thomas, E. 2003. "Transmittal of Unsaturated Testing of Bare Spent UO_2 Fuel Fragments: Data Report, Argonne National Laboratory." Interoffice memorandum from E. Thomas (BSC) to J.C. Cunnane, July 2, 2003, 0702037939, with attachment. ACC: MOL.20030702.0116; MOL.20030311.0097.

Tombacz, E.; Abraham, I.; Gilde, M.; and Szanto, F. 1990. "The pH-Dependent Colloidal Stability of Aqueous Montmorillonite Suspensions." *Colloids and Surfaces, 49,* 71–80. Amsterdam, The Netherlands: Elsevier. TIC: 246046.

Torrero, M.E.; Baraj, E.; de Pablo, J.; Gimenez, J.; and Casas, I. 1997. "Kinetics of Corrosion and Dissolution of Uranium Dioxide as a Function of pH." *International Journal of Chemical Kinetics, 29,* (4), 261–267. New York, New York: John Wiley & Sons. TIC: 246160.

Williams, N.H. 2003. "Contract No. DE-AC-28-01RW12101—Revision to Report No. TDR-CRW-SE-000022, WBS 9.1.2." Letter from N.H. Williams (BSC) to B. Hamilton-Ray (DOE/ORD), April 7, 2003, NHW:jmt–0331036688, with enclosure. ACC: MOL.20030520.0367.

Wilmot, E.L. 1981. *Transportation Accident Scenarios for Commercial Spent Fuel.* SAND80-2124. Albuquerque, New Mexico: Sandia National Laboratories. ACC: HQO.19871023.0215.

Wilson, C.N. 1990a. *Results from NNWSI Series 2 Bare Fuel Dissolution Tests*. PNL-7169. Richland, Washington: Pacific Northwest Laboratory. ACC: NNA.19900814.0048.

Wilson, C.N. 1990b. *Results from NNWSI Series 3 Spent Fuel Dissolution Tests*. PNL-7170. Richland, Washington: Pacific Northwest Laboratory. ACC: NNA.19900329.0142.

Witte, M.C.; Chun, R.C.; and Schwartz, M.W. 1989. "Dynamic Impact Effects on Spent Fuel Assemblies." *9th International Symposium on the Packaging and Transportation of Radioactive Materials, Washington, D.C., June 11–16, 1989. 1*, 186–194. Oak Ridge, Tennessee: Oak Ridge National Laboratory. TIC: 240741.

Wolery, T.J. 1992. *EQ3NR, A Computer Program for Geochemical Aqueous Speciation-Solubility Calculations: Theoretical Manual, User's Guide, and Related Documentation (Version 7.0).* UCRL-MA-110662 PT III. Livermore, California: Lawrence Livermore National Laboratory. ACC: MOL.19980717.0626.

Wolery, T.J. and Daveler, S.A. 1992. *EQ6, A Computer Program for Reaction Path Modeling of Aqueous Geochemical Systems: Theoretical Manual, User's Guide, and Related Documentation (Version 7.0).* UCRL-MA-110662 PT IV. Livermore, California: Lawrence Livermore National Laboratory. TIC: 205002.

Wronkiewicz, D.J.; Bates, J.K.; Buck, E.C.; Hoh, J.C.; Emery, J.W.; and Wang, L.M. 1997. *Radiation Effects in Moist-Air Systems and the Influence of Radiolytic Product Formation on Nuclear Waste Glass Corrosion.* ANL-97/15. Argonne, Illinois: Argonne National Laboratory. TIC: 234821.

9.2 CODES, STANDARDS, REGULATIONS, AND PROCEDURES

10 CFR 63. Energy: Disposal of High-Level Radioactive Wastes in a Geologic Repository at Yucca Mountain, Nevada. Readily available.

40 CFR 197. Protection of Environment: Public Health and Environmental Radiation Protection Standards for Yucca Mountain, Nevada. Readily available.

9.3 DATA, LISTED BY DATA TRACKING NUMBER

GS020408312272.003. Collection and Analysis of Pore Water Samples for the Period from April 2001 to February 2002. Submittal date: 04/24/2002.

LL000107951021.107. Radionuclide Inventory in Spent Fuel. Submittal date: 01/12/2000.

LL010902212241.026. CSNF Alteration Phase Porosity Estimates. Submittal date: 09/21/2001.

LL030300112241.027. Uranium Dissolution Rates from Uranium Dioxide. Submittal date: 03/03/2003.

LL991001251021.090. Draft—CSNF Waste Form Degradation: Unsaturated Drip Tests—G2020 Analysis and Modeling Report. Submittal date: 10/04/1999.

MO0006J13WTRCM.000. Recommended Mean Values of Major Constituents in J-13 Well Water. Submittal date: 06/07/2000.

MO0212UCC034JC.002. Mass Transport of Solids in Effluent Solution During Miniature Waste Package Corrosion. Submittal date: 12/09/2002.

MO0301ANLGNN01.527. Glass Unsaturated (Drip) Test Results (BSC Test Plan: SITP-02-WF-002): Boron Release. Submittal date: 01/15/2003.

MO0301ANLSF001.450. Initial Release Fractions and Fractional Release Rates (Per Day) for Rod Segment Tests (BSC Test Plan: SITP-02-WF-001, REV 0). Submittal date: 01/15/2003.

MO0301ANLSF001.451. Summary of Fractional Release Rate Data (Per Day) for Fuel Fragment Tests (BSC Test Plan: SITP-02-WF-001, REV 0). Submittal date: 01/15/2003.

MO0302PNLDUFTD.000. Flowthrough Dissolution Data. Submittal date: 02/28/2003.

MO0302SPATHDYN.000. Thermodynamic Data Input Files - Data0.YMP.R2. Submittal date: 02/05/2003.

MO0302UCC034JC.003. Graphical X-Ray Diffractometer Data and Mineral Analysis of Filtered Solids from Effluent Solution During Miniature Waste Package Corrosion. Submittal date: 02/10/2003.

MO0304PNLLPHDD.000. Low pH Dissolution Data. Submittal date: 04/09/2003.

MO0306ANLGIM01.525. Glass Immersion Test Results (BSC Test Plan: SITP-02-WF-002); Concentrations and pH. Submittal date: 06/12/2003.

MO0306ANLGIM02.525. Glass Immersion Test Results (BSC Test Plan: SITP-02-WF-002); Normalized Mass Losses. Submittal date: 06/12/2003.

MO0306ANLGVH01.526. Glass Vapor Hydration Test Results (BSC Test Plan: SITP-02-WF-002). Submittal date: 06/12/2003.

MO0306ANLSF001.459. Colloids Generated from Irradiated N Reactor Fuel, Data Report. Submittal date: 06/04/2003.

MO0308ANLGPC01.528. Immersion Tests for Glass Composition Dependence. Submittal date: 08/15/2003.

MO0402SPAHWCIG.002. Heat and Water Chemistry Output from Igneous Intrusion. Submittal date: 02/23/2004.

MO0403SPAIPCHM.004. Abstractions of In-Package Chemistry for TSPA-LA. Submittal date: 03/15/2004.

MO0404SPAIPCHM.005. Abstractions of In-Package Chemistry for TSPA-LA. Submittal date: 04/29/2004.

SN0001T0810599.008. Stainless Steel in Waste Packages for TSPA-SR (Total System Performance Assessment-Site Recommendation). Submittal date: 01/18/2000.

APPENDIX A

IN-PACKAGE CHEMISTRY ENVIRONMENT (RESPONSE TO CLST 3.02 AIN-1, ENFE 3.03, TSPAI 3.14, AND GEN 1.01 (COMMENTS 116 AND 126))

Note Regarding the Status of Supporting Technical Information

This document was prepared using the most current information available at the time of its development. This Technical Basis Document and its appendices providing Key Technical Issue Agreement responses that were prepared using preliminary or draft information reflect the status of the Yucca Mountain Project's scientific and design bases at the time of submittal. In some cases this involved the use of draft Analysis and Model Reports (AMRs) and other draft references whose contents may change with time. Information that evolves through subsequent revisions of the AMRs and other references will be reflected in the License Application (LA) as the approved analyses of record at the time of LA submittal. Consequently, the Project will not routinely update either this Technical Basis Document or its Key Technical Issue Agreement appendices to reflect changes in the supporting references prior to submittal of the LA.

APPENDIX A

IN-PACKAGE CHEMISTRY ENVIRONMENT (RESPONSE TO CLST 3.02 AIN-1, ENFE 3.03, TSPAI 3.14, AND GEN 1.01 (COMMENTS 116 AND 126))

This appendix provides a response to Key Technical Issue (KTI) agreements Container Life and Source Term (CLST) 3.02 Additional Information Needed (AIN)-1, Evolution of the Near Field Environment (ENFE) 3.03, Total System Performance Assessment and Integration (TSPAI) 3.14, and General Agreement (GEN) 1.01 (Comments 116 and 126). These agreements relate to the in-package chemistry environment.

A.1 KEY TECHNICAL ISSUE AGREEMENTS

A.1.1 CLST 3.02 AIN-1, ENFE 3.03, TSPAI 3.14, and GEN 1.01 (Comments 116 and 126)

Agreement CLST 3.02 was reached during the U.S. Nuclear Regulatory Commission (NRC)/U.S. Department of Energy (DOE) Technical Exchange and Management Meeting on CLST held September 12 and 13, 2000, in Las Vegas, Nevada (Schlueter 2000). Subissues 1, 2, 3, 4, and 6 were discussed at that meeting.

In-Package Chemistry for Waste Forms (BSC 2001a),[1] which addresses agreement CLST 3.02, was provided to the NRC in March 2001 (Brocoum 2001). After reviewing the document, the NRC determined that additional information was needed to close the agreement, resulting in CLST 3.02 AIN-1.

Agreement ENFE 3.03 was reached during the NRC/DOE Technical Exchange and Management Meeting on Evolution of the Near Field Environment held January 9 through 12, 2001, in Pleasanton, California (Reamer 2001). ENFE KTI subissues 1, 2, 3, and 4 were discussed at that meeting.

Agreement TSPAI 3.14 was reached during the NRC/DOE Technical Exchange and Management Meeting on TSPAI held August 6 through 10, 2001, in Las Vegas, Nevada (Reamer and Gil 2001a).

The wording of these agreements and AIN is as follows:

CLST 3.02

> In the revision to the "Summary of In-Package Chemistry for Waste Forms," AMR, address specific NRC questions regarding radiolysis, incoming water, localized corrosion, corrosion products, transient effects, and a sensitivity study on differing dissolution rates of components. DOE stated that these specific questions are currently being addressed in the revision of the "Summary of In-Package Chemistry for Waste Forms" AMR, ANL-EBS-MD-000050 and related AMRs and calculations. To be available in January 2001.

[1] This document's title and number differ from that identified in the original agreement for KTI CLST 3.02.

CLST 3.02 AIN-1

1. Provide the technical basis for the corrosion rates and the likely corrosion mechanisms of internal waste package components.

2. Provide the technical justification and appropriate ranges for the model abstraction parameters for each internal component of the waste package.

3. Provide the results of sensitivity analyses using current values of the parameters included in the model abstractions.

4. Provide the technical basis for the in-package water chemistry, taking into account the formation of locally aggressive environments in crevices and tight spaces inside the waste package that can enhance the degradation of waste forms and the solubility of radionuclides.

5. Provide documentation which validates the use of EQ3/6 to predict the formation of secondary phases resulting from high level waste glass dissolution.

6. Provide the technical bases for ignoring the role of halides in the dissolution process.

ENFE 3.03

Provide analyses to verify that the bulk-scale chemical processes dominate the in-package chemical environment. The DOE will provide analyses justifying the use of bulk chemistry as opposed to local chemistry for solubility and waste form degradation models. These analyses will be documented in an update to the Miscellaneous Waste-Form FEPs AMR (ANL-WIS-MD-000009) or in an update to the Summary of In-Package Chemistry for Waste Forms AMR (ANL-EBS-MD-000050), expected to be available in FY 02.

TSPAI 3.14[2]

DOE should account for the full range of environmental conditions for the in-package chemistry model (ENG4.1.1).

DOE will update the in-package chemistry model to account for scenarios and their associated uncertainties required by TSPA. This will be documented in the In-Package Chemistry AMR (ANL-EBS-MD-000056) expected to be available to NRC in FY 2003.

GEN 1.01 was reached during the NRC/DOE Technical Exchange and Management Meeting on Range of Thermal Operating Temperatures held September 18 and 19, 2001. At that meeting, the NRC provided additional comments that relate to agreements CLST 3.02 and TSPAI 3.14.

[2] The content of ENG4.1.1 (Cornell 2001) is adequately represented within the text of TSPAI 3.14.

These resulted in GEN 1.01, Comments 116 and 126. The DOE provided an initial response to those comments at the meeting (Reamer and Gil 2001b). Specific pages and chapter cited as part of GEN 1.01, Comments 116 and 126, are from *FY01 Supplemental Science and Performance Analyses, Volume 1: Scientific Bases and Analyses* (BSC 2001b).

GEN 1.01 (Comment 116)

> Page 10-22: What does the calculation that shows the rate of water consumption is 27 times greater than the diffusional inflow suggest about the chemical conditions inside the package? Are the simulations for in-package chemistry assuming a bathtub model appropriate?

GEN 1.01 (Comment 126)

> In Chapter 9, the assessment of in-package chemistry did not consider the spatial heterogeneity. Provide the rationales for the homogeneity.

A.1.2 Related Key Technical Issue Agreements

Per the DOE request to the NRC (Ziegler 2002), KTI agreements CLST 4.02 and CLST 4.03 were subsumed into CLST 3.02 and CLST 3.03 (Schlueter 2002) because the wording and response for agreements CLST 4.02 and CLST 4.03 were the same as those for agreements CLST 3.02 and CLST 3.03, respectively.

A.2 RELEVANCE TO REPOSITORY PERFORMANCE

The chemical reactions that occur inside a breached waste package exert strong controls over the nature and extent of radionuclide transport from the waste form into the engineered barrier system and ultimately into the geosphere. Because they collectively determine both the chemical speciation and abundance of mobile radionuclides in effluents, the reactions that occur during waste form degradation are critical to predictions of repository performance. The waste form degradation model incorporates corrosion rates of waste form materials (steel, fuel, and glass) and assumed compositional ranges of incoming fluids as inputs and calculates the formation of secondary phases and changes in fluid composition.

The in-package chemistry model must account for the full ranges of environmental conditions that may be encountered within the waste package. Local processes within the waste package could produce high or low pH values, which could enable cladding corrosion, increased waste reaction, and accelerated radionuclide mobilization. For example, widely ranging pH values can affect the solubility of radionuclide-bearing phases and hence, the quantities of radionuclides released and made available for transport. Other potentially important parameters include seepage water chemistry, temperature, and corrosion rates. Model inputs must be adequately modeled in isolation, and a physically realistic accounting of water balances inside the degrading waste form must be made. It must also be demonstrated that the complete ensemble of reactions is treatable and that the model sufficiently addresses all likely environmental conditions. The waste form degradation model must adequately predict the chemical reactivity of the waste form under the variety of conditions expected at Yucca Mountain. If these conditions are not met, the

chemical form of radionuclides might potentially be incorrectly predicted (e.g., dissolved versus colloidal) and the actual mobile mass of the radionuclide might be incorrectly estimated.

A.3 RESPONSE

A.3.1 CLST 3.02 AIN-1

The inputs used in the in-package chemistry model cover a realistic range of processes and parameters. *In-Package Chemistry Abstraction* (BSC 2004a) includes a suite of reaction path calculations in which input fluid compositions, waste form materials, temperatures, and fluid flux rates are considered. The abstraction procedure is adequate and appropriate on the basis of sensitivity testing and validation of the model. The technical basis for the model is summarized in Section 3 of this technical basis document and has been outlined in considerable detail in *In-Package Chemistry Abstraction* (BSC 2004a). Confidence has been established that the in-package chemistry model adequately captures the appropriate material properties and the range of conditions required to assess repository performance.

Corrosion rates and mechanisms for alloys used in the in-package chemistry model were derived from project-specific degradation experiments and industry handbook data (BSC 2004a). The specific values used were chosen according to the temperature range considered in the in-package chemistry model (25°C to 90°C), which was within the range of temperatures used in the experiments (BSC 2002). The values used are also the same as those used in the geochemical study and sensitivity analysis performed to analyze the corrosion of 21-PWR commercial spent nuclear fuel (SNF) waste packages (BSC 2002).

Abstraction parameters used in the analysis of waste package internal components are listed in Table A-1 and described in the context of the abstraction calculations in *In-Package Chemistry Abstraction* (BSC 2004a, Section 6.5). To provide portable inputs to TSPA, the results of reaction path calculations are abstracted into reasonably simple parameterizations that effectively envelop actual results. The abstraction procedure is described in *In-Package Chemistry Abstraction* (BSC 2004a, Chapter 8).

Table A-1. Input References for the Waste Package Components used in *In-Package Chemistry Abstraction*

Material/Property	Input	Reference
21-PWR commercial SNF waste package geometric information	Waste Package Component Dimensions	BSC 2004b, Table 1a; BSC 2003; Punatar 2001, p. 2–5
Codisposal waste package geometric information	Waste Package Component Dimensions	BSC 2003; DOE 2000, Section 3
Periodic table of the elements and mass list of radioactive isotopes	Atomic Weight of the Elements and Isotopes	Audi and Wapstra 1995; Parrington et al. 1996
Stainless Steel Type 316	Corrosion rate	DTN: MO0401SPAMCRAE.000
	Density	ASTM G 1-90 1999, Table XI, p. 7
	Composition	ASME 1998, Section II, SA-240, Table 1, p. 366, for composition of 316; ASM International 1987, p. 931, for C and N content of 316
Stainless Steel Type 304L	Corrosion rate	DTN: MO0401SPAMCRAE.000
	Density	ASTM G 1-90 1999, Table XI, p. 7
	Composition	ASTM A 240/A 240M-99b 2000, Table 1, p. 2
Carbon Steel Type A516	Corrosion rate	DTN: MO0401SPAMCRAE.000
	Density	ASTM A 20/A 20M-95a 1995, p. 21
	Composition	ASME 1998, Section II, SA-516/SA-516M, Table 1, p. 925
Aluminum Alloy 6061	Corrosion rate	ASM International 1987, Table 12, p. 603
	Density	ASTM G 1-90 1999, Table X1.1
	Composition	ASME 1998, Section II, SB-209, Table 1, p. 236
Aluminum Alloy 1100	Corrosion rate	ASM International 1987, Table 12, p. 603
	Density	ASTM G 1-90 1999, Table XI, p. 7
	Composition	ASTM B 209-96 1996, Table 1, p. 7
Neutronit[a]	Corrosion rate	DTN: MO0401SPAMCRAE.000
	Density	DTN: MO0109RIB00049.001; For B content ASTM A 887–89 2000, Table 1, S30463, S30464, and S30466
	Composition	
High-Level Radioactive Waste Glass	Density	BSC 2003; Stout and Leider 1994, Table 6.4
	Composition	BSC 2003; Baxter 1988, Table 10
N Reactor Fuel	Composition	BSC 2003; DOE 2000, Table 3-1
Commercial SNF	Isotopic Inventory	BSC 2003; BSC 2001c, Attachment III Disk 1 of 9, ATT III/ LPM1/ uniform_profile/ 3.5/ ft71-case10.N04
Goethite	Surface properties	Langmuir 1997, p. 345, Table 10.2

Source: BSC 2004a, Table 7.

NOTE: PWR = pressurized water reactor.
[a] A nickel alloy interspersed with gadolinium (ASTM designation UNS N06464) is recommended to replace Neutronit as the absorber material. The effects of this change on in-package chemistry should be negligible because deleting the Neutronit does not significantly change the quantity of available stainless steel; the low corrosion rates of the nickel alloy relative to stainless steel will result in slightly higher in-package pH (i.e., less aggressive pH), and gadolinium will form phosphates that are fairly insoluble (Loros and Williams 2004).

Sensitivity analyses were performed (BSC 2004a, Section 6.7) to (1) determine the uncertainty range for ionic strength; (2) expand the temperature and CO_2 partial pressure ranges; and (3) demonstrate how inputs such as the waste package design configuration (including sulfur content), chromium, and seepage composition affect the model output. The results of the sensitivity analyses are described in Section A.4.1.

The possibility of corrosion occurring in crevices and tight spaces, accompanied by potentially enhanced waste package degradation and radionuclide solubilities, was addressed in the in-package chemistry model, in part, by calculating the chemistry resulting from corrosion of individual waste package internal components. The resulting heterogeneous processes were not directly considered in the in-package chemistry model because the waste form components are initially spread uniformly throughout the waste package and degradation will tend to make the mix of components more homogeneous. Since a fluid capable of transporting radionuclides from the waste form would have to either move or be continuous over distances greater than about 1 m, and pH would be buffered by waste package components and waste forms to the extent that pH extremes would not occur, chemical transport would minimize the effects of spatial heterogeneity, if there was any heterogeneity initially.

The EQ3/6 model is appropriate for modeling glass degradation. Basaltic glass is considered to be an accurate natural analog for high-level radioactive waste glass (Grambow et al. 1986). EQ3/6 runs predict that high-level radioactive waste glass degradation will result in the formation of a host of secondary minerals typical of altered natural glass. Thus, it is reasonable to expect EQ3/6 models of high-level radioactive waste glass alteration to roughly mimic natural alteration of basaltic glass.

The role of metal halides on waste package and fuel degradation has been evaluated using ferric chloride and excluded from further consideration in the total system performance assessment for the license application (TSPA-LA) model because of the low likelihood that conditions necessary for metal halides to impact corrosion exist in the Yucca Mountain in-package environment. Specifically, as pH levels below 4.5 are not expected inside breached waste packages, it is highly unlikely that such low pH conditions will occur.

A.3.2 ENFE 3.03 and GEN 1.01 (Comment 126)

It is impossible to anticipate the exact paths by which water molecules will move through degraded waste forms. Consequently, there is no absolute certainty regarding which waste form components a given volume of water will interact with. However, for heterogeneous chemical processes to persist and leave a waste package without coming into contact with other fluids or solids, a fluid capable of transporting radionuclides from the waste form would have to either move or be continuous over distances greater than about 1 m. Accordingly, there is ample indication that spatial heterogeneity will not significantly alter the overall course of waste form degradation. The calculated pH is the crucial feature of the in-package chemistry model because it is used as input in the fuel and glass degradation models, in calculations of radionuclide solubility and retardation, and in the estimation of colloid stability. The reactants that would tend to buffer very high or low pH values (corrosion product surfaces, uranyl hydroxide solids, and stainless steels) are more abundant and tend to react more quickly than those components that might cause local pH extremes (e.g., high-level radioactive waste glass).

The dissolution of high-level radioactive waste glass is the only factor likely to produce extreme pH values. However, only in the unlikely scenario of a fluid contacting the glass inside the package could extreme pH levels persist. Subsequent contact with degrading metals generally results in near-neutral pH fluids. Deprotonation of corrosion product surfaces would likewise drive pH levels back toward neutral. Dissolution of schoepite, an important component of codisposal packages, will also keep pH values near neutral. Consequently, these chemical principles strongly support the conclusion that spatial heterogeneity has a negligible impact.

A.3.3 TSPAI 3.14

Model inputs have been treated both separately and in ensembles of reactions in such a way that the model sufficiently reproduces all likely environmental conditions expected at Yucca Mountain. Analyzed scenarios include the effects of intrusion of magma into the waste form (BSC 2004c), seismic damage, water accumulation in the waste form through seepage, water accumulation through vapor condensation, and heterogeneously distributed reactions of water with waste form components (BSC 2004a). A range of fluid compositions have also been considered that bound the compositions of fluids likely to prevail inside the repository over long periods of time. Input fluid compositions have been shown to have little effect on output fluid compositions (Section 3.4 of this technical basis document).

A.3.4 GEN 1.01 (Comment 116)

In previous model descriptions, the model required more water for the described reactions than was available (BSC 2004a). The water supplied by diffusion was estimated to be 1/27 of that required by the bathtub model. The two unsaturated models currently adopted (condensation of water films from the vapor phase and water film development from dripping into the waste package) resolve that inconsistency.

The information in this report is responsive to agreements ENFE 3.03, TSPAI 3.14, and GEN 1.01 (Comments 116 and 126) made between the DOE and NRC and responsive to AIN request CLST 3.02 AIN-1. The report contains the information that DOE considers necessary for NRC review for closure of these agreements.

A.4 BASIS FOR THE RESPONSE

A.4.1 CLST 3.02 AIN-1

As described in Section A.3.1, corrosion rates and mechanisms for alloys used in the in-package chemistry model were derived from project-specific degradation experiments and industry handbook data (BSC 2004a; Table 3-4 of this technical basis document). The specific values used were chosen according to the applicable temperature range of the in-package chemistry model (from 25°C to approximately 100°C), which was within the range of temperatures used in the experiments (BSC 2002). The values used are also the same as those used in the geochemical study and sensitivity analysis that was performed to analyze the corrosion of 21-PWR commercial SNF waste packages (BSC 2002). *Total System Performance Assessment (TSPA) Model for Site Recommendation* (CRWMS M&O 2000) demonstrated that corrosion rates are not sensitive parameters.

Abstraction parameters used in the analysis of waste package internal components are listed in Table A-1 and described in the context of the abstraction calculations in *In-Package Chemistry Abstraction* (BSC 2004a, Section 6.5). The parameters were taken primarily from handbook data and DOE technical product output and include waste and alloy corrosion rates; waste package component dimensions; physical properties and chemical compositions; water compositions and diffusion fluxes; and corrosion product properties. The reactions of waste package components with water were calculated for single components and for combinations of components in order to capture the situation most likely to prevail, as well as to assess potential extreme chemical conditions from the less likely situation in which single components are allowed to degrade in isolation.

Sensitivity testing (or abstraction model validation) using current values of parameters included in the model abstractions is described in *In-Package Chemistry Abstraction* (BSC 2004a, Section 6.7 and Attachment II). These tests were performed to (1) determine the uncertainty range for ionic strength; (2) expand the temperature and CO_2 partial pressure ranges; and (3) demonstrate how inputs such as the waste package design configuration (including sulfur content), chromium, and seepage composition affect the model output.

Figures A-1, A-2, and A-3 illustrate the behavior of specific processes and their responses to the varying of certain parameters. These processes are themselves parts of a complex ensemble of processes that occur simultaneously within the waste package. For example, surface complexation of steel corrosion products, which is discussed in Section A.4.2, has a profound moderating effect on pH. This process was not included in the sensitivity runs described here. As a result, pH resulting from the corrosion of steel appears in the figures to reach lower values than are expected or considered possible, given the overall chemistry that is expected to develop within the waste package.

The following conclusions were drawn. First, incoming water compositions have little effect on in-package pH and ionic strength (see Appendix B, Figures B-1 and B-2). Second, the oxidation state of chromium has little effect on overall pH history. Figure A-1 illustrates that the effects on pH and ionic strength of chromium(III) and chromium(VI) are small. Figure A-2 shows that CO_2 partial pressure has little effect on pH and ionic strength for both commercial SNF and codisposed waste, although sulfur (which causes the degradation of Carbon Steel Type A516) has a large influence on pH but a lesser effect on ionic strength.

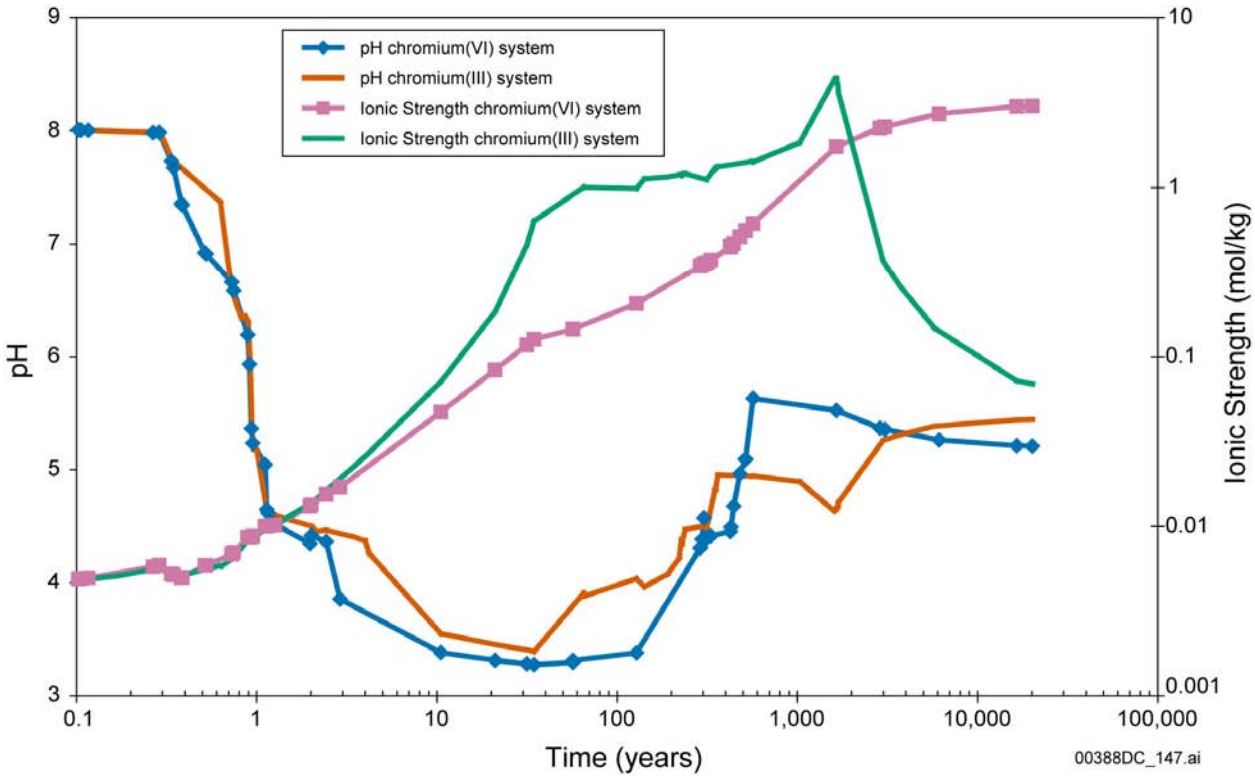

Source: BSC 2004a, Figure 16.

Figure A-1. pH and Ionic Strength Outputs from a Model Run Showing the Effects of Chromium(III) and Chromium(VI)

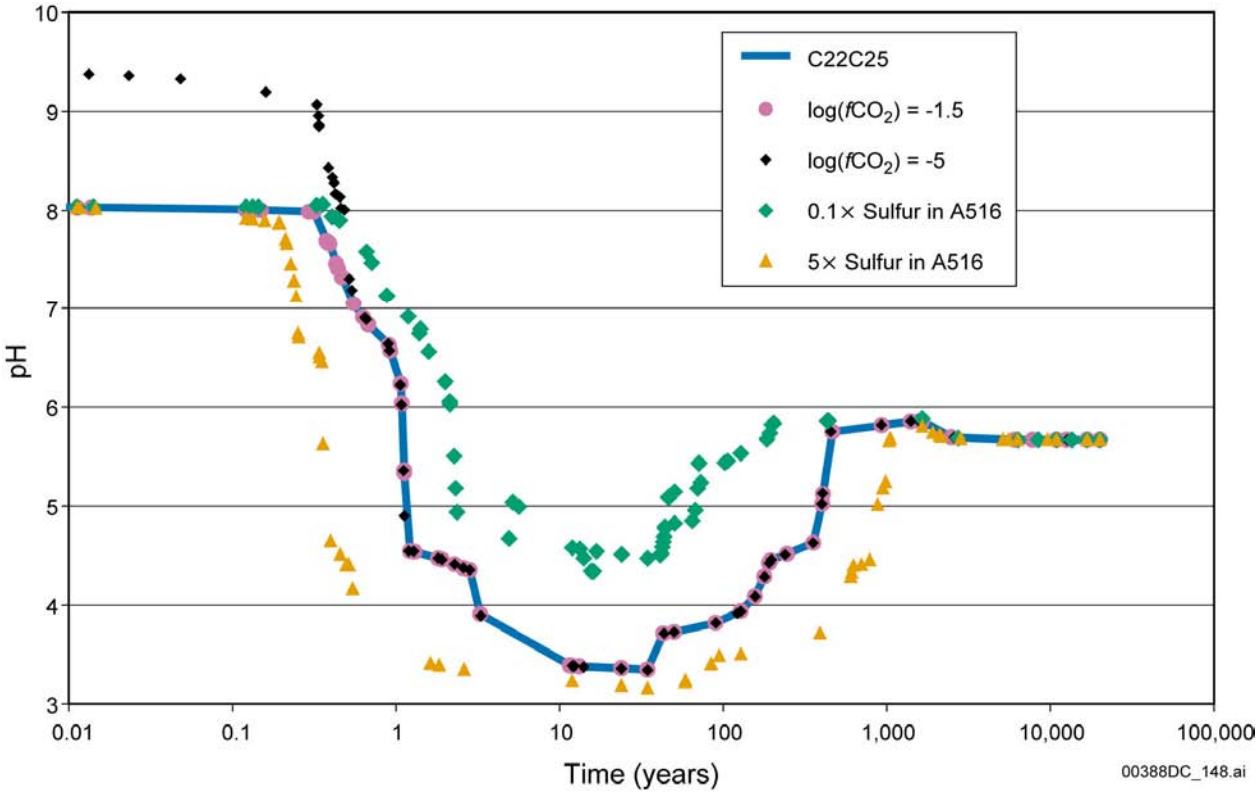

Source: BSC 2004a, Figure 17.

NOTE: C22C25 represents commercial SNF, 1.5 L/yr water flux, calcium–pore water, 10% fuel exposure, at 25°C.

Figure A-2. Effect of pCO_2 and Sulfur Content of Carbon Steel Type A516 on pH of Commercial Spent Nuclear Fuel

The quantity of sulfur contained in the A516 steel had a strong influence on the system pH during the period when A516 was degrading (Figure A-2). Increasing the sulfur content tended to lower the pH, and decreasing the sulfur tended to moderate the pH compared to the base case. Replacing Carbon Steel Type A516 with Type S31600 resulted in more moderate early pH and similar late pH. Increased temperature results in lowering the pH for commercial spent nuclear fuel and codisposed waste. This effect is due to the increased dissociation of the water molecule as temperature increases.

Increased water flux results in more rapid stabilization of the chemistry (Figure A-3) close to the initial incoming water composition. Figure A-3 shows that as the water flux was increased, the simulation would end at progressively earlier times; this was caused by the lack of change in the chemistry, which terminates the computer run. This result is a product of the reactants dissolution being kinetically controlled and the lack of significant reaction of the water and reactants. Similarly, increasing the corrosion rates of the metal alloy components has the same impact on the chemistry as decreasing the water flux (i.e., the contact time of the water with the alloy determines the degree of reaction) (see Section 6.6.5 of this technical basis document).

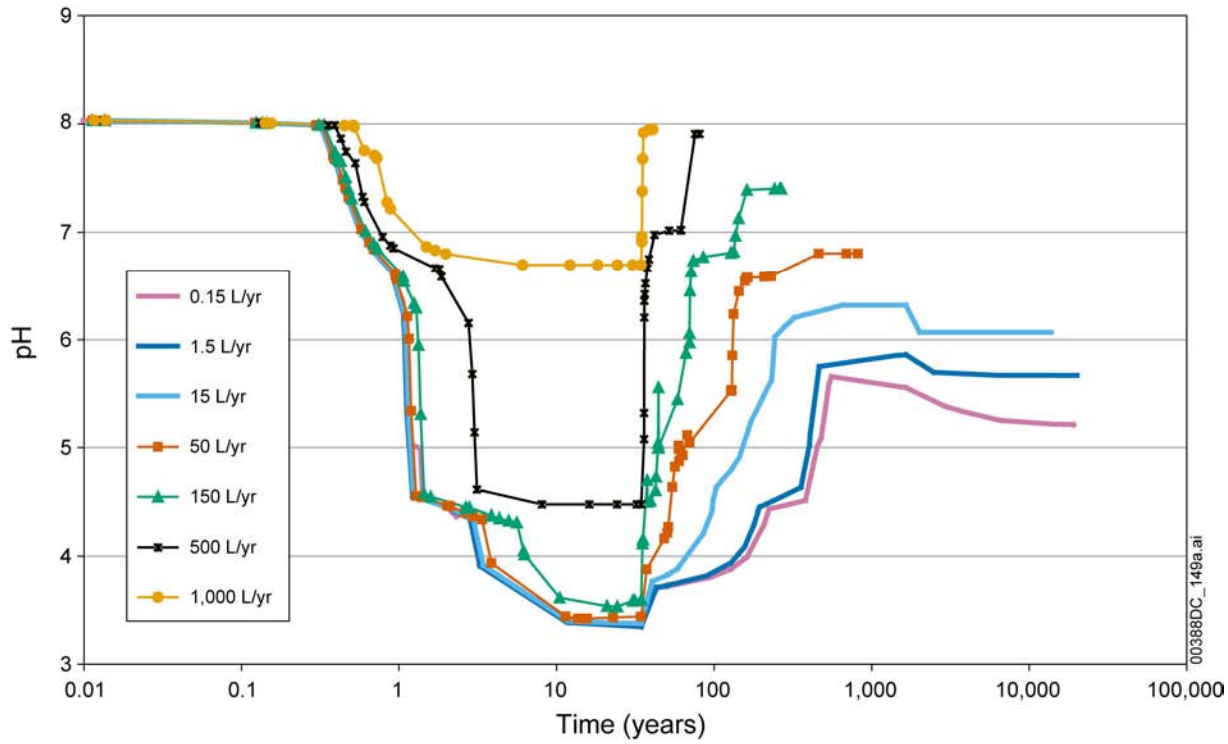

Source: BSC 2004a, Figure 20.

NOTE: Cases run using calcium–pore water, 10% fuel exposure, at 25°C.

Figure A-3. Effect of Water Flux on pH for a Commercial Spent Nuclear Fuel Waste Package

The uncertainty range for ionic strength is discussed in Section 3.5.2.3 of this technical basis document and illustrated in Figure A-4. This range accounts for uncertainties in carbon dioxide partial pressures, as well as for the possibility of lower ionic strengths resulting from surface complexation effects.

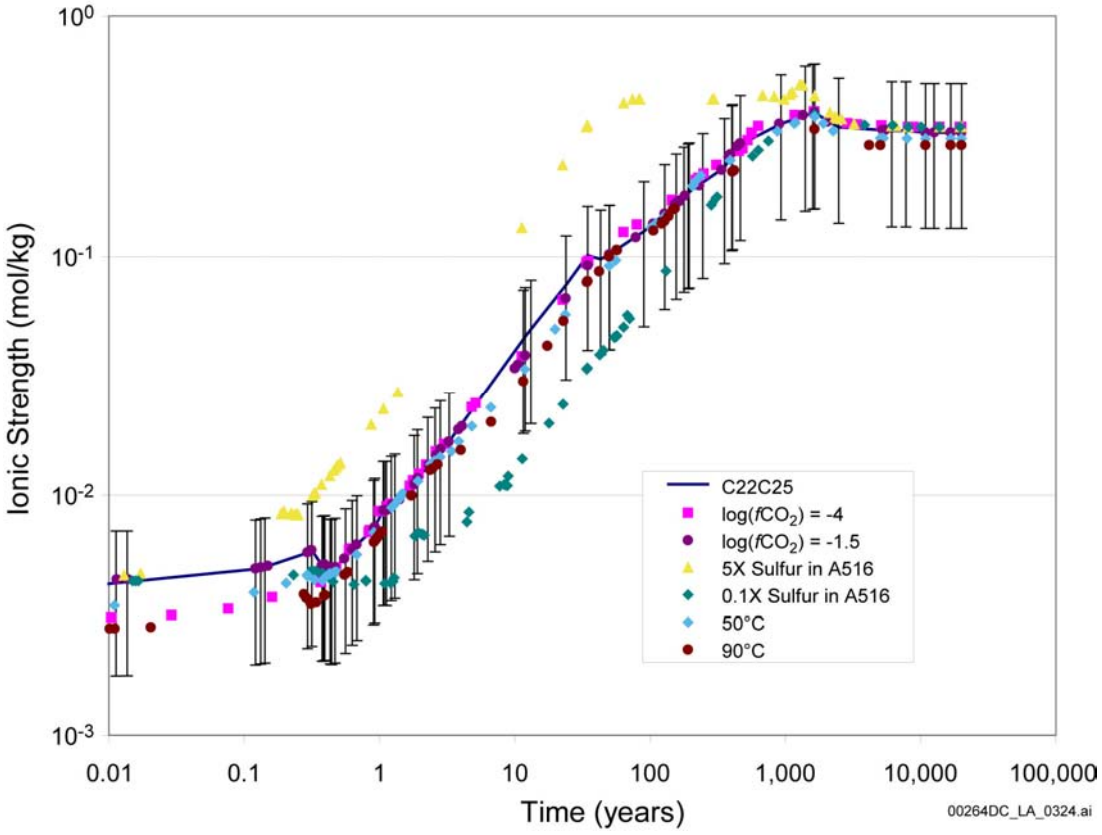

Source: DTN: MO0403SPAIPCHM.004.

NOTE: C22C25 represents commercial SNF, 1.5 L/yr water flux, calcium–pore water, 10% fuel exposure, at 25°C.

Figure A-4. Commercial Spent Nuclear Fuel Ionic Strength Profile with Error Bars

It is reasonable to speculate that if fluids were to accumulate in crevices and tight spaces inside the waste package, low pH conditions could develop and, in the extreme case, result in cladding failure. The potential for these low-volume fluids to significantly reduce the pH is small because the presence of abundant ferric (hydr)oxide corrosion products will constrain pH levels near neutral by sorbing protons from solution.

High-level radioactive waste glass degradation is predicted in EQ3/6 runs to result in the formation of a number of secondary minerals, particularly chalcedony, sodium-nontronite (a clay), borax ($Na_2[B_4O_5(OH)_4]:8H_2O$), nahcolite ($NaHCO_3$), microcline ($KAlSi_3O_8$), calcite, and saponite (a clay). Basaltic glass is considered to be an accurate natural analog for high-level radioactive waste glass (Grambow et al. 1986). Except for the presence of boron and the subsequent formation of secondary borate phases, it is reasonable to expect EQ3/6 models of high-level radioactive waste glass alteration to roughly mimic natural alteration of basaltic glass if the comparison is valid. The fact that chalcedony, clays, calcite, and microcline are routinely observed in the weathering of basalt glass in natural environments suggests that EQ3/6 is a valid tool for modeling the formation of secondary phases during high-level radioactive waste glass alteration.

Ferric chloride (and other halides) are unlikely to impact corrosion processes within the in-package environment. In the drip scenario, seepage water enters the waste package. This water contains dissolved species, including chloride and bicarbonate ions. Ferric chloride (and fluoride) may form and, with nitric acid from radiolysis, tend to lower pH. However, the bicarbonate ion tends to raise pH, and ferric hydroxide forms from waste package corrosion above about pH 3. Dissolution of such metal oxide and hydroxide minerals (primarily iron) tends to drive pH upward. Thus, a set of competing chemical reactions occurring in the waste package tends to maintain pH at moderate values and prohibit deviations to extremely low pH. As pH values below 4.5 are not expected inside breached waste packages, it is highly unlikely that the low pH conditions needed for ferric chloride (or other halide-associated) impacts will ever occur.

A.4.2 ENFE 3.03 and GEN 1.01 (Comment 126)

Schoepite, which with iron corrosion products dominates the composition of the alteration products from time periods of 500 years and beyond, dissolves at acid pH to consume protons and at above neutral pH to produce protons. These two reactions constitute a negative feedback that resists pH deviations to high or low pH and ultimately limits pH values near the schoepite solubility minimum of pH 6.5 to 7 (BSC 2004a, Section 6.8), which shifts to lower pH as the ambient carbon dioxide pressure increases (BSC 2004a, Figure 6.7-1).

Consideration of the steels and glass in isolation from the schoepite points to another mechanism by which alkalinity increases from high-level radioactive waste glass dissolution are resisted: chromium oxidizes to CrO_4^{2-} above pH 6.5, but forms $HCrO_4^-$ below pH 6.5. For this reason, ambient pH has an important effect on proton production by steel degradation. Specifically, at a pH less than or equal to 6.5, steel degradation either consumes protons or produces relatively small amounts of them, while at a pH greater than 6.5, degradation of both Stainless Steel Types 304L and 316 produces relatively large amounts of protons. This mechanism constrains pH values close to 6.5 and counters proton consumption by glass degradation.

The fact that proton consumption prevails at pH values greater than or equal to 6.5, but proton production amplifies above pH 6.5 indicates that long-term pH values will converge toward 6.5 as long as sufficient steel and high-level radioactive waste glass exist in the package. Note that there is more than twice as much Stainless Steel Type 316 as high-level radioactive waste glass and roughly 20% more Stainless Steel Type 304L than high-level radioactive waste glass.

The revised *In-Package Chemistry Abstraction* (BSC 2004a, Sections 6.6.1.1 and 6.6.2.1) demonstrates that the reactions of the individual waste form components (steels, glass, fuel) produce fluids with pH values that are close to neutral. The exceptions are Carbon Steel Type A516 and Stainless Steel Type 304L steel degradation, which both produce protons, and high-level radioactive waste glass, which generates alkalinity. Explicit consideration of the pH-buffering of corrosion products indicates that Carbon Steel Type A516 degradation will actually produce near neutral fluids (BSC 2004a, Section 6.8). Stainless Steel Type 304L degradation is also unlikely to result in acid pH solutions because it dissolves very slowly (BSC 2004a, Section 6.5.1.1), so proton production is likely to be diluted by incoming fluids. High-level radioactive waste glass dissolution can produce locally high pH levels because of its high base cation content. However, there is far more steel than high-level radioactive waste glass in codisposal packages, and large amounts of schoepite are estimated to form as well. Dissolution

of either steel or schoepite consumes alkalinity and would tend to make the persistence of high pH levels in the waste form unlikely. In particular, relatively rapid dissolution of schoepite would tend to drive pH levels towards its solubility minimum, near neutral pH.

pH is the critical feature of concern to the in-package chemistry model and is controlled by an ensemble of processes that occur throughout the waste package. Reactants that tend to buffer pH levels (i.e., corrosion product surfaces, uranyl hydroxide solids, and stainless steels) are more abundant and tend to be faster reacting than components such as high-level radioactive waste glass that might cause local pH extremes. The presence of multiple processes capable of providing a negative-feedback control over high pH is discussed in Section 3.4 of this technical basis document and in *In-Package Chemistry Abstraction* (BSC 2004a, Section 6.8). In summary, the dissolution of high-level radioactive waste glass is the only way to generate locally extreme pHs. Because high-level radioactive waste glass is present in minor amounts (and dissolves more slowly) relative to other pH-buffering reactants, the potential for long-term persistence of extreme pH levels is considered remote.

A.4.3 TSPAI 3.14

The updated *In-Package Chemistry Abstraction* (BSC 2004a) considers wide ranges in input fluid compositions and ambient gas (oxygen and carbon dioxide) partial pressures; the presence and absence of cladding; the effects of an igneous intrusion (BSC 2004c); degradation in the presence of water condensate and seepage; and wide ranges in the fluxes of both condensate and seepage. A pH range of 4.5 to 8.1 is found to adequately account for the full range of in-package conditions.

Higher fluid fluxes tend to result in fluid pH values close to the original input values, which tend to be close to neutral. Low fluid fluxes (condensate or seepage) allow the accumulation of salts and, as expected, result in higher ionic strengths; pH values close to neutral share this tendency.

Sensitivity calculations have considered the impacts of higher and lower ambient carbon dioxide and oxygen levels. None of the conditions affects the output pH significantly. This is true for carbon dioxide primarily because the kinetics of the reactions controlling proton production and consumption are not strong functions of carbon dioxide levels. High carbon dioxide levels might result from biomass production on the drift floor. Redox conditions lower than ambient might occur as a result of the shielding of fuel by corrosion product accumulation. While lowered redox states would affect solubilities, they do not affect pH materially.

As emphasized elsewhere in this document, a number of pH-buffering solid-solution reactions tend to anchor local and bulk pH close to neutral. These reactions include schoepite dissolution; steel degradation; and proton uptake, release, or both, by corrosion products. Ambient cycling of oxygen through the mountain sets the upper oxygen partial pressure and the nominal carbon dioxide levels. The assemblage of reactions has the effect of driving output chemistries toward a common endpoint despite the large variation in possible initial environmental conditions.

A.4.4 GEN 1.01 (Comment 116)

In previous model descriptions, the model required more water for the described reactions than was available (BSC 2004a). The water supplied by diffusion was estimated to be 1/27 of that

required by the bathtub model. The two unsaturated models currently adopted (condensation of water films from the vapor phase and water film development from dripping into the waste package) resolve that inconsistency. Both the no-drip and the seepage dripping model have separate process models and separate abstraction models, thus allowing implementation of nondripping (water vapor condensation) and dripping (seepage dripping model) models in the TSPA-LA. For both of these models, the chemical reaction of the waste package components with a liquid was simulated as a function of time.

A.5 REFERENCES

A.5.1 Documents Cited

ASME (American Society of Mechanical Engineers) 1998. *1998 ASME Boiler and Pressure Vessel Code*. 1998 Edition with 1999 and 2000 Addenda. New York, New York: American Society of Mechanical Engineers. TIC: 247429.

ASM International 1987. *Corrosion*. Volume 13 of *Metals Handbook*. 9th Edition. Metals Park, Ohio: ASM International. TIC: 209807.

Audi, G. and Wapstra, A.H. 1995. *Atomic Mass Adjustment, Mass List for Analysis*. Upton, New York: Brookhaven National Laboratory, National Nuclear Data Center. TIC: 242718.

Baxter, R.G. 1988. *Defense Waste Processing Facility Wasteform and Canister Description*. DP-1606, Rev. 2. Aiken, South Carolina: E.I. du Pont de Nemours & Company, Savannah River Plant. TIC: 8704.

Brocoum, S. 2001. "Transmittal of Analysis and Model Reports (AMR) and other Items Addressing Key Technical Issue (KTI) Technical Exchanges." Letter from S.J. Brocoum (DOE) to C.W. Reamer (NRC), March 30, 2001, with enclosure. ACC: MOL.20010529.0119.

BSC (Bechtel SAIC Company) 2001a. *In-Package Chemistry for Waste Forms.* ANL-EBS-MD-000056 REV 00. Las Vegas, Nevada: Bechtel SAIC Company. ACC: MOL.20010322.0490.

BSC 2001b. *FY01 Supplemental Science and Performance Analyses, Volume 1: Scientific Bases and Analyses.* TDR-MGR-MD-000007 REV 00. Las Vegas, Nevada: Bechtel SAIC Company. ACC: MOL.20010712.0062.

BSC 2001c. *PWR Assembly End-Effect Reactivity Evaluation*. CAL-UDC-NU-000006 REV 00. Las Vegas, Nevada: Bechtel SAIC Company. ACC: MOL.20010412.0158.

BSC 2002. *Geochemistry Model Abstraction and Sensitivity Studies for the 21 PWR CSNF Waste Packages*. MDL-DSU-MD-000001 REV 00. Las Vegas, Nevada: Bechtel SAIC Company. ACC: MOL.20021107.0154.

BSC 2003. *Repository Design Project, Repository/PA IED Emplacement Drift Committed Materials 1 of 2*. 800-IED-WIS0-00301-000-00A. Las Vegas, Nevada: Bechtel SAIC Company. ACC: ENG.20030627.0003.

BSC 2004a. *In-Package Chemistry Abstraction*. ANL-EBS-MD-000037 REV 03B. Las Vegas, Nevada: Bechtel SAIC Company. ACC: MOL.20040609.0094.

BSC 2004b. *D&E/PA/C IED Typical Waste Package Components Assembly*. 800-IED-WIS0-00202-000-00B. Las Vegas, Nevada: Bechtel SAIC Company. ACC: ENG.20040202.0010.

BSC 2004c. *Igneous Intrusion Impacts on Waste Packages and Waste Forms*. MDL-EBS-GS-000002 REV 01. Las Vegas, Nevada: Bechtel SAIC Company. ACC: DOC.20040421.0002.

Cornell, V. 2001. *Analysis of Resolution Status Key Technical Issue: Total System Performance Assessment and Integration Subissue 3: Model Abstraction*. Slide presentation at U.S. Nuclear Regulatory Commission/U.S. Department of Energy Technical Exchange and Management Meeting on Total System Performance Assessment and Integration, August 6 through 10, 2001. ACC: MOL.20010921.0129.

CRWMS M&O (Civilian Radioactive Waste Management System Management and Operating Contractor) 2000. *Total System Performance Assessment (TSPA) Model for Site Recommendation*. MDL-WIS-PA-000002 REV 00. Las Vegas, Nevada: CRWMS M&O. ACC: MOL.20001226.0003.

DOE (U.S. Department of Energy) 2000. *N Reactor (U-Metal) Fuel Characteristics for Disposal Criticality Analysis*. DOE/SNF/REP-056, Rev. 0. Washington, D.C.: U.S. Department of Energy, Office of Environmental Management. TIC: 247956.

Grambow, B., Jercinovic, M.J., Ewing, R.C., and Byers, C.D. 1986. "Weathered Basalt Glass: A Natural Analogue for the Effects of Reaction Progress on Nuclear Waste Glass Alteration." *Scientific Basis for Nuclear Waste Management IX, Symposium held September 9-11, 1985, Stockholm, Sweden*. Werme, L.O., ed. *50*, 263–272. Pittsburgh, Pennsylvania: Materials Research Society. TIC: 203664.

Langmuir, D. 1997. *Aqueous Environmental Geochemistry*. Upper Saddle River, New Jersey: Prentice Hall. TIC: 237107.

Loros, E. and Williams, N.H. 2004. Meeting Minutes, Bechtel SAIC Company, LLC, Technical Review Board (TMRB) Meeting, April 22, 2004. Las Vegas, Nevada: Bechtel SAIC Company. ACC: MOL.20040622.0297.

Parrington, J.R.; Knox, H.D.; Breneman, S.L.; Baum, E.M.; and Feiner, F. 1996. *Nuclides and Isotopes, Chart of the Nuclides*. 15th Edition. San Jose, California: General Electric Company and KAPL, Inc. TIC: 233705.

Punatar, M.K. 2001. *Summary Report of Commercial Reactor Criticality Data for Crystal River Unit 3*. TDR-UDC-NU-000001 REV 02. Las Vegas, Nevada: Bechtel SAIC Company. ACC: MOL.20010702.0087.

Reamer, C.W. 2001. "U.S. Nuclear Regulatory Commission/U.S. Department of Energy Technical Exchange and Management Meeting on Evolution of the Near-Field Environment (January 9–12, 2001)." Letter from C.W. Reamer (NRC) to S. Brocoum (DOE/YMSCO), January 26, 2001, with enclosure. ACC: MOL.20010810.0033.

Reamer, C.W. and Gil, A.V. 2001a. Summary Highlights of NRC/DOE Technical Exchange and Management Meeting on Total System Performance Assessment and Integration. Meeting held August 6–10, 2001. Las Vegas, Nevada. Washington, D.C.: U.S. Nuclear Regulatory Commission. ACC: MOL.20010921.0121.

Reamer, C.W. and Gil, A.V. 2001b. Summary Highlights of NRC/DOE Technical Exchange and Management Meeting of Range on Thermal Operating Temperatures, September 18–19, 2001. Washington, D.C.: U.S. Nuclear Regulatory Commission. ACC: MOL.20020107.0162.

Schlueter, J. 2000. U.S. Nuclear Regulatory Commission/U.S. Department of Energy Technical Exchange and Management Meeting on Container Life and Source Term (September 12–13, 2000). Letter from J. Schlueter (NRC) to S. Brocoum (DOE/YMSCO), October 4, 2000, with enclosure. ACC: MOL.20010731.0161.

Schlueter, J. 2002. "Container Life and Source Term Agreements." Letter from J. R. Schlueter (NRC) to J. D. Ziegler (NRC). July 2, 2002. ACC: MOL.20020819.0277.

Stout, R.B. and Leider, H.R., eds. 1994. *Preliminary Waste Form Characteristics Report, Version 1.0*. UCRL-ID-108314, Rev. 1. Livermore, California: Lawrence Livermore National Laboratory. ACC: MOL.19960314.0440.

Ziegler, J.D. 2002. "Transmittal of Information Addressing Key Technical Issue (KTI) Container Life and Source Term (CLST) Agreements 4.02, 4.03, 4.04, And 4.05." Letter from J. D. Ziegler (DOE) to J. R. Schlueter (NRC), June 21, 2002. ACC: MOL.20020815.0586.

A.5.2 Codes, Standards, and Regulations

ASTM A 20/A 20M-95a. 1995. *Standard Specification for General Requirements for Steel Plates for Pressure Vessels*. West Conshohocken, Pennsylvania: American Society for Testing and Materials. TIC: 240026.

ASTM A 240/A 240M-99b. 2000. *Standard Specification for Heat-Resisting Chromium and Chromium-Nickel Stainless Steel Plate, Sheet, and Strip for Pressure Vessels*. West Conshohocken, Pennsylvania: American Society for Testing and Materials. TIC: 248529.

ASTM A 887-89 (Reapproved 2000). 2000. *Standard Specification for Borated Stainless Steel Plate, Sheet, and Strip for Nuclear Application.* West Conshohocken, Pennsylvania: American Society for Testing and Materials. TIC: 249544.

ASTM B 209–96. 1996. *Standard Specification for Aluminum and Aluminum-Alloy Sheet and Plate*. West Conshohocken, Pennsylvania: American Society for Testing and Materials. TIC: 247078.

ASTM G 1-90 (Reapproved 1999). 1999. *Standard Practice for Preparing, Cleaning, and Evaluating Corrosion Test Specimens.* West Conshohocken, Pennsylvania: American Society for Testing and Materials. TIC: 238771.

A.5.3 Data, Listed by Data Tracking Number

MO0109RIB00049.001. *Waste Package Material Properties: Neutron Absorbing Materials*. Submittal date: 09/17/2001.

MO0401SPAMCRAE.000. *Materials Corrosion Rates in Aqueous Environments*. Submittal date: 01/16/2004.

MO0403SPAIPCHM.004. *Abstractions of In-Package Chemistry for TSPA-LA*. Submittal date: 03/15/2004.

APPENDIX B

EFFECTS OF RADIOLYSIS AND ENGINEERED MATERIALS ON IN-PACKAGE CHEMISTRY (RESPONSE TO CLST 3.03 AIN-1 AND CLST 3.04 AIN-1)

Note Regarding the Status of Supporting Technical Information

This document was prepared using the most current information available at the time of its development. This Technical Basis Document and its appendices providing Key Technical Issue Agreement responses that were prepared using preliminary or draft information reflect the status of the Yucca Mountain Project's scientific and design bases at the time of submittal. In some cases this involved the use of draft Analysis and Model Reports (AMRs) and other draft references whose contents may change with time. Information that evolves through subsequent revisions of the AMRs and other references will be reflected in the License Application (LA) as the approved analyses of record at the time of LA submittal. Consequently, the Project will not routinely update either this Technical Basis Document or its Key Technical Issue Agreement appendices to reflect changes in the supporting references prior to submittal of the LA.

APPENDIX B

EFFECTS OF RADIOLYSIS AND ENGINEERED MATERIALS ON IN-PACKAGE CHEMISTRY (RESPONSE TO CLST 3.03 AIN-1 AND CLST 3.04 AIN-1)

This appendix provides a response to Key Technical Issue (KTI) agreements Container Life and Source Term (CLST) 3.03 Additional Information Needed (AIN)-1 and CLST 3.04 AIN-1. These agreements relate to the effects of radiolysis and engineered materials on in-package chemistry.

B.1 KEY TECHNICAL ISSUE AGREEMENTS

B.1.1 CLST 3.03 AIN-1 and CLST 3.04 AIN-1

Agreements CLST 3.03 and CLST 3.04 were reached during the U.S. Nuclear Regulatory Commission (NRC)/U.S. Department of Energy (DOE) Technical Exchange and Management Meeting on CLST held September 12 and 13, 2000, in Las Vegas, Nevada (Schlueter 2000). Subissues 1, 2, 3, 4, and 6 were discussed at that meeting.

In-Package Chemistry for Waste Forms (BSC 2001), which addresses agreements CLST 3.03 and CLST 3.04, was provided to the NRC in March 2001 (Brocoum 2001). After reviewing the document, the NRC determined that the effect of radiolysis on cladding corrosion was not discussed in the DOE analysis. Also, according to the NRC, the report did not discuss the applicability of abstractions for incoming water, taking into account information provided in *Environment on the Surfaces of the Drip Shield and Waste Package Outer Barrier* (CRWMS M&O 2000). The NRC, therefore, asked for specific additional information to close these agreements, resulting in CLST 3.03 AIN-1 and CLST 3.04 AIN-1 (Reamer 2001).

The NRC AIN request for agreement CLST 3.03 (for commercial spent nuclear fuel (SNF) stored in commercial SNF waste packages) was also applicable to CLST 4.03 (for DOE SNF and DOE high-level radioactive waste stored in codisposal waste packages). Similarly, the AIN request for agreement CLST 3.04 was applicable to CLST 4.04 (for DOE SNF and DOE high-level radioactive waste). Accordingly, this appendix provides responses to the AINs that the NRC requested for agreements CLST 3.03, 3.04, 4.03, and 4.04. This approach is consistent with the DOE letter request dated June 21, 2002 (Ziegler 2002), and the NRC letter concurrence dated July 2, 2002 (Schlueter 2002).

The wording for agreements CLST 4.03 and CLST 4.04 is identical to the wording for agreements CLST 3.03 and CLST 3.04, respectively. The wording of these agreements and AINs is as follows:

CLST 3.03 and CLST 4.03

> Provide a more detailed calculation on the in-package chemistry effects of radiolysis. DOE stated that the calculations recently performed as discussed at the 9/12/00 Technical Exchange and preceding teleconferences are being documented. These calculations will be referenced and justified in the revision of

the Summary of In-Package Chemistry for Waste Forms AMR, ANL-EBS-MD-000050 and will be available in January 2001.

CLST 3.04 and CLST 4.04

Need consistency between abstractions for incoming water and sensitivity studies conducted for in-package calculations, in particular, taking into account the interaction of engineered materials on the chemistry of water used for input to in-package abstractions. DOE stated that the revision of the Summary of In-Package Chemistry for Waste Forms AMR, ANL-EBS-MD-000050 will discuss the applicability of abstractions for incoming water, taking into account the revised Environment on the Surfaces of the Drip Shield and Waste Package Outer Barrier AMR. The revision will be available in January 2001.

CLST 3.03 AIN-1 and CLST 4.03 AIN-1

Provide additional information on the dose rate calculation as a function of time for typical fuels in the waste package and the technical basis for 50 R/hr dose rate.

CLST 3.04 AIN-1 and CLST 4.04 AIN-1

Provide documentation, which shows consistency between abstractions for incoming water and sensitivity studies conducted for in-package calculations.

B.1.2 Related Key Technical Issue Agreements

There are no other KTI agreements directly related to agreements CLST 3.03, 3.04, 4.03, and 4.04.

B.2 RELEVANCE TO REPOSITORY PERFORMANCE

B.2.1 CLST 3.03 AIN-1

Radiolysis can affect in-package chemistry, particularly with regard to the formation of nitric acid (HNO_3), which could promote the corrosion of zirconium alloy cladding. Higher cladding corrosion rates could lead to higher dissolution rates of commercial SNF and result in higher radionuclide release rates from the engineered barrier system. These higher radionuclide release rates could, in turn, result in higher doses to the reasonably maximally exposed individual (RMEI). The critical question in agreement CLST 3.03 is whether radiolysis (gamma, neutron, and alpha) of humid air can produce HNO_3 in quantities sufficient to corrode zirconium alloy cladding.

B.2.2 CLST 3.04 AIN-1

Seepage water entering a damaged waste package may vary in chemical composition. If in-package fluid chemistries resulting from the reaction of seepage water with the waste form and waste package components are found to be sensitive to the compositions of the waters that initially enter a package, the performance of the repository could be affected.

B.3 RESPONSE

B.3.1 CLST 3.03 AIN-1

Radiolysis occurs when radiation passes through a material and transfers energy to it, resulting in chemical reactions. In aqueous solutions and air–water–vapor systems, a large number of possible radicals and molecules containing hydrogen and oxygen may form. Two species, HNO_3 and hydrogen peroxide (H_2O_2), are of particular concern because of their potential to alter the in-package chemistry (BSC 2004a, Attachment III) and promote the corrosion of zirconium alloy cladding. The amount of HNO_3 and H_2O_2 produced is directly proportional to the amount of energy deposited in the material and thus, is directly proportional to the dose rate. Hence, the NRC requested further information on dose rate as a function of time.

The DOE initial response stated that very high concentrations of HNO_3 (14.2 mol/L) are needed to promote the corrosion of zirconium alloy cladding and that buildups of such concentrations are not likely because: (1) the dose rate after waste package breach is low; (2) some of the nitric oxide may escape through waste package breaches, thereby producing less HNO_3; and (3) dripping water flushes away HNO_3 absorbed in the water film during a long period (Reamer 2001).

In the drip scenario, seepage water enters the waste package. This water contains dissolved species, including chloride and bicarbonate ions. Ferric chloride (and fluoride) may form and, with HNO_3, tend to control and promote Zircaloy corrosion. However, bicarbonate ion tends to raise pH, and ferric hydroxide forms from waste package corrosion above about pH 3. Dissolution of such metal oxide and hydroxide minerals (primarily iron) tends to drive pH upward. Thus, a set of competing chemical reactions occurring in the waste package tends to maintain pH at moderate values and prohibit excursions to extremely low pH.

The NRC finds the foregoing arguments acceptable, for the most part, but notes that the calculation for HNO_3 concentration is based on a dose rate of 50 R/hr, a value not previously documented by the DOE. Data (presented in Section B.4.1) show that with an assumed package failure at 500 years (chosen to provide an arbitrarily high dose rate), the gamma dose rate has declined to less than 6 R/hr, about 1 order of magnitude lower than the dose rate used in the analysis.

The NRC also notes that the analysis ignores the radiolysis effect of alpha particles that may escape from cladding-perforated fuels. While gamma and neutron radiation decline to insignificant levels with respect to radiolytic effects after a few centuries, alpha radiation will persist for a few thousand years. However, due to the nature of alpha radiolysis, the chemical species produced are less aggressive oxidants than are the products of gamma and neutron radiolysis. Furthermore, the dose rate will be lower than the unrealistically high dose rate modeled in the sensitivity analysis for the gamma dose rate (see Section B.4.1). On these bases, it is concluded that alpha radiation persisting after gamma and neutron radiation decline will not promote Zircaloy-cladding corrosion.

B.3.2 CLST 3.04 AIN-1

In-Package Chemistry Abstraction (BSC 2004a) documents that the compositions of fluids resulting from in-package chemical reactions are largely insensitive to the composition of the seepage entering the package. Three thermally perturbed fluid compositions abstracted in *Engineered Barrier System: Physical and Chemical Environment Model* (BSC 2004b) were used as inputs to a sensitivity analysis (BSC 2004a, Section 6.7.1). The three water compositions represent different carbon dioxide fugacity (fCO_2) and temperature conditions.

Inputs used in the in-package chemistry abstraction (BSC 2004a, Section 6.5) also included three water compositions: calcium–pore water; sodium–pore water; and J-13 well water. The calcium– and sodium–pore water compositions were used because they were obtained from core samples taken near the repository site. The J-13 composition was used for comparison purposes.

The results from the two sets of sensitivity runs show that pH and ionic strength vary little with input water chemistry. Comparisons of two pairs of water composition output from the sensitivity analysis (BSC 2004a, Section 6.7.1) are presented in Section B.4.2.

This information in this report is responsive to AIN requests CLST 3.03 AIN-1 and CLST 3.04 AIN-1. This report contains the information that the DOE considers necessary for NRC review for closure of these agreements.

B.4 BASIS FOR RESPONSE

B.4.1 CLST 3.03 AIN-1

Dose Rates–Gamma dose rates outside pressurized water reactor SNF rods are shown in Table B-1. These rates are taken from *Gamma and Neutron Radiolysis in the 21-PWR Waste Package from Ten to One Million Years* (BSC 2002, Tables 15 and 17). Neutron dose rates are roughly 4 orders of magnitude lower than gamma dose rates for the time period discussed; they are listed in *Gamma and Neutron Radiolysis in the 21-PWR Waste Package from Ten to One Million Years* (BSC 2002). Doses are from the central nine SNF assemblies and were calculated using the software code MCNP. The pressurized water reactor SNF assembly used in the calculation was a Babcock and Wilcox 15-by-15 assembly, and it was assumed to have 4.0 wt % initial U^{235}, 48 GWd/MTU burnup, and 21-year decay time. The waste package containing the 21-PWR was assumed to fail, resulting in a pressure of 1 atm. The temperature was assumed to be 90°C with relative humidity between 40% and 90%. The rationale for this assumption is that the waste package has failed and been exposed to the atmosphere; the temperature and relative humidity ranges correspond to conditions under which nitrate production was measured (BSC 2002, Section 3.11). The dose rates shown in Table B-1 are for two moist air conditions. Other assumptions are documented in *Gamma and Neutron Radiolysis in the 21-PWR Waste Package from Ten to One Million Years* (BSC 2002).

Table B-1. Gamma Dose Rates outside Pressurized Water Reactor Spent Nuclear Fuel Rods

Age (Years)	Dose Rate at Relative Humidity 40%, Temperature 90°C (R/hr)	Dose Rate at Relative Humidity 90%, Temperature 90°C (R/hr)
10	7.81×10^4	7.82×10^4
15	5.75×10^4	5.76×10^4
20	4.69×10^4	4.69×10^4
25	4.02×10^4	4.02×10^4
35	3.04×10^4	3.04×10^4
50	2.10×10^4	2.10×10^4
70	1.31×10^4	1.31×10^4
100	6.51×10^3	6.50×10^3
150	2.05×10^3	2.05×10^3
200	6.46×10^2	6.46×10^2
250	2.07×10^2	2.07×10^2
350	2.52×10^1	2.52×10^1
500	5.54	5.54
700	4.65	4.65
1,000	4.29	4.29
1,500	4.07	4.07
2,000	3.83	3.83
2,500	3.75	3.75
3,500	3.65	3.65
5,000	3.52	3.52
7,000	3.39	3.39
10,000	3.24	3.24

Source: BSC 2002, Table 15.

The dose rate of 50 R/hr occurs around 325 years, as shown in Table B-1. The dose rate at 500 years is only about 6 R/hr. Thus, using a dose rate of 50 R/hr to calculate HNO_3 production overestimates such production by about 1 order of magnitude and is, therefore, a conservative value.

Alpha Radiolysis–Because alpha activity in SNF decreases more slowly than gamma and neutron activity, it is possible that oxidizing conditions and HNO_3 formation could persist for some time (a few thousand years) after gamma and neutron radiation became ineffective (a few centuries). However, due to the nature of alpha radiation, fewer reactive chemical species form in response to water radiolysis than do in the case of neutron and gamma radiation, which results in chemical conditions significantly less conducive to Zircaloy corrosion.

For low-linear-energy-transfer radiation, such as gamma radiation, the formation of oxygen- and hydrogen-bearing radicals and free electrons (e.g., $H_3O^+(aq)$, OH^-, $e^-(aq)$) is favored over molecular species (e.g., H_2, H_2O_2). Alpha radiation is high-linear-energy-transfer radiation and has the opposite effect (i.e., formation of more molecular species). The oxidizing effect of molecular species is lower than that of radicals (Christensen and Sunder 2000). Because Zircaloy is less susceptible to corrosion from H_2O_2 than from HNO_3, and because HNO_3 does

not significantly affect Zircaloy degradation at the concentrations anticipated, prolonged alpha radiation will likewise have a minimal effect on Zircaloy cladding integrity.

B.4.2 CLST 3.04 AIN-1

In-Package Chemistry Abstraction (BSC 2004a) demonstrates that the compositions of fluids resulting from in-package chemical reactions are largely insensitive to the composition of the seepage entering the package. Three thermally perturbed fluid compositions abstracted in *Engineered Barrier System: Physical and Chemical Environment Model* (BSC 2004b) were used as inputs to a sensitivity analysis using the in-package chemistry model (BSC 2004a, Section 6.7.1). The three water compositions represent different fCO_2 and temperature conditions. In the in-package chemistry abstraction (BSC 2004a, Section 6.5), inputs also included three different water compositions: calcium–pore water; sodium–pore water; and J-13 well water. The calcium– and sodium–pore water compositions were used because they were obtained from core samples taken near the repository site. The J-13 water composition was used for comparison purposes.

The EQ6 runs were set up to reflect the increased temperature and fCO_2, and both the commercial SNF and high-level radioactive waste glass kinetic rate coefficients were recalculated at the new temperatures (BSC 2004a, Tables 18 and 19). The EQ6 runs were executed at these conditions using both the thermally perturbed seepage compositions and the calcium–pore water composition for comparative purposes. Perturbed seepage compositions are presented in Table B-2; the compositions for sodium–pore water, calcium–pore water, and J-13 well water are presented in Table B-3. Fluids can be formed with compositions outside of the ranges considered in this analysis, particularly in the early stages of the repository when temperatures are high and evaporative concentration of seepage on the drip shield and waste package surface occurs. While evaporative concentration can lead to anomalous fluid chemistries, it also results in substantially lower fluid fluxes, which, in turn, limit long-term transport of radionuclides.

Table B-2. Thermally Perturbed Seepage Compositions

Parameter	Units	Input File Names		
		10006	20013	51
Temperature	°C	56.2	40.2	91.8
$Log(fCO_2)$	–	−1.950	−2.198	-2.532
pH	–	7.78	7.94	8.14
HCO_3^-	mol/kg	6.58×10^{-3}	6.92×10^{-3}	2.04×10^{-3}
Ca^{2+}	mol/kg	4.40×10^{-4}	5.73×10^{-4}	7.24×10^{-5}
Cl^-	mol/kg	7.12×10^{-4}	5.61×10^{-4}	7.34×10^{-4}
F^-	mol/kg	7.81×10^{-4}	6.43×10^{-4}	9.77×10^{-4}
K^+	mol/kg	4.55×10^{-4}	2.76×10^{-4}	5.02×10^{-4}
Mg^{2+}	mol/kg	5.19×10^{-5}	8.51×10^{-5}	2.54×10^{-7}
Na^+	mol/kg	7.49×10^{-3}	7.31×10^{-3}	4.27×10^{-3}
SO_4^{2-}	mol/kg	3.94×10^{-4}	3.55×10^{-4}	1.18×10^{-4}
SiO_2(aq)	mol/kg	2.43×10^{-3}	1.79×10^{-3}	4.15×10^{-3}
NO_3^-	mol/kg	6.58×10^{-5}	3.97×10^{-5}	3.10×10^{-4}
NH_3(aq)	mol/kg	1.00×10^{-12}	1.00×10^{-12}	1.00×10^{-12}
Al^{3+}	mol/kg	3.73×10^{-9}	1.50×10^{-9}	6.09×10^{-8}

Source: DTN: MO0303MWDSCMAB.000; 10006: CS2000/16.5thc_w4_r.xls, 20013: CS1000/7.3 thc6_w5_r.xls, and 51: SD-9/990.4 thc6_w6_r.xls are pointers from the DTN in *Engineered Barrier System: Physical and Chemical Environment Model* (BSC 2004b).

Table B-3. Input Water Compositions for In-Package Chemistry

Parameter	Units	Calcium–Pore Water ECRB-SYS-CS1000/7.3-7.7/UC	Sodium–Pore Water ECRB-SYS-CS2000/16.3-16.5/UC	J-13 Well Water
Ca	mol/kg	2.35×10^{-3}	2.02×10^{-3}	3.24×10^{-4}
Mg	mol/kg	7.45×10^{-4}	1.36×10^{-4}	8.27×10^{-5}
Na	mol/kg	1.70×10^{-3}	5.22×10^{-3}	1.99×10^{-3}
K	mol/kg	1.94×10^{-4}	1.56×10^{-4}	1.29×10^{-4}
Si	mol/kg	6.99×10^{-4}	6.99×10^{-4}	1.02×10^{-3}
N	mol/kg	4.19×10^{-5}	6.61×10^{-6}	1.42×10^{-4}
C	mol/kg	6.76×10^{-3}	8.62×10^{-3}	2.49×10^{-3}
Cl	mol/kg	5.92×10^{-4}	6.77×10^{-4}	2.01×10^{-4}
F	mol/kg	1.79×10^{-4}	3.16×10^{-4}	1.15×10^{-4}
S	mol/kg	3.75×10^{-4}	3.23×10^{-4}	1.95×10^{-4}
pH	pH	7.6	7.4	7

Source: BSC 2004a, Table 2.

The steady-state chemistries of incoming fluids after reaction with waste form components are anchored near neutral. Figures B-1 and B-2 show the sensitivity of pH and ionic strength to different incoming water compositions for a commercial SNF waste package and a codisposal waste package, respectively. The simulation results are in close agreement even though the initial fluid compositions were different, which implies that incoming water composition has little influence over the in-package pH and ionic strength.

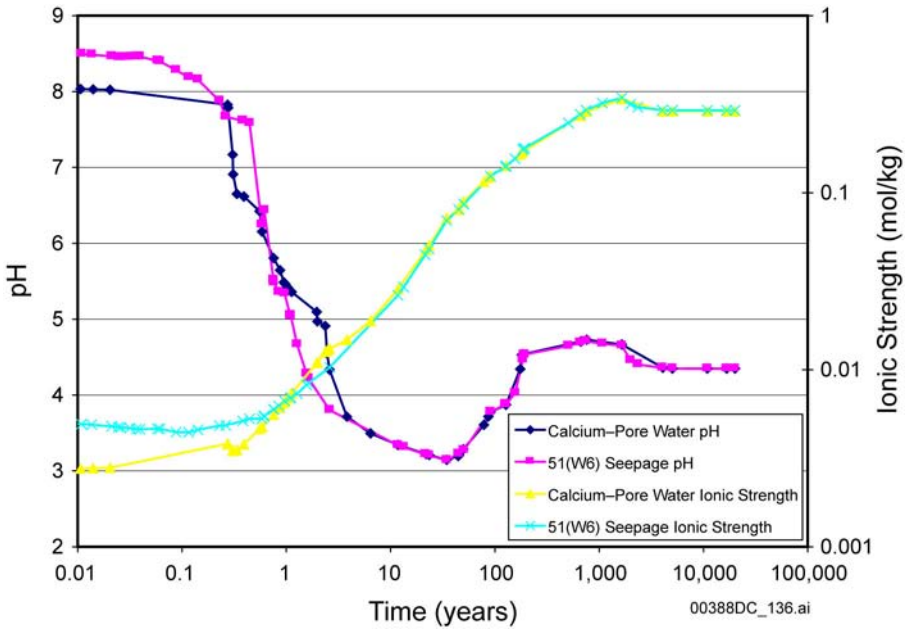

Source: BSC 2004a, Figure 14.

Figure B-1. Comparison of Thermally Perturbed Composition 51 (W6) with Calcium–Pore Water (W5) for a Commercial Spent Nuclear Fuel Waste Package

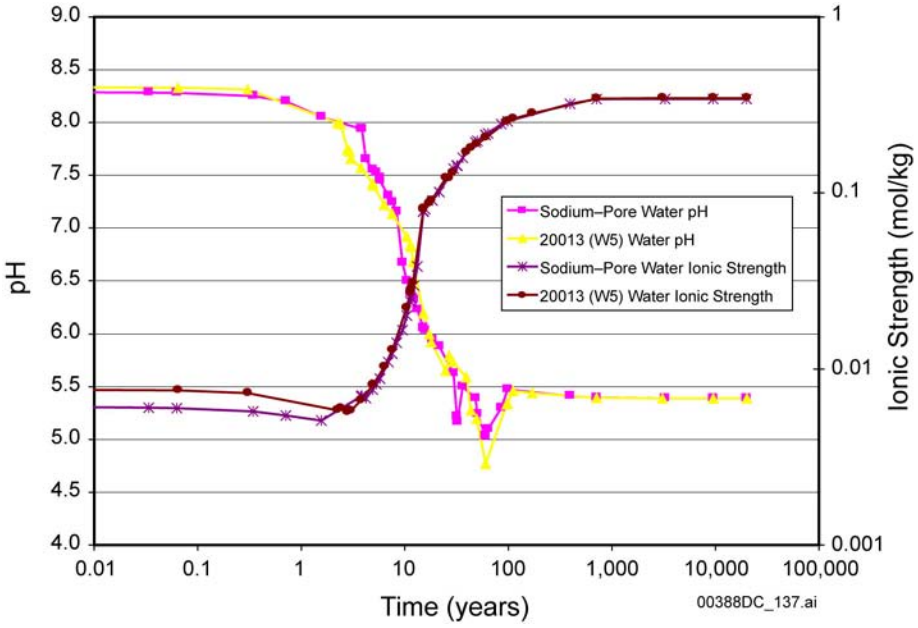

Source: BSC 2004a, Figure 15.

Figure B-2 Comparison of Thermally Perturbed Composition 20013 (W5) with Sodium–Pore Water (W4) for a Codisposal Waste Package

Results indicated that pH and ionic strength vary little with input water chemistry (Sections 3.4 and 3.7 of this technical basis document) and that phases produced from in-package chemical interactions are similar and have similar quantities for all input water chemistries. The

comparison could have been made using J-13 water as the starting composition, rather than the sodium– or calcium–pore water, and the results would have been the same. In *In-Package Chemistry Abstraction* (BSC 2004a, Section 6), it was demonstrated that the in-package chemistry was virtually the same, irrespective of the starting water chemistry: J-13 water, sodium–pore water, and calcium–pore water all resulted in virtually the same in-package chemistry. Thus, comparing J-13 well water with the thermally perturbed water would have resulted in the same in-package chemistry.

B.5 REFERENCES

B.5.1 Documents Cited

Brocoum, S. 2001. "Transmittal of Analysis and Model Reports (AMR) and Other Items Addressing Key Technical Issue (KTI) Technical Exchanges." Letter from S. Brocoum (DOE) to C.W. Reamer (NRC), March 30, 2001, with enclosure. ACC: MOL.20010529.0119.

BSC (Bechtel SAIC Company) 2001. *In-Package Chemistry for Waste Forms.* ANL-EBS-MD-000056 REV 00. Las Vegas, Nevada: Bechtel SAIC Company. ACC: MOL.20010322.0490.

BSC 2002. *Gamma and Neutron Radiolysis in the 21-PWR Waste Package from Ten to One Million Years.* 000-00C-DSU0-00700-00-00A. Las Vegas, Nevada: Bechtel SAIC Company. ACC: MOL.20021004.0002.

BSC 2004a. *In-Package Chemistry Abstraction*. ANL-EBS-MD-000037 REV 03B. Las Vegas, Nevada: Bechtel SAIC Company. ACC: MOL.20040609.0094.

BSC 2004b. *Engineered Barrier System: Physical and Chemical Environment Model.* ANL-EBS-MD-000033 REV 02. Las Vegas, Nevada: Bechtel SAIC Company. ACC: DOC.20040212.0004.

Christensen, H. and Sunder, S. 2000. "Current State of Knowledge of Water Radiolysis Effects on Spent Nuclear Fuel Corrosion." *Nuclear Technology, 131*, (1), 102–123. La Grange Park, Illinois: American Nuclear Society. TIC: 254040.

CRWMS M&O (Civilian Radioactive Waste Management System Management and Operating Contractor) 2000. *Environment on the Surfaces of the Drip Shield and Waste Package Outer Barrier.* ANL-EBS-MD-000001 REV 00. Las Vegas, Nevada: CRWMS M&O. ACC: MOL.20000328.0590.

Reamer, C.W. 2001. "Container Life and Source Term Key Technical Issue Agreements." Letter from C.W. Reamer (NRC) to S.J. Brocoum (DOE/YMSCO), December 21, 2001, 0111021102, with enclosure. ACC: MOL.20020402.0608.

Schlueter, J. 2000. U.S. Nuclear Regulatory Commission/U.S. Department of Energy Technical Exchange and Management Meeting on Container Life and Source Term (September 12–13, 2000). Letter from J. Schlueter (NRC) to S. Brocoum (DOE/YMSCO), October 4, 2000, with enclosure. ACC: MOL.20010731.0161.

Schlueter, J. 2002. U.S. Nuclear Regulatory Commission/U.S. Department of Energy Technical Exchange and Management Meeting on Container Life and Source Term (September 12–13, 2000). Letter from J. Schlueter (NRC) to J. Ziegler (DOE/YMSCO), July 2, 2002, with enclosure. ACC: MOL.20020819.0277.

Ziegler, J.D. 2002. Transmittal of Information Addressing Key Technical Issue (KTI) Container Life and Source Term (CLST) Agreements 4.02, 4.03, 4.04, and 4.05. Letter from J.D. Ziegler (DOE) to J.R. Schlueter (NRC), June 21, 2002. ACC: MOL.20020815.0586.

B.5.2 Data, Listed by Data Tracking Number

MO0303MWDSCMAB.000. THC Seepage Chemistry Model Abstraction Binning EQ3 Input, Pickup and Output Files. Submittal date: 03/06/2003.

APPENDIX C

DEMONSTRATION OF THE ADEQUACY OF THE IN-PACKAGE CHEMISTRY MODEL RESULTS (RESPONSE TO ENFE 3.04 AND CLST 3.05)

Note Regarding the Status of Supporting Technical Information

This document was prepared using the most current information available at the time of its development. This Technical Basis Document and its appendices providing Key Technical Issue Agreement responses that were prepared using preliminary or draft information reflect the status of the Yucca Mountain Project's scientific and design bases at the time of submittal. In some cases this involved the use of draft Analysis and Model Reports (AMRs) and other draft references whose contents may change with time. Information that evolves through subsequent revisions of the AMRs and other references will be reflected in the License Application (LA) as the approved analyses of record at the time of LA submittal. Consequently, the Project will not routinely update either this Technical Basis Document or its Key Technical Issue Agreement appendices to reflect changes in the supporting references prior to submittal of the LA.

APPENDIX C

DEMONSTRATION OF THE ADEQUACY OF THE IN-PACKAGE CHEMISTRY MODEL RESULTS (RESPONSE TO ENFE 3.04 AND CLST 3.05)

This appendix provides a response to Key Technical Issue (KTI) agreements Container Life and Source Term (CLST) 3.05 and Evolution of the Near Field Environment (ENFE) 3.04. These agreements relate to demonstrating the adequacy of the in-package chemistry model.

C.1 KEY TECHNICAL ISSUE AGREEMENTS

C.1.1 ENFE 3.04 and CLST 3.05

Agreement CLST 3.05 was reached during the U.S. Nuclear Regulatory Commission (NRC)/U.S. Department of Energy (DOE) Technical Exchange and Management Meeting on Container Life and Source Term held September 12 to 13, 2000, in Las Vegas, Nevada (Schlueter 2000). Subissues 1, 2, 3, 4, and 6 were discussed at that meeting.

Agreement ENFE 3.04 was reached during the NRC/DOE Technical Exchange and Management Meeting on Evolution of the Near Field Environment held January 9 and 12, 2001, in Pleasanton, California (Reamer 2001). ENFE KTI subissues 1, 2, 3, and 4 were discussed at that meeting. There have been no specific submittals to the NRC or meetings subsequent to the original technical exchange on this subject.

Wording of the agreements is as follows:

ENFE 3.04

> Complete validation of in-package chemistry models. Agreement #5 for CLST Subissue 3 addresses testing plans. Model validation based on this testing and further analysis will be documented in an update to the Summary of In-Package Chemistry for Waste Forms AMR (ANL-EBS-MD-000050), expected to be available in FY 02.

CLST 3.05

> Provide the plan for experiments demonstrating in-package chemistry, and take into account subsequent NRC comments, if any. DOE stated that the current planning provides for the analysis of additional in-package chemistry model support. This analysis will determine which parts of the model are amenable to additional support by testing, and which parts are more amenable to sensitivity analysis, or use of analogs. Based on these results, longer range testing will be considered. If testing is determined to be appropriate, test plans will be written in FY01 and made available to the NRC.

C.1.2 Related Key Technical Issue Agreements

Per the DOE request to the NRC (Ziegler 2002), KTI agreement CLST 4.05 was subsumed into CLST 3.05 (Schlueter 2002) because the wording and response for agreement CLST 4.05 was the same as agreement CLST 3.05.

This agreement is related to agreements Evolution of the Near Field Environment (ENFE) 3.03, ENFE 3.04, and CLST 3.02 in that they address the in-package chemistry modeling.

C.2 RELEVANCE TO REPOSITORY PERFORMANCE

In-package chemistry will have a significant impact on the degradation of the waste form, which in turn impacts the rate at which radionuclides can be mobilized. Mobilized radionuclides will form the source term for transport of radionuclides through the engineered barrier system and release to the unsaturated zone. Therefore, understanding the in-package chemistry is important to repository performance.

The primary outputs of the calculations are pH and ionic strength; other outputs are fluoride, chloride, total carbonate concentration, and Eh.

C.3 RESPONSE

The information in this report is responsive to agreements CLST 3.05 and ENFE 3.04 made between the DOE and NRC. The report contains the information that DOE considers necessary for NRC review for closure of these agreements.

C.3.1 ENFE 3.04

The revised in-package chemistry abstraction has been validated (BSC 2004, Section 7). Validation of the in-package chemistry model was accomplished with a combination of an independent technical review (surface complexation model) and comparison of the model response with analog data presented in peer-reviewed literature (physical chemistry model). Validation of the in-package physical chemistry model requires it predict the general features of corrosion product assemblages observed in corrosion of metals. It also requires that the broad ranges of pH and ionic strength it predicts be consistent with pH values and ionic strengths observed in analog natural systems where the same, or similar, mechanisms prevail. The critical features of the in-package physical chemistry model are production of large amounts of metal (hydr)oxide corrosion products**,** alkaline waters (pH greater than 8) by interaction of dilute solutions with waste form glass components, acidic (pH greater than 3) waters by interaction of incoming solutions with waste form metallic components (primarily Carbon Steel Type A516 and Stainless Steel Type 304) and high-ionic-strength solutions (greater than 1 mol/L) by reaction with waste form components over long periods of time. Corrosion products are similar to those seen when steels are corroded under oxidizing conditions. Ionic strength and pH values have been validated by comparing them with analog chemistries of natural waters, in which pH values rarely exceed 8.5 and range below 5 only for very specific reasons (e.g., the presence of high concentrations of reduced sulfur or organic acids) that will not be present at Yucca Mountain. The surface complexation in-package chemistry model was validated by an independent technical reviewer. The model validation provides confidence that the results of

both the physical chemistry and surface complexation in-package chemistry models provide outputs that are representative of potential water–waste package chemistries that potentially could occur at Yucca Mountain.

C.3.2 CLST 3.05

Developing an adequate understanding of in-package chemistry was accomplished through a nexus of data analyses, model runs, and model validation. These efforts provide confidence that the in-package chemistry model will be representative of the range of chemical conditions likely to occur in the water that contacts the internals of the waste package. Development of a robust in-package chemistry model was accomplished by consideration of an expanded input set, which included both environmental and system parameters. Confidence in the model output was bolstered by comparison to natural analogs. As a result of incorporating parameter uncertainty (for these system, environmental, and material parameters most sensitive to the in-package chemistry evolution) and reasonably constraining the model using natural analogs, additional testing to address specific water–in-package material interactions is not necessary.

C.4 BASIS FOR THE RESPONSE

C.4.1 ENFE 3.04

Movement of liquid or vapor phase water through cracks or other openings in the waste package is anticipated to trigger a series of coupled, nonlinear chemical processes dominated by degradation of fuel and steel components inside the waste package. The interacting processes are collectively termed waste package source term processes and must be effectively predicted because they largely control the in-package pH, ionic strength, carbonate concentration, Eh, fluoride concentration, and chloride concentration. In turn, these parameters are used in other models either directly, in the case of pH, carbonate concentration, and ionic strength, or indirectly, as is the case of Eh, fluoride, and chloride. Table C-1 lists the models and the in-package parameters where direct inputs are used to calculate a numerical value and indirect inputs are qualitatively used to determine if the model is applicable.

Table C-1. In-Package Chemistry Feed Parameters to Waste Form Submodels

Waste Form Submodel I	Direct Input	Indirect Input
Solubility	pH	Ionic strength, Eh, fluoride
Commercial Spent Nuclear Fuel Degradation Rate	pH, carbonate concentration	
High-Level Radioactive Waste Glass Degradation Rate	pH	
Colloid Concentration	Ionic strength	pH
Cladding		pH, chloride

The pH is the most important output parameter from the in-package chemistry abstraction because it has the greatest influence in determining rates of radionuclide release from waste packages. Thus, confidence that the in-package chemistry model represents the in-package environment translates to confidence that the model output pH covers the potential pH range of the actual in-package pH. Confidence that the model output pH range is representative is gained

via extensive model-exercised sensitivity analyses and model validation exercises, including comparisons to natural analogs.

The other output parameters used as direct input to waste form submodels include the total carbonate concentration and ionic strength. The carbonate concentration is calculated directly from thermodynamic relationships using the pH, temperature, and partial pressure of carbon dioxide as inputs. Thus, if the pH is calculated correctly, then the total carbonate concentration is calculated correctly as well. Note that temperature and partial pressure of carbon dioxide are input feeds to the in-package chemistry model. The ionic strength is used to determine if colloids are stable as a suspension in solution. If the ionic strength exceeds a threshold value, then the colloids are no longer stable and do not remain in solution, however, if below the threshold the ionic strength is used to calculate the colloid concentration.

The critical features of the in-package chemistry model are production of: (1) alkaline waters (pH between 8 and 10) by interaction of dilute solutions with waste form glass components; (2) acidic (pH greater than 3) waters by interaction of incoming solutions with waste form metallic components (primarily Carbon Steel Type A516 steel and Stainless Steel Type 304); (3) high-ionic-strength solutions (greater than 1 mol/L) by prolonged reaction with waste form components; and (4) buffering of low-pH fluids to moderate pH by interaction with corrosion products (surface complexation reactions with iron oxyhydroxides).

Validation of the in-package physical chemistry model is accomplished by showing that the broad ranges of pH and ionic strength it predicts are consistent with the pH levels and ionic strengths observed in natural systems where the same, or similar, mechanisms prevail (BSC 2004).

The in-package chemistry model consists of three input elements:

1. **System Properties**–Water distribution and mode of occurrence inside of the waste package

2. **Environmental Properties**–Temperature, gas partial pressures, water flux rates

3. **Material Properties**–Compositions, degradation and corrosion rates, masses and surfaces areas.

The combination of properties from these three input elements constitutes the conceptual model of the in-package chemistry model. Variability of the properties within each of the input elements provides the basis for the range of model response. Thus, if the range of values used from each input element is representative of the actual system, then the model output will capture the system behavior. Investigation of the sensitivity of variability of the system properties and environmental and material properties is incorporated in *In-Package Chemistry Abstraction* (BSC 2004, Sections 6.6 and 6.7).

The system properties describe the distribution and mode of occurrence of water within a waste package. The waste package is modeled as unsaturated; that is, not all of the void space is occupied with liquid water, some of it is occupied with gas. Water may enter the waste package either as a vapor phase, which presumably condenses and forms a layer of liquid water on the

waste package components surfaces, or as seepage, which drips onto the failed waste package and streams through the waste package. In the no-drip model, each waste package component was examined individually as a single reactant to determine each component's contribution to chemistry, and ensembles of the various waste package components were examined to determine chemical effects of the reactant combinations. In the seepage dripping model, the waste package components are considered together, and the resulting chemistry is that of a well-mixed single-cell flow-through batch reactor. Due to the geometric complexity of the waste package interior, the large degree of uncertainty in explicitly modeling a single pathway in the myriad of water flow pathways inside of a failed waste package, and the influence of surface complexation and mineral equilibria reactions on system pH, it was determined that the most robust model was the model that included all of the waste package components because it was the simplest model that retained all of the chemical trends observed in the single component and ensemble model results.

The environmental properties are those parameters that define the in-drift and in-package environment. The temperature range, partial pressure of carbon dioxide, the water flux values, and initial water composition used in the model are all sufficiently broad to include a wide range of eventual in-drift and in-package environments. The temperature range was varied from 25°C to 90°C (BSC 2004, Section 6.7.5) to determine its influence on pH and ionic strength. The partial pressure of carbon dioxide was varied between 10^{-5} to $10^{-1.5}$ bars (BSC 2004, Section 6.7.3) to determine if the pH varied with changes in CO_2 partial pressure. The total carbonate abstraction is cast in terms of pH, temperature, and CO_2 partial pressure. The water flux rate was varied from 0.15 to 1,000 L/yr (BSC 2004, Section 6.7.4) to determine the rate at which the incoming seepage composition was affected by the reactions with the waste package. Note that increasing the water flux rate has the same influence on the model results as decreasing the corrosion rates of the alloys; the contact time of the water and metal alloy determine the degree of reaction that is possible.

The material properties include the alloy and waste form compositions, the seepage water compositions, the alloy and waste form corrosion or degradation rates, and the waste package geometric information, which is used to calculate the masses and surface areas of the reactants. The composition of the alloys is well-defined handbook information (BSC 2004, Section 4.1.3). In the case of Carbon Steel Type A516, the sulfur content, which was identified as the primary contributor to the low pH trends observed in the model output, was varied to determine the magnitude of its influence on the model response (BSC 2004, Section 6.7.3). The geometry of the commercial SNF and codisposal waste packages used in the model report (BSC 2004, Section 4.1.3) was based on design information. Additional analyses were performed to determine the influence on the model results of replacing the Carbon Steel Type A516 in the commercial SNF waste package with Stainless Steel Type 316 (BSC 2004, Section 6.7.6) as may be the case for a naval waste package. The impact of seepage water composition on in-package chemistry was explored and shown to have only a minor influence on the in-package chemistry (BSC 2004, Sections 6.6.1.2, 6.6.2.2, and 6.7.1).

Aqueous corrosion of metals in industrial settings under oxidizing conditions tends to result in the accumulation of iron(III)-containing corrosion products (Stumm and Morgan 1996, pp. 720 to 724, 799 to 800; Snoeyink and Jenkins 1980, pp. 363, 379 to 380), such as predicted by the in-package chemistry model (BSC 2004, Sections 6.6.1.2 and 6.6.2.2). Oxidation of aluminum metal likewise results in the formation of a passivating aluminum oxide surface layer (Snoeyink

and Jenkins 1980, pp. 363, 375) similar to that predicted in the in-package chemistry model (BSC 2004, Sections 6.6.1.2 and 6.6.2.2). Therefore, the ability of the in-package chemistry model to accurately predict mineral assemblages that resulted from similar reactants lends confidence that the model is robust.

Alkaline pH values are routinely observed when glass degrades under laboratory conditions or in the field (Berner and Berner 1996), although pH values above 10 are rarely seen in natural waters (Langmuir 1997, p. 410). When they do occur, it is generally because the waters have interacted with a base-containing silicate (e.g., ultramafic mineral assemblages) not in contact with atmospheric CO_2 (Hem 1985, p. 64). This scenario is unlike the situation expected to prevail at Yucca Mountain, where atmospheric carbon dioxide is expected. Moreover, pH excursions above approximately 10 in fluid-mineral systems are also limited by precipitation of metal-carbonate minerals, deprotonation of aqueous species (e.g., silica, $Al(OH)_3(aq)$), proton loss from mineral surface groups, and, most importantly, by schoepite dissolution. The results in *In-Package Chemistry Abstraction* (BSC 2004, Section 6.8.2) indicate that the maximum pH inside codisposal N Reactor waste packages will not exceed 7, independent of temperature and CO_2 fugacity due to a variety of buffering reactions (e.g., schoepite dissolution). At water flux rates greater than 150 L/yr, waste package pH may equal 8 or the input pH.

A number of predicted reactions prevent any pH excursions to values below approximately 4.5, the most important being protonation of iron corrosion products via surface complexation. These are discussed in detail in the in-package chemistry model (BSC 2004, Section 6.8). Natural waters having pH values below 4.5 generally occur because of the presence of abundant organic acids or the oxidation of metal sulfide groups (Langmuir 1997, p. 162), both in the absence of effective pH-buffering reactions. Organic acids are not expected at Yucca Mountain, and sulfide levels are too low to result in acidic pHs (BSC 2004, Section 6.8). In other words, because conditions that favor pH lower than 4.5 (low acid-buffering capacity and high sulfur or organic acids or both) are absent in the in-package chemistry model, the lower limit of pH (approximately 4.5) estimated by the in-package chemistry model is consistent with natural observations.

The in-package surface chemistry model is an analytic derivation of pH and considers the major physical-chemical reactions and their effects on pH and how these interactions with iron corrosion products will ultimately influence the effluent pH. This analytical model and its results are supported by surface complexation calculations (BSC 2004, Section 6.9) that demonstrate the validity of the analytical model. The physical chemistry of the system and the surface chemistry are intricately linked and ideally would be combined in a fully coupled in-package chemistry model. However, it was not possible to construct such a model due to the necessity of maintaining continuity with the reaction-path geochemical modeling approach, which does not couple surface complexation reactions with the physical chemistry of the system. The software used in modeling the in-package physical chemistry, EQ3/6 v7.2b (Wolery and Daveler 1992), is a reaction-path code which simulates the interaction of water with a set of reactants under various user-specified conditions. At this time, EQ3/6 v7.2b does not have the facility to simulate the coupled process of the degradation of the reactant metal alloys and the simultaneous precipitation of corrosion products and the influence surface complexation reactions of the bulk fluid with the corrosion products. Software, such as PHREEQC, version 2.3 (BSC 2002), which is similar to EQ3/6 and does have the facility to model surface

complexation reactions and was used to confirm the results of the analytic surface complexation model (BSC 2004, Section 6.9). However, PRHEEQC was not used in a fully coupled mode because of its limited capability to perform reaction tracing, an operation at which EQ6 excels.

Surface complexation describes the electrostatic interactions of charged ions in solution with high surface area charged mineral surfaces, such as clays and iron (hydr)oxide corrosion products. The immobile charged surfaces of the mineral phases act to retain ions in solution so that the bulk solution properties, such as pH, are altered. In the waste package environment where the predominant alteration phases are iron corrosion products, which by their nature carry an electrical charge and have extremely high surfaces areas (BSC 2004, Table 12), the influence of the corrosion products on the solution chemistry is potentially important. The effect of surface complexation on the in-package pH was estimated analytically in the in-package chemistry model report (BSC 2004) because it was not possible to model the effects directly using the reaction-path software.

In a multireactant system, such as the waste package interior, the evolution of the chemistry is most influenced by reactants that react rapidly, contain elements that have the potential to perturb the ambient chemical conditions, and are present in large enough quantities to exert a chemical change on the system. For these reasons, Carbon Steel Type A516 is considered to be of primary importance because of its high corrosion rate (BSC 2004, Table 9) relative to the other reactants, the presence of reduced sulfur in its composition which lowers system pH when oxidized, and its abundance in the waste package. During the period of rapid corrosion of Carbon Steel Type A516, a large quantity of ferric (hydr)oxides will accumulate in the waste packages in about 200 years, and the oxidation of sulfur will tend to lower the system pH. Occurring simultaneously with Carbon Steel Type A516 corrosion are corrosion and degradation of the other waste package metal alloys and SNF, although at much slower rates than the Carbon Steel Type A516. While the system chemistry would be dominated by Carbon Steel Type A516 corrosion, the complexity of the system chemistry would be increased by the corrosion/degradation of the other waste package components. The steel alloys would form ferric (hydr)oxides and other metal corrosion products (e.g., pyrolusite), the aluminum alloys would form gibbsite and clay minerals, and, while the SNF would form primarily schoepite, the high-level radioactive waste glass would form clays, nearly all of the degradation products of the non-Carbon Steel Type A516 waste package components are phases with surface complexation properties. Considering only the reaction of Carbon Steel Type A516 would tend to underestimate the number of surface sites available for the surface complexation reactions, as well as the nature of the sites (e.g., site density). In an actual degrading waste package, the potential for surface complexation and pH buffering would be greater than in the simplified system, which only considers Carbon Steel Type A516 corrosion products.

It is during the 0- to 600-year postclosure period that the analytic surface complexation model was used to predict the in-package pH. The reasons for limiting the application of the surface complexation model to this period are (1) increasing uncertainty in the ferric (hydr)oxide mineral assemblage as a function of time and (2) this relatively brief period of low pH, as predicted by the EQ6 physical chemistry model, would be most influenced by the presence of surface complexation reactions. By not overapplying the surface complexation model, its output underestimates the magnitude of the potential surface complexation reactions that could take place in a degrading waste package. For commercial SNF, the pH was calculated as a

distribution that was a function of the partial pressure of carbon dioxide. Surface complexation tends to mediate pH to a range between approximately pH 4.5 to 8.

The results presented in *In-Package Chemistry Abstraction* (BSC 2004, Sections 6.6, 6.7 and 6.8) illustrate that variations in the model properties influence the pH time trajectories for the physical chemistry of the system. The surface complexation model tends to buffer low pH values, while mineral equilibria tends to limit alkaline pH values limiting the range between approximately 4.5 and 8. The ionic strength uncertainty terms, which were derived based on the results of the sensitivity analyses, and water flux rate functionality of ionic strength abstractions provide confidence that the ionic strength calculated by the model is representative the of the system. Model validation exercises, coupled with extensive sensitivity analyses, provide a high level of confidence that the system pH and ionic strength will fall within the model output ranges for these parameters.

C.4.2 CLST 3.05

Confidence that the model output brackets the range of chemistries from a degrading waste package was gained by prudent choice of model inputs combined with a large array of sensitivity analyses. The three input elements identified in Section C.4.1 and the properties within each comprise the in-package chemistry model.

The system element comprises the mode of occurrence and distribution of water within the waste package. For both the commercial SNF and the codisposal waste packages, the range in output physical chemistry was simulated for water vapor condensing and accumulating in the waste package and seepage dripping and flowing through the waste package. The effect on the chemistry of individual and groups, or ensembles, of reactants was examined to gain understanding of the role of water distribution within the waste package. The results of these analyses can be found in *In-Package Chemistry Abstraction* (BSC 2004, Sections 6.6.1 and 6.6.2).

The material element includes the waste package design information (used to calculate the masses and surface areas of each waste package component), the composition of the waste package components and spent nuclear fuel, the composition of the incoming seepage, the corrosion rates of the metal alloys, and the degradation rates of the commercial SNF and high-level radioactive waste glass. Variations in these inputs were examined for their influence on the model response. The results of these analyses can be found in *In-Package Chemistry Abstraction* (BSC 2004, Section 6.7).

The environmental element includes the temperature, the partial pressure of carbon dioxide, and rate of water flux through the waste package. These parameters were varied over a wide range of values to account for a large number of possible waste package environments. The results of these analyses can be found in *In-Package Chemistry Abstraction* (BSC 2004, Section 6.7).

Based on the results of the sensitivity analyses and the large number of eventual waste package conditions that the sensitivity analyses encompass, the need for future testing is unnecessary.

C.5 REFERENCES

Berner, E.K. and Berner, R.A. 1996. *Global Environment: Water, Air, and Geochemical Cycles*. Upper Saddle River, New Jersey: Prentice Hall. TIC: 253965.

BSC (Bechtel SAIC Company) 2002. *Software Code: PHREEQC.* V2.3. PC. 10068-2.3-01.

BSC 2004. *In-Package Chemistry Abstraction.* ANL-EBS-MD-000037 REV 03B. Las Vegas, Nevada: Bechtel SAIC Company. ACC: MOL.20040609.0094.

Hem, J.D. 1985. *Study and Interpretation of the Chemical Characteristics of Natural Water*. 3rd Edition. Geological Survey Water-Supply Paper 2254. Washington, D.C.: U.S. Government Printing Office. ACC: NNA.19940427.0181.

Langmuir, D. 1997. *Aqueous Environmental Geochemistry.* Upper Saddle River, New Jersey: Prentice Hall. TIC: 237107.

Reamer, C.W. 2001. "U.S. Nuclear Regulatory Commission/U.S. Department of Energy Technical Exchange and Management Meeting on Evolution of the Near-Field Environment (January 9–12, 2001)." Letter from C.W. Reamer (NRC) to S. Brocoum (DOE/YMSCO), January 26, 2001, with enclosure. ACC: MOL.20010810.0033.

Schlueter, J.D. 2000. "U.S. Nuclear Regulatory Commission/U.S. Department of Energy Technical Exchange and Management Meeting on Container Life and Source Term (September 12-13, 2000)." Letter from J. Schlueter (NRC) to S. Brocoum (DOE/YMSCO), October 4, 2000, with enclosure. ACC: MOL.20010731.0161.

Schlueter, J.D. 2002. "U.S. Nuclear Regulatory/U.S. Department of Energy Technical Exchange and Management Meeting on Container Life and Source Term (September 12-13, 2000)." Letter from J. Schlueter (NRC) to J. Ziegler (DOE/YMSCO), July 2, 2002, with enclosure. ACC: MOL.20020819.0277.

Snoeyink, V.L. and Jenkins, D. 1980. *Water Chemistry*. New York, New York: John Wiley & Sons. TIC: 256179.

Stumm, W. and Morgan, J.J. 1996. *Aquatic Chemistry, Chemical Equilibria and Rates in Natural Waters.* 3rd Edition. New York, New York: John Wiley & Sons. TIC: 246296.

Wolery, T.J. and Daveler, S.A. 1992. *EQ6, A Computer Program for Reaction Path Modeling of Aqueous Geochemical Systems: Theoretical Manual, User's Guide, and Related Documentation (Version 7.0).* UCRL-MA-110662 PT IV. Livermore, California: Lawrence Livermore National Laboratory. ACC: MOL.19980701.0459.

Ziegler, J.D. 2002. "Transmittal of Information Addressing Key Technical Issue (KTI) Container Life and Source Term (CLST) Agreements 4.02, 4.03, 4.04, AND 4.05." Letter from J.D. Ziegler (DOE/YMSCO) to J.R. Schlueter (NRC), June 21, 2002, OL&RC:TCG-1262. ACC: MOL.20020815.0586.

INTENTIONALLY LEFT BLANK

APPENDIX D

LOCALIZED CORROSION AND STRESS CORROSION CRACKING IN CLADDING (RESPONSE TO CLST 3.06 AIN-1, CLST 3.07, CLST 3.08 AIN-1, CLST 3.09 AIN-1, AND GEN 1.01 (COMMENT 124))

Note Regarding the Status of Supporting Technical Information

This document was prepared using the most current information available at the time of its development. This Technical Basis Document and its appendices providing Key Technical Issue Agreement responses that were prepared using preliminary or draft information reflect the status of the Yucca Mountain Project's scientific and design bases at the time of submittal. In some cases this involved the use of draft Analysis and Model Reports (AMRs) and other draft references whose contents may change with time. Information that evolves through subsequent revisions of the AMRs and other references will be reflected in the License Application (LA) as the approved analyses of record at the time of LA submittal. Consequently, the Project will not routinely update either this Technical Basis Document or its Key Technical Issue Agreement appendices to reflect changes in the supporting references prior to submittal of the LA.

APPENDIX D

LOCALIZED CORROSION AND STRESS CORROSION CRACKING IN CLADDING (RESPONSE TO CLST 3.06 AIN-1, CLST 3.07, CLST 3.08 AIN-1, CLST 3.09 AIN-1, AND GEN 1.01 (COMMENT 124))

This appendix provides a response to Key Technical Issue (KTI) agreements Container Life and Source Term (CLST) 3.06 Additional Information Needed (AIN)-1, CLST 3.07, CLST 3.08 AIN-1, CLST 3.09 AIN-1, and General Agreement (GEN) 1.01 (Comment 124). These agreements relate to localized corrosion and stress corrosion cracking in cladding.

D.1 KEY TECHNICAL ISSUE AGREEMENTS

D.1.1 CLST 3.06 AIN-1, CLST 3.07, CLST 3.08 AIN-1, CLST 3.09 AIN-1, and GEN 1.01 (Comment 124)

Agreements CLST 3.06, CLST 3.07, CLST 3.08, and CLST 3.09 were reached during the U.S. Nuclear Regulatory Commission (NRC)/U.S. Department of Energy (DOE) Technical Exchange and Management Meeting on CLST held September 12 to 13, 2000, in Las Vegas, Nevada (Schlueter 2000).

The NRC reviewed documents related to these CLST agreements, and, as a result, several AIN items were identified. With regard to CLST 3.06, the NRC reviewed *In-Package Chemistry for Waste Forms* (BSC 2001), *Clad Degradation–Summary and Abstraction* (CRWMS M&O 2001), and *Clad Degradation–Local Corrosion of Zirconium and Its Alloys Under Repository Conditions* (CRWMS M&O 2000a) and determined that these documents did not satisfy the agreement. The NRC asked for specific additional information to close the agreement, resulting in CLST 3.06 AIN-1 (Reamer 2001).

With regard to CLST 3.08, the NRC reviewed the following documents: *Initial Cladding Condition* (CRWMS M&O 2000b), *Thermal History of Cladding in a 21 PWR SNF WP Loaded with Average Fuel* (CRWMS M&O 2000c), *Abstraction of NFE Drift Thermodynamic Environment and Percolation Flux* (CRWMS M&O 2000d), and *Multiscale Thermohydrologic Model* (CRWMS M&O 2000e). As a result of that review, the NRC requested additional information to close the agreement, resulting in CLST 3.08 AIN-1 (Reamer 2001).

With regard to CLST 3.09, the NRC reviewed *Clad Degradation–Summary and Abstraction* (CRWMS M&O 2001) and determined that the document did not satisfy the agreement. As a result, the NRC requested additional information to close the agreement, resulting in CLST 3.09 AIN-1 (Reamer 2001).

The wording of each agreement and AIN is as follows:

CLST 3.06

> Provide additional technical basis for the failure rate and how the rate is affected by localized corrosion. DOE stated that the technical basis for local corrosion conditions will be added to by additional discussion of local chemistry in the

Summary of In-package Chemistry for Waste Forms revision ANL-EBS-MD-000050 which will be available in January 2001. Current Clad Degradation Summary Abstraction Section 6.3, ANL-WIS-MD-000007 and Clad Degradation - Local Corrosion of Zirconium and its Alloys Under Repository Conditions, ANL-EBS-MD-000012 contain the overall technical basis.

CLST 3.06 AIN-1

1) Provide the technical basis to define the chemical composition of the in-package water and its evolution with time.

2) Provide the technical basis for excluding the effect of localized corrosion in the form of pitting promoted by chloride.

3) Provide clarification on whether or not DOE assumes that acidic conditions will be present inside the waste packages and the pH range expected if acidic conditions prevail.

4) Provide additional information on the environmental conditions, in terms of chemical composition, prevailing inside breached waste packages.

CLST 3.07

Provide data to address chloride induced localized corrosion and SCC under the environment predicted by in-package chemistry modeling. DOE stated that the technical basis for the models used for localized corrosion and SCC will be expanded in future revisions of the Clad Degradation Summary Abstraction AMR, ANL-WIS-MD-000007, available by LA.

CLST 3.08

Provide the documentation on the distribution for cladding temperature and stress used for hydride embrittlement. DOE stated that the stresses are documented in the Initial Cladding Conditions AMR, ANL-EBS-MD-000048. CAL-UDC-ME-000001 contains the waste package internal temperatures. Waste package surface temperatures were provided within the TSPA model (ANL-EBS-HS-000003, Rev 00, ICN 01 and ANL-EBS-MD-000049). The updated versions of these documents will be available in January 2001.

CLST 3.08 AIN-1

1) Provide additional information to justify that the temperature is not sufficiently high for dissolution of some of the precipitated hydrides.

2) Provide additional information regarding the accuracy and validity of the stress and temperature data.

CLST 3.09

> Provide a technical basis for critical stress that is relevant for the environment in which external SCC takes place. DOE stated that critical stress from SCC experiments under more aggressive conditions will be cited in the Revision of the Cladding Degradation Summary Abstraction AMR, ANL-WIS-MD-000007, which will be available in January 2001.

CLST 3.09 AIN-1

> Provide specific information on the critical stress required for the occurrence of stress corrosion cracking initiated from the external surface of the fuel cladding in the presence of the possible in-package environments.

The NRC/DOE Technical Exchange and Management Meeting on Range of Thermal Operating Temperatures was held September 18 to 19, 2001 (Reamer and Gil 2001). At that meeting, the NRC provided additional comments that relate to the CLST Key Technical Issues (KTIs) discussed in this appendix, including GEN 1.01 (Comment 124) (Reamer and Gil 2001). Agreement GEN 1.01 was reached. Wording of these agreements and of the DOE initial response to the general agreement comments is as follows:

GEN 1.01 (Comment 124)

> In p. 7-74, Ferric Chloride generation is very remote spatially. Provide the basis for the hypothesis.
>
> NRC Clarification: Correct page number is 7-64, Section 7.3.7.1:
>
> Although useful in ranking a range of alloys, these standard tests utilize aggressive environments (in particular, a ferric chloride solution) that are not directly relevant to expected waste package surface environments because the potential for ferric chloride generation is very remote.
>
> The NRC expressed a concern that DOE models might neglect the potential accelerating effect of ferric chloride on corrosion/degradation of waste package materials and fuel cladding materials. NRC requested clarification about DOE's intent to evaluate the potential role of ferric chloride in waste package and fuel cladding degradation.

DOE Initial Response to GEN 1.01 (Comment 124)

> Electrochemical corrosion testing is determining the effect that minor constituents will have on the waste package corrosion processes. This will include the effects of ferric ion in the aqueous test solutions. Activities will also determine the extent that minor constituents can concentrate in the aqueous solutions. This work is covered under existing KTI agreement CLST 1.1.

Per existing KTI agreement CLST 3.7, a ferric-chloride local clad corrosion model is being developed that will be documented in a future revision of the Clad Degradation Summary Abstraction AMR.

D.1.2 Related Key Technical Issue Agreements

There are no other KTI agreements directly related to agreements CLST 3.06, 3.07, 3.08, and 3.09.

D.2 RELEVANCE TO REPOSITORY PERFORMANCE

Intact cladding is a crucial impediment to corrosion of fuel and the export of radionuclides because radionuclides cannot be released from spent nuclear fuel (SNF) with intact cladding. Clad corrosion is, therefore, potentially an important factor that must be considered in calculations of repository performance. Local corrosion of cladding requires low pH values and high dissolved concentrations of metal halide complexes.

Stress corrosion cracking mechanisms can also contribute to cladding failure and accelerate radionuclide release.

For stress corrosion cracking to occur, a cladding manufacturing defect, corrosion pit, or other small cladding crack must exist, and stresses and stress intensity factors must be large enough to promote stress corrosion cracking.

D.3 RESPONSE

The information in this report is responsive to agreements CLST 3.07 and GEN 1.01 (Comment 124) made between the DOE and NRC and responsive to AIN requests CLST 3.06 AIN-1, CLST 3.08 AIN-1, and CLST 3.09 AIN-1. The report contains the information that the DOE considers necessary for NRC review for closure of these agreements.

D.3.1 CLST 3.06 AIN-1

Item-1–The technical basis for the time-dependent chemical composition of the in-package water is documented in *In-Package Chemistry Abstraction* (BSC 2004a) for water interactions in commercial SNF waste packages (BSC 2004a, Section 6.6.1) and codisposal (N Reactor SNF and high-level radioactive waste glass) waste packages (BSC 2004a, Section 6.6.2). A summary of in-package chemistry evolution is presented in Section 3.4. The in-package chemistry model simulates chemical interactions of water with the waste package materials and the waste form. The results from the in-package chemistry model include time concentration histories of the elements and their aqueous complexes constituting the waste package, waste form, seepage, and gas composition. Results also include time histories of pH, Eh, ionic strength, and mineralogical phase abundance. The in-package chemistry model abstraction simplifies these results for use in the TSPA-LA.

Item 2–Zirconium alloys are susceptible to pitting in a particularly aggressive combination of chloride (Cl^-) ions, ferric ions (Fe^{3+}), or hydrogen peroxide (H_2O_2). However, because pH levels below pH 4.5 and Fe^{3+} levels above 1 ppm are not predicted by the in-package chemistry model,

the acid conditions and high Fe^{3+} levels needed for localized corrosion cannot be achieved (dissolved Fe^{3+} will be limited by ferric hydroxide solubility, which is low at pH 3 and above). The mechanisms for pH control are described in Appendix A of this document and treated in quantitative detail in Section 3.

Item 3–In-package pH levels are not expected to drop below 4.5. Calculations pointing to the absence of low pH conditions are central to the conclusion that localized corrosion will not be an important factor inside a breached waste package. As discussed in Section 3.5.1 in this technical basis document, analyses in *In-Package Chemistry Abstraction* (BSC 2004a, Section 6.8) indicate that low pH will not occur.

Item 4–A summary of in-package chemistry (pH, Eh, ionic strength, fluoride concentration, chloride concentration, and total carbonate concentration) evolution is presented in Section 3.4. The technical basis for environmental conditions in the waste packages is found in *In-Package Chemistry Abstraction* (BSC 2004a, Sections 6 and 8).

D.3.2 CLST 3.07 and GEN 1.01 (Comment 124)

CLST 3.07–The technical basis for the response to this KTI agreement is based on the feature, event, and process (FEP) screening argument presented in *Clad Degradation–FEPs Screening Arguments* (BSC 2004b, Table 7-1, FEP 2.1.02.16.0A, Section 6.6). Stress corrosion cracking results from simultaneous action of a tensile stress and a corrosive environment and requires a certain chemical environment and sufficiently high stresses (stress intensity factors at the crack tip). Chloride-induced stress corrosion cracking could occur on the outside of the cladding but requires that the passive layer of oxides on the zirconium surface be unstable. These are the same conditions under which pitting occurs. As demonstrated in FEP 2.1.02.160A, the chemical conditions for pitting and for stress corrosion cracking do not exist in the waste package because the repassivation potential exceeds the corrosion potential. As a result, the passive layer of oxides on the zirconium surface is not unstable. The zirconium pitting model (BSC 2003) describes the conditions in which pitting is observed at high concentrations of chlorides at extremely low pH (below −0.6), which can lead to the general dissolution of the protective zirconium oxide film. Figure D-1 demonstrates the chemical conditions in which pitting would occur. No pitting is predicted to occur for any chemical conditions that were associated with Zircaloy cladding in the repository. Chemical conditions expected to prevail inside the waste package would represent a location in the extreme lower left corner of Figure D-1. Analyses in these references concluded that cladding failures caused by chloride-induced stress corrosion cracking are not anticipated and can be excluded from consideration in the TSPA-LA.

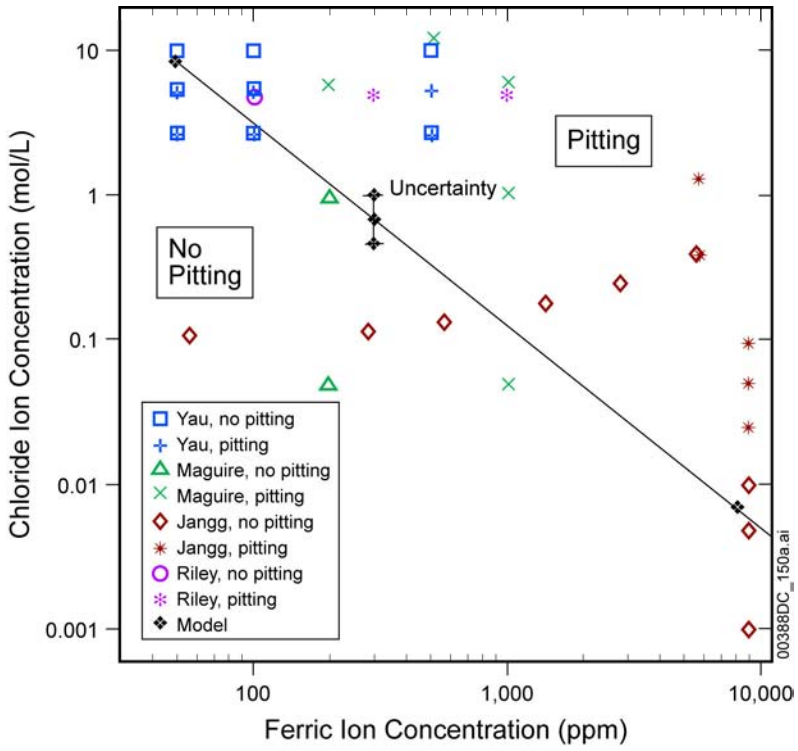

Source: BSC 2003, Figure 7-1.

NOTE: Data used for this graph are being updated; these updates, however, will not impact conclusions obtained herein.

Figure D-1. Experimental Measurements of Pitting and Pitting Model

GEN 1.01 (Comment 124)–The role of ferric chloride on waste package and fuel degradation has been evaluated and excluded from further consideration in the TSPA-LA model because of the low likelihood that the conditions for ferric chloride to impact corrosion exist in the in-package environment. A zirconium-pitting model (BSC 2003) was developed to investigate the chemical conditions at which pitting occurs. Zirconium alloys are susceptible to pitting in a particularly aggressive combination of chloride (Cl^-) ions, ferric ions (Fe^{3+}), or hydrogen peroxide (H_2O_2). The model predicts the conditions where pitting is observed. No pitting was predicted to occur in the predicted in-package environment. In a sensitivity study in which acid production from radiolysis was increased by a factor of 10, no pitting was predicted to occur. Results from the application of this model support the TSPA-LA treatment that when the in-package pH is above 3, the cladding will not fail from either pitting or general corrosion (BSC 2004b, Section 6.6). In a sensitivity study, the pH was artificially suppressed to 2.2, and yet pitting was still not predicted to occur.

D.3.3 CLST 3.08

Because of a close tie between temperature and stress, CLST 3.08 AIN-1 and CLST 3.08 AIN-2 will be addressed together.

Stresses and stress intensity factors are too low for crack propagation, and cladding failure by delayed hydride cracking is unlikely. Maximum temperatures are too low to dissolve much hydrogen, most rods have stresses too low for hydride reorientation, and cladding failure by hydride reorientation is unlikely. Lastly, hydrogen axial migration is limited at the 268°C maximum temperature expected during emplacement.

Clad Degradation–FEPs Screening Arguments (BSC 2004b, Section 6.12) presents the accuracy and validity of the cladding stress and temperature data that impact the defensibility of the screening arguments. The screening arguments are based on the maximum fuel rod temperature, which is estimated for the center rod and maximum fuel loading conditions to be approximately 268°C. Maximum stress intensity factors at 268°C are approximately 10% of the critical stress intensity factor threshold for crack propagation for moist chloride. At the 268°C maximum temperature, less than 5% of the fuel rods would be candidates for hydride reorientation. Those fuel rods that may be candidates for hydride reorientation also would require that high stress exist in order for hydride reorientation to occur. Less than 1% of the fuel rods would have stresses sufficiently high to result in some level of reorientation. At the 268°C maximum temperature, a temperature gradient between the hotter and cooler portions of a fuel rod of at least 50°C would be required for hydride axial migration to occur. Predicted temperature gradients are 19°C, which would be insufficient to result in axial migration.

D.3.4 CLST 3.09

The information requested supports the screening of FEP 2.1.02.21.0A, stress corrosion cracking of cladding. This FEP has been excluded from further consideration in the TSPA-LA because of low consequence in the in-package environment. In order for stress corrosion cracking to occur, conditions similar to those that would support pitting must be present at a cladding manufacturing defect, corrosion pit, or other small cladding crack, and stresses and stress intensity factors must be large enough to promote stress corrosion cracking. The chemical environment necessary to promote either pitting or stress corrosion cracking will not exist in the in-package environment. Even if such chemical conditions were to occur, the stresses and stress intensity factors are too low for stress corrosion cracking to occur, as discussed in Section D.4.4. Details on the technical basis for the critical stress state in which external stress corrosion cracking takes place are found in *Clad Degradation–FEPs Screening Arguments* (BSC 2004b, Table 7-1, FEP 2.1.02.16.0A, Section 6.6, and FEP 2.1.02.21.0A, Section 6.11).

The maximum pressure, stresses, and stress intensity factors occur either at the time of maximum temperature or at the end of the regulatory period of 10,000 years, depending on the gas release fraction for helium (BSC 2004b, Section 6.11). Conservatively using 100% helium gas release, maximum stress intensity factors (K_I) are in the range of approximately a mean value of 0.47 to a maximum of 2.7 MPa-m$^{0.5}$. This is less than the critical stress (K_{ISCC}) of 28 MPa-m$^{0.5}$ for moist chlorine at 70°C (or 24 MPa-m$^{0.5}$ at 100°C) measured by Cox (1990, Figure 20, p. 15), which is pertinent to the case of external cracking. Therefore, stress corrosion cracking is not expected.

D.4 BASIS FOR THE RESPONSE

D.4.1 CLST 3.06 AIN-1

D.4.1.1 CLST 3.06 AIN-1 Item 1

The temporal evolution of in-package chemistry is described in Section 3.4.

The technical basis of the in-package chemistry model is an assemblage of mass action and mass balance expressions that permit the anticipation of waste form steel and water interaction over time. Kinetic rate constants and dependencies capture the broad scale features of irreversible processes and an updated thermodynamic database reproduces the characteristics of reversible processes. The outputs of the model are reasonable when compared against the observed behavior of natural waters. The chemistry of fluids inside the waste package is controlled by the breakdown of waste package components. Changing the flow rate changes the output pH and ionic strength. Raising the flow rate causes pH and ionic strengths to be closer to that of the input fluid. Increasing the fuel exposure (i.e., decreasing clad coverage), also affects model outputs by raising fuel degradation, via the increase in the fuel surface area, leading to more moderate pH conditions due to buffering by schoepite formation.

Over the first 100 years when the degraded waste form consists primarily of A516 corrosion products and intact fuel, pH will be held to near-neutral by the surface properties of the corrosion products, which are the most abundant proton donor/acceptors in the package. Over longer time periods, when the degraded waste form will consist of schoepite, dissolving steels, and possibly high-level radioactive waste glass, the pH will be anchored near neutral by dissolution reactions of schoepite that consume protons at acidic pH values and release them at alkaline pH values. Lastly, the in-package chemistry calculations assume that reaction of steel components will proceed unhindered by corrosion product buildup until the steels are completely dissolved. It also assumes that corrosion product sites will themselves remain available for interaction with ambient solutions. In reality, corrosion product buildup will likely prevent access of water and oxygen to the fresh metal (as well as fuel and high-level radioactive waste glass) surfaces and hinder further reaction. Waste form degradation will then proceed in a stochastic fashion: corrosion products forming and stopping degradation, followed by sloughing off of protective layers and reinitiation of corrosion.

D.4.1.2 CLST 3.06 AIN-1 Item 2

The effect of localized corrosion in the form of pitting has been excluded from the TSPA-LA model because its inclusion in the TSPA-LA modeling would have a low consequence. The technical basis for excluding the effect of localized corrosion of the cladding in the form of pitting promoted by chloride is contained in *Clad Degradation–FEPs Screening Arguments* (BSC 2004b, Section 6.6). This conclusion is based on the results from a pitting model for zirconium-alloy cladding (BSC 2003) and assumes that the in-package pH will not fall below 4.5. This model predicts the chemical conditions that cause pitting of zirconium cladding used on commercial SNF. Zirconium alloys are susceptible to pitting in a particularly aggressive combination of chloride (Cl^-) ions, ferric ions (Fe^{3+}), or hydrogen peroxide (H_2O_2). In order to predict cladding failure from chloride pitting, a review of the literature for pitting rates and

electrochemical data for various zirconium alloys was conducted. Based on this review of the literature, failure criteria were constructed based on an electrochemical definition of pitting as the condition at which the corrosion potential exceeds repassivation potential (i.e., E_{corr} greater than E_{rp}).

Figure D-1 shows experimental measurements of pitting corrosion and the clad pitting model. No pitting is predicted to occur for any chemical conditions that were associated with Zircaloy cladding in the repository. Note that Fe^{3+} levels of 1 ppm (a level never exceeded in the in-package chemistry calculations) would require chloride levels exceeding 10 mol/L (equally unlikely even under conditions of high evaporation) for clad pitting to occur. In-package chemistry calculations point to maximal levels of Fe^{3+} to be 1 ppm; chloride levels never exceed 0.001 mol/L. In other words, the chemical conditions expected to prevail inside the package would represent a location in the extreme lower left corner of Figure D-1.

In sensitivity studies in which acid production from radiolysis increased by a factor of 10 or the pH was artificially suppressed to 2.2, the pitting model predicted a corrosion potential less than the repassivation potential, and, as a result, no pitting was predicted to occur. Even at the minimum pH predicted in the in-package chemistry model, no pitting is predicted to occur (BSC 2003, Section 6.6.). In-package chemistry predictions are compared with chemical conditions necessary for pitting as determined by the pitting model in Figure D-1. The chemistry conditions in which pitting has been observed and on which the pitting model is based, are illustrated in relation to the model and its uncertainty range in the screening argument for FEP 2.1.02.16.0A (BSC 2003, Section 6.6, Figure 6.6-2).

D.4.1.3 CLST 3.06 AIN-1 Item 3

Waste package pH is expected to remain between 4.5 and 8.1. The technical basis for this is discussed below, in *In-Package Chemistry Abstraction* (BSC 2004a, Section 6.8), and in Section 3.2. Dissolution of Carbon Steel Type A516 has the potential to lower pH due to the oxidation of elemental sulfur to sulfuric acid. Degradation of other alloys and fuels results in roughly neutral pH.

The A516 dissolution reaction is:

$$\begin{aligned} &Fe_{1.76}Mn_{0.019}C_{0.0233}Si_{0.0103}P_{0.00113}S_{0.00109} + mH_2O + pO_2 \\ &\rightarrow 0.00109SO_4^{2-} + 0.00113(H_3PO_4 + H_2PO_4^{-} + HPO_4^{2-}) + 0.0103H_4SiO_4 \\ &+ 0.0233(H_2CO_3 + HCO_3^{-}) + 0.019MnO_2 + (1.76 - X)FeOOH \\ &+ X(>Fe\text{-}O\text{-}H + >Fe\text{-}O\text{-}H_2^{+} + >Fe\text{-}O^{-} + >Fe\text{-}O\text{-}CO_3^{-}) + nH^{+} \end{aligned} \qquad \text{(Eq. D-1)}$$

where X is the amount of iron in FeOOH (moles) that is exposed to solution, m is moles of water, and p is partial pressure. Note that the uncharged species in Equation D-1 are not included in Equation D-2 because they do not contribute directly to the pH. However, as weak acids they do contribute to the overall buffer capacity of the solution.

Given an *X* value of 0.176 (10% of iron sites, a reasonable value for goethite (BSC 2004a)) for dissolution of 1 mol of Carbon Steel Type A516 into a near-neutral solution:

$$n = 2[SO_4^{2-}] + [H_2PO_4^-] + 2[HPO_4^{2-}] + [HCO_3^-] + [>Fe\text{-}O^-] + [>Fe\text{-}O\text{-}HCO_3^-] - [>Fe\text{-}O\text{-}H_2^+] \quad \text{(Eq. D-2)}$$

Similarly, charge balance for a solution in contact with carbon dioxide gas at 0.001 atm and into which 1 mol of A516 was dissolved would be

$$(H^+) + (>Fe\text{-}O\text{-}H_2^+) = 2[SO_4^{2-}] + [H_2PO_4^-] + 2[HPO_4^{2-}]$$

$$+ (OH^-) + (HCO_3^-) + (>Fe\text{-}O^-) + (>Fe\text{-}O\text{-}HCO_3^-) \quad \text{(Eq. D-3)}$$

The equation above can be solved for pH as a function of fixed partial pressure of CO_2, given the following surface complexation constants (Dzombak and Morel 1990) and other existing thermodynamic relations.

$$>Fe\text{-}OH_2^+ \leftrightarrow >Fe\text{-}O\text{-}H + H^+ \quad K_1 = [>Fe\text{-}O\text{-}H][H^+]/[>Fe\text{-}OH_2^+] = 10^{-7.29}$$

$$>Fe\text{-}OH \leftrightarrow >Fe\text{-}O^- + H^+ \quad K_2 = [>Fe\text{-}O^-][H^+]/[>Fe\text{-}OH] = 10^{-8.93}$$

$$>Fe\text{-}O\text{-}H + H^+ + CO_3^{2-} \leftrightarrow >Fe\text{-}HCO_3^- + H_2O$$

$$K_{CO3} = [>Fe\text{-}HCO_3^-]a_{H2O}/[>Fe\text{-}OH][H^+][\ CO_3^{2-}] = 10^{12.78} \quad \text{(Eq. D-4)}$$

where >Fe denotes sites exposed at the FeOOH–solution interface. Performing the algebraic calculation above allows the prediction of the pH values that will result from Carbon Steel Type A516 degradation as a function of carbon dioxide levels (Table D-1) during the period from 0 to 600 years when surface complexation is implemented. Consideration of the corrosion product surface chemistry suggests that the pH of fluids in contact with degrading Carbon Steel Type A516 will not be acidic but rather will be close to neutral. To summarize, the lack of acid-generating reactions in the waste package will prevent acidic conditions from prevailing.

Table D-1. Calculated pHs

log(*f*CO_2) (atm)	pH
−5.0	8.1
−4.5	8.1
−4.0	8.0
−3.5	7.9
−3.0	7.7
−2.5	7.5
−2.0	7.3
−1.5	7.0
−1.0	6.8

Source: BSC 2004a, Table 61.

D.4.1.4 CLST 3.06 AIN-1 Item 4

Three scenarios are modeled in TSPA-LA. In the nominal (no volcanoes or earthquakes) scenario, water drips or condenses into the waste form where it encounters a large amount of steel and some fuel (clad in the case of commercial SNF) or high-level radioactive waste glass. The water will be near neutral, oxidizing, and carrying ambient levels of carbon dioxide. Corrosion of low carbon steel in the first 3 to 5 decades will cause the formation of large quantities of ferric (hydr)oxide corrosion products. Water encountering fuel in commercial SNF packages will initiate dissolution of the fuel if the cladding has failed because of manufacturing defects or damage during fuel handling activities. In codisposal waste packages, DOE SNF will immediately begin to corrode, as will high-level radioactive waste glass. The resulting pH of fluids inside the waste form will be held close to neutral by a combination of corrosion product surface chemistry and a pH-buffering dissolution of uranium(VI)-hydroxides, stainless steels, and glass. Dissolved concentrations of neptunium, plutonium, americium, and uranium will be limited to the near-neutral pH solubilities of their respective oxides or other less soluble minerals. At early and late time periods, when ionic strengths are calculated to be large, colloids will tend to agglomerate inside the waste form. Late-term high ionic strengths occur due to the long-term accumulation of dissolved solids. In between, dilute conditions might allow the export of radionuclides attached to colloidal hosts. Waste form degradation in the seismic scenario will proceed as in the nominal case; however, some fraction of the clad will be destroyed as a result of the seismic activity, allowing more commercial SNF to be dissolved. Seismic scenario pH levels will be close to neutral and likely buffered by the presence of uranium and other metal hydroxide phases. In the third scenario, when a volcano sends basalt into the drift, dispersing the fuel into the basalt matrix, the chemistry of basalt–water seepage interaction will control the breakdown of fuel and the release of radionuclides. Igneous intrusion scenario pH levels will be somewhat above neutral and reflect the influence of base cation leaching from the basalt matrix.

D.4.2 CLST 3.07 and GEN 1.01 (Comment 124)

CLST 3.07–Stress corrosion cracking (Cox 1973, Abstract; Farina et al. 2002, p. 5; Yau and Webster 1987, p. 718) is the propagation of an existing crack on the surface of a metal because of the presence of a chemical in the crack tip. Stress corrosion cracking requires a certain chemical environment and sufficiently high stresses (stress intensity factors at the crack tip). Chloride-induced stress corrosion cracking could occur on the outside of the cladding, with the requirement that the passive layer of oxides on the zirconium surface be first chemically attacked. These are the same conditions under which pitting occurs. As demonstrated in *Pitting Model for Zirconium Alloyed Cladding at YMP* (BSC 2003, Section 8.2) and in the response to CLST 3.06 AIN-2, the chemical conditions for pitting and stress corrosion cracking do not exist in the Yucca Mountain environment. See *Clad Degradation–FEPs Screening Arguments* (BSC 2004b, Section 6.6) for the screening of the pitting corrosion FEP. Consequently, chloride-induced stress corrosion cracking is not expected in the waste package environment.

Even if the chemical environment for stress corrosion cracking existed, stresses and stress intensities are too low for stress corrosion cracking to occur. Stresses and stress intensity factors on the cladding are estimated in *Clad Degradation–FEPs Screening Arguments* (BSC 2004b, Section 6.11) at three times in the waste package: (1) at initial emplacement time, (2) at the time of maximum cladding temperature, and (3) at the regulatory period of 10,000 years. The

conditions at the time of maximum temperature (10 years from closure, 268°C (BSC 2004b, Table A-3)) are determined by using the ideal-gas law and the initial temperature conditions. The conditions at 10,000 years are also obtained by adjusting for helium production from alpha decay and assuming that all of the helium is released from the fuel matrix. The mean temperature at 10,000 years for average loading is estimated to be 61°C (the maximum temperature at 10,000 years for maximum loading is estimated to be 73°C, which is used in the pressure and stress calculations) (BSC 2004b, Table A-3). The mean pressure at 10,000 years, which includes helium production and released fission gas, is estimated to be 13 MPa. Stress intensity factors vary from a mean value of 0.47 to a maximum of 2.7 MPa-$m^{0.5}$, shown in Table D-2. This is compared to the threshold stress intensity factor for stress corrosion cracking, the value at which crack propagation will start but with a very slow propagation velocity. Threshold values from the open literature for various chemical solutions are shown in Table D-3. The lowest value from the open literature in Table D-3 is 4 MPa-$m^{0.5}$. The threshold stress intensity factor (K_{ISCC}) of 28 MPa-$m^{0.5}$ for moist chlorine is included in this table and is pertinent to the case of external cracking (Cox 1990, Figure 20, p. 15). Since the estimated stress intensities are less than each threshold value in Table D-3, chloride-induced cracking is not expected.

Table D-2. Temperature, Pressure, Stress, and Stress Intensity Factors for Three Different Times

Parameter		Ambient Temperature Properties	Properties at Peak Temperature	Properties at Peak Temperature, Regulatory Limit
Time	Time (years)	0	10	10,000
Temperature	Temperature (°C)	27	268	73
Pressure	Mean (MPa)	4.8	8.7	13
	95% (MPa)	7.3	13	16
	98% (MPa)	8.9	16	18
	Maximum (MPa)	18	32	28
Stress	Mean (MPa)	38	69	107
	95% (MPa)	62	111	137
	98% (MPa)	76	136	154
	Maximum (MPa)	146	263	233
Stress Intensity[a]	Mean (MPa-$m^{0.5}$)	0.26	0.47	0.73
	95% (MPa-$m^{0.5}$)	0.61	1.09	1.34
	98% (MPa-$m^{0.5}$)	0.77	1.38	1.56
	Maximum (MPa-$m^{0.5}$)	1.52	2.73	2.42

Source: BSC 2004b, Table 6.11-1.

NOTE: [a] For a sharp crack (Reed-Hill 1973, p. 800).

Table D-3. Threshold Stress Intensity Factors for Zirconium Alloys from the Open Literature

Reference	Solution	K_{ISCC}
Cox 1990, Figure 14, p. 12	3 mol/L Potassium Iodide (KI)	12 (100°C) to 22 (22°C) MPa-$m^{0.5}$
Cox 1990, Figure 15, p. 12	1 mol/L KBr + 0.25 mol/L Br_2	12 MPa-$m^{0.5}$ (22°C)
Cox 1990, Figure 20, p. 15	Chlorine (Moist)	28 MPa-$m^{0.5}$ (70°C)
Cox 1990, Figure 20, p. 15	Iodine + air	13 MPa-$m^{0.5}$ (22°C)
Cox 1990, Figure 20, p. 15	Nitrate/Iodide Melt	5 MPa-$m^{0.5}$
Cox 1990, Figure 7a, p. 7	Hydrogen Gas (6.7 to 86 kPa)	20 to 28 MPa-$m^{0.5}$ (Zirc4)
Cox 1990, Figure 7b, p. 7	Hydrogen Gas (1 to 100 kPa)	13 to 22 MPa-$m^{0.5}$ (Zirc2)
Tasooji et al. 1984, Figure 12, p. 612	Iodine, 0.001 kg/m^2	4.0 to 15 MPa-$m^{0.5}$ (Zirc2, value varies with texture, 300°C)

GEN 1.01 (Comment 124)–The potential role of ferric chloride in waste package and fuel cladding degradation is evaluated in *Clad Degradation–FEPs Screening Arguments* (BSC 2004b, Sections 6.5 and 6.6). Zirconium and its alloys resist localized corrosion, such as pitting, crevice corrosion, and stress corrosion cracking, in all but concentrated acidic metal halide solutions that are themselves not predicted to occur in the repository. Temperature has little effect on the process.

A zirconium-pitting model (BSC 2003) was developed to investigate the chemical conditions at which pitting occurs. Zirconium alloys are susceptible to pitting in a particularly aggressive combination of chloride (Cl^-) ions, ferric ions (Fe^{3+}), or hydrogen peroxide (H_2O_2). The model predicts the chemical conditions under which pitting is expected to occur. Details of the analysis are documented in *Clad Degradation–FEPs Screening Arguments* (BSC 2004b, Section 6.6). Figure D-1 shows the chemical conditions in which pitting would occur and the chemical regions predicted. No pitting was predicted to occur in the waste package environment because the appropriate chemical conditions do not exist there. In sensitivity studies where acid production from radiolysis was increased by a factor of 10 and the pH was artificially suppressed to 2.2, no pitting was predicted to occur.

Results from the application of this model support the TSPA-LA treatment that the cladding will not fail from either pitting or general corrosion in the Yucca Mountain environment. As predicted from the in-package chemistry analysis (BSC 2004a, Attachment III) and the pitting model (BSC 2003, Section 8.2), pitting is not expected to occur.

The pitting model was generated using data for as-polished samples, but commercial SNF is coated with thick oxides (54 μm mean, 5% to 95% μm range of 5.3 to 112 μm) (CRWMS M&O 2000b, Section 6.4). These oxides will affect the corrosion potential (open circuit potential) because of the high electrical resistance of the coating. Zirconium samples with oxides elevate the corrosion potential above the as-polished corrosion potential and repassivation potential, but no pitting corrosion was observed, even when exposed to 5 mol/L $FeCl_3$ (BSC 2004b, Section 6.6).

As further validation of the pitting model and its results, a review of the literature for pitting observations for various zirconium alloys was conducted and conditions under which pitting

occurs were documented (BSC 2004b, Section 6.6). A comparison of the chemistry and the regions where pitting is observed shows that cladding failure from pitting is unlikely. Concentrations of chlorides and ferric ions predicted in the in-package chemistry model are many orders of magnitude lower than those necessary for pitting; therefore, cladding failure from pitting is not expected.

D.4.3 CLST 3.08

Because of the close tie between temperature and stress, CLST 3.08 AIN-1 and CLST 3.08 AIN-2 will be addressed jointly.

The information below is taken from *Clad Degradation–FEPs Screening Arguments* (BSC 2004b, Section 6.1.2) and is addressed as FEP 2.1.02.22.0A, hydride cracking of cladding. Three subissues from the FEP screening argument rely on temperature and stress data: delayed hydride cracking (of cladding), hydride reorientation (of cladding), and hydride axial migration (of cladding). These subissues are relevant to this KTI agreement response and are discussed below.

The FEPs screening arguments for the three subissues above rely on estimates of the maximum fuel rod temperatures. The stresses and stress intensities are a function of temperature. Table D-4 gives the temperature history for the rod located in the waste package center location (hottest location). Both the mean (average) and the maximum rod temperatures are presented.

Table D-4. Time-Dependence of Temperatures for Center Rod, Average and Maximum Fuel Loading

Time (Years)	Temperature, Average Loading, Average Waste Package Temperature (°C)	Temperature, Maximum Fuel Loading, Maximum Waste Package Temperature (°C)
0	159	214
5	208	260
10	219	268
15	221	266
20	220	264
30	214	254
90	181	212
130	169	197
290	145	170
950	111	131
3,000	82	99
6,000	71	85
10,000	61	73

Source: BSC 2004b, Appendix A, Table A-3.

The pressure, stress, and stress intensity factors are presented in Table D-2 for three times. The stress intensity factor is a measure of the concentration of stress at the tip of existing cracks. The peak temperature occurs at 10 years after closure of the repository. Using 100% helium gas release, the mean, 95%, and 99% values of pressure are higher at 10,000 years than at 10 years; however, the maximum value is actually higher at 10 years. Table D-2 shows that the maximum stress intensity factors are about 2.7 MPa-$m^{0.5}$. As the table also shows, most rods have significantly lower stress intensities. These stress intensities are less than the critical stress intensity (K_{ISCC}) of 28 MPa-$m^{0.5}$ for moist chlorine measured by Cox (1990, Figure 20, p. 15). Therefore, cracking is not expected.

Details of how the temperature profiles are generated are given in *Clad Degradation–FEPs Screening Arguments* (BSC 2004b, Appendix A). Stress and stress intensity factors of Table D-2 are used in the screening arguments of the FEPs presented in *Clad Degradation–FEPs Screening Arguments* (BSC 2004b, Sections 6.11 and 6.12).

At the peak temperature of 268°C for the center rod of the hottest waste package, the saturation limit for hydrogen is about 44 ppm (BSC 2004b, Table 6.12-2). That is, for all the hydrides to dissolve at 268°C and for hydride reorientation to occur, the initial hydrogen concentration must be less than 44 ppm. No more than 5% of the fuel has an average hydrogen concentration of 44 ppm or less; hence, less than 5% of the fuel could have all its hydrogen go into solution and, thus, be a candidate for reorientation.

Analyses conclude that hydride reorientation is of low likelihood because stresses and temperatures are too low for hydride reorientation to occur (BSC 2004b, Section 6.12.4). These analyses have shown that most of the fuel and the cladding material will maintain sufficient fracture toughness, even if hydride reorientation did occur, so that failure would not be expected. At the maximum cladding temperature of 2 68°C, the stress would have to be greater than 174

MPa before reorientation would occur. This corresponds to a stress value of about 94 MPa at room temperature. It is estimated (CRWMS M&O 2000b, Figure 26) that only 0.45% of the rods could have stresses this high and might undergo some reorientation. This is a small amount of the total inventory and supports the screening argument of low consequence. Hydride reorientation has been excluded on the basis of low consequence since few, if any, rods may undergo reorientation, and such reoriented rods may not fail.

Hydride axial migration, if it were to occur to a significant extent, could result in increased cladding failure. Analyses (BSC 2004b, Section 6.12.5) have shown that little or no hydride axial migration is expected because of a lack of large temperature gradients (the driving force for axial migration along the rod) in the waste packages and the low peak temperatures (which limit the amount of hydrogen in solution).

Hydrides can form in cooler parts of the rod, such as the end sections, because the hydrogen can dissolve into the fuel-cladding metal matrix at a warmer area, diffuse toward the cooler area, and condense there. McMinn et al. (2000, Figure 15) give the solubility of hydrogen. The solubility varies depending on whether hydrogen is dissolving or precipitating to form hydrides. McMinn et al. (2000, Figure 15) show that a minimum of 42°C temperature difference between the hot location and cold location in the cladding is needed to move the hydrogen. At temperatures below 200°C, temperature differences of more than 75°C are needed to axially move the hydrogen. At a peak cladding-center temperature of 268°C, at least a difference of about 50°C is needed to move and precipitate hydrogen. After repository closure, temperature differences of 19 C° are predicted (CRWMS M&O 2000c, Table 6-4). Therefore, little or no axial migration is expected based on the difference between condensation and dissolution solubility.

D.4.4 CLST 3.09

The chemical environment in the waste package, as discussed in Section D.4.2, is not sufficiently aggressive for pitting or stress corrosion cracking on the outer fuel cladding surface to occur. Even if an aggressive chemical environment existed in waste packages, stresses and stress intensities are too low for stress corrosion cracking to occur. Table D-2 gives the pressure, stresses, and stress intensity distributions for cladding at three times and temperatures. Details of how the entries in this table were determined can be found in *Clad Degradation–FEPs Screening Arguments* (BSC 2004b, Section 6.11).

During the times of interest (peak temperature or helium pressure) the stress intensity factors vary from 0.47 mean value to 2.7 MPa-$m^{0.5}$ maximum. This is compared to the threshold stress intensity factor for stress corrosion cracking, the value at which crack propagation will start, but with a very slow propagation velocity. If the stress intensity factor exceeds the threshold, failure will occur. Table D-3 gives the threshold values for various chemical solutions and temperatures. All values in the table are greater than or equal to 4 MPa $m^{0.5}$. The threshold stress intensity factor (K_{ISCC}) of 28 MPa-$m^{0.5}$ for moist chlorine is included in this table and is pertinent to the case of external cracking. The initial source of these stress intensity factors is Cox (1990, Figure 20, p. 15). Since the estimated stress intensities are less than the threshold values, chloride-induced cracking is not expected.

D.5 REFERENCES

BSC (Bechtel SAIC Company) 2001. *In-Package Chemistry for Waste Forms*. ANL-EBS-MD-000056 REV 00. Las Vegas, Nevada: Bechtel SAIC Company. ACC: MOL.20010322.0490.

BSC 2003. *Pitting Model for Zirconium Alloyed Cladding at YMP*. MDL-WIS-MD-000001 REV 00. Las Vegas, Nevada: Bechtel SAIC Company. ACC: DOC.20031017.0003.

BSC 2004a. *In-Package Chemistry Abstraction*. ANL-EBS-MD-000037 REV 03B. Las Vegas, Nevada: Bechtel SAIC Company. ACC: MOL.20040325.0129.

BSC 2004b. *Clad Degradation–FEPs Screening Arguments*. ANL-WIS-MD-000008 REV 01. Las Vegas, Nevada: Bechtel SAIC Company. ACC: DOC.20040322.0001.

Cox, B. 1973. "Stress Corrosion Cracking of Zircaloy-2 in Neutral Aqueous Chloride Solutions at 25 C." *Corrosion, 29*, (4), 157–166. Houston, Texas: National Association of Corrosion Engineers. TIC: 248988.

Cox, B. 1990. "Environmentally-Induced Cracking of Zirconium Alloys – A Review." *Journal of Nuclear Materials, 170*, 1–23. Amsterdam, The Netherlands: North-Holland. TIC: 234774.

CRWMS M&O (Civilian Radioactive Waste Management System Management and Operating Contractor) 2000a. *Clad Degradation–Local Corrosion of Zirconium and Its Alloys Under Repository Conditions.* ANL-EBS-MD-000012 REV 00. Las Vegas, Nevada: CRWMS M&O. ACC: MOL.20000405.0479.

CRWMS M&O 2000b. *Initial Cladding Condition.* ANL-EBS-MD-000048 REV 00 ICN 01. Las Vegas, Nevada: CRWMS M&O. ACC: MOL.20001002.0145.

CRWMS M&O 2000c. *Thermal History of Cladding in a 21 PWR SNF WP Loaded with Average Fuel*. CAL-UDC-ME-000001 REV 00. Las Vegas, Nevada: CRWMS M&O. ACC: MOL.20000216.0105.

CRWMS M&O 2000d. *Abstraction of NFE Drift Thermodynamic Environment and Percolation Flux*. ANL-EBS-HS-000003 REV 00 ICN 01. Las Vegas, Nevada: CRWMS M&O. ACC: MOL.20001206.0143.

CRWMS M&O 2000e. *Multiscale Thermohydrologic Model*. ANL-EBS-MD-000049 REV 00 ICN 01. Las Vegas, Nevada: CRWMS M&O. ACC: MOL.20001208.0062.

CRWMS M&O 2001. *Clad Degradation – Summary and Abstraction.* ANL-WIS-MD-000007 REV 00 ICN 01. Las Vegas, Nevada: CRWMS M&O. ACC: MOL.20010214.0229.

Dzombak, D.A. and Morel, F.M.M. 1990. *Surface Complexation Modeling, Hydrous Ferric Oxide*. New York, New York: John Wiley & Sons. TIC: 224089.

Farina, S. B.; Duffo, G.S.; and Galvele, J.R. 2002. "Stress Corrosion Cracking of Zirconium and Zircaloy-4 in Iodine Containing Solutions." *Corrosion/2002, 57th Annual Conference & Exposition, April 7-11, 2002, Denver, Colorado.* Paper No. 02436. Houston, Texas: NACE International. TIC: 253841.

McMinn, A.; Darby, E.C.; and Schofield, J.S. 2000. "The Terminal Solid Solubility of Hydrogen in Zirconium Alloys." *Zirconium in the Nuclear Industry: Twelfth International Symposium, Toronto, Canada, 15-18 June 1998.* Sabol, G.P. and Moan, G.D., eds. Pages 173–195. West Conshohocken, Pennsylvania: American Society for Testing and Materials. TIC: 247102.

Reamer, C.W. 2001. "Container Life and Source Term Key Technical Agreements." Letter from C.W. Reamer (NRC) to S. Brocoum (DOE/YMSCO), December 21, 2001, with enclosure. ACC: MOL.20020402.0608.

Reamer, C.W. and Gil, A.V. 2001. Summary Highlights of NRC/DOE Technical Exchange and Management Meeting of Range on Thermal Operating Temperatures, September 18–19, 2001. Washington, D.C.: U.S. Nuclear Regulatory Commission. ACC: MOL.2002017.0162.

Reed-Hill, R.E. 1973. *Physical Metallurgy Principles.* 2nd Edition. New York, New York: D. Van Nostrand Company. TIC: 237154.

Schlueter, J. 2000. U.S. Nuclear Regulatory Commission/U.S. Department of Energy Technical Exchange and Management Meeting on Container Life and Source Term (September 12–13, 2000). Letter from J. Schlueter (NRC) to S. Brocoum (DOE/YMSCO), October 4, 2000, with enclosure. ACC: MOL.20010731.0161.

Tasooji, A.; Einziger, R.E.; and Miller, A.K. 1984. "Modeling of Zircaloy Stress-Corrosion Cracking: Texture Effects and Dry Storage Spent Fuel Behavior." *Zirconium in the Nuclear Industry, Sixth International Symposium, Vancouver, British Columbia, June 28- July 1, 1982.* Franklin, D.G. and Adamson, R.B., eds. ASTM STP 824. Pages 595–626. Philadelphia, Pennsylvania: American Society for Testing and Materials. TIC: 241417.

Yau, T.L. and Webster, R.T. 1987. "Corrosion of Zirconium and Hafnium." *Corrosion, 13,* 707–721 of *ASM Handbook.* Formerly 9th Edition, *Metals Handbook.* Materials Park, Ohio: ASM International. TIC: 240704.

APPENDIX E

TOTAL SYSTEM PERFORMANCE ASSESSMENT IMPLEMENTATION OF IN-PACKAGE CHEMISTRY (RESPONSE TO TSPAI 3.08)

Note Regarding the Status of Supporting Technical Information

This document was prepared using the most current information available at the time of its development. This Technical Basis Document and its appendices providing Key Technical Issue Agreement responses that were prepared using preliminary or draft information reflect the status of the Yucca Mountain Project's scientific and design bases at the time of submittal. In some cases this involved the use of draft Analysis and Model Reports (AMRs) and other draft references whose contents may change with time. Information that evolves through subsequent revisions of the AMRs and other references will be reflected in the License Application (LA) as the approved analyses of record at the time of LA submittal. Consequently, the Project will not routinely update either this Technical Basis Document or its Key Technical Issue Agreement appendices to reflect changes in the supporting references prior to submittal of the LA.

APPENDIX E

TOTAL SYSTEM PERFORMANCE ASSESSMENT IMPLEMENTATION OF IN-PACKAGE CHEMISTRY (RESPONSE TO TSPAI 3.08)

This appendix provides a response to Key Technical Issue (KTI) agreement Total System Performance Assessment and Integration (TSPAI) 3.08. This agreement relates to implementation of in-package chemistry in total system performance assessment (TSPA).

E.1 KEY TECHNICAL ISSUE AGREEMENT

Agreement TSPAI 3.08 was reached during the U.S. Nuclear Regulatory Commission (NRC)/U.S. Department of Energy (DOE) Technical Exchange and Management Meeting on TSPAI held August 6 through 10, 2001, in Las Vegas, Nevada (Reamer and Gil 2001a).

E.1.1 TSPAI 3.08

The wording of the agreement is as follows:

TSPAI 3.08[1]

> Provide the technical basis (quantification) for the abstraction of in-package chemistry and its implementation into the TSPA which will demonstrate that the utilization of the weighted-moving-average methodology will not result in an underestimation of risk (ENG3.1.3).
>
> DOE will provide the technical basis (quantification) for the abstraction of in-package chemistry and its implementation into the TSPA, which will demonstrate that the implementation methodology will not result in an underestimation of risk. The technical basis will be documented in TSPA-LA and is expected to be available in FY 2003.

General agreement (GEN) 1.01 was reached during the NRC/DOE Technical Exchange and Management Meeting on Range of Thermal Operating Temperatures, held September 18 to 19, 2001, in Las Vegas, Nevada. Associated with that meeting, the DOE provided initial responses to GEN 1.01 (Comment 126) that referred in part to TSPAI 3.08 (Reamer and Gil 2001b). Comment 126, however, is addressed entirely in Appendix A.

E.1.2 Related Key Technical Issue Agreements

There are no other KTI agreements directly related to agreement TSPAI 3.08.

[1] The content of ENG3.1.3 (Cornell 2001) is adequately represented within the text of TSPAI 3.08.

E.2 RELEVANCE TO REPOSITORY PERFORMANCE

The in-package chemistry (water chemistry, pH, ionic strength, Eh, fluoride concentration, chloride concentration, and total carbonate concentration) can potentially impact radionuclide and colloid concentration and transport, as well as waste package and waste form component degradation in TSPA for the license application (TSPA-LA). The calculation of time-dependent chemical parameters in combination with the weighted-moving average method of calculating waste package failure times could potentially underestimate waste package and waste form degradation and radionuclide transport.

E.3 RESPONSE

The model calculates the time-varying chemical conditions in the waste package for each time step of the TSPA-LA calculations (Section 3.5 of this technical basis document).

Once a waste package fails and degradation of the waste form and package components commences, pH values are expected to remain within a range of 4.5 to 8.1 during the first 600 years after breach and within a range of 4.5 to 7 after 600 years (nominal and seismic scenarios; see below) (BSC 2004, Sections 6.6.1.1 and 6.6.2.1). Potentially low pH from the corrosion of steel waste package components, particularly during the first 600 years after package failure, would be buffered by the corrosion product goethite; potentially high pH from the corrosion of high-level radioactive waste glass would be counteracted by corrosion of the large amount of steel in the codisposal packages. The difference in the upper end of the pH range (pH 8.1 at times less than 600 years after breach, versus pH 7 at times greater than 600 years after breach) is not significant.

The information in this report is responsive to agreement TSPAI 3.08 made between DOE and NRC. This report contains the information that DOE considers necessary for NRC review for closure of this agreement.

E.4 BASIS FOR THE RESPONSE

The weighted-moving average methodology for calculating the time-phased failure of waste packages will be used in the TSPA-LA in combination with a set of calculations that determine the time-varying chemical conditions that will evolve in a waste package once it has failed (Section 3.4 of this technical basis document) (BSC 2004, Section 6). The time-varying chemical conditions are obtained with the in-package chemistry model (BSC 2004).

With the weighted-moving average methodology (using the same approach in the TSPA-LA model as that used in *Total System Performance Assessment (TSPA) Model for Site Recommendation* (CRWMS M&O 2000), the average waste package failure time is calculated as the average duration that each failed waste package within a bin has been breached; it is calculated for each percolation flux subregion (bin) and for nondripping and dripping conditions. For each bin, a curve is used to represent the fraction of waste packages failed at any given time. Due to differences in the numbers of packages in the bins, waste package failures are realized at different times in different bin environments.

The in-package chemistry model simulates the chemistry inside of a failed waste package (i.e., the chemistry of the fluid that reacts with the waste package components and the waste forms). The in-package chemistry model begins calculation of the fluid chemistry resulting from waste form and package component degradation in the TSPA-LA model when the first package fails and an aqueous phase is present within the waste package (i.e., when the waste package temperature falls below 100°C). In each time-step of the TSPA-LA calculations, the particular chemical condition (e.g., pH, ionic strength, Eh, total carbonate, chloride, or fluoride concentration) is abstracted into response surfaces or parameter distributions that are sampled to establish the chemical condition for a particular computational realization in the TSPA-LA.

In the in-package chemistry calculations used in the TSPA for the site recommendation model, pH in a breached waste package dropped to low values within about 50 years after breach, primarily due to corrosion of sulfur-bearing steel alloys and became more moderate after about 500 years (CRWMS M&O 2000). Under these circumstances, the weighted-moving average methodology for calculating waste package failure time could underestimate the duration of low-pH conditions. However, refinements in the in-package chemistry calculations (see below) used in TSPA-LA make the effects of time averaging insignificant due to the similar pH ranges prior to and after 600 years. The likelihood that a combination of a relatively late-failing package with calculated time-varying chemical conditions could reduce releases and underestimate risk is small because the pH within the waste package will avoid extremes throughout the time analyzed.

Constant Moderate Chemistry–pH values are expected to remain within a range of 4.5 to 8.1 during the first 600 years after breach and within a range of 4.5 to 7 after 600 years (nominal and seismic scenarios). Although time-varying pH is calculated only for commercial SNF waste packages, for completeness this discussion describes the chemistry within both commercial SNF and codisposal packages. The revised *In-Package Chemistry Abstraction* (BSC 2004, Sections 6.6.1.1 and 6.6.2.1) demonstrates that reaction of the individual waste form components (steels, glass, fuel) produces fluids with pH values that are near neutral. The three exceptions are Carbon Steel Type A516 and Stainless Steel Type 304L steel degradation, which both produce protons (acid conditions), and high-level radioactive waste glass, which generates alkalinity. Explicit consideration of the pH-buffering of corrosion products indicates that Carbon Steel Type A516 degradation will actually produce near-neutral fluids (BSC 2004, Section 6.8). Stainless Steel Type 304L degradation is similarly unlikely to result in acid pH solutions because it dissolves very slowly (BSC 2004, Section 6.5.1.1); hence, proton production is likely to be diluted by incoming fluids. High-level radioactive waste glass dissolution can produce locally high pH values because of its high base cation content. However, there is far more steel than high-level radioactive waste glass in codisposal packages, and large amounts of schoepite are estimated to form as well. Dissolution of either consumes alkalinity and would tend to make the persistence of high pH values unlikely in the waste form. In particular, relatively rapid dissolution of schoepite would tend to drive pH values toward its solubility minimum near-neutral pH. The presence of multiple processes capable of providing a negative-feedback control over high pH is discussed in Section 3.4 of this technical basis document and in *In-Package Chemistry Abstraction* (BSC 2004, Section 6.8). The dissolution of high-level radioactive waste glass is the only way to generate locally extreme pHs. Because high-level radioactive waste glass is present in minor amounts (and dissolves more slowly) relative to other

pH-buffering reactants, the potential for long-term persistence of extreme pHs is considered remote.

The difference in the upper end of the pH range (pH 8.1 at times less than 600 years after breach, versus pH 7 at times greater than 600 years after breach) and its effect on waste form degradation rates do not adversely affect chemistry, since the degradation rates of commercial SNF at pH 7 and 8.1 are essentially the same. While codisposal waste packages are not affected by the weighted-moving average methodology, it is worth noting that high-level radioactive waste glass has a lower degradation rate at the higher pH value and is, therefore, conservative.

The difference in the upper end of the pH range has a mixed effect on actinide solubilities. Neptunium has a lower solubility at pH 8.1 than pH 7 at lower fCO_2 values and a higher solubility at pH 8.1 at higher fCO_2 values (roughly an order of magnitude higher between pH 7 and 8.1). Protactinium shows a similar pattern.

Uranium solubility is controlled by one of three phases (schoepite, Na-boltwoodite, or $NA_3UO_2(CO_3)_3$, depending on the pH and the fCO_2 (BSC 2004, Section 6.7). There is a complex functionality of dissolved uranium to both pH and the fCO_2 (BSC 2004, Figure 6.7-2). Thus, for any of the uranium controlling phases, the trend in the uranium concentration at different pH values can be either by increasing or decreasing, depending on fCO_2.

Plutonium solubility is flat between pH 7 and 8.1 at higher fCO_2 values and lower at pH 8.1 at lower fCO_2 values. Americium solubility follows a roughly similar pattern. Thorium solubility is higher at pH 8.1 for all fCO_2 values.

In conclusion, the moderate chemistry anticipated in a breached waste package will result in pH values that will vary within narrow limits over time. This means that the pH during the first 600 years after waste package failure will not be greatly different from the pH beyond that period. As a result, the use of the weighted-moving average method for calculation of progressive waste package failure due to localized corrosion processes is not likely to underestimate dose to the reasonably maximally exposed individual.

E.5 REFERENCES

BSC (Bechtel SAIC Company) 2004. *In-Package Chemistry Abstraction.* ANL-EBS-MD-000037 REV 03B. Las Vegas, Nevada: Bechtel SAIC Company. ACC: MOL.20040609.0094.

Cornell, V. 2001. *Analysis of Resolution Status Key Technical Issue: Total System Performance Assessment and Integration Subissue 3: Model Abstraction.* Slide presentation at U.S. Nuclear Regulatory Commission/U.S. Department of Energy Technical Exchange and Management Meeting on Total System Performance Assessment and Integration, August 6 through 10, 2001. ACC: MOL.20010921.0129.

CRWMS M&O (Civilian Radioactive Waste Management System Management and Operating Contractor) 2000. *Total System Performance Assessment (TSPA) Model for Site Recommendation*. MDL-WIS-PA-000002 REV 00. Las Vegas, Nevada: CRWMS M&O. ACC: MOL.20001226.0003.

Reamer, C.W. and Gil, A.V. 2001a. Summary Highlights of NRC/DOE Technical Exchange and Management Meeting on Total System Performance Assessment and Integration. Meeting held August 6–10, 2001, Las Vegas, Nevada. Washington, D.C.: U.S. Nuclear Regulatory Commission. ACC: MOL.20010921.0121.

Reamer, C.W. and Gil, A.V. 2001b. Summary Highlights of NRC/DOE Technical Exchange and Management Meeting of Range on Thermal Operating Temperatures, September 18–19, 2001. Washington, D.C.: U.S. Nuclear Regulatory Commission. ACC: MOL.20020107.0162.

INTENTIONALLY LEFT BLANK